University of Padova

Department of Department of Physics and Astronomy “Galileo Galilei”

Master Thesis in Astrophysics and Cosmology

Neutrino Self–Interactions in the Dodelson–Widrow Mechanism

Supervisor
Prof. Francesco D’Eramo
University of Padova

Master Candidate
Finn Anthony Mulder

Student ID
2106228

Academic Year
2024-2025

Abstract

Sterile neutrinos have long been accepted as minimal possible Standard Model extensions due to their simplicity and ability to generate low-mass active neutrinos through the Seesaw mechanism. Furthermore, due to its feeble interaction, the heavy neutrino mass eigenstate can remain cosmologically long-lived and avoid thermalization, making it an attractive dark matter candidate. Dodelson and Widrow showed how to produce a sterile population compatible with the required dark matter energy density, but the necessary active-sterile mixing is ruled out by X-ray bounds on the radiative decay of the sterile neutrino. In order to explain dark matter using sterile neutrinos, one must thus provide for a mechanism that allows for the mixing angle to assume lower values. We reproduce the effect of sterile neutrino self-interactions mediated by a scalar on their production, and in agreement with the literature, we find that a part of the parameter space is not in tension with cosmological bounds for a small enough scalar mass. Then, as a new contribution to the literature, we evaluate the effect of spin-1 boson mediated self-interactions on sterile neutrino production, and find that it is able to saturate the dark matter energy density requirement for even lower mixing angles.

Contents

ABSTRACT

1 INTRODUCTION 1

2 THE STANDARD MODEL AND ITS DRAWBACKS 3
- 2.1 Gauge Structure of the Standard Model . . . 3
  - 2.1.1 Lorentz Symmetries and Gauge Theory . . . 3
  - 2.1.2 $SU(3)_c \times SU(2)_L \times U(1)_Y$ . . . 5
- 2.2 Electroweak Symmetry Breaking . . . 7
  - 2.2.1 The Higgs Mechanism . . . 8
  - 2.2.2 Vector Boson Masses . . . 10
  - 2.2.3 Fermion Masses . . . 12
- 2.3 Flavour Structure and Mixing . . . 13
  - 2.3.1 Quark Flavour Mixing . . . 13
  - 2.3.2 CP Violation . . . 15
  - 2.3.3 Flavour Changing Neutral Currents . . . 17
- 2.4 Problems in the Standard Model . . . 19
  - 2.4.1 Neutrino masses . . . 19
  - 2.4.2 Dark Matter . . . 19
  - 2.4.3 Baryon Asymmetry . . . 21
  - 2.4.4 Dark Energy . . . 22
  - 2.4.5 Strong CP Problem . . . 23
  - 2.4.6 Hierarchy Problem . . . 24
  - 2.4.7 Unification of Coupling Constants . . . 24

3 EMPIRICAL EVIDENCE FOR NEUTRINO MASSES 26
- 3.1 Neutrinos Before the Standard Model . . . 26
- 3.2 The Solar Neutrino Problem . . . 28
  - 3.2.1 Discovery and Confirmation of the SNP . . . 28
  - 3.2.2 SNO . . . 29
- 3.3 Neutrino Oscillations in Vacuum . . . 30
  - 3.3.1 Standard Neutrino Oscillation Probability . . . 30
  - 3.3.2 CP Violation in Neutrino Oscillations . . . 33
- 3.4 Neutrino Oscillations in Matter . . . 34
  - 3.4.1 Effective Potentials . . . 34
  - 3.4.2 Flavour Evolution in Matter . . . 36
  - 3.4.3 The MSW effect . . . 38
- 3.5 Extension to Three-Neutrino Mixing . . . 43
  - 3.5.1 Important Results from n-Neutrino Mixing . . . 43
  - 3.5.2 3-Neutrino Mixing in Vacuum . . . 46
  - 3.5.3 3-Neutrino Mixing in Matter . . . 49

4 NEUTRINOS BEYOND THE STANDARD MODEL 53
4.1 Dirac and Majorana masses . . . 53
4.1.1 Dirac Spinors . . . 53
4.1.2 Majorana Spinors . . . 54
4.1.3 Dirac and Majorana Masses for Neutrinos . . . 55
4.1.4 Lepton Number Violation . . . 61
4.1.5 Neutrino Oscillations and Majorana Masses . . . 61
4.2 Seesaw Mass mechanisms . . . 62
4.2.1 The Weinberg Operator and the EFT Approach . . . 62
4.2.2 The Type I Seesaw Mechanism . . . 64
4.2.3 Type II . . . 69
4.2.4 Type III . . . 69
4.2.5 Inverse Seesaw . . . 70
4.2.6 The νSMEFT . . . 70

5 THE DODELSON–WIDROW MECHANISM 72
5.1 Sterile Neutrino Boltzmann Equations . . . 73
5.1.1 Rates and Angles from Thermal Field Theory . . . 75
5.1.2 Notes on the Potentials . . . 76
5.2 Solving the Equation . . . 78
5.3 DW Sterile Neutrinos as Dark Matter . . . 82
5.3.1 X-Ray Constraints . . . 83
5.3.2 Cosmological Constraints . . . 85

6 SELF-INTERACTIONS 87
6.1 Sterile Self-Interactions through Scalars . . . 87
6.1.1 Setting up the Boltzmann Equation . . . 87
6.1.2 Light Mediators . . . 91
6.1.3 Intermediate Mass Range . . . 94
6.1.4 Available Parameter Space . . . 97
6.2 Active Self-Interactions through Scalars . . . 99
6.2.1 Setting up the Boltzmann Equation . . . 100
6.2.2 Solving the Boltzmann Equation . . . 102
6.2.3 Discussion of the Parameter Space . . . 104
6.3 Sterile Self-Interaction through Vectors . . . 105
6.3.1 The (Effective) Model . . . 105
6.3.2 Light Mediator Boltzmann Equations . . . 107
6.3.3 Solving the Boltzmann Equations . . . 108

7 CONCLUSIONS 112

APPENDIX A CALCULATION OF AMPLITUDES AND RATES 114
A.1 Amplitudes . . . 114
A.1.1 Identities for 4-Component Spinors . . . 114
A.1.2 Obtaining $-i\mathcal{M}_{\nu_s\nu_s\to\nu_s\nu_s}$ . . . 115
A.1.3 $\overline{|\mathcal{M}_{\nu_s\nu_s\to\nu_s\nu_s}|}^2$ . . . 118
A.1.4 Obtaining $-i\mathcal{M}_{\nu_s\nu_s\to\phi\phi}$ . . . 120

A.1.5 $\overline{|\mathcal{M}_{\nu_s\nu_s\to\phi\phi}|^2}$ . . . 121
A.2 Cross sections . . . 121
A.3 Rates . . . 122
A.3.1 Sterile-sterile interaction rates via scalar mediators . . . 122
A.3.2 Interaction Rates and Thermal Averaging . . . 124
A.3.3 Moments of Scalar Final States . . . 124
A.3.4 Active–active interaction rates . . . 125
A.3.5 Sterile-sterile interaction rates for vector mediators . . . 126

APPENDIX B CALCULATION OF SCALAR MEDIATOR COLLISION TERMS 128
B.0.1 Oscillation-Based Processes . . . 129
B.0.2 Two-to-two Scattering . . . 130

APPENDIX C DESCRIPTION OF NUMERICAL CODE 131
C.1 Dodelson-Widrow Integration . . . 131
C.2 Solving the Scalar Mediator Differential Equations . . . 132
C.2.1 Light Mediator Limit . . . 134
C.2.2 Including Number Changing Processes . . . 136
C.2.3 Scanning the Parameter Space . . . 138
C.3 Solving the Vector Mediator Differential Equations . . . 140
C.3.1 Variable Redefinitions . . . 140
C.3.2 Coding considerations . . . 143

BIBLIOGRAPHY 145

ACKNOWLEDGMENTS 160

1

Introduction

The Standard Model (SM) of particle physics, while renowned for its predictive power, is manifestly incomplete. Several empirical facts of different origins point to this. Among them are the existence of dark matter, cosmological questions such as the baryon asymmetry of the Universe, and the strong CP and hierarchy problem from a particle physics point of view. Perhaps most directly, however, there are neutrino oscillations. This observation demonstrates that neutrinos possess non-zero masses—a feature absent in the minimal Standard Model. To explain such masses, one of the theoretically most economical extensions of the SM introduces new particles: right-handed gauge-singlet fermions called sterile neutrinos. Unlike the familiar active species, these states carry no Standard Model charges. They interact only via their mixing with active neutrinos. Sterile states are also not constrained by electroweak symmetry breaking and do not require the Higgs mechanism to acquire mass. As a result, their masses are essentially free parameters. These can span a wide range of scales, from sub-eV to well beyond the electroweak scale. This flexibility is of particular theoretical significance, as it allows for so-called seesaw mechanisms. In these, heavy sterile states generate the tiny active neutrino masses observed in oscillation experiments.

Although the neutrality of the sterile neutrino under the SM charges makes the particle difficult to detect, it also provides an attractive dark matter candidate. A state with only feeble interactions can remain cosmologically long-lived and evade thermalization. This avoids the strong constraints that rule out most weakly interacting species. This observation motivated Dodelson and Widrow. They proposed that sterile neutrinos produced via active-sterile oscillations in the early Universe could account for the observed dark matter fraction [DW94b]. Despite their ability to produce significant abundances, this minimal production mechanism faces severe constraints. These arise primarily from X-ray observations of sterile neutrino decays, which effectively exclude the original scenario across all of the relevant parameter space [Aba17; B M+20].

To realize sterile neutrinos as the dominant dark matter component anyway, numerous extensions have been proposed that evade these X-ray constraints. Such extensions typically introduce additional interactions that modify the sterile neutrino Boltzmann equation 5.1.21, thereby changing production epochs, rates, and in some cases decay signatures. Among the more minimal approaches are the addition of self-interactions between active neutrinos [Gou+20b; Kel+20; Ben+22], self-interactions among sterile neutrinos [JF19; Bri+21; AV24], and sterile–active interactions [Bri+21]. More elaborate models introduce additional SM singlets [MNS14; MT15; PK08] or invoke dark entropy production [HV17].

In this thesis, we focus on such modifications of the Dodelson–Widrow mechanism. In particular, we successfully reproduce the DM production through light scalar-mediated sterile self-interactions, originally produced in [AV24]. The resulting parameter space is swept over and discussed. We also mention results from the analogous active self-interacting scenario for completeness [Gou+20a]. As a new contribution to the literature, we replicate the modified Dodelson–Widrow mechanism in the case of a spin-1 boson mediating sterile neutrino self-interactions. The resulting dark matter yield is computed for a light mediator scenario. We find that such an interaction allows for a stronger production than a scalar mediated one, permitting the mixing between the active and sterile sectors to be even smaller, therefore evading X-ray constraints more effectively.

The thesis is structured as follows: in Chapter 2 we revise the basic theory of the electroweak section of the Standard Model, including a discussion on its shortcomings. Then, in Chapter 3, we argue why oscillation observations require neutrino masses, and we derive some useful phenomenological results related to oscillation probabilities. After this, we introduce sterile neutrinos and relevant field theoretical concepts in Chapter 4. The Dodelson–Widrow mechanism is reproduced in Chapter 5, accompanied by the astrophysical and cosmological bounds leading to its exclusion. Finally, in Chapter 6, we turn our eyes to modified Dodelson–Widrow mechanisms. In 6.1, we rederive and present known results on sterile self-interactions through scalars. Afterwards, in 6.2, we present the analogous active case. The new results are then derived and shown in 6.3, after which all is summarised in Chapter 7.

2
The Standard Model and its Drawbacks

The dominant modern approach to describing a quantum field theory is through gauge theory, and the current standard model of particle physics, the Standard Model (SM) for short, is one such variant. Any gauge theory has three main determining characteristics:

1. its symmetry groups;
2. its matter content;
3. its mechanism for symmetry breaking.

The aim of this section is to define the standard model according to these aspects. In the first section, we briefly discuss some fundamental theoretical preliminaries before giving the full gauge structure of the SM. In the sections after, we will massage this structure further to explain particle masses through the Higgs mechanism, discuss how it brings about mixing in the quark sector, before finally discussing the problems the current model still faces.

2.1 GAUGE STRUCTURE OF THE STANDARD MODEL

2.1.1 LORENTZ SYMMETRIES AND GAUGE THEORY

Before we introduce the gauge symmetries and matter content present in the Standard Model, it is useful to briefly recap the main results from representation theory of the Lorentz group and from general gauge theory.

Since QFT arose as the fusion of quantum mechanics and special relativity, it is natural that Lorentz invariance lies at the heart of the theory. Special relativity requires the invariance of a theory under all Lorentz transformations (i.e., 3 boosts and 3 spatial rotations), which implies that all physical quantities entering the theory must be constructed to remain invariant under such transformations. The fundamental building blocks of the theory should thus either transform trivially themselves or manifest themselves together in such a way that their transformations cancel to a trivial net effect. We can form a group of Lorentz transformations called the Lorentz group, and then all objects that have well-defined transformation properties under the Lorentz group are described by its representations. We can thus introduce objects that either transform trivially or under any of the representations of the Lorentz group. The group of Lorentz transformations preserving direction of time and orientation is called the *proper orthochronous Lorentz group*. Mathematically, it is $SO(1,3)^+$, and its representations are known to consist of

- the trivial representation 1, transforming spin-0 scalars;
- the fundamental representation 4, transforming spin-1 four vectors;
- the tensor product $4 \otimes 4$ transforming spin-2 tensors, which are decomposable into a trivial representation, an irreducible representation of dimension 6 transforming antisymmetric tensors, and an irreducible representation of dimension 9 transforming symmetric tensors.

The spin values are assigned by considering the various $SO(1,3)^+$ representations under its subgroup $SO(3)$, where spin corresponds to the eigenvalues of the quadratic Casimir operator J^2 of its corresponding algebra $\mathfrak{so}(3)$. In order to include spin-1/2 particles, however, we must consider the double cover of the Lorentz group, which is $\mathrm{SL}(2,\mathbb{C})$. Under the local isomorphism $\mathrm{SL}(2,\mathbb{C}) \simeq SU(2)_L \times SU(2)_R$, the representations of the Lorentz group are classified by tensor products of the form (j_L, j_R), where j_L and j_R denote the spin under the respective $SU(2)$ subgroups. These include the representations that we saw before, but additionally introduce, among others:

- the trivial representation $1 \otimes 1$ or $(0,0)$, corresponding to spin-0 scalars;
- the Weyl spinor representations $2 \otimes 1$ and $1 \otimes 2$, or in terms of spin values $(\frac{1}{2}, 0)$ and $(0, \frac{1}{2})$, describing two-component left- and right-handed spinors, respectively.

An important consequence of the structure of these representations is that Weyl spinors are the fundamental building blocks of matter fields. The description of elementary particles in terms of the left- and right-handed Weyl components, transforming independently, is referred to as the chiral structure of the model. A $(\frac{1}{2}, 0)$ spinor transforms non-trivially under $SU(2)_L$ and trivially under $SU(2)_R$, and vice versa for $(0, \frac{1}{2})$. These components are not mixed under Lorentz transformations but are exchanged under parity, which swaps the $SU(2)_L$ and $SU(2)_R$ factors. A four vector is described by the $(\frac{1}{2}, \frac{1}{2})$ representation restricted by the reality condition.

In addition to Lorentz symmetry, a theory is also described by its gauge symmetries. Those symmetries are used to describe interactions between the various matter components. A general intuition can be created by the generalization of invariance under a local phase factor. From quantum mechanics, we know that observables do not depend on overall phase factors, say a general state transformation

$$|\psi\rangle \to e^{i\alpha}|\psi\rangle. \tag{2.1.1}$$

If one attempts to generalise this to a local phase $e^{i\alpha(x)}$, where $\alpha(x)$ is an arbitrary function of x^μ, troubles with the formal definition of the derivative emerge, since $e^{i\alpha(x)}$ can be different from $e^{i\alpha(x+h)}$. A non-ambiguous expression requires the redefinition of the derivative to the covariant derivative

$$\partial_\mu \to D_\mu = \partial_\mu + igA_\mu, \tag{2.1.2}$$

where g is an overall scale called the coupling constant and A_μ is a vector field that acts as a connection, encoding how the internal phase of the field varies from point to point across spacetime. This implies that kinetic terms of fields respecting the invariance under a local phase factor naturally contain an interaction term with a vector-like field A_μ. Even stronger, we see that the requirement of invariance under a symmetry introduces vector-like particles and their interactions with the other particles. The symmetry group (or gauge group) corresponding to a local phase factor is $U(1)$, but one can also consider more complex symmetry groups like $SU(N)$ or other non-abelian groups. Although the generalization to non-abelian groups requires some rigour, the idea is similar and one can generally state that: *for a symmetry group with N generators, N new* *massless bosons are introduced to the theory, and each generator corresponds to a conserved charge.*

Once the matter representations and the gauge groups are specified, one should write every renormalizable operator in the Lagrangian that respects Lorentz, gauge, and CPT symmetry. Remembering the determining characteristics of a gauge theory from the beginning of this chapter, we will now first introduce the symmetry groups of the SM.

2.1.2 $SU(3)_c \times SU(2)_L \times U(1)_Y$

The gauge group of the Standard Model is

$$SU(3)_c \times SU(2)_L \times U(1)_Y,$$

and can be seen to consist of the product of 3 simple Lie groups. A distinction is generally made between the colour component $SU(3)_c$ and the electroweak part $SU(2)_L \times U(1)_Y$. The fundamental representations and emerging gauge bosons will be listed in table 2.1, and it can be seen that the fundamental objects transforming under the groups are $SU(3)_c$ triplets, $SU(2)_L$ doublets, and $U(1)_Y$ singlets.

gauge group	gauge bosons	fundamental representation	dimension
$SU(3)_c$	$G^1_\mu, \ldots, G^8_\mu$	$\exp\{i\theta^a \frac{\lambda^a}{2}\}$	3
$SU(2)_L$	$W^1_\mu, W^2_\mu, W^3_\mu$	$\exp\{i\theta^j \frac{\sigma^j}{2}\}$	2
$U(1)_Y$	B_μ	$\exp\{i\alpha Y\}$	1

Table 2.1: Gauge groups and their fundamental representations, where σ^j are the Pauli matrices and λ^a the Gell-Mann matrices. The strong gauge bosons $G^1_\mu, \ldots, G^8_\mu$ are the gluons.

So far, without having introduced any fermionic fields, the only gauge-invariant Lagrangian that can be written[*] is

$$\mathcal{L}_1 = -\frac{1}{4} G^a_{\mu\nu} G^{a\mu\nu} - \frac{1}{4} W^i_{\mu\nu} W^{i\mu\nu} - \frac{1}{4} B_{\mu\nu} B^{\mu\nu}, \tag{2.1.3}$$

where the various field strength tensors are described by

$$G^a_{\mu\nu} = \partial_\mu G^a_\nu - \partial_\nu G^a_\mu + g_s f^{abc} G^b_\mu G^c_\nu, \tag{2.1.4}$$

$$W^i_{\mu\nu} = \partial_\mu W^i_\nu - \partial_\nu W^i_\mu + g \varepsilon^{ijk} A^j_\mu A^k_\nu, \tag{2.1.5}$$

$$B_{\mu\nu} = \partial_\mu B_\nu - \partial_\nu B_\mu, \tag{2.1.6}$$

with f^{abc} the $SU(3)$ structure constants and ε^{ijk} the fully antisymmetric tensor, and g_s and g the coupling constants of $SU(3)_c$ and $SU(2)_L$ respectively. The next task is to add the correct matter fields to the model. Note that all matter fields transform under one-dimensional representations of $U(1)_Y$, meaning their hypercharges are not fixed by group structure but are instead assigned explicitly. In contrast, the charges under non-Abelian groups such as $SU(2)_L$ and $SU(3)_c$ are determined by the dimensionality of the representation the field transforms under. We can thus classify matter fields by $(n_{SU(3)}, m_{SU(2)}, Y)$, as done in table 2.2, where n and m denote the dimensionality of the corresponding representations and Y their hypercharge.

Weyl fermions that transform as triplets under $SU(3)_c$ are called quarks, while the matching singlets are called leptons. Weyl fermions that transform as doublets under $SU(2)_L$ are called left-handed, while the corresponding singlets are right-handed. Note that the left- and right-handed separation of $SU(2)_L$ follows the separation of left- and right-handed from the Lorentz group, so in fact it is more precise to say that left-handed Weyl fermions enter as doublets and are charged under $SU(2)_L$, while the right-handed Weyl fermions are singlets and neutral under $SU(2)_L$. The difference in charge of the two types of Weyl fermions explicitly breaks parity symmetry and requires a description using chiral structure. One could, however, theoretically add $SU(2)_L$ doublets which are not left-handed Weyl fermions, so one should remain conscious of the distinction between the gauge and the Lorentz symmetries.

---

[*] One can also write the so-called dual terms, a discussion on these terms is given in section 2.4.5.

There are three families of quarks, indicated by the index i for q_L^i in Table 2.2, and three families of fermions indicated similarly for ℓ_L^i and ℓ_R^i. The right-handed quarks also come in three families, but not in $SU(2)_L$ doublets, so a separation is made for the families of positively charged quarks p_R^i and negatively charged quarks n_R^i. Note that the neutrinos, i.e., components of the leptonic $SU(2)_L$ doublets with isospin $T_3 = +\frac{1}{2}$, have no right-handed counterpart with $T_3 = 0$ in the Standard Model, as we have never measured such a particle. The remaining right-handed leptons also come in three families, denoted by ℓ_R^i. Sometimes it is handy to explicitly denote the families of individual components of $SU(2)_L$ doublets, and that will be done by p_L^i, n_L^i, ν_L^i and e_L^i.

	Quarks	**Leptons**
L	$\underline{(3, 2, \frac{1}{3})}$ $q_L^i : \begin{pmatrix} u_L \\ d_L \end{pmatrix}, \begin{pmatrix} c_L \\ s_L \end{pmatrix}, \begin{pmatrix} t_L \\ b_L \end{pmatrix}$	$\underline{(1, 2, -1)}$ $\ell_L^i : \begin{pmatrix} \nu_{e_L} \\ e_L \end{pmatrix}, \begin{pmatrix} \nu_{\mu_L} \\ \mu_L \end{pmatrix}, \begin{pmatrix} \nu_{\tau_L} \\ \tau_L \end{pmatrix}$
R	$\underline{(3, 1, \frac{4}{3})}$ $p_R^i : u_R, c_R, t_R$ $\underline{(3, 1, -\frac{2}{3})}$ $n_R^i : d_R, s_R, b_R$	$\underline{(1, 1, -2)}$ $\ell_R^i : e_R, \mu_R, \tau_R$

Table 2.2: Matter fields of the Standard Model, separated as quarks and leptons, and as left- and right-handed Weyl spinors. The isospin T_3 for the $SU(2)_L$ singlet fields is 0, for the upper component of the doublet we have $T_3 = +\frac{1}{2}$ and for the lower component we have $T_3 = -\frac{1}{2}$. Note that the triplet structure of the quarks is not explicitly written out, and that every quark family should be seen as transforming in 3-dimensional colour space.

Once the matter fields are determined, one is able to add their kinetic terms to the Lagrangian and attempt to construct a potential. Note, however, that for a mass term we must couple a left-handed fermion to a right-handed one, which would break the $SU(2)_L$ gauge invariance, so we are not yet able to explain the fermion masses. For a more detailed description of mass terms, see or Section 4.1.3. The full covariant derivative will couple a Weyl fermion to the gauge bosons belonging to the symmetry under which it is charged. Since the spinors in the Lagrangian are generally described by four-component spinors satisfying the Dirac equation, i.e. Dirac spinors, the Weyl fermions can be thought of as a four component spinor with only two entries[†].

[†] A Weyl fermion is conventionally introduced via projection operators: $\ell_{L,R} = P_{L,R}\ell$, with $P_{L,R} = \frac{1}{2}(1 \mp \gamma^5)$. Since a Weyl fermion transforms under the fundamental representation of the Lorentz group, however, this is slightly misleading, as it suggests that Dirac fermions are more fundamental.

The covariant derivatives then appear in the Lagrangian with leptons as

$$\mathcal{L}_2^{\text{leptons}} = \sum_{\text{families}} \left[i\bar{\ell}_L\gamma^\mu D_\mu \ell_L + i\bar{\ell}_R\gamma^\mu D_\mu \ell_R \right], \text{ with} \tag{2.1.7}$$

$$D_\mu \ell_L = \left(\partial_\mu - ig\frac{\sigma^i}{2} W_\mu^i - ig' Y_L B_\mu \right) \ell_L, \tag{2.1.8}$$

$$D_\mu \ell_R = \left(\partial_\mu - ig' Y_R B_\mu \right) \ell_R. \tag{2.1.9}$$

and for quarks as

$$\mathcal{L}_2^{\text{quarks}} = \sum_{\text{families}} \left[i\bar{q}_L\gamma^\mu D_\mu q_L + i\bar{p}_R\gamma^\mu D_\mu p_R + i\bar{n}_R\gamma^\mu D_\mu n_R \right], \text{ with} \tag{2.1.10}$$

$$D_\mu q_L = \left(\partial_\mu - ig_s\frac{\lambda^a}{2} G_\mu^a - ig\frac{\sigma^i}{2} W_\mu^i - ig' Y B_\mu \right) q_L, \tag{2.1.11}$$

$$D_\mu q_R = \left(\partial_\mu - ig_s\frac{\lambda^a}{2} G_\mu^a - ig' Y B_\mu \right) q_R, \tag{2.1.12}$$

with g_s, g and g' being the coupling constants of $SU(3)_c$, $SU(2)_L$ and $U(1)_Y$ respectively, and where the explicit labelling of the fermionic families with i is omitted. This now yields the gauge-invariant Lagrangian including fermions as

$$\begin{aligned} \mathcal{L}_{1+2} =& \mathcal{L}_1 + \mathcal{L}_2 \\ =& -\frac{1}{4} G_{\mu\nu}^a G^{a\,\mu\nu} - \frac{1}{4} W_{\mu\nu}^i W^{i\,\mu\nu} - \frac{1}{4} B_{\mu\nu} B^{\mu\nu} \\ &+ \sum_{\text{families}} \left[i\bar{q}_L\gamma^\mu D_\mu q_L + i\bar{u}_R\gamma^\mu D_\mu u_R + i\bar{d}_R\gamma^\mu D_\mu d_R \right. \\ &\qquad \left. + i\bar{\ell}_L\gamma^\mu D_\mu \ell_L + i\bar{\ell}_R\gamma^\mu D_\mu \ell_R \right]. \end{aligned} \tag{2.1.13}$$

The resulting Lagrangian describes the massless fermionic content of the Standard Model interacting with gauge fields via covariant derivatives, each defined according to the fermion's transformation properties under $SU(3)_c \times SU(2)_L \times U(1)_Y$. The chiral structure is made explicit: left-handed fermions transform non-trivially under $SU(2)_L$, while their right-handed counterparts are singlets, leading to distinct gauge couplings for each chiral sector. The absence of mass terms is a direct consequence of gauge symmetry and the irreducible chiral representations under which the matter fields transform. At this stage, the Lagrangian defines a fully consistent and gauge-invariant theory of massless fermions and gauge bosons.

2.2 Electroweak Symmetry Breaking

From a theoretical standpoint, the Standard Model Lagrangian built up to this point satisfies all the requirements of gauge invariance, renormalizability, and anomaly cancellation. Yet, it fails to account for the observed masses of the fermions, which cannot be added explicitly without breaking the gauge symmetry. From a modern perspective, this deficiency is not a flaw, but rather a signal that mass generation must occur through a dynamical mechanism compatible with the underlying gauge principles, called spontaneous symmetry breaking (SSB). The exact mechanism for SSB is the third determining classification of a modern gauge theory. Additionally, we have not yet found the symmetry that describes the electromagnetic interaction, $U(1)_{\text{em}}$, which means that we should either add it to our symmetry group or we should demonstrate that this symmetry already lies hidden in our current construction. Through the Higgs mechanism we will see that $U(1)_{\text{em}}$ is in fact a linear combination of $U(1)_Y$ and a $U(1)$ subgroup of $SU(2)_L$, which can already be guessed by realising the the electric charge Q is correctly described for all our particles as the combination

$$Q = T_3 + \frac{Y}{2}. \tag{2.2.1}$$

In the following section, we introduce the Higgs field and analyse how its vacuum state allows for the construction of gauge-invariant mass terms and the electromagnetic interaction.

2.2.1 The Higgs Mechanism

Spontaneous symmetry breaking is a mechanism that introduces a field to the system in such a way that it respects the gauge symmetries of the theory as written in the Lagrangian, but with a potential constructed in such a manner that its vacuum state no longer respects some of the symmetries. For every generator that corresponds to a transformation that no longer leaves the system invariant if the new field is in its vacuum state, we say that the generator is broken. In field theories with spontaneously broken *global* symmetries, the Goldstone theorem guarantees the appearance of massless scalar excitations, the so-called Goldstone bosons, corresponding to each broken generator, seemingly worsening the problem of the excess of massless particles. In gauge theories, on the other hand, these would-be Goldstone bosons are absorbed by the gauge fields via the Higgs mechanism, providing the degrees of freedom necessary for the gauge bosons to acquire mass. As a result, no new physical massless scalars appear in the spectrum. We shall see this process in detail for the gauge symmetries of the Standard Model.

In the electroweak case, we hope to obtain, from the full ELW gauge symmetry, a $U(1)$ group describing the electromagnetic interaction with charges described by equation 2.2.1. This is achieved through the addition of a Lorentz scalar Φ with an appropriate symmetry-breaking vacuum state, i.e.

$$SU(2)_L \times U(1)_Y \xrightarrow{\langle\Phi\rangle_0} U(1)_{\text{em}}. \tag{2.2.2}$$

Under $SU(2)_L$, Φ should transform as a doublet which has components

$$\Phi = \begin{pmatrix} \varphi_1 + i\varphi_2 \\ \varphi_3 + i\varphi_4 \end{pmatrix} \equiv \begin{pmatrix} \varphi^+ \\ \varphi^0 \end{pmatrix} \text{ and } Y(\Phi) = 1, \tag{2.2.3}$$

and thus with a covariant derivative

$$D_\mu \Phi = \left(\partial_\mu - ig\frac{\sigma^i}{2}W^i_\mu - ig'B_\mu\right)\Phi. \tag{2.2.4}$$

The Lagrangian obtains a scalar kinetic term and a potential term

$$\mathcal{L}_3 = (D_\mu\Phi)^\dagger(D_\mu\Phi) - V(\Phi), \tag{2.2.5}$$

and a Yukawa interaction term

$$\mathcal{L}_4 = M_e^{ij}\bar{\ell}^i_L\Phi\ell^j_R + M_p^{ij}\bar{q}^i_L\tilde{\Phi}p^j_R + M_n^{ij}\bar{q}^i_L\Phi n^j_R + \text{ h.c.}, \tag{2.2.6}$$

where $\tilde{\Phi} = i\sigma_2\Phi$ such that $Y(\tilde{\Phi}) = -1$, and M_f are matrices that describe the mixing among the various left- and right-handed Weyl fermions. So far, we have added, in a sense, a regular field, since we have not yet imposed any symmetry-breaking potential. To do so, the potential assigned to Φ can be given by

$$V(\Phi) = -\mu^2\Phi^\dagger\Phi + \lambda(\Phi^\dagger\Phi)^2, \tag{2.2.7}$$

with μ^2 and λ are taken as positive, which is minimized for

$$\langle \Phi^\dagger \Phi \rangle_0 = \langle |\varphi^+|^2 + |\varphi^0|^2 \rangle_0 = \frac{v^2}{2}, \text{ with } v \equiv \left(\frac{\mu^2}{\lambda}\right)^{\frac{1}{2}}. \tag{2.2.8}$$

As can be seen from equation 2.2.3, Φ contains two complex fields, corresponding to four real degrees of freedom. A non-zero vacuum expectation value (VEV) can be assigned to a specific component of Φ, thereby selecting a particular vacuum configuration. Although the Higgs potential is symmetric under $SU(2)_L$ rotations, the specific choice of a vacuum configuration is not: applying an $SU(2)_L$ rotation to the vacuum transforms it into a physically distinct state. Thus, while the form of the theory remains symmetric, the vacuum breaks the symmetry spontaneously, marking a fundamental difference between the invariance of the potential and the invariance of the chosen field configuration. In order to find out which configuration may occur in nature, we make use of equation 2.2.1 and the fact that $U(1)_{\text{em}}$ remains unbroken. For the upper and lower components of the doublet, we find respectively that

$$Q_{\varphi^+} = T_{3\varphi^+} + \frac{1}{2} Y_{\varphi^+} = +\frac{1}{2} + \frac{1}{2} = 1, \text{ and} \tag{2.2.9}$$

$$Q_{\varphi^0} = T_{3\varphi^0} + \frac{1}{2} Y_{\varphi^0} = -\frac{1}{2} + \frac{1}{2} = 0. \tag{2.2.10}$$

In order to preserve the electromagnetic charge after symmetry breaking, we must have a neutral vacuum state, which implies that the non-zero VEV must be acquired by the lower component, i.e.,

$$\langle \Phi \rangle_0 = \langle 0 | \Phi | 0 \rangle = \begin{pmatrix} 0 \\ \frac{v}{\sqrt{2}} \end{pmatrix}. \tag{2.2.11}$$

We can rewrite Φ as an expansion of zero-VEV fields around its vacuum,

$$\Phi(x) = \frac{1}{\sqrt{2}} \begin{pmatrix} \theta_1(x) + i\theta_2(x) \\ v + h(x) - i\theta_3(x) \end{pmatrix}, \tag{2.2.12}$$

which for arbitrarily small θ_i can be parametrized as

$$\Phi(x) = \exp\{i\theta_i(x)\sigma^i/v\} \begin{pmatrix} 0 \\ \frac{1}{\sqrt{2}}(v + h(x)) \end{pmatrix}. \tag{2.2.13}$$

Written as the exponentiation of the Pauli matrices, it is clear to see that the parametrization has the same structure as an $SU(2)$-transformation. We can use this to apply, at the Lagrangian level, a gauge transformation to the fields such that

$$\Phi(x) \to \Phi'(x) = U\Phi(x) \tag{2.2.14}$$

$$\equiv \exp\{-i\theta_i(x)\sigma^i/v\}\Phi(x) \tag{2.2.15}$$

$$= \frac{1}{\sqrt{2}} \begin{pmatrix} 0 \\ v + h(x) \end{pmatrix} \tag{2.2.16}$$

$$\equiv \frac{v + h(x)}{\sqrt{2}}\chi, \text{ with } \chi = \begin{pmatrix} 0 \\ 1 \end{pmatrix}. \tag{2.2.17}$$

This gauge is called the *unitary gauge*. The d.o.f. from θ_i are rotated away, and only the VEV and a scalar boson $h(x)$ - the Higgs boson - remains. The fields in this gauge will be denoted as primed, with the remaining fields transforming into Spontaneous symmetry breaking occurs when $\Phi'(x)$ transitions from a symmetric

$$\begin{gathered}
\ell'_L = U(\theta)\ell_L \quad \ell'_R = \ell_R \\
q'_L = U(\theta)q_L \quad p'_R = p_R \quad n'_R = n_R \\
\tfrac{\sigma\cdot W_\mu}{2} \to U(\theta)\left(\tfrac{\sigma\cdot W_\mu}{2}\right)U^{-1}(\theta) - \tfrac{i}{g}[\partial_\mu U(\theta)]U^{-1}(\theta) \\
B'_\mu = B_\mu
\end{gathered}$$

Table 2.3: Redefinitions of chiral fields and vector bosons into the unitary gauge, denoted by a prime.

excited state to its vacuum state. Once the state is in its vacuum configuration one can expand the Lagrangian in terms of v and $h(x)$. In particular, one can rewrite equations 2.2.5 and 2.2.6 as

$$\begin{aligned}
\mathcal{L}_3 =& \frac{(v+h(x))^2}{2}\chi^\dagger\left(\frac{g}{2}\sigma\cdot W'_\mu + \frac{g'}{2}B'_\mu\right)\left(\frac{g}{2}\sigma\cdot W'^\mu + \frac{g'}{2}B'^\mu\right)\chi \qquad (2.2.18)\\
& - \mu^2 h^2 - \lambda v h^3 - \frac{\lambda}{4}h^4 \\
\mathcal{L}_4 =& \frac{v+h(x)}{\sqrt{2}}\left(M_e^{ij}\overline{e}'^i_L\ell'^j_R + M_p^{ij}\overline{p}'^i_L p'^j_R + M_n^{ij}\overline{n}'^i_L n'^j_R + \text{ h.c.}\right). \qquad (2.2.19)
\end{aligned}$$

2.2.2 VECTOR BOSON MASSES

The net effect of the asymmetry of the vacuum state of Φ is that the vector bosons couple to its VEV, replicating the structure of a mass term. To see this we are only to consider the bosonic terms from equation 2.2.18 which are proportional to v^2:

$$\begin{aligned}
\mathcal{L}_3 \supset& \frac{v^2}{2}\chi^\dagger\left(\frac{g}{2}\sigma\cdot W'_\mu + \frac{g'}{2}B'_\mu\right)\left(\frac{g}{2}\sigma\cdot W'^\mu + \frac{g'}{2}B'^\mu\right)\chi \qquad (2.2.20)\\
=& \frac{v^2}{8}\left(g^2[(W'^1_\mu)^2 + (W'^2_\mu)^2] + (gW'^3_\mu - g'B'_\mu)^2\right) \qquad (2.2.21)\\
\equiv& M_W^2 W^+_\mu W^{-\mu} + \frac{1}{2}M_Z^2 Z_\mu Z^\mu. \qquad (2.2.22)
\end{aligned}$$

Here we have defined $W^\pm_\mu \equiv (W'^1_\mu \mp iW'^2_\mu)/\sqrt{2}$ and $M_W^2 = g^2v^2/4$. The Z-boson is defined as a linear combination of W'^3_μ and B'_μ derived from the diagonalisation of the mass matrix in

$$\begin{aligned}
\frac{1}{2}M_Z^2 Z_\mu Z^\mu &= \frac{v^2}{8}(gW'^3_\mu - g'B'_\mu)^2 \qquad (2.2.23)\\
&= \frac{v^2}{8}\begin{pmatrix} W'^3_\mu & B'_\mu \end{pmatrix}\begin{pmatrix} g^2 & -gg' \\ -gg' & g'^2 \end{pmatrix}\begin{pmatrix} W'^{3\mu} \\ B'^\mu \end{pmatrix} \qquad (2.2.24)\\
&\equiv \frac{1}{2}\begin{pmatrix} Z_\mu & A_\mu \end{pmatrix}\begin{pmatrix} M_Z^2 & 0 \\ 0 & 0 \end{pmatrix}\begin{pmatrix} Z^\mu \\ A^\mu \end{pmatrix}, \qquad (2.2.25)
\end{aligned}$$

leading to a mass $M_Z^2 = v^2(g^2 + g'^2)/4$. The orthogonal transformation characterising the diagonalisation is, in terms of the Weinberg angle $\tan\theta_W = \frac{g'}{g}$, given by

$$Z_\mu = \cos\theta_W W'^3_\mu - \sin\theta_W B'_\mu, \tag{2.2.26}$$

$$A_\mu = \sin\theta_W W'^3_\mu + \cos\theta_W B'_\mu. \tag{2.2.27}$$

To summarise, one sees that the asymmetry of the vacuum state of the doublet Φ has led to mass terms of the electroweak bosons. The four d.o.f. present in Φ have been removed and redistributed amongst three originally massless vector bosons as longitudinal components, and one remaining scalar field $h(x)$. The manifestation of these d.o.f. as mass terms becomes clear in the unitary gauge, after explicitly expanding the terms as done above. Although other gauge choices retain the Goldstone fields explicitly, physical predictions remain unchanged, and observable quantities such as vector boson masses are gauge-independent. The emergence of a mass term proportional to a specific linear combination of the original vector bosons W^1_μ and W^2_μ defines a new basis, namely their mass basis. These mass eigenstates $W^\pm$ no longer align with the original gauge basis, so it will be useful to rephrase the ELW covariant derivative of equation 2.1.8 accordingly and express it in terms of $W^\pm_\mu$, Z_μ, and A_μ. This rephrasing will illuminate the charged current, previously described by $V - A$ theory, and introduce an additional neutral current. Using the correct charges from the various fermions of table 2.2, we see the interaction terms from the covariant derivative to be described by

$$\begin{aligned}
\bar{f}_{L,R} i\not{D} f_{L,R} \supset & \sum_{\text{families}} \bar{\ell}'_L \left(\frac{g}{2}\sigma^i \not{W}'^i - i\frac{g'}{2}\not{B}' \right) \ell'_L - \bar{q}'_L \left(\frac{g}{2}\sigma^i \not{W}'^i + \frac{g'}{6}\not{B}' \right) q'_R \\
& - \bar{l}'_R g' \not{B}' l'_R + \bar{p}'_R \frac{2g'}{3} \not{B}' p'_R - \bar{n}'_R \frac{g'}{3} \not{B}' n'_R \\
= & \sum_{\text{families}} \frac{g}{2} \left(\bar{\ell}'_L \sigma^i \gamma_\mu \ell'_L + \bar{q}'_L \sigma^i \gamma_\mu q'_L \right) W'^{i\mu} \\
& + \frac{g}{2} \left(-\bar{\ell}'_L \gamma_\mu \ell'_L + \frac{1}{3} \bar{q}'_L \gamma_\mu q'_L - 2\bar{\ell}'_R \gamma_\mu \ell'_R + \frac{4}{3} \bar{p}'_R \gamma_\mu p'_R + \bar{n}'_R \gamma_\mu n'_R \right) B'_\mu \\
\equiv & \sum_{\text{families}} (g J^1_\mu W^{1\prime\mu} + g J^2_\mu W^{2\prime\mu}) + (g J^3_\mu W^{3\prime\mu} + \frac{1}{2} g' J^Y_\mu B'^\mu) \\
= & \sum_{\text{families}} \frac{g}{\sqrt{2}} \left(J^+_\mu W^{+\mu} + J^-_\mu W^{-\mu} \right) + \left(e J^{\text{em}}_\mu A^\mu + \frac{g}{\cos\theta_W} J^0_\mu Z^\mu \right) \\
\equiv & \mathcal{L}_{\text{CC}} + \mathcal{L}_{\text{NC}},
\end{aligned} \tag{2.2.28}$$

with $e = g\sin\theta_W$, and where we define the various currents as

$$J^i_\mu = \sum_{f=\ell',q'} \bar{f}_L \frac{\sigma^i}{2} \gamma_\mu f_L, \tag{2.2.29}$$

$$J^Y_\mu = \sum_{f=\ell',q'} \bar{f}_L \gamma_\mu Y_f f_L + \sum_{f=\ell,p,n} \bar{f}_R \gamma_\mu Y_f f_R, \tag{2.2.30}$$

$$J^\pm = J^1_\mu \pm J^2_\mu, \tag{2.2.31}$$

$$J^{\text{em}}_\mu = J^3_\mu + \frac{1}{2} J^Y_\mu, \tag{2.2.32}$$

$$J^0_\mu = J^3_\mu - \sin^2\theta_W J^{\text{em}}_\mu . \tag{2.2.33}$$

One can see that in the new basis the $W^{\pm}$-bosons only couple to the charged currents $J^{\pm}$, and since $J^{\pm}$ consist only of left-chiral fermions this implies that the charged current maximally violates parity, as was described before by current-current interactions in V-A theory. This can now be understood as a low-energy effective description of the charged current, namely, after integrating out the $W^{\pm}$ bosons, we get

$$\mathcal{L}_{\mathrm{CC}}^{\mathrm{eff}} = \frac{-g^2}{2M_W^2} J_\mu^+ J^{-\mu}. \tag{2.2.34}$$

Also in the new basis, the current proportional to A^μ is found to be in accordance with equation 2.2.1. Aside from J^{em}, we then see the appearance of J^0 as a neutral current, coupled to Z^μ. Just a in the charged current we can integrate out the heavy $Z-$boson from the system to find a low-energy effective description of the current, namely

$$\mathcal{L}_{\mathrm{NC}}^{\mathrm{eff}} = \frac{-g^2}{2\cos^2\theta_W M_Z^2} J_\mu^0 J^{0\mu} = \frac{-g^2}{2M_W^2} J_\mu^0 J^{0\mu}. \tag{2.2.35}$$

The experimental confirmation of this current by the Gargamelle collaboration in 1973 provided one of the first direct evidences for neutral currents through the observation of neutrino-induced reactions without accompanying charged leptons [Has+73a; Has+73b; Has+74], and was considered amongst the strongest evidence for the SM.

2.2.3 Fermion Masses

From the Yukawa sector of the Lagrangian, equation 2.2.19, we see that the VEV of the doublet component φ^0 effectively acts as a mass term for the fermions. If there were one family of fermions, the Yukawa sector would look like

$$\mathcal{L}_{v-\mathrm{fermion}} = \frac{v}{2}[y_e \bar{e}'_L e'_R + y_u \bar{u}'_L u'_R + y_d \bar{d}'_L d'_R], \tag{2.2.36}$$

where the Yukawa couplings y_f determine the masses of the various fermions. Note then that the fermions are written in the basis used to describe their NC and CC interaction, so we say that the mass eigenstates correspond to the weak eigenstates. In reality, however, there are three families of fermions, which generalise the Lagrangian to

$$\mathcal{L}_{v-\mathrm{fermion}} = \frac{v}{\sqrt{2}}[\bar{\ell}'^i_L M_e^{ij} l'^j_R + \bar{p}'^i_L M_p^{ij} p'^j_R + \bar{n}'^i_L M_n^{ij} n'^j_R], \tag{2.2.37}$$

where now the Yukawa couplings become (3×3)-matrices which are in general neither diagonal, symmetric, nor even hermitian. A consequence is that terms like $M_e^{12} \bar{e}'_L \mu'_R$ are generally present, mixing the various weak eigenstates. One important fact to consider, though, is that the weak interaction does not distinguish the various fermionic families, i.e., it transforms the families of fermionic doublets in a similar way. So one can redefine, for example, the leptonic $SU(2)_L$ doublets to be linear combinations of the old weak basis in such a way that it matches the mass basis of the charged leptons. For quarks, this becomes more ambiguous, since due to the generality of M_p^{ij} and M_d^{ij}, the mass bases of the positively and negatively charged quarks in terms of the original weak basis can be different. We will mathematically formalise the implications of the mass terms for leptons in the next few paragraphs, and then dedicate more time to studying the case for quarks separately in the next section.

A general matrix M^{ij} can be diagonalized by bi-unitary transformations, meaning that for a given mass matrix M we have unitary matrices S and T such that

$$S^\dagger M T = M_{\mathrm{d}}, \tag{2.2.38}$$

with M_d a diagonal matrix. Applying this to our Lagrangian, we can rewrite the mass matrix for the leptons as

$$\bar{e}'^i_L M^{ij}_e \ell'^j_R = (\bar{e}'_L S)^i (S^\dagger M T)^{ij} (T^\dagger \ell'_R)^j \tag{2.2.39}$$
$$= \bar{e}^i_L M^{ij}_d \ell^j_R \tag{2.2.40}$$

with

$$e'^i_L = S^{ij} e^j_L \tag{2.2.41}$$
$$\ell'^i_R = T^{ij} \ell^j_R. \tag{2.2.42}$$

This new unprimed basis describes the fermions in terms of their mass eigenstates, so as they propagate, while the primed basis forms the weak eigenstates through which they rotate in gauge space. To see whether the choice of the new basis has any implications for our gauge interactions, we consider the leptonic charged current

$$J^+_{\ell\mu} = \bar{\ell}^i_L \gamma_\mu \tau^+ \ell^i_L \tag{2.2.43}$$
$$= \bar{\nu}'^i_L \gamma_\mu e'^i_L \tag{2.2.44}$$
$$= \bar{\nu}^i_L (S^\dagger_{(\nu)} S_{(e)})^{ij} \gamma_\mu e^j_B, \tag{2.2.45}$$

where τ^+ is the raising operator in $SU(2)_L$ space, and $S_{(\nu)}$ and $S_{(e)}$ denote the basis transformation matrices of equation 2.2.41 for left-handed neutrinos and charged leptons respectively. It is clear to see that any modification of the charged current is encoded in the matrix $V^{ij} \equiv (S^\dagger_{(\nu)} S_{(e)})^{ij}$. Since neutrinos are massless, however, the choice for $S_{(\nu)}$ is arbitrary, and we can choose it in such a way that $V = \mathbb{I}$, leaving the charged current unchanged in the new basis. Due to the unitarity of $S_{(e)}$ it is easy to see that this holds trivially for the neutral current, of which the consequences will be discussed in section 2.3.3.

2.3 Flavour Structure and Mixing

For quarks, the treatment of the charged current in the mass basis is not as straightforward as for leptons, due to the presence of a right-handed counterpart for both components of the q_L doublets. We will redo the derivation of the previous section to demonstrate the difference and discuss some important related concepts.

2.3.1 Quark Flavour Mixing

If we apply the basis transformation equivalent to equation 2.2.41 to the quarks,

$$q'_L = S q_L \tag{2.3.1}$$
$$q'_R = T q_R \tag{2.3.2}$$

we obtain the quarkic charged current

$$
\begin{aligned}
J^{+}_{(q)\mu} &= \bar{q}'^{i}_{L}\gamma_{\mu}\tau^{+}q'^{i}_{L} && (2.3.3)\\
&= \bar{p}'^{i}_{L}\gamma_{\mu}n'^{i}_{L} && (2.3.4)\\
&= \bar{p}^{i}_{L}\gamma_{\mu}(S^{\dagger}_{(p)}S_{(n)})^{ij}n^{j}_{L} && (2.3.5)\\
&\equiv \bar{p}^{i}_{L}\gamma_{\mu}U^{ij}n^{j}_{L}, && (2.3.6)
\end{aligned}
$$

where $U \equiv U_{\text{CKM}} = (S^{\dagger}_{(p)}S_{(n)})$ is called the Cabibbo–Kobayashi–Maskawa matrix, or CKM matrix for short, which describes in essence the misalignment between the two mass bases. Since both the positive and negative quarks have mass terms (in contrast to the charged vs neutral leptons), both $S_{(p)}$ and $S_{(n)}$ are unitary matrices derived from diagonalizing different arbitrary matrices M_p and M_n respectively. The lack of restriction imposed on the latter two matrices implies that we can say little *a priori* about the structure of U other than that it is the product of two unitary matrices. In particular, there is no reason this matrix should be unity, like in the leptonic sector. Defining a new basis for the negative quarks as

$$
\begin{pmatrix} d'' \\ s'' \\ b'' \end{pmatrix} = U \begin{pmatrix} d \\ s \\ b \end{pmatrix} \tag{2.3.7}
$$

we can construct the quark doublets as

$$
q^{i}_{L} : \begin{pmatrix} u \\ d'' \end{pmatrix}_{L} \begin{pmatrix} c \\ s'' \end{pmatrix}_{L} \begin{pmatrix} t \\ b'' \end{pmatrix}_{L}. \tag{2.3.8}
$$

Since $d'' = U_{11}d + U_{12}s + U_{13}b$ we can clearly see that a mixing of the various mass eigenstates takes place whenever an $SU(2)$ rotation occurs. The charged current for, for example, the up quark will thus look like

$$
\begin{aligned}
J^{+}_{(u)\mu} &= \bar{u}'_{L}\gamma_{\mu}d'_{L} && (2.3.9)\\
&= \bar{u}_{L}\gamma_{\mu}d''_{L} && (2.3.10)\\
&= \bar{u}_{L}\gamma_{\mu}(U_{11}d_{L} + U_{12}s_{L} + U_{13}b_{L}). && (2.3.11)
\end{aligned}
$$

If we want to understand the amount of mixing between the various mass eigenstates, we require information on U. The coefficients are determined by experiment and not by theory, but we can attempt to parametrize the matrix to understand its components better. A general complex (3×3)—matrix contains 9 components of the form $U_{ij} = R_{ij}e^{i\delta_{ij}}$, and thus is determined by 18 parameters. We can remove some of these parameters by redefinitions of the quark fields, however. By redefining, for example, the positively charged quark fields by the complex phase δ_{11}, we obtain

$$
q^{1}_{L} = \begin{pmatrix} u_{L} \\ U_{11}d_{L} + U_{12}s_{L} + U_{13}b_{L} \end{pmatrix} \rightarrow e^{-i\delta_{11}}q^{1}_{L} = \begin{pmatrix} u'_{L} \\ R_{11}d_{L} + U'_{12}s_{L} + U'_{13}b_{L} \end{pmatrix},
$$

and through δ_{21} and δ_{31} similarly for c_L and t_L. By redefinition of the s and b fields we can then also remove two more phases, say δ_{12} and δ_{13}. The resulting structure of the doublets is then

$$
\begin{pmatrix} u' \\ R_{11}d + R_{12}s' + R_{13}b' \end{pmatrix}_{L}; \begin{pmatrix} c' \\ R_{21}d + R_{22}e^{i\delta_{1}}s' + R_{23}e^{i\delta_{2}}b' \end{pmatrix}_{L};
$$

$$\begin{pmatrix} t' \\ R_{31}d + R_{32}e^{i\delta_3}s' + R_{33}e^{i\delta_4}b' \end{pmatrix} . \tag{2.3.12}$$

If we apply an overall phase, we leave U invariant, since only relative phases affect the structure of $S^{\dagger}_{(p)}S_{(n)}$. This means, in particular, that we can only absorb 5 phases using 6 quark fields. Additionally, since we require quark masses to be real, we must transform left- and right-handed fields by the same phase, so also in terms of chirality we have exhausted our field redefinition abilities. The net result is that we are left with 13 parameters: 9 R_{ij}s and 4 δ_is. Due to the unitarity condition $U^{\dagger}U = UU^{\dagger} = \mathbb{I}$, however, we should still be able to impose more restrictions.

The restriction coming from the unitarity condition are generally classified as three normalization conditions, $\sum\limits_{j} |V_{ij}|^2$ for $i = 1, 2, 3$, and six orthogonality conditions, $\sum\limits_{j}^{i \neq k} V^{*}_{ji}V_{jk} = 0$, for $i, k = 1, 2, 3$. These restrictions bring our final number of parameters to four, of which three are needed to form a real 3×3 orthogonal matrix, thus leaving only one independent complex phase. The explicit parametrization can be done in many ways, but one of the standard choices takes the form

$$U_{\text{CKM}} = \begin{pmatrix} 1 & 0 & 0 \\ 0 & c_{23} & s_{23} \\ 0 & -s_{23} & c_{23} \end{pmatrix} \begin{pmatrix} c_{13} & 0 & s_{13}e^{-i\delta} \\ 0 & 1 & 0 \\ -s_{13}e^{i\delta} & 0 & c_{13} \end{pmatrix} \begin{pmatrix} c_{12} & s_{12} & 0 \\ -s_{12} & c_{12} & 0 \\ 0 & 0 & 1 \end{pmatrix} \tag{2.3.13}$$

$$= \begin{pmatrix} c_{12}c_{13} & s_{12}c_{13} & s_{13}e^{-i\delta} \\ -s_{12}c_{23} - c_{12}s_{23}s_{13}e^{i\delta} & c_{12}c_{23} - s_{12}s_{23}s_{13}e^{i\delta} & s_{23}c_{13} \\ s_{12}s_{23} - c_{12}c_{23}s_{13}e^{i\delta} & -c_{12}s_{23} - s_{12}c_{23}s_{13}e^{i\delta} & c_{23}c_{13} \end{pmatrix}, \tag{2.3.14}$$

where $s_{ij} = \sin\theta_{ij}$, $c_{ij} = \cos\theta_{ij}$, and $\delta \equiv \delta_{\text{CKM}}$ is the complex phase. For an overview of modern bounds on these parameters, consider consulting the Particle Data Group review [Wor+22a].

2.3.2 CP VIOLATION

The complex phase δ in the CKM matrix has severe consequences for the discrete symmetries in the Standard Model, as it allows for CP violation in the quark sector. This is made clear by explicitly computing the CP transformation of the charged current. The individual doublets transform as

$$\bar{p}_L \xrightarrow{\text{CP}} -p_L^T\mathcal{C}^{-1}\gamma^0 D^{\dagger}(\vec{\xi}_p) \tag{2.3.15}$$

$$\bar{n}_L \xrightarrow{\text{CP}} D(\vec{\xi}_n)\gamma^0\mathcal{C}\bar{n}_L^T, \tag{2.3.16}$$

where $D(\vec{\xi}_p)$ and $D(\vec{\xi}_n)$ are unspecified diagonal matrices describing CP phases of the quark fields, with $\vec{\xi}_p = (\xi_u, \xi_c, \xi_t)$ and $\vec{\xi}_n = (\xi_d, \xi_s, \xi_b)$. Using these expression one finds the current to transform as

$$J^{+\mu}_{(q)} \xrightarrow{\text{CP}} -p_L^T\mathcal{C}^{-1}\gamma^0\gamma^{\mu}\gamma^0\mathcal{C}D^{\dagger}(\vec{\xi}_p)U_{\text{CKM}}D(\vec{\xi}_n)\bar{n}_L^T \tag{2.3.17}$$

$$= -p_L^T(-\gamma^{\mu *})D^{\dagger}(\vec{\xi}_p)U_{\text{CKM}}D(\vec{\xi}_n)\bar{n}_L^T \tag{2.3.18}$$

$$= -\bar{n}_L^T\gamma^{\mu\dagger}D(\vec{\xi}_n)U_{\text{CKM}}D^{\dagger}(\vec{\xi}_p)p_L^T \tag{2.3.19}$$

$$= -\bar{n}_L^T D(\vec{\xi}_n)U_{\text{CKM}}D^{\dagger}(\vec{\xi}_p)\gamma_{\mu}p_L^T. \tag{2.3.20}$$

The $W-$boson transforms as

$$W_\mu \xrightarrow{\text{CP}} e^{i\xi_W} W^{\mu\dagger}, \tag{2.3.21}$$

where ξ_W is again an undetermined CP phase. All together, this leads the transformation of the charged current interaction term as

$$J^{+\mu}_{(q)} W_\mu \xrightarrow{\text{CP}} e^{i\xi_W} \bar{n}_L D(\vec{\xi}_n) U^T D^\dagger(\vec{\xi}_p) \gamma^\mu p_L W^{\mu\dagger}. \tag{2.3.22}$$

Since the Lagrangian contains also the hermitian conjugate of charged current interaction, we can compare this with the transformation

$$\begin{aligned} \left(J^{+\mu}_{(q)} W_\mu\right)^\dagger &= W^\dagger_\mu J^{+\mu\dagger}_{(q)} \\ &= W^\dagger_\mu n^\dagger_L U^\dagger \gamma^0 \gamma^\mu \cancel{\gamma^0 \gamma^{0\dagger}} p_L \\ &= \bar{n}_L U^\dagger \gamma_\mu p_L W^{\mu\dagger}, \end{aligned} \tag{2.3.23}$$

where we used that $\gamma^\mu W_\mu = \gamma_\mu W^\mu$. We see that the transformations 2.3.17 and 2.3.23 look fairly similar, and are in fact equal if we require

$$-e^{i\xi_W} D(\vec{\xi}_n) U^T D^\dagger(\vec{\xi}_p) = U^\dagger. \tag{2.3.24}$$

If we choose $\xi_W = \pi$ and manipulate the expression slightly further (for a full step-by-step derivation see [GK07], page 121) we find that this equation holds if and only if the complex phase is zero, i.e.

$$U = U^* \iff \text{CP symmetry}. \tag{2.3.25}$$

So if the phase of the CKM matrix is non-zero, we necessarily obtain CP-violating processes in the weak interaction, and if we measure only CP symmetric processes, we must have that $\delta_{\text{CKM}} = 0$. As mentioned, there are many different ways to parametrize the CKM matrix and thus there are many different ways to rephrase the condition $\delta_{\text{CKM}} = 0$. One question that does not depend on the explicit parametrization, however, is how this condition takes form in the mass matrices M_p^{ij} and M_n^{ij} from which the mixing matrix is derived. It can be shown that in order to obtain CP violation, the quarks must satisfy 14 conditions [GK07]:

1-6 No pair of positively charged quarks or negatively charged quarks have the same mass.

7-12 No mixing angle equals either 0 or $\frac{\pi}{2}$.

13, 14 The physical phase is neither 0 nor π.

Although it seems like conditions 13 and 14 are enough to require that U_{CKM} is real, the degeneracy of quark masses intuitively introduces another symmetry, allowing for the absorption of one more phase. One can rewrite all 14 conditions into one condition [Eid+04],

$$\det C \neq 0, \tag{2.3.26}$$

with C defined as the commutator of the original mass matrices appearing in the Yukawa sector, $C = -i[M_p M_p^\dagger, M_n M_n^\dagger]$. In terms of the quark masses and the elements of the CKM matrix, this can be expressed as

$$\det C = -2J(m_c^2 - m_u^2)(m_t^2 - m_u^2)(m_t^2 - m_c^2) \tag{2.3.27}$$

$$(m_s^2 - m_d^2)(m_b^2 - m_d^2)(m_b^2 - m_s^2), \tag{2.3.28}$$

where

$$J = \mathfrak{Im}[U_{us}U_{cv}U^*_{ub}U^*_{cs}] \tag{2.3.29}$$

is the Jarlskog invariant. The attractive aspect of this formulation is that the Jarlskog invariant is a parameter-independent formulation, i.e. it is invariant under reparametrizations of U_{CKM} or phase transformations of the quark fields. Such quartic products are in general called *rephasing invariants*, and they are measurable quantities. In this case [Eid+04], $J = (2.88 \pm 0.33) \times 10^{-5}$.

2.3.3 Flavour Changing Neutral Currents

An important argument in favour of the Standard Model is the natural suppression of flavour changing neutral currents (FCNC). FCNCs are processes in which a fermion changes flavour without changing its electric charge (or isospin), mediated by a neutral boson such as Z^0_μ. Historically, there was no understanding as to why their corresponding decays, like $K^0_S \to \mu^+\mu^-$ from Figure 2.3.1, are suppressed so much with respect to the non-leptonic decays, like $K^0_S \to \pi^0\pi^0$. The explanation is presented in the Glashow-Illiopoulos-Maiani (GIM) mechanism [GIM70], which predicted (even more, required) the existence of the charm quark c_L which should form the $T_3 = \frac{1}{2}$ component of an $SU(2)_L$ doublet with s_L, analogous to the $(u, d)_L$ doublet. In modern terms, this mechanism is embedded in the electroweak gauge theory, and the suppression of FCNCs is directly understood from the structure of the Lagrangian. We have found c_L, and all fermions with similar charge and helicity should transform identically under $SU(2)_L \times U(1)_Y$, which means that the Z boson can not mix the various mass eigenstates.

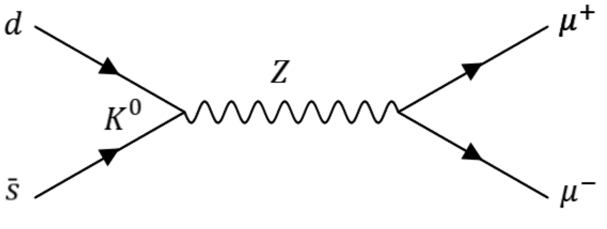

Figure 2.3.1: Feynman diagram of hypothetical K^0-decay. K^0_S is a superposition of states, $K^0_S = \frac{d\bar{s}-s\bar{d}}{\sqrt{2}}$.

The current bound on the branching ratio of muonic K^0_S decays lies around 10^{-9} [Aai+17]. As mentioned, this suppression requires the presence of the charm quark, which we will demonstrate at tree-level and at first order. As for tree-level FCNCs, we can explicitly repeat the exercise in equation 2.3.5 for the neutral current, starting from a weak eigenstate basis, which leads to

$$\begin{aligned} J^0_{(q_L)\mu} &= \bar{q}'^i_L\gamma_\mu\left(\frac{\sigma^3}{3} - \sin^2\theta_W Q\right)q'^i_L \\ &= \bar{q}^i_L(S^\dagger_{(q)})^{ik}\gamma_\mu\left(\frac{\sigma^3}{2} - \sin^2\theta_W Q\right)(S_{(q)})^{kj}q^j_L \\ &= \bar{q}^i_L\gamma_\mu\left((S^\dagger_{(q)}\frac{\sigma^3}{2}S_{(q)})^{ij} - \sin^2\theta_W(S^\dagger_{(q)}QS_{(q)})^{ij}\right)q^j_L \\ &= \delta_{ij}\bar{q}^i_L\gamma_\mu\left(\frac{\sigma^3}{2} - \sin^2\theta_W Q\right)q^j_L, \end{aligned} \tag{2.3.30}$$

and

$$\begin{aligned} J^0_{(q_R)\mu} &= \bar{q}'^i_R \gamma_\mu \left(-\sin^2\theta_W Q\right) q'^i_R \\ &= \bar{q}^i_R (S^\dagger_{(q_R)})^{ik} \gamma_\mu \left(-\sin^2\theta_W Q\right) (S_{(q_R)})^{kj} q^j_R \\ &= \bar{q}^i_R \gamma_\mu \left(-\sin^2\theta_W (S^\dagger_{(q_R)} Q S_{(q_R)})^{ij}\right) q^j_R \\ &= \delta_{ij} \bar{q}^i_R \gamma_\mu \left(-\sin^2\theta_W Q\right) q^j_R, \end{aligned} \tag{2.3.31}$$

in which the basis transformation matrices cancel to produce Kronecker deltas and thus do not induce mixing. FCNCs are therefore predicted to be absent at tree-level. At second order, effective flavour-changing neutral currents are possible through two charged currents, so box diagrams of the form

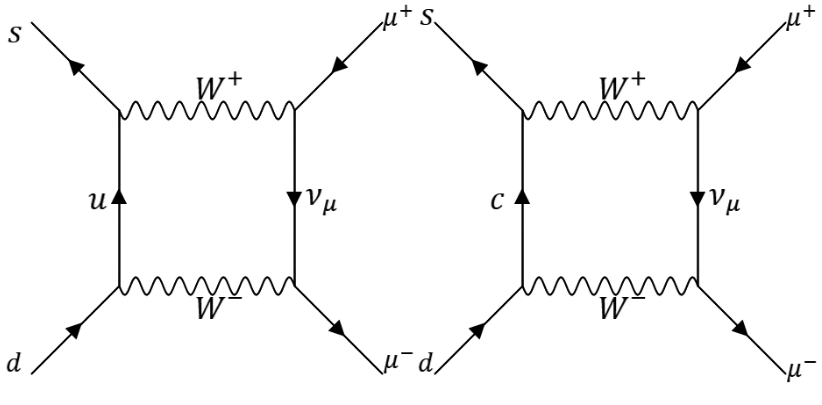

Figure 2.3.2: Box diagrams contributing to flavour-changing neutral currents (FCNCs) at second order.

can arise. If one were to explicitly calculate out the diagram for only a strange quark, one would find the branching ratios to be proportional to

$$\mathcal{M}(K^0_S \to \mu^-\mu^+) \sim G_F^2 M_W^2 \tag{2.3.32}$$

$$\mathcal{M}(K^0_S \to \pi^0\pi^0) \sim G_F, \tag{2.3.33}$$

which is in contradiction with the relative 10^{-9} order suppression of the muonic decay. If one adds the charm quark to the calculation, however, a cancellation occurs. The loop amplitudes involving the up quark and charm quark contributions appear with opposite sign due to the orthogonality of the quark mixing matrix, removing the dependence on M_W^2. The amplitudes take the form

$$\mathcal{M}(K^0_S \to \mu^-\mu^+) \sim G_F^2 (m_c^2 - m_u^2), \tag{2.3.34}$$

which is greatly suppressed with respect to the amplitude in equation 2.3.32, and which predicts the current bound if loop factor and other suppressions are taken into account [Aai+17]. This shows, therefore, that the introduction of the $c-$quark and the orthogonality of the CKM matrix guarantee the suppression of the decay. Even more, an effective FCNC at second order through the charged current is only present if the difference in mass between the quarks is non-zero. This means that the mass difference of the quarks can be inferred from the branching ratios.

This suppression mechanism is not only relevant for rare kaon decays such as $K^0_S \to \mu^+\mu^-$, but also plays an important role in understanding neutral kaon mixing. The transition $K^0 \leftrightarrow \bar{K}^0$, a $\Delta S = 2$ flavor-changing process, arises at second order in the weak interaction and proceeds via box diagrams involving internal up-type quarks and W bosons. The amplitude suppression is similar: in a model with only three light quarks, the resulting amplitude would scale with $G_F^2 M_W^2$ and be many orders of magnitude larger than observed. However, with the inclusion of the charm quark, just like in the case of leptonic decay, the leading contribution cancels in the limit $m_c = m_u$, and the amplitude becomes proportional to $G_F^2(m_c^2 - m_u^2)$.

This suppression is not only theoretically satisfying, it is also practically essential: because the mixing amplitude is small and under good theoretical understanding, it becomes possible to extract smaller effects, like those coming from CP violation. In particular, the interference between mixing and decay amplitudes in the neutral kaon system allows for the measurement of indirect CP violation. The smallness of the FCNC background ensures that this CP-violating contribution is not overruled by larger flavour-conserving or tree-level effects.

2.4 PROBLEMS IN THE STANDARD MODEL

The acceptance of the Standard Model has been the result of many celebrated experimental confirmations, its most notable successes being probably the accurate prediction [Wei67] and subsequent discovery of the W and Z bosons [UA183], the top and charm quarks [CDF95; BNL74], and more recently the Higgs boson [Aad+12]. It has withstood decades of precision testing, perhaps to the disappointment of physicists hoping for new physics, across the various sectors. The classic examples are the predicted values of the muon and electron anomalous moment [Aoy+20; HFG08], but also electroweak precision observables (EWPOs) like $Z-$boson mass and width, CKM unitarity tests, and Higgs coupling measurements have not left much room for new physics. Despite these successes and precision measurements, however, there are still many unsatisfactory aspects of the theory leading to the general consensus that there should be physics beyond the standard model (BSM). To conclude our overview of the SM, we will discuss the most pressing arguments for BSM physics in this section.

2.4.1 NEUTRINO MASSES

The strongest evidence of physics beyond the Standard Model lies probably in the neutrino sector. Throughout the previous chapter, we have treated neutrinos as massless left-handed fermions, but in the past five decades it has become indisputable that this description is incomplete. Neutrino oscillations [Mes06] are, so far, only to be properly explained if a mass term is introduced for at least two neutrinos, requiring either the introduction of right-handed neutrino fields or the violation of the symmetry group of the SM. Direct neutrino mass experiments like KARTIN have, on the other hand, put strict upper limits on their masses, currently measured to be at least 6 orders of magnitude smaller than the electron mass [Ake+22]. A satisfying explanation for neutrino masses should thus not only introduce a mass mechanism, but should also introduce a dynamical mechanism for why these masses are so small. The subject of neutrino masses will be central to the rest of this thesis, and a full discussion of the various mass mechanisms and their implications is found in the next two chapters.

2.4.2 DARK MATTER

Another compelling reason for new physics is the current lack of SM candidate particles for dark matter (DM). Dark matter refers to any matter that is observed only through its gravitational effect on its surroundings, while not emitting or absorbing any type of radiation for us to directly observe. There is substantial evidence for the existence of dark matter, and a list containing the most stringent ones will be given.

Cluster dynamics
Observations of galaxy clusters, such as the Coma Cluster, show that the galaxies move with velocities too high to be gravitationally bound by the visible matter alone. Applying the virial theorem reveals a discrepancy between the kinetic energy of the galaxies and the gravitational potential implied by luminous matter, suggesting a large component of unseen mass, i.e., dark matter [Zwi33; Rin+16].

Galactic rotation curves
Measurements of rotational velocities of stars and gas in spiral galaxies reveal that these velocities remain roughly constant at large radii from the galactic centre, instead of falling off as expected from the distribution of visible matter. This indicates the presence of a massive, extended dark matter halo surrounding galaxies [RF70; SR01].

Dwarf galaxies
Dwarf spheroidal galaxies exhibit extremely high mass-to-light ratios. Their internal stellar velocity dispersions imply the presence of much more mass than is visible in stars or gas. These systems are among the most dark matter-dominated environments known and provide strong constraints on dark matter models [Mat98; WMO+09].

Gravitational lensing
Strong and weak gravitational lensing studies of galaxies and clusters often show lensing effects far exceeding what can be accounted for by visible matter alone, according to general relativity. The distribution of gravitational potentials inferred from lensing maps is consistent with the presence of dark matter [Zwi37; Clo+06].

Nucleosynthesis
Big Bang Nucleosynthesis (BBN) predicts the abundances of light elements like helium, deuterium, and lithium based on the baryon density of the universe. The observed abundances agree with predictions only if baryonic matter makes up roughly 5% of the total energy density, implying the remaining dark matter must be non-baryonic in nature [ABG48; Cyb+16].

Cluster gas in X-rays
Galaxy clusters contain hot, ionized gas that emits X-rays due to bremsstrahlung radiation. The temperature and distribution of this gas suggest that it should escape the cluster's gravitational pull unless there is additional unseen mass providing confinement. This mass is attributed to dark matter [Fel+66; VKF+06].

Background radiation
The anisotropies observed in the Cosmic Microwave Background (CMB) serve as a precise cosmological probe of the early universe. The angular power spectrum of temperature fluctuations, particularly the relative heights and positions of the acoustic peaks, is sensitive to the total matter content, the baryon-to-photon ratio, and the expansion history. Data from the Planck satellite have shown that the observed spectrum is only consistent with a universe where approximately 26% of the energy density is in the form of non-baryonic, cold dark matter. These measurements are highly model-independent, relying primarily on linear perturbation theory and well-understood plasma physics, and disfavour warm or self-interacting dark matter in significant quantities [Agh+20].

Structure formation
The growth of cosmic structures from primordial fluctuations requires a significant amount of cold, non-relativistic matter. Without dark matter, gravitational collapse would be too slow to form galaxies and clusters within the age of the universe. Dark matter accelerates structure formation by providing gravitational wells around which baryonic matter can accumulate [Pee82; Blu+84; Agh+20; Abb+22].

Cluster collisions

The Bullet Cluster (1E 0657-56) provides arguably the most direct empirical evidence for dark matter. In this system, two galaxy clusters have recently collided. The hot intracluster gas, which constitutes most of the baryonic mass, was slowed and displaced due to its electromagnetic interactions, emitting strong X-rays. However, gravitational lensing maps reveal that the majority of the gravitational mass lies with the collisionless galaxies that passed through the interaction unaffected. This spatial offset between the baryonic matter and the inferred gravitational potential is a direct indication of a non-baryonic, collisionless mass component—dark matter. This observation is particularly powerful because it directly challenges modified gravity scenarios and supports a particle-based interpretation of dark matter [Clo+06; BCG+06]

There are generally two ways of attempts to treating the dark matter problem. The first is to modify gravity in order to fit a new gravitational theory to the observed movement of the visible matter consistent with the Standard Model [Mil83; Bek04; FM12]. The opposite approach is to introduce matter to the Standard Model in such a way that it is able to explain the observed DM behaviour. Due to the large varieties of scales on which gravity should be modified, and due to the successes of general relativity, the second approach is the more popular and sane one. Despite the many suggestions for DM candidates over the years [BHS05; Ber10], none of the proposed particles have ever been found in the lab. There is no strong evidence for any particular DM candidate, but candidates that are not yet excluded in all of their parameter space include weakly interacting massive particles (WIMPs), axions, sterile neutrinos, and light dark sector particles such as dark photons or millicharged particles [JKG96; Apr+18; PQ77a; Du+18; DW94a; Boy+19; Hol86; Bat+17].

2.4.3 Baryon Asymmetry

Around 5% of the energy content of the universe is made up of visible baryons [Agh+20], while there is virtually no evidence for any anti-baryonic presence in the cosmos (for a somewhat outdated overview see [Cas06]). The question that naturally arises is how this matter-antimatter imbalance came about, given natural initial conditions. There are generally two types of initial conditions that might be considered natural: a purely symmetric matter-antimatter distribution $n_b = n_{\bar{b}}$, or a different abundance of the same order of magnitude, i.e. $n_\mathrm{b} = \mathcal{O}(1) n_{\bar{\mathrm{b}}}$, with n denoting number density.

If one considers a symmetric initial distribution one can compute the final baryon-photon number density fraction after freeze-out, which leads to $\frac{n_\mathrm{b}}{n_\gamma} = \mathcal{O}(10^{-19})$ at freeze-out temperature $T_f^b = \mathcal{O}(20)\mathrm{MeV}$, while the observed fraction is of order $\frac{n_\mathrm{b}}{n_\gamma} = \mathcal{O}(10^{-10})$. This means that if one allowed for the baryon vs anti-baryon to annihilate until freeze-out, we would have an abundance of around 9 orders of magnitude. A mechanism for turning anti-baryons into baryons must therefore be active way before freeze-out.

If one were to discard symmetric initial conditions, the observed distribution would require an extreme fine-tuning. Using the current number density of baryons, the corresponding initial fraction of baryons vs anti-baryons would be about

$$\frac{n_\mathrm{b}}{n_{\bar{\mathrm{b}}} \simeq \frac{10^{10}+1}{10^{10}}},$$

or $n_\mathrm{b} = (1 + \mathcal{O}(10^{-10})) \times n_{\bar{\mathrm{b}}}$. This means that general initial conditions do not solve the asymmetry today, so a mechanism must be introduced in order to avoid a finite-tuned solution.

A particle interaction allowing for a net production of (anti-)baryons requires several properties, first laid out by Sakharov in 1967 [Sak91][Sak67]. The interaction should

1. violate baryon number symmetry;
2. violate C, P, and CP symmetry;
3. occur out of thermal equilibrium.

The first condition is fairly intuitive; the second condition requires, in particular, CP violation in order to make sure the net baryon-producing rate is different from the net anti-baryon-producing rate, and the third condition ensures that this reaction occurs only one way, for which thermal equilibrium can not be present. Several known processes satisfy one or more of these conditions. Baryon number violation appears naturally through electroweak sphaleron processes [KRS85], and CP violation occurs within the quark sector via the CKM matrix, and in principle also via the lepton sector if neutrinos are massive particles [FY86]. Furthermore, many environments in the early universe provide the required departure from equilibrium, such as first-order phase transitions. However, the observed CP violation in the Standard Model is insufficient to account for the observed baryon asymmetry, and no experimentally confirmed baryogenesis mechanism currently explains the discrepancy.

2.4.4 DARK ENERGY

Another mismatch between standard cosmological theory and the Standard Model of particle physics lies in the value of the cosmological constant, Λ. The most general action for Einstein gravity together with the Standard Model is

$$S_E = \int d^4x\sqrt{-g}\left(\frac{1}{16\pi G}R - \Lambda + \mathcal{L}_{\text{SM}}\right), \tag{2.4.1}$$

in which the cosmological constant can take on any particular value. By studying the different effects of (non-relativistic) matter, radiation, or Λ on the Friedman equations, one is able to determine their fractional contribution to the total energy density present in the universe. The present standard theoretical model of cosmology, the $\Lambda-$CDM model, predicts the presence of the cosmological constant, with observational constraints leading to a value of about $\Lambda_{\text{obs}}^{\frac{1}{4}} \sim 10^{-3}$ eV.

From a QFT perspective, one is also able to make predictions on the energy density of the vacuum. This vacuum energy from quantum fields arises from their zero-point fluctuations, which contribute to the energy-momentum tensor in the same way as a cosmological constant, allowing the two to be compared. In a special relativistic quantum field theory one generally removes this energy by a redefinition of zero energy, but in general relativity this is no longer possible. If one were to cut off the vacuum energy at the Planck scale, where our theory of gravity is expected to break down, we find the discrepancy between the values of Λ to be

$$\frac{\rho_{\text{vac}}^{\text{QFT}}}{\rho_{\text{obs}}^{\Lambda}} \sim 10^{120}. \tag{2.4.2}$$

This is clearly an indication that there are major inconsistencies between the Λ-CDM model and the Standard Model. Even if we were to sweep the zero point energy under the rug, as is often too gladly done, a strong disagreement between the models would still arise. We have seen that the mass of the W-boson can be used to measure the vacuum expectation value of the Higgs field (see Section 2.2.2), which even in special relativity would induce a $\Lambda-$like contribution to the action. The discrepancy between the vacuum energy from spontaneous symmetry breaking and the observed value is

$$\frac{|\Lambda_{\text{SSB}}|}{\Lambda_{\text{obs}}} \sim 10^{56}. \tag{2.4.3}$$

Since a bare Λ, i.e., the cosmological constant without vacuum fluctuations, can take on any given value, one could choose the value in such a way that they together cancel. The two values are not known to be in any way related, however, so this would be the largest fine-tuning problem so far.

In most BSM theories like string theory or grand unified theories, the problem only worsens [Pol06; BP00; Dou03; Mar12; Wei89]. Anthropic arguments are currently considered one of the most viable explanations, which only underlines how disastrous the problem really is [Wei87; Sus03].

2.4.5 STRONG CP PROBLEM

The strong CP problem, in essence, asks why there is no CP violation in the strong sector, even though a CP-violating term is allowed to be present. There are two theoretical contributions to such a term, and current measurements of CP violation in the strong sector require them to cancel through fine-tuning up to 7 significant decimals [t H76; PQ77b; Wei78; Cre+79; Bak+06; Abe+20; Hoo19].

If one attempts to write every Lorentz- and gauge-invariant renormalizable term for a pure gauge theory, one would obtain the Lagrangian

$$\mathcal{L} = -\frac{1}{4}F^{\mu\nu}F_{\mu\nu} - \frac{\theta}{4}F^{\mu\nu}\tilde{F}_{\mu\nu}, \tag{2.4.4}$$

where $\tilde{F}_{\mu\nu} = \varepsilon^{\mu\nu\rho\sigma}F_{\rho\sigma}$ is the dual field strength tensor with $\varepsilon^{\mu\nu\rho\sigma}$ the totally antisymmetric tensor, and θ is a parameter denoting the strength of the term relative to the kinetic term. The dual term violates CP symmetry, and thus θ determines the strength of CP-violating interactions. The reason why one generally does not encounter the dual term in the Lagrangian is because it can be written, both for abelian and non-abelian groups, as a total derivative

$$\frac{1}{8}\tilde{F}^{\mu\nu}F_{\mu\nu} = \partial_\mu K^\mu, \tag{2.4.5}$$

where K^μ is a current depending on the vector field (in the non-abelian case generally referred to as the Chern-Simons current). In the action we integrate over this derivative, which through Stokes' theorem then becomes a boundary term, i.e.

$$\frac{1}{8}\int\limits_{V^4} d^4x F^{\mu\nu}\tilde{F}_{\mu\nu} = \int\limits_{V^4} d^4x \partial_\mu K^\mu = \int\limits_{\partial V^4} d\sigma K_\perp, \tag{2.4.6}$$

where σ is a 3-volume unit of the boundary ∂V^4, and $K_\perp$ denotes the component of K^μ orthogonal to the boundary. For abelian gauge theories, field configurations typically vanish at infinity, and gauge transformations are trivial at the boundary. This means that the surface term vanishes, and thus for these groups the dual term is physically irrelevant. The problem for non-abelian gauge groups, on the other hand, is that gauge transformations are not necessarily trivial at the boundary. Mathematically, this is due to the fact that Lie groups are (by definition) also topological manifolds, meaning that one can consider their fundamental group. Abelian groups have a trivial fundamental group, while non-abelian groups do not. The result is that the boundary terms discussed above do not trivially vanish, and thus for non-abelian groups one can expect a term proportional $F_{\mu\nu}\tilde{F}^{\mu\nu}$ in the Lagrangian. For QCD the dual term is generally written as $\frac{\theta_{\text{QCD}}}{32\pi^2}g_s^2 G\tilde{G}$.

Additionally, we have seen that the CP violation in the weak quark sector arises due to relative phases of the left-handed quark fields. Aside from that, we have a global phase of the mass matrices that introduces CP violation in the strong sector, which manifests itself proportional to the dual term as $\arg\det(M_p M_n)$. We don't have any symmetries requiring further restrictions on the Yukawa matrices, so the global phase can take on an arbitrary value. A charitable natural value could be of order $\mathcal{O}(10^{-3})$.

The two contributions can be combined into one parameter,

$$\bar{\theta} = \theta_{\text{QCD}} - \arg\det \mathcal{M}_p\mathcal{M}_n, \tag{2.4.7}$$

which determines the total amount of strong CP violation. Bounds on $\bar{\theta}$ are deduced from the electric dipole moment of the neutron, with current measurements restricting $\bar{\theta} < 10^{-10} - 10^{-11}$ [YZF21]. Within the SM, $\bar{\theta}$ is simply a free parameter, much like the electron mass or the gauge couplings, so its smallness cannot be explained from first principles. The real puzzle only arises once one assumes a UV completion of the SM, which must simultaneously accommodate maximal CP violation in the electroweak sector while ensuring its near absence in QCD—a highly nontrivial requirement commonly referred to as the strong CP problem.

2.4.6 HIERARCHY PROBLEM

As we have seen, the chiral symmetry in the Standard Model prevents direct mass terms for the fermions to be present, and the very nature of the force-carrying bosons, i.e., the gauge bosons, allows only for initially massless bosons. It is then through SSB that they acquire mass, as we saw in section 2.2.2 and 2.2.3. In order to preserve the symmetries, a massless fermion can not obtain mass from self-energy corrections, so we can understand that the mass shift induced by loop corrections must be proportional to its bare mass value. Any divergence in this mass shift must then be dimensionless, only to be realised by a logarithmic divergence,

$$\delta m_e \xrightarrow[\Lambda\to\infty]{} \frac{3\alpha}{4\pi} m_{e_0} \log\left(\frac{\Lambda^2}{m_{e_0}^2}\right). \tag{2.4.8}$$

The Higgs scalar, on the other hand, has explicit mass terms in its potential and is not protected by the same symmetries, which allows for power-law divergences in the loop corrections. The first-order mass shift is then not proportional to its own mass, but to its coupling constant with the heaviest particle, in our case the top quark, and an energy scale Λ, so

$$\delta m_H^2 \xrightarrow[\Lambda\to\infty]{} -\frac{|y_t|^2}{8\pi^2}\Lambda^2 + \dots . \tag{2.4.9}$$

Λ is the maximum momentum of the virtual particles that we can assign using our current theory. Since we expect the Standard Model to break down at the Planck scale, $\mathcal{M}_{\text{Pl}} \sim 10^{18}$GeV, one generally takes Λ to be $\mathcal{M}_{\text{Pl}}$. The question then is, why do the higher order corrections to the Higgs mass, all of the order of the Planck scale, cancel out in such a way that the mass of the Higgs reduces to a mere 100GeV? There is no symmetry enforcing these cancellations, so this is only explained by an extreme fine-tuning.

2.4.7 UNIFICATION OF COUPLING CONSTANTS

After the success of the unification of the weak and electromagnetic interaction, the quest for further unification of the gauge groups of the standard model became popular. Gauge coupling unification addresses the question of whether the different gauge interactions of the Standard Model might emerge from a single unified gauge group at high energies. At low energies, each sector has its own distinct coupling constant and thus different interaction strengths. However, in QFT, the coupling constants are not fixed: they run with energy scale due to quantum corrections, as described by the renormalization group equations.

The β-functions for each gauge coupling g_i $(i = 1, 2, 3)$ determine their scale dependence through

$$\mu \frac{dg_i}{d\mu} = \beta_i(g_i), \tag{2.4.10}$$

and at one-loop order, these functions take the form $\beta_i = \frac{b_i}{16\pi^2} g_i^3$, where the b_i coefficients depend on the matter content of the theory. For the Standard Model particle spectrum, the running couplings do not unify: extrapolated to high energies, the three gauge couplings g_1, g_2, and g_3 come close but fail to meet at a single point. This near-miss gives hope that the Standard Model may be part of a larger group, such as a Grand Unified Theory (GUT), which would only become manifest at energies many orders of magnitude above the electroweak scale. In particular, the introduction of new particles at intermediate scales, such as those predicted by supersymmetric extensions of the Standard Model, can modify the β-functions such that unification does occur at an energy around 10^{16} GeV.

Despite the aesthetic appeal and theoretical motivation, there is currently no experimental evidence for gauge coupling unification, nor a fully established model that consistently incorporates all observed features of particle physics. Moreover, predictions such as proton decay—common in GUTs—remain unconfirmed. It should be remembered that the absence of exact unification within the Standard Model is not an inconsistency or a contradiction of the theory, but rather an inelegance.

3

Empirical Evidence for Neutrino Masses

As briefly mentioned in the previous section, neutrino masses are the most commonly accepted form of BSM physics, and the description of a neutrino as a massless (solely left-handed) fermion is currently believed to be incomplete. The idea of assigning masses to the neutrinos is, however, not a new one, as both the possibility of massive and massless neutrinos was mentioned by Pauli at the Solvay conference in 1933 [Pau34]. The neutrino mass has been a topic of debate throughout most of its history, and new manifestations of the topic are still studied today. That neutrinos have mass is now, on the contrary, generally agreed upon, most prominently due to the discovery and solution of the solar neutrino problem (SNP). We will give a brief overview of the historical development and motivation of neutrino theory up until the proposal of neutrino oscillations, then we will discuss its confirmation by SNO as a solution to the SNP, and finally give a formal treatment of neutrino oscillation theory both in vacuum and in matter.

3.1 NEUTRINOS BEFORE THE STANDARD MODEL

The story of neutrinos starts perhaps with the discovery of the radiation of uranium salts, by Henri Becquerel in 1896 [Bec96], and the radiation of polonium by Pierre and Marie Curie [CC98] two years after. E. Rutherford discovered that radiation came in two different types, which he coined alpha and beta radiation [Rut99], and P. Villard discovered that a third type existed, which he called gamma [Vil00]. The second of the three types was found to consist of electrons only, by P. and M. Curie in 1902 [CC02], yet the energy spectrum of the emitted electrons was definitively measured to be continuous in 1927 in a calorimeter experiment by Ellis and Wooster [EW27].

In 1930, W. Pauli proposed, in order to solve the problem of energy conservation and spin-statistics due to this continuous spectrum, the existence of a neutral weakly interacting fermion to be emitted during β-decay, which should have a mass not exceeding that of an electron [Pau30]. This particle was named the neutrino by E. Fermi two years later, and Fermi and Perrin independently concluded in 1933 [Fer34a; Per33] that its mass must be much smaller than that of the electron, due to the shape of the energy spectrum. In 1934, Fermi introduced a quantitative theory of β-decay [Fer34b], describing it as a four-fermion contact interaction involving a neutron, proton, electron, and neutrino. This effective interaction theory, now known as Fermi's theory of weak interactions, laid the groundwork for understanding neutrino behaviour, making it the first successful theoretical framework to predict neutrino processes.

In 1934, Bethe and Peierls famously argued that neutrino detection was practically impossible due to its vanishingly small interaction cross section [BP34]. Nevertheless, in 1946, Pontecorvo proposed a practical method based on inverse beta decay, suggesting the use of the reaction $\nu_e +^{37}\text{Cl} \rightarrow e^- +^{37}\text{Ar}$ as a detection channel, with the Sun and nuclear reactors as intense sources [Pon46].

This concept was realized a decade later by Reines and Cowan, who placed a detector near the Savannah River nuclear reactor. After improving their original setup to suppress backgrounds, they successfully observed neutrino-induced inverse beta decay events with statistical significance exceeding 4σ [Cow+56]. This marked the first direct detection of the neutrino.

Following the discovery of the electron neutrino, the question arose whether the neutrinos produced in pion decay, observed in processes like $\pi^+ \rightarrow \mu^+ + \nu_\mu$, were identical to those from beta decay. The absence of the decay $\mu \rightarrow e\gamma$, predicted if only one type of neutrino existed, strongly hinted at a second neutrino species. In 1962, an experiment at Brookhaven National Laboratory confirmed this hypothesis. Using a high-intensity proton beam to generate pions, a flux of neutrinos was produced via pion decay-in-flight. Muons emerging from neutrino interactions in a neon-filled spark chamber provided clear evidence for a new lepton-flavour specific interaction channel. The detected neutrinos were identified as muon neutrinos, ν_μ, thereby establishing the existence of a second neutrino flavour [Dan+62; Sch60]. Parallel ideas were independently developed by Pontecorvo, who proposed a similar experimental approach in the Soviet Union, though it was not pursued at the time [Pon59].

Around the same time, insights into the nature of weak interactions were taking shape. In 1956, T.D. Lee and C.N. Yang proposed that parity may not be conserved in weak decays, challenging quite a fundamental assumption of quantum field theory [LY56; LY57]. Their hypothesis was confirmed in 1957 in an experiment by C.S. Wu and collaborators, who demonstrated parity violation in the beta decay of cobalt-60 nuclei [Wu+57]. This finding established that the weak interaction differentiates between left- and right-chiral fermions. Shortly thereafter, Goldhaber et al. devised an experiment showing that neutrinos produced in beta decay are left-handed, possessing negative helicity [GGS58]. These discoveries laid the basis for the development of the V–A theory of weak interactions by Feynman, Gell-Mann, Marshak, and Sudarshan, which successfully unified weak processes under a single chiral framework and accounted for the observed maximal parity violation [FG58; MS57].

The Standard Model of particle physics, formulated in the late 1960s, provided a unified description of electromagnetic and weak interactions. Building on Glashow's original $SU(2)_L \times U(1)_Y$ proposal from 1961 [Gla61], the Glashow–Weinberg–Salam theory introduced spontaneous symmetry breaking through the Higgs mechanism [Hig64b; Hig64a; Hig66; EB64; GHK64], which allowed for massive gauge bosons, as we saw in 2.2.2. Neutrinos appeared as massless left-handed particles. The theory became fully viable after 't Hooft and Veltman demonstrated its renormalizability [t H71; tV72; Vel77], and its predictions were confirmed by the discovery of weak neutral currents in neutrino scattering at CERN's Gargamelle experiment [Has73a; Has73b; Bie74], and later at Fermilab [Bal74].

While the Standard Model fixed neutrinos as massless, interest in neutrino masses had not vanished, and even mixing had emerged much earlier. Inspired by the analogy with $K^0 \leftrightarrow \bar{K}^0$ oscillations [GP55], Pontecorvo proposed in 1957 that neutrinos might undergo transitions into antineutrinos [Pon57b; Pon57a]. He initially considered this in the context of Majorana neutrinos and interpreted early, ultimately incorrect, reports of reactor antineutrino detection by Davis as possible signs of $\bar{\nu} \rightarrow \nu$ oscillations. However, the V–A theory, developed soon after [FG58; MS57], implied that right-handed neutrinos produced in such a transition would be sterile, limiting the physical relevance of this process. A more realistic scenario emerged in 1967 when Maki, Nakagawa, and Sakata introduced the idea that flavour eigenstates could be linear combinations of mass eigenstates, analogous to quark mixing [MNS62]. Although their formalism was not yet fully connected to oscillation phenomenology, it laid the foundation for later developments. In the same year, Pontecorvo proposed a more intuitive two-flavour mixing framework, later expanded with Gribov in 1969 to include massive neutrinos and oscillations between ν_e and ν_μ [Pon68b; GP69a]. During the 1970s, this framework was generalized to multiple flavours and incorporated into quantum field theory, particularly through the work of Eliezer and Swift [ES76], Fritzsch and Minkowski [FM76], and Bilenky and Pontecorvo [BP76b; BP78]. These studies made clear that oscillations could only occur if neutrinos had mass and if flavour states were nontrivial superpositions of mass eigenstates, a possibility that remained outside the Standard Model's original formulation. This formalism provided a framework in which neutrinos are treated as coherent quantum states undergoing flavour oscillations if their mass eigenstates are non-degenerate. Although the Standard Model, as formulated, assumes massless neutrinos and thus cannot accommodate such phenomena, the theoretical developments by Pontecorvo, Gribov, Bilenky, and others allowed for a treatment of oscillations independently of the Standard Model [GP69b; BP76a; BP76b]. Pontecorvo had already then pointed out that flavour transitions could lead to a deficit in the observed solar neutrino flux [Pon68a], a hypothesis which became the motivation for future measurements. More specifically, they led to the design of the first dedicated experiments aimed at detecting solar neutrinos and testing the existence of flavour oscillations, which we will describe in the next section.

3.2 The Solar Neutrino Problem

3.2.1 Discovery and Confirmation of the SNP

The triggering experiment for a rich history of neutrino oscillation measurements was the Homestake experiment, or Brookhaven Solar Neutrino Experiment, initiated in the late 1960s by R. Davis, Jr. and collaborators [**davis**]. The goal was to measure neutrinos emitted by the sun through the Pontecorvo-Alvarez inverse $\beta-$decay in a Cl-Ar system,

$$\nu_e +^{37}\text{Cl} \rightarrow^{37}\text{Ar} + e^-. \tag{3.2.1}$$

A tank of 6×10^5 litres of tetrachloroethylene (C_2Cl_4) placed almost 1500 meters underground formed the detector, and the processes targeted neutrinos produced in the subdominant PPIII chain of helium production. The Argon that is produced by the neutrinos in the detector is extracted after around two months using chemical methods, from which these types of *radiochemical* detectors obtain their name. The measured neutrino flux after the first extraction in 1968 was around a third of the flux predicted by the standard solar model (SSM) of [Bah+63; BU88], and continued measurements in the following 25 years confirmed this value [Cle+98; Abd+99; Ham+99]. The question of these missing neutrinos is what became known as the solar neutrino problem (SNP). A disadvantage of the chlorine-based detector used in the Homestake experiment is, however, that the energy threshold for the neutrino to be detected in the corresponding interaction is fairly high at $E_\nu^{\text{th}} = 814\,\text{keV}$ [Wor+22b], in particular, higher than the energies of neutrinos emitted in the dominant PPI chain. In order to confirm that the neutrino deficit was not due to a misunderstanding of the SSM at specific energy levels, measurements of neutrinos produced in the PPI chain were proposed. Since the energy of these neutrinos is lower, radiochemical experiments allowing for a low energy threshold were suggested, in particular, the gallium inverse $\beta-$decay reaction

$$\nu_e +^{71}\text{Ga} \rightarrow^{71}\text{Ge} + e^-, \tag{3.2.2}$$

with threshold $E_\nu^{\text{th}} = 233\,\text{keV}$. To this end, two radiochemical experiments were proposed and built: SAGE, located in Baksan, and GALLEX, at Gran Sasso. The results from both SAGE and GALLEX (and later its successor GNO) confirmed the solar neutrino deficit of around half of the expected neutrinos, now in the lower energy range. This strongly validated the SNP and suggested that the problem was not restricted to high-energy neutrinos or due to experimental errors.

The Kamiokande experiment represented the next significant development in the study of solar neutrinos, characterized by the use of Cherenkov detectors. There are three important benefits of Cherenkov detectors over the earlier radiochemical techniques. Firstly, they are able to measure the neutrinos "real time", while radiochemical detectors require the extraction of the products after every few weeks, effectively integrating the interaction rates over long time periods. Secondly, the underlying scattering process involves both charged and neutral current interactions, allowing detection of all neutrino flavours. Thirdly, they are able to measure information on the kinematic properties of the measured neutrino. The detector, initially constructed in the Kamioka mine to search for proton decay, employed 3000 tons of water monitored by photomultiplier tubes (PMTs) to identify neutrinos through their elastic scattering off electrons,

$$\nu_i + e^- \to \nu_i + e^-, \text{ where } i = e, \mu, \tau.$$

The emitted Cherenkov radiation, produced by the recoiling electrons, provided directional information that allowed the separation of neutrino events from background noise. A later upgrade, Kamiokande-II, reduced the energy threshold to around 6.5 MeV, making the experiment primarily sensitive to high-energy neutrinos originating from ^{8}B decay in the Sun. This methodology was further advanced with the construction of Super-Kamiokande (SK), which began operation in 1996. Containing 50 kilotons of pure water and equipped with more than 11,000 inward-facing PMTs, the detector achieved a lower energy threshold of about 3.5 MeV, again enhancing sensitivity to solar neutrinos. Measurements from both Kamiokande and Super-Kamiokande revealed a consistent deficit in the observed neutrino flux compared to predictions from the SSM, again of around a half. Furthermore, early data from Super-Kamiokande showed no significant energy spectrum distortion or directional asymmetry, placing strong limits on various explanations for the observed discrepancy [BKS98; BGP02; Fuk+98; Fuk+01]. Even though the detector was able to measure muon and tau neutrinos, their sensitivity was much lower, not allowing for the individual identification of these flavours, nor for a direct measurement of the flavour conversion responsible for the missing electron neutrinos. This meant in essence that these experiments we not yet able to fully account for the missing neutrinos, but were the definitive sign of the origin of the SNP in the neutrino physics, and not in the SSM.

3.2.2 SNO

SK started operating in April 1996, and at this time, twenty years had passed since the theory of vacuum neutrino oscillations was formally proposed by Pontecorvo [Pon68b], and around 10 years after the analogous theory for matter. If one were able to measure the total neutrino flux from the Sun together with their respective flavour fractions, one would be able to search for a direct correspondence with theory. The Sudbury Neutrino Observatory (SNO) set out to do so by measuring solar neutrinos through three different processes,

$$\begin{aligned} \text{CC} \quad & \nu_e + d \to p + p + e^-, \\ \text{NC} \quad & \nu_i + d \to p + n + \nu_i, \\ \text{ES} \quad & \nu_i + e^- \to \nu_i + e^-, \end{aligned}$$

with $i = e, \mu, \tau$. The SNO detector consisted of 1,000 tonnes of heavy water (D_2O), contained within a transparent acrylic sphere and surrounded by a light water shield to suppress external backgrounds. Cherenkov light produced by charged particles in both the inner D_2O and outer H_2O volumes was detected by an array of photomultiplier tubes mounted on a surrounding structure. Unlike water Cherenkov experiments such as Super-Kamiokande, SNO's use of deuterium enabled the detection of solar neutrinos through the three distinct processes above. The charged current (CC) channel allowed for a direct measurement of the solar electron neutrino flux, while the neutral current (NC) interaction provided a measure of the total flux of active neutrinos independent of flavour. By comparing the observed rates in these channels, SNO found that the total active neutrino flux was in agreement with the predictions of the standard solar model, but that only roughly one-third of the neutrinos retained their electron flavour upon detection. The electron scattering (ES) measurement, which was also sensitive to non-electron neutrinos with reduced cross-section, further supported this result when combined with data from Super-Kamiokande.

This pattern of results provided conclusive evidence that electron neutrinos produced in the solar core undergo flavour transformation before reaching Earth. SNO thus resolved the long-standing solar neutrino problem by confirming the presence of neutrino oscillations, consistent with the large mixing angle (LMA) solution of the MSW effect in solar matter [Ahm+02].

3.3 NEUTRINO OSCILLATIONS IN VACUUM

The confirmation of neutrino oscillations is equivalent to the confirmation of neutrino mass terms, which have important implications for the leptonic sector. As briefly discussed in the historical overview, the origin of neutrino mixing has strong similarities to the origins of flavour mixing in the quark sector. If neutrinos are massive, there is no reason for their mass eigenstates to correspond to their flavour eigenstates, and a misalignment between the mass basis of the charged leptons and their corresponding neutrinos is naturally present. This misalignment is encoded in the PMNS matrix, the equivalent of the CKM matrix, after Pontecorvo, Maki, Nakagawa and Sakata [MNS62]. The flavour basis can be constructed from the mass basis as

$$\begin{pmatrix} \nu_\mathrm{e} \\ \nu_\mu \\ \nu_\tau \end{pmatrix} = U_\mathrm{PMNS} \begin{pmatrix} \nu_1 \\ \nu_2 \\ \nu_3 \end{pmatrix} = \begin{pmatrix} U_{\mathrm{e}1} & U_{\mathrm{e}2} & U_{\mathrm{e}3} \\ U_{\mu 1} & U_{\mu 2} & U_{\mu 3} \\ U_{\tau 1} & U_{\tau 2} & U_{\tau 3} \end{pmatrix} \begin{pmatrix} \nu_1 \\ \nu_2 \\ \nu_3 \end{pmatrix}, \tag{3.3.1}$$

and the unitarity of U_PMNS also allows for the reverse operation. There are, just as for the CKM matrix, parametrizations of U_PMNS to single out the independent parameters. These will be discussed in Section 4.2.2.

Neutrino oscillations occur due to this misalignment, and can be considered as similar to the oscillation in the mixed Kaon system. If a coherent group of neutrinos is produced in a weak eigenstate, their various mass components will propagate at different velocities. This means that the respective fraction of the various mass eigenstates changes over time (or distance), and thus also the respective probabilities of measuring a certain weak eigenstate. We will now discuss this idea in full formality, first in vacuum and then in matter.

3.3.1 STANDARD NEUTRINO OSCILLATION PROBABILITY

A neutrino with flavour α and momentum $\vec{p}$ produced through a weak interaction consists of the linear combination of mass eigenstates. In the following derivation, the mass eigenstates will be approximated to be plane waves*,

$$|\nu_\alpha\rangle = \sum_k U^*_{\alpha k}|\nu_k\rangle, \tag{3.3.2}$$

where the number of massive eigenstates is larger or equal than 3. From the unitarity of U_{PMNS} we have (considering a finite normalization volume)

$$\langle \nu_i|\nu_j\rangle = \delta_{ij}, \qquad \langle \nu_\alpha|\nu_\beta\rangle = \delta_{\alpha\beta}. \tag{3.3.3}$$

The superposition of states can be described quantum mechanically, and for state $|\nu_k\rangle$ with energy $E_k = \sqrt{\vec{p}_k^{\,2} + m_k^2}$ the time evolution of the state after a given distance L is

$$|\nu_\alpha(t,L)\rangle = \sum_k U^*_{\alpha k} e^{-iE_k t + p_k L}|\nu_k(0)\rangle \equiv \sum_k U^*_{\alpha k} e^{-iE_k t + p_k L}|\nu_k\rangle. \tag{3.3.4}$$

Now, by expressing the mass eigenstate $|\nu_k\rangle$ above in terms of its flavour components, we obtain

$$\begin{aligned} |\nu_\alpha(t,L)\rangle &= \sum_k U^*_{\alpha k} e^{-iE_k t + p_k L} \sum_\beta U_{\beta k}|\nu_\beta\rangle & (3.3.5)\\ &= \sum_\beta \left(\sum_k U^*_{\alpha k} e^{-iE_k t + p_k L} U_{\beta k} \right)|\nu_k\rangle. & (3.3.6) \end{aligned}$$

We now have an expression that describes how a pure flavour state α becomes a superposition of the other flavour states as a function of time and distance travelled. This can be directly applied to find the amplitude for a transition $\nu_\alpha \to \nu_\beta$ at a time t and distance L,

$$A_{\nu_\alpha \to \nu_\beta}(t,L) \equiv \langle \nu_\beta|\nu_\alpha(t,L)\rangle = \sum_k U^*_{\alpha k} U_{\beta k} e^{-iE_k t + p_k L}, \tag{3.3.7}$$

and the corresponding probability

$$P_{\nu_\alpha \to \nu_\beta}(t,L) = |A_{\nu_\alpha \to \nu_\beta}(t,L)|^2 = \sum_{k,j} U^*_{\alpha k} U_{\beta k} U_{\alpha j} U^*_{\beta j} e^{-i(E_k - E_j)t + i(p_k - p_j)L}. \tag{3.3.8}$$

In order to obtain the conventional results, at this point some approximations are to be made. The correct way to continue is to now assume equal energy of the various massive components, and use the dispersion relations to eliminate differences in momentum accordingly. It is equivalent and more common, however, to assume an equal momentum and use the ultrarelativistic velocity of the neutrino to argue that $L = t$, as then $E = |\vec{p}|$. Although it does not change the final outcome, one should realize that the latter two assumptions are not justified, since the various mass eigenstates realistically have varying momenta, and because in the plane wave approximation it makes no sense to speak about $L = t$, as a plane-wave is not localized. The justification for using these assumptions comes from a more complete treatment in quantum field theory, where neutrinos are modelled as wave packets produced and detected in localized interactions. In this framework, the standard oscillation formula is recovered under well-defined coherence and localization conditions. These results validate the use of simplified quantum mechanical approximations, despite their formal incon-

---

[*] For all relevant measurable purposes, a full QFT treatment will yield the same result. For a discussion consult [GK07], Section 8.1.1.

sistencies.

If we thus make the assumption that the momenta for the components are equal, we can approximate the dispersion relation to $E_k \simeq E + \frac{m_k^2}{2E}$, with $E = |\vec{p}|$ for both neutrinos. This then yields

$$E_k - E_j = \frac{m_k^2 - m_j^2}{2E} \equiv \frac{\Delta m_{kj}^2}{2E}. \tag{3.3.9}$$

As explained before, $E = |\vec{p}|$ becomes useful in the ultra-relativistic limit, and as we generally have more information on the distance to the source than the time travelled, we approximate $t \sim L$, where L is the distance from the source to the detector. We can now write our probability as

$$P_{\nu_\alpha \to \nu_\beta}(L, E) = \sum_{k,j} U_{\alpha k}^* U_{\beta k} U_{\alpha j} U_{\beta j}^* \exp\left(-i \frac{\Delta m_{kj}^2 L}{2E} \right). \tag{3.3.10}$$

It should be noted that this probability depends on two parameters, L and E, and two constants of nature, Δm_{ij}^2 and $U_{\alpha i}$. If we are able to gain knowledge on the specific values of E and L, we can thus obtain information on the mass differences and elements of the mixing matrix. Additionally it is of importance that the products $U_{\alpha k}^* U_{\beta k} U_{\alpha j} U_{\beta j}^*$, of elements of U_{PMNS}, are invariant under a rephasing of the leptons or a reparametrization of the mass matrix. They are, in fact, rephasing invariants, as mentioned briefly in section 2.3.2, and are thus invariant under any additional complex phase in the system.

There are some useful ways to rewrite probability 3.3.10 that highlight different aspects. The starting point of the preceding derivation was the production of a neutrino through a weak process, after which the massive neutrino components would propagate coherently in superposition. Since the values of U_{PMNS} are unchanging and non-zero, there is also a probability for *incoherent* states to be detected as neutrinos of a specific flavour, purely due to mixing, which should be constant in time. We can thus separate our expression 3.3.10 in terms of a constant component and an oscillatory component related to interference, as

$$P_{\nu_\alpha \to \nu_\beta}(L, E) = \sum_k |U_{\alpha k}|^2 |U_{\beta k}|^2 + 2\mathfrak{Re} \sum_{k>j} U_{\alpha k}^* U_{\beta k} U_{\alpha j} U_{\beta j}^* \exp\left(-2\pi i \frac{L}{L_{kj}^{\text{osc}}} \right), \tag{3.3.11}$$

where the oscillation length is given by

$$L_{kj}^{\text{osc}} = \frac{4\pi E}{\Delta m_{kj}^2}. \tag{3.3.12}$$

Since the exponential term oscillates rapidly for $L \gg L^{\text{osc}}$, integrating over variations of this scale averages out to zero, and only the constant term remains. The measurement of averaged or incoherent oscillations can thus be used to effectively measure the constant term. Alternatively, we could identify the constant term above as related to the real part of the rephasing invariant,

$$\sum_k |U_{\alpha k}|^2 |U_{\beta k}|^2 = \delta_{\alpha\beta} - 2 \sum_{k>j} \mathfrak{Re}\left[U_{\alpha k}^* U_{\beta k} U_{\alpha j} U_{\beta j}^* \right], \tag{3.3.13}$$

so that we can use Euler's identity to rewrite the exponential and get

$$P_{\nu_\alpha\to\nu_\beta}(L,E) = \delta_{\alpha\beta} - 4\sum_{k>j}\mathfrak{Re}\left[U^*_{\alpha k}U_{\beta k}U_{\alpha j}U^*_{\beta j}\right]\sin^2\left(\frac{\Delta m^2_{kj}L}{4E}\right)$$
$$+ 2\sum_{k>j}\mathfrak{Im}\left[U^*_{\alpha k}U_{\beta k}U_{\alpha j}U^*_{\beta j}\right]\sin\left(\frac{\Delta m^2_{kj}L}{2E}\right). \tag{3.3.14}$$

One of the advantages of this form is in its computation of survival probabilities, which is the probability to detect a flavour α after emitting the same flavour α, i.e. $P_{\nu_\alpha\to\nu_\alpha}$. If $\alpha=\beta$, then the rephasing invariant is purely real, so one can rewrite the survival probability as

$$P_{\nu_\alpha\to\nu_\alpha}(L,E) = 1 - 4\sum_{k>j}|U_{\alpha k}|^2|U_{\alpha j}|^2\sin^2\left(\frac{\Delta m^2_{kj}L}{4E}\right). \tag{3.3.15}$$

The other aspect that the form 3.3.14 emphasizes is the difference in probabilities for antineutrino oscillations $\bar\nu_\alpha \to \bar\nu_\beta$. In general the derivation for amplitudes of antineutrino transitions is similar to that of neutrino oscillations, only the mixing matrix U_{PMNS} is conjugated. This manifests itself visibly in the form of 3.3.14 as

$$P_{\bar\nu_\alpha\to\bar\nu_\beta}(L,E) = \delta_{\alpha\beta} - 4\sum_{k>j}\mathfrak{Re}\left[U^*_{\alpha k}U_{\beta k}U_{\alpha j}U^*_{\beta j}\right]\sin^2\left(\frac{\Delta m^2_{kj}L}{4E}\right)$$
$$- 2\sum_{k>j}\mathfrak{Im}\left[U^*_{\alpha k}U_{\beta k}U_{\alpha j}U^*_{\beta j}\right]\sin\left(\frac{\Delta m^2_{kj}L}{2E}\right), \tag{3.3.16}$$

since only the sign of the purely imaginary contribution is flipped.

3.3.2 CP VIOLATION IN NEUTRINO OSCILLATIONS

Precision measurements of neutrino versus antineutrino oscillations can reveal information on the conservation of discrete symmetries in the neutrino sector. For example, a CPT transformation would correspond to a conversion of the channel $\nu_\alpha \to \nu_\beta$ into $\bar\nu_\beta \to \bar\nu_\alpha$, and CPT violation could therefore be measured through the amplitude

$$A^{\text{CPT}}_{\alpha\beta} = P_{\nu_\alpha\to\nu_\beta} - P_{\bar\nu_\beta\to\bar\nu_\alpha}. \tag{3.3.17}$$

More relevant and less speculative, however, is the measurement of the CP-violating phase of U_{PMNS} in a similar way. CP transformations substitute neutrinos with antineutrinos of opposite helicity, and vice versa, leading to measurable amplitudes

$$A^{\text{CP}}_{\alpha\beta} = P_{\nu_\alpha\to\nu_\beta} - P_{\bar\nu_\alpha\to\bar\nu_\beta}. \tag{3.3.18}$$

Using equations 3.3.14 and 3.3.16 we can easily compute this amplitude as

$$A^{\text{CP}}_{\alpha\beta}(L,E) = 4\sum_{k>j}\mathfrak{Im}\left[U^*_{\alpha k}U_{\beta k}U_{\alpha j}U^*_{\beta j}\right]\sin\left(\frac{\Delta m^2_{kj}L}{2E}\right), \tag{3.3.19}$$

which is non-zero only if $\beta\neq\alpha$. Since we expect CPT to be a symmetry, CP violation must be accompanied by the violation of T symmetry, reversing the temporal direction of the channel. This transformation corresponds to swapping final and initial states, so the amplitude of T violation in the oscillation probabilities can be measured by

$$A^{T}_{\alpha\beta} = P_{\nu_\alpha \to \nu_\beta} - P_{\nu_\beta \to \nu_\alpha}. \tag{3.3.20}$$

Note that through CPT symmetry we find that $\nu_\beta \to \nu_\alpha$ is equivalent to $\bar{\nu}_\alpha \to \bar{\nu}_\beta$, and so

$$A^{\mathrm{T}}_{\alpha\beta} = A^{\mathrm{CP}}_{\alpha\beta}. \tag{3.3.21}$$

3.4 NEUTRINO OSCILLATIONS IN MATTER

Neutrino oscillations as proposed by Pontecorvo [Pon68b], and as worked out in modern terms in the previous paragraphs, are not able to explain the solar neutrino problem. The oscillation probabilities should account for the matter that the neutrinos traverse, and especially the different effect that electron-rich matter has on electron neutrinos with respect to muon and tau neutrinos. In particular, when passing through matter with fluctuating density, resonant flavour transitions appear due to coherent forward scattering. Coherent scattering refers to a quantum mechanical interaction in which the wave-function of the incident particle remains in a pure, uncollapsed state after interacting with a medium, allowing amplitudes from multiple scattering centres to add coherently (i.e., with well-defined relative phases), typically resulting in a net forward scattering effect. In this process, no transfer of energy or momentum, and no excitation of electrons or nuclei occur, in contrast to incoherent scattering, which only becomes significant for extreme densities found in supernovae or neutron stars [Sto87a; NR88a]. The overall effect of this scattering can be described by an effective potential, which can then be used to model the evolution of the various flavours, and can be worked out without too much difficulty in the case of 2 neutrinos.

The propagation of neutrinos through matter was originally considered by Wolfenstein [Wol78] for constant densities, and later generalised to varying matter densities by Mikheev and Smirnov [MS85; MS86; Hax86], hence it is named the MSW effect.

3.4.1 EFFECTIVE POTENTIALS

The theory we set out to develop has the aim to be relevant for solar neutrinos propagating towards the earth, so in the derivation we assume that the neutrinos have energies below around 20 MeV, and all matter is electron-rich matter (this scenario is also relevant for reactor-produced neutrinos propagating through earth-like matter). This means, first of all, that the diagrams that contribute to the amplitude are those of the charged current for electron neutrinos, and the neutral current for all neutrino flavours. Additionally,

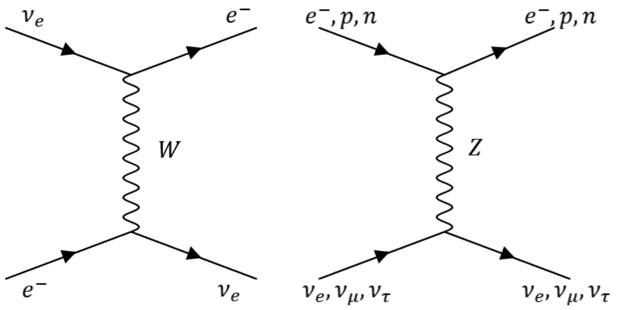

Figure 3.4.1: Diagrams describing the different electroweak contributions to neutrino-background scattering in electron-rich matter.

we can safely say that all solar neutrinos have energies much lower than the mass of the W boson, so we can approximate the diagrams with a four-fermion interaction. For the charged current, we obtain the effective Hamiltonian

$$\begin{aligned}
\mathcal{H}_{\text{eff}}^{(\text{CC})}(x) &= -\mathcal{L}_{\text{eff}}^{(\text{CC})} && (3.4.1)\\
&= \frac{G_F}{\sqrt{2}}[\bar{\nu}_e(x)\gamma^\rho(1-\gamma^5)e(x)][\bar{e}(x)\gamma_\rho(1-\gamma^5)\nu_e(x)] && (3.4.2)\\
&= \frac{G_F}{\sqrt{2}}[\bar{\nu}_e(x)\gamma^\rho(1-\gamma^5)\nu_e(x)][\bar{e}(x)\gamma_\rho(1-\gamma^5)e(x)], && (3.4.3)
\end{aligned}$$

where the last equality is justified by a Fierz transformation. We would like, eventually, to write this as an effective potential term for the neutrinos, so we must replace the individual electron fields with their average contribution. In the frame of the background matter, this average contribution is found by integrating over a statistical distribution of the electron energy depending on the background temperature, i.e., $f = f(E_e, T)$, such that the normalization is given by the total number of electrons, i.e.,

$$\int \mathrm{d}^3 p\, f(E_e, T) = N_e V, \tag{3.4.4}$$

with N_e the number density and V the considered volume. Applying this to our effective Hamiltonian yields

$$\begin{aligned}
\overline{\mathcal{H}_{\text{eff}}^{(\text{CC})}}(x) =& \frac{G_F}{\sqrt{2}}[\bar{\nu}_e(x)\gamma^\rho(1-\gamma^5)\nu_e(x)]\\
&\times \int d^3 p_e f(E_e, T)\frac{1}{2}\sum_{h=\pm 1}\langle e^-(p_e, h_e)|\bar{e}(x)\gamma_\rho(1-\gamma^5)e(x)|e^-(p_e, h_e)\rangle, && (3.4.5)
\end{aligned}$$

where the integral averages over the energy distribution, the sum averages over the contributions from both helicity states, and the matrix element evaluates the contribution of a single electron state (with fixed momentum and helicity) to the effective weak current experienced by the neutrino. The matrix element is worked out ([GK07], 9.10) to reduce to

$$\frac{1}{2}\sum_{h=\pm 1}\langle e^-(p_e, h_e)|\bar{e}(x)\gamma_\rho(1-\gamma^5)e(x)|e^-(p_e, h_e)\rangle = \frac{p_{e\rho}}{E_e V}, \tag{3.4.6}$$

so the expression becomes

$$\overline{\mathcal{H}_{\text{eff}}^{(\text{CC})}}(x) = \frac{G_F}{\sqrt{2}}\frac{1}{V}\int \mathrm{d}^3 p_e f(E_e, T)\bar{\nu}_e(x)\frac{\not{p}_e}{E_e}(1-\gamma^5)\nu_e(x). \tag{3.4.7}$$

The integral now only runs over f and $\frac{\not{p}_e}{E_e}$, so expanding γ_μ explicitly gives

$$\int \mathrm{d}^3 p_e f(E_e, T)\frac{\not{p}_e}{E_e} = \int \mathrm{d}^3 p_e f(E_e, T)\left(\gamma^0 - \frac{\vec{p}_e\cdot\vec{\gamma}}{E_e}\right) = N_e V\gamma^0, \tag{3.4.8}$$

since the second term vanishes due to the integrand being odd. This results in the effective Hamiltonian

$$\begin{aligned}
\overline{\mathcal{H}_{\text{eff}}^{(\text{CC})}}(x) &= \sqrt{2}G_F N_e \bar{\nu}_{eL}(x)\gamma^0\nu_{eL}(x) && (3.4.9)\\
&\equiv V_{\text{CC}}\bar{\nu}_{eL}(x)\gamma^0\nu_{eL}(x). && (3.4.10)
\end{aligned}$$

For the neutral current, a similar calculation can be done, taking into account that neutrinos can interact with both fermions and baryons through their quark components. Since the contributions to the potential are equal but opposite for the electrons and protons, only the neutrons contribute to the potential

$$V_{\mathrm{NC}} = -\frac{1}{2}\sqrt{2}G_F N_n, \tag{3.4.11}$$

with N_n the number density of neutrons. The definitive effective Hamiltonian for both currents is thus given by

$$\overline{\mathcal{H}_{\mathrm{eff}}}(x) = \sum_{\alpha=e,\mu,\tau} V_\alpha \bar{\nu}_{\alpha L}(x)\gamma^0 \nu_{\alpha L}(x), \tag{3.4.12}$$

where the potentials are given by

$$V_\alpha = V_{\mathrm{CC}}\delta_{\alpha e} + V_{\mathrm{NC}} = \sqrt{G_F}\left(N_e\delta_{\alpha e} - \frac{1}{2}N_n\right). \tag{3.4.13}$$

The effective potentials are present as a universal background term throughout the matter, but the actual potential energy given to the neutrino depends on its helicity. It is only present of left-chiral neutrinos, of course, but for massive neutrinos, helicity no longer is equivalent to chirality. A formal treatment for neutrinos as wave-packets (wp) is given in [GK07], page 327, where the potential energy is explicitly computed as

$$\mathcal{V}_\alpha^{(h)} \equiv \langle \nu_\alpha^{\mathrm{wp}} | \int \mathrm{d}^3x \overline{\mathcal{H}_{\mathrm{eff}}}(x) | \nu_\alpha^{\mathrm{wp}} \rangle \tag{3.4.14}$$

and the results on left- versus right-chiral neutrinos, or antineutrinos, is summarised by

$$\mathcal{V}_\alpha^{(-)} \simeq V_\alpha, \qquad \mathcal{V}_\alpha^{(+)} \simeq V_\alpha \frac{m_{\nu_\alpha}^2}{4}\left\langle \frac{1}{E^2} \right\rangle \tag{3.4.15}$$

$$\overline{\mathcal{V}}_\alpha^{(-)} \simeq -V_\alpha \frac{m_{\nu_\alpha}^2}{4}\left\langle \frac{1}{E^2} \right\rangle \qquad \overline{\mathcal{V}}^{(+)} \simeq -V_\alpha. \tag{3.4.16}$$

Note in particular the dependence on the neutrino mass for the opposite-helicity neutrinos. If the neutrinos and the background consist of both matter and antimatter, the average contribution from a potential cancels out, which prevents any net effect from matter. That scenario is relevant in, for example, the early universe.

3.4.2 Flavour Evolution in Matter

The next step is to understand how the potentials affect the oscillation probabilities from before. We will treat the transition amplitude like a quantum state to which we will apply the Schrödinger equation using the total effective Hamiltonian. This total Hamiltonian consists of $\mathcal{H}_0$, for which the massive neutrino components are the eigenstates with eigenvalues E_k, and $\mathcal{H}_I$, for which the flavour components are the eigenstates with eigenvalues given in 3.4.15. So for an ultrarelativistic left-handed neutrino

$$\mathcal{H}_0|\nu_k\rangle = E_k|\nu_k\rangle = \sqrt{\vec{p}_k^{\,2} + m_k^2}|\nu_k\rangle, \qquad \mathcal{H}_I|\nu_\alpha\rangle = V_\alpha|\nu_\alpha\rangle. \tag{3.4.17}$$

Since we are mostly interested in left-handed ultrarelativistic neutrinos, we will only consider those for this derivation. In terms of mass eigenstates, they can be expressed as

$$|\nu_\alpha\rangle = \sum_k U^*_{\alpha k}|\nu_k\rangle, \tag{3.4.18}$$

just as before. We define the transition amplitude as

$$\psi_{\alpha\beta}(t) \equiv \langle\nu_\beta|\nu_\alpha(t)\rangle, \qquad \text{with} \qquad \psi_{\alpha\beta}(0) = \delta_{\alpha\beta}. \tag{3.4.19}$$

The time evolution of the amplitude is determined by the time evolution of the flavour state, so we apply the Schrödinger equation to find

$$\begin{aligned} i\frac{d}{dt}\psi_{\alpha\beta}(t) &= \langle\nu_\beta|i\frac{d}{dt}|\nu_\alpha(t)\rangle \\ &= \langle\nu_\beta|\mathcal{H}|\nu_\alpha(t)\rangle \\ &= \left(\sum_k U_{\beta k}\langle\nu_k|\mathcal{H}_0 + \langle\nu_\beta|\mathcal{H}_I\right)|\nu_\alpha(t)\rangle \\ &= \sum_\eta\left(\sum_k U_{\beta k}E_k U^*_{\eta k} + \delta_{\beta\eta}V_\beta\right)\psi_{\alpha\eta}(t). \end{aligned} \tag{3.4.20}$$

In order to make the equation slightly more workable, we would like to remove the terms that are common to all flavours and thus do not induce a relative phase, but a common phase. Similarly to how oscillations in vacuum only depend on mass differences and not on absolute masses, we can remove one mass from the energy and replace the other mass terms with the differences. We can also remove the common momentum and the shared potential generated by the neutral current. Additionally, since we are considering ultrarelativistic neutrinos, we say $t = x$. After an appropriate phase shift, our equation thus becomes

$$i\frac{d}{dx}\psi_{\alpha\beta}(x) = \sum_\eta\left(\sum_k U_{\beta k}\frac{\Delta m^2_{1k}}{2E}U^*_{\eta k} + \delta_{\beta e}\delta_{\eta e}V_{\text{CC}}\right)\psi_{\alpha\eta}(x). \tag{3.4.21}$$

We have now considered the probability for the transition of a neutrino $\nu_\alpha$to a neutrino ν_β after some time t. It is conventional to define a vector

$$\Upsilon_\alpha \equiv \begin{pmatrix}\psi_{\alpha e}\\ \psi_{\alpha\mu}\\ \psi_{\alpha\tau}\end{pmatrix}, \tag{3.4.22}$$

which contains the transition probability for any of the flavours. By applying the appropriate values for Δm^2_{1k} and exercising the Kronecker deltas, we can write the vector equation

$$\begin{aligned} i\frac{d}{dx}\Upsilon_\alpha(x) &= \frac{1}{2E}(U\mathbb{M}^2U^\dagger + \mathbb{A})\Upsilon_\alpha(x) &(3.4.23)\\ &\equiv \mathcal{H}_F\Upsilon_\alpha(x), &(3.4.24)\end{aligned}$$

where

$$\mathbb{M} = \begin{pmatrix} 0 & 0 & 0 \\ 0 & \Delta m^2_{21} & 0 \\ 0 & 0 & \Delta m^2_{31} \end{pmatrix}, \qquad \mathbb{A} = \begin{pmatrix} A_{\mathrm{CC}} & 0 & 0 \\ 0 & 0 & 0 \\ 0 & 0 & 0 \end{pmatrix}, \qquad U = U_{\mathrm{PMNS}}, \tag{3.4.25}$$

and following convention one has defined $A_{\mathrm{CC}} \equiv 2EV_{\mathrm{CC}} = 2\sqrt{2}EG_F N_e$. From this final form, one is able to convince oneself that any diagonal matrix, for example, a total complex phase, applied to the amplitudes leaves the equation invariant. Note that from equation 3.4.21 one can generalise to any given number of neutrino flavours, not just three, so the formula can be applied also to a two-neutrino scenario.

3.4.3 The MSW effect

The next task is to explicitly solve the evolution equation for three neutrinos for a specific parametrization of the PMNS matrix, given an initial neutrino ν_α. In practice, this is quite difficult, so a more rudimentary exercise would be to follow the evolution for only two flavours. This is not irrelevant to practical application, however, since a two-flavour oscillation can effectively model three-neutrino mixing. Even more, many experiments are not sensitive to the mixing of three neutrinos, since electron-rich matter distinguishes only electron vs non-electron neutrinos through the charged current. In particular, there is no real difference in the propagation of a ν_μ or a ν_τ through solar or earth-like matter, aside from their different massive components. The final result of this section, Parke's formula, has been used to a great extent to describe solar neutrino oscillations.

In the case of two-neutrino mixing, the flavour states can be taken to be the electron neutrino and either a ν_μ, a ν_τ, or a linear combination of the two. Only two mass states are considered, and thus only one mass difference $\Delta m^2 \equiv \Delta m^2_{21} = m_2^2 - m_1^2$ is present. The mixing matrix can be parametrized using a single angle θ, like how the quark matrix is parametrized by the Cabibbo angle for two generations, which is done by

$$U = \begin{pmatrix} \cos\theta & \sin\theta \\ -\sin\theta & \cos\theta \end{pmatrix}, \qquad \text{with} \quad 0 \leq \theta \leq \frac{\pi}{2}. \tag{3.4.26}$$

For an overview of the 2-neutrino oscillation probabilities in vacuum as in section 3.3.1 consider reading [GK07] from page 260 onwards, but the import result is the transition probability

$$P_{\nu_\alpha \to \nu_\beta}(L, E) = \sin^2 2\theta \sin^2\left(\frac{\Delta m^2 L}{4E}\right), \qquad (\alpha \neq \beta). \tag{3.4.27}$$

The essence of the next derivation is to see how this probability differs for 2-neutrino oscillations in matter.

Taking only flavours ν_e and ν_μ, and mass states ν_1 and ν_2, satisfying

$$\begin{pmatrix} \nu_e \\ \nu_\mu \end{pmatrix} = U \begin{pmatrix} \nu_1 \\ \nu_2 \end{pmatrix} = \begin{pmatrix} \cos\theta & \sin\theta \\ -\sin\theta & \cos\theta \end{pmatrix} \begin{pmatrix} \nu_1 \\ \nu_2 \end{pmatrix} \tag{3.4.28}$$

we can rewrite equation 3.4.23 as

$$\begin{aligned} i\frac{d}{dt}\begin{pmatrix}\psi_{ee}\\ \psi_{e\mu}\end{pmatrix} &= \frac{1}{2E}(U\mathbb{M}^2U^\dagger + \mathbb{A})\begin{pmatrix}\psi_{ee}\\ \psi_{e\mu}\end{pmatrix} \\ &= \frac{1}{4E}\begin{pmatrix}-\Delta m^2\cos 2\theta + A_{\mathrm{CC}} & \Delta m^2\sin 2\theta \\ \Delta m^2 \sin 2\theta & \Delta m^2\cos 2\theta - A_{\mathrm{CC}}\end{pmatrix}\begin{pmatrix}\psi_{ee}\\ \psi_{e\mu}\end{pmatrix}, \qquad (3.4.29)\end{aligned}$$

with the corresponding initial state

$$\begin{pmatrix}\psi_{ee}(0)\\ \psi_{e\mu}(0)\end{pmatrix} = \begin{pmatrix}1\\ 0\end{pmatrix}. \tag{3.4.30}$$

We can see that the potential A_{CC} affects the evolution of the amplitudes. The transition and survival probabilities are just the squares of the amplitudes, namely

$$P_{\nu_e\to\nu_\mu}(x) = |\psi_{e\mu}(x)|^2, \qquad P_{\nu_e\to\nu_e}(x) = |\psi_{ee}(x)|^2 = 1 - P_{\nu_e\to\nu_\mu}(x). \tag{3.4.31}$$

The mixing matrix U determines the mixing in vacuum, and this enters the equation as an effective flavour Hamiltonian $\mathcal{H}_F = \frac{1}{2E}(U\mathbb{M}U^\dagger + \mathbb{A})$, which is explicitly written out in 3.4.29. The resulting matrix is not diagonal, however, so we could aim to diagonalise it by the orthogonal transformation

$$U_M^T\mathcal{H}_F U_M = \mathcal{H}_M, \tag{3.4.32}$$

with

$$\mathcal{H}_M = \frac{1}{4E}\mathrm{diag}(-\Delta m_M^2, \Delta m_M^2). \tag{3.4.33}$$

The unitary matrix U_M that diagonalises the effective flavour Hamiltonian represents an effective mixing matrix, or equivalently, a rotation with an effective mixing angle, that depends on the explicit structure of $\mathcal{H}_F$. The diagonal matrix $\mathcal{H}_M$ can be interpreted as an effective square-mass difference matrix, also depending on the matter that it is considered in. Explicitly, they are given by

$$U_M = \begin{pmatrix}\cos\theta_M & \sin\theta_M \\ -\sin\theta_M & \cos\theta_M\end{pmatrix}, \tag{3.4.34}$$

$$\Delta m_M^2 = \sqrt{(\Delta m^2\cos 2\theta - A_{\mathrm{CC}})^2 + (\Delta m^2 \sin 2\theta)^2}, \tag{3.4.35}$$

with

$$\tan 2\theta_M = \frac{\tan 2\theta}{1 - \frac{A_{\mathrm{CC}}}{\Delta m^2\cos 2\theta}}. \tag{3.4.36}$$

In terms of our new parameters equation 3.4.29 becomes

$$i\frac{d}{dt}\begin{pmatrix}\psi_{ee}\\ \psi_{e\mu}\end{pmatrix} = U_M\mathcal{H}_M U_M^\dagger\begin{pmatrix}\psi_{ee}\\ \psi_{e\mu}\end{pmatrix} \tag{3.4.37}$$

$$= \frac{1}{4E}\begin{pmatrix}-\Delta m_M^2\cos 2\theta_M & \Delta m_M^2 \sin 2\theta_M \\ \Delta m_M^2\sin 2\theta_M & \Delta m_M^2\cos 2\theta_M\end{pmatrix}\begin{pmatrix}\psi_{ee}\\ \psi_{e\mu}\end{pmatrix}. \tag{3.4.38}$$

We will take a moment just to summarise where we are. In matter, electrons interact through the CC with electron neutrinos, and this brings about an effective potential A_{CC}. Adding this to our evolution equation, we obtain a new evolution governed by an effective Hamiltonian, which is given in equation 3.4.29. This new effective Hamiltonian can also be decomposed into a mixing matrix and a new diagonal Hamiltonian, just as how the original Hamiltonian had the form $\mathrm{diag}(E_1, E_2)$ in the mass eigenstate basis, only the new basis uses an effective mixing angle and an effective mass difference, θ_M and Δm_M. So what matter effectively does, is change the mixing angle θ such that the mass components of the flavour states change in their respective fraction. Not to be missed is that the expression for the effective mixing angle θ_M in 3.4.36 contains the presence of a resonance at

$$A^{\mathrm{R}}_{\mathrm{CC}} = \Delta m^2 \cos 2\theta, \tag{3.4.39}$$

or in terms of electron number density,

$$N^{\mathrm{R}}_e = \frac{\Delta m^2 \cos 2\theta}{2\sqrt{2} E G_F}. \tag{3.4.40}$$

At this resonance, the effective mixing angle becomes maximal, so θ_M becomes $\pi/4$. Note also that this induced a measurable difference in the propagation of neutrinos versus antineutrinos in a normal matter background. The potential V_{CC} flips sign for neutrinos versus antineutrinos (see 3.4.15), and the corresponding flip also occurs for $A_{\mathrm{CC}} \propto V_{\mathrm{CC}}$, implying that for antineutrinos the resonance ensues when $\cos 2\theta$ is negative, while for neutrinos it must be positive, which can only occur for $\theta > \frac{\pi}{4}$ or $\theta < \frac{\pi}{4}$ respectively.

So far, we have considered a general matter background, but an important nuance arises when we consider the difference in propagation through matter of constant or varying densities. In constant densities, the situation is fairly similar to the vacuum scenario, only with a different mixing angle. A new angle defines a new mass eigenstate basis, but since the new angle is equal everywhere throughout the matter, the mass eigenstates propagate independently from each other. The mass eigenstates are, in a sense, the propagation eigenstates. In matter of varying density, the mass eigenstates are no longer the propagation eigenstates due to the changing of the mixing angle θ_M along the path of propagation. This means that the different mass eigenstates are no longer completely decoupled. In order to formalise these ideas, we apply a basis transformation

$$\Psi_e \to \Phi_e \equiv U_M^T \Psi_e, \qquad \text{with} \quad \Phi_e = \begin{pmatrix} \varphi_{e1} \\ \varphi_{e2} \end{pmatrix}, \tag{3.4.41}$$

where the vector entries now denote the amplitude of the transition $\nu_1^M \to \nu_e$, and ν_1^M is a matter eigenstate for a specific corresponding matter density. We apply the basis transformation to evolution equation 3.4.38 to get

$$i\frac{d}{dx}\begin{pmatrix} \varphi_{e1} \\ \varphi_{e2} \end{pmatrix} = \frac{1}{4E}\begin{pmatrix} -\Delta m_M^2 & -4Ei\frac{d\theta_M}{dx} \\ 4Ei\frac{d\theta_M}{dx} & \Delta m_M^2 \end{pmatrix}\begin{pmatrix} \varphi_{e1} \\ \varphi_{e2} \end{pmatrix}. \tag{3.4.42}$$

The derivatives in the off-diagonal components are due to the derivative acting on $\Psi_e = U_M \Phi_e$, so an additional dU_M/dx adds to the right-hand side. It is precisely this derivative in which the earlier discussed behaviour is concealed, since for matter varying in density it induces a mixing between the different mass eigenstates. The initial condition is just the transformed initial condition from 3.4.30. We are now ready to compute the explicit probabilities for constant matter, matter of slowly varying density, and matter of rapidly varying density.

Constant matter density
This scenario is very similar to the vacuum scenario, only with a different mixing angle and effective mass difference. The transition probability is given by

$$P_{\nu_e \to \nu_\mu}(x) = \sin^2 2\theta_M \sin^2\left(\frac{\Delta m_M^2 x}{4E}\right), \tag{3.4.43}$$

with oscillation length

$$L_M^{\text{osc}} = \frac{4\pi E}{\Delta m_M^2}. \tag{3.4.44}$$

Slowly varying matter density

It is conventional to define the *adiabaticity parameter*

$$\gamma = \frac{\Delta m_M^2}{4E|d\theta_M/dx|}, \tag{3.4.45}$$

which measures the magnitude of the effective mass difference w.r.t. the magnitude of the variation of the effective mixing angle. Slowly varying matter density corresponds to a large adiabaticity parameter, or an adiabatic evolution. In this case the off-diagonal components of 3.4.42 can be neglected, and just the cumulative phase induced by the changing of Δm_M^2 should be added to the initial states, i.e.

$$\varphi_{e1}(x) = \exp\left(i\int_0^x \frac{\Delta m_M^2(x')}{4E}\,dx'\right)\varphi_{e1}(0), \tag{3.4.46}$$

$$\varphi_{e2}(x) = \exp\left(-i\int_0^x \frac{\Delta m_M^2(x')}{4E}\,dx'\right)\varphi_{e2}(0). \tag{3.4.47}$$

This leads to a survival probability

$$\begin{aligned} P^{\text{adiabatic}}_{\nu_e\to\nu_e}(x) =& \frac{1}{2} + \frac{1}{2}\cos 2\theta_M^{(i)}\cos 2\theta_M^{(f)} && (3.4.48)\\ &+ \frac{1}{2}\sin 2\theta_M^{(i)}\sin 2\theta_M^{(f)}\cos\left(\int_0^x \frac{\Delta m_M^2(x')}{2E}\,dx'\right), && (3.4.49) \end{aligned}$$

where $\theta_M^{(i)}$ is the effective mixing angle at the point of production, and $\theta_M^{(f)}$ at the point of detection. The vacuum probability is recovered by taking Δm_M^2 to be constant and removing it from the integral. Detectors on earth are practically in vacuum (from a neutrino perspective that is), and due to the large distances from the source, the rapid oscillation of the cosine tends to average out within the sensitivity range of detectors. This reduces the probability to

$$\begin{aligned} P^{\text{adiabatic}}_{\nu_e\to\nu_e}(x) =& \frac{1}{2} + \frac{1}{2}\cos 2\theta_M^{(i)}\cos 2\theta_M^{(f)} && (3.4.50)\\ =& \frac{1}{2} + \frac{1}{2}\cos 2\theta_M^{(i)}\cos 2\theta. && (3.4.51) \end{aligned}$$

Rapidly varying matter density

Rapidly varying matter corresponds to a low adiabaticity parameter, or a dominance in the off-diagonal components. A dominance of the off-diagonal terms leads to significant transitions between the effective mass eigenstates. While this does not immediately translate into a direct gain or loss of electron neutrinos, it enhances the oscillatory behaviour during propagation, allowing net flavour conversions to occur more efficiently along the path. The strongest violation of adiabaticity occurs at the smallest value of γ, and this point is called the point of maximum violation of adiabaticity (MVA). The MVA point can be calculated by expanding A_{CC} in equation 3.4.45, and one can reduce the condition to

$$\left.\frac{d^2\cos 2\theta_M}{dx^2}\right|_{x=x_{\mathrm{MVA}}}=0. \tag{3.4.52}$$

The resonance point had the condition

$$cos2\theta_M\Big|_{x=x_R}=0, \tag{3.4.53}$$

so they do not generally align, except for when the density varies linearly or when vacuum mixing is very small. In order to understand how the probabilities are affected, we must not only consider initial conditions for the state but also for the density. The most relevant example is the case where electron neutrinos are produced in a region of high density and then propagate towards a region of low density, crossing the resonance point, as is the case for solar neutrinos detected on Earth. The probabilities now get enhanced or reduced based on the transition rate from/to the other mass state, denoted by $A^R_{kj}=\langle\nu^M_j|\nu^M_k\rangle$, and a relative phase, as in the slowly-varying case, is still present. The full expression reads

$$\begin{aligned}\varphi_{e1}(x)=&\left[\cos\theta_M^{(i)}\exp\left(i\int_0^{x_R}\frac{\Delta m_M^2(x')}{4E}\,dx'\right)A^R_{11}\right.\\&\left.+\sin\theta_M^{(i)}\exp\left(-i\int_0^{x_R}\frac{\Delta m_M^2(x')}{4E}\,dx'\right)A^R_{21}\right]\exp\left(i\int_{x_R}^{x}\frac{\Delta m_M^2(x')}{4E}\,dx'\right),\end{aligned} \tag{3.4.54}$$

$$\begin{aligned}\varphi_{e2}(x)=&\left[\cos\theta_M^{(i)}\exp\left(i\int_0^{x_R}\frac{\Delta m_M^2(x')}{4E}\,dx'\right)A^R_{12}\right.\\&\left.+\sin\theta_M^{(i)}\exp\left(-i\int_0^{x_R}\frac{\Delta m_M^2(x')}{4E}\,dx'\right)A^R_{22}\right]\exp\left(-i\int_{x_R}^{x}\frac{\Delta m_M^2(x')}{4E}\,dx'\right).\end{aligned} \tag{3.4.55}$$

The phases are separated at the resonance point x_R, reflecting the evolution before and after the possible non-adiabatic transition. Just as with the non-adiabatic probability, for large distances, the rapid oscillation induces an elimination of the phases, and the probability averages out to

$$\begin{aligned}\overline{P}_{\nu_e\to\nu_e}=&\cos^2\theta\cos^2\theta_M^{(i)}|A^R_{11}|^2+\cos^2\theta\sin^2\theta_M^{(i)}|A^R_{21}|^2\\&+\sin^2\theta\cos^2\theta_M^{(i)}|A^R_{12}|^2+\sin^2\theta\sin^2\theta_M^{(i)}|A^R_{22}|^2.\end{aligned} \tag{3.4.56}$$

This expression no longer depends on the distance from the source to the detector, but just on the transition amplitudes at the resonance point. By defining

$$P_c\equiv|A^{\mathrm{R}}_{21}|^2=|A^{\mathrm{R}}_{12}|^2=1-|A^{\mathrm{R}}_{11}|^2=1-|A^{\mathrm{R}}_{22}|^2, \tag{3.4.57}$$

we find a final expression called the Parke formula,

$$\overline{P}_{\nu_e\to\nu_e}=\frac{1}{2}+\left(\frac{1}{2}-P_c\right)\cos 2\theta_M^{(i)}\cos 2\theta. \tag{3.4.58}$$

The next and final task for a true probability would be to calculate the transition probability at the resonance, P_c, but we will refrain from lengthening the discussion. There are many relevant density profiles, and thus many different corresponding expressions for P_c. For the Sun, a good approximation is

$$P_c=\exp\left[-\frac{\pi}{2}\frac{\Delta m^2\sin^2 2\theta}{2E\cos 2\theta|\frac{\partial}{\partial x}\ln N_e(x_R)|}(1-\tan^2\theta)\right]. \tag{3.4.59}$$

The Parke formula proves especially useful in the context of solar neutrinos, which are produced in the core of the Sun, where matter effects are significant. In this high-density environment, the effective mixing angle $\theta_M^{(i)}$ can differ a lot from its vacuum counterpart, and the MSW resonance may be crossed as neutrinos propagate outward. Depending on the energy of the neutrinos and the specific values of the mixing parameters, the resonance crossing can be either adiabatic or non-adiabatic, leading to different flavour transition outcomes. For instance, in the experimentally established Large Mixing Angle (LMA) region, the resonance is crossed adiabatically for most solar neutrino energies, resulting in an efficient and energy-dependent flavour conversion. On the other hand, for Small Mixing Angle (SMA) solutions, the transition is often non-adiabatic, yielding a sharply energy-dependent survival probability. The order of magnitude of the mixing angles was not known at the time of the first experiments, but the SMA solution is currently no longer considered an option.

3.5 EXTENSION TO THREE-NEUTRINO MIXING

Although many qualitative features of neutrino oscillations can be described by a two-flavour framework, the physical reality involves mixing among all three known neutrino flavours. In the three-neutrino scheme, the flavour states are related to the mass eigenstates via the PMNS matrix, as we saw before, which can be parametrized by three mixing angles $(\theta_{12}, \theta_{23}, \theta_{13})$ and a CP-violating phase δ_{CP}. In some scenarios, the 3-neutrino mixing can be fully modelled by a two-mixing case, yet this does not always hold. It is the goal of this section to understand the particular case of three-neutrino mixing, and when it is or is not reducible to a two-neutrino model, without going deep into the derivation. First, some general n-neutrino mixing results will be discussed, then 3-neutrino mixing in vacuum, and finally the most realistic case of 3-neutrino mixing in matter.

3.5.1 IMPORTANT RESULTS FROM n-NEUTRINO MIXING

There are two important and relevant limits from a general mixing scenario of n neutrinos with mass eigenstates $\nu_1, \nu_2, \ldots, \nu_N$. The first that will be considered is called a *large* Δm^2 *dominance*, which holds when there are two groups of mass eigenstates with small squared-mass differences, with a large squared-mass difference between the groups, as described in image 3.5.1. If one considers equation 3.3.10 , one sees that a large squared-mass difference induces a more rapid oscillation in the transition probability with respect to a small difference. This implies that at short distances, the oscillation probability between any flavour state becomes such that only the large square-mass differences contribute to the sum. If we consider the left-hand case of figure 3.5.1, so we say that states $\nu_1, \ldots, \nu_{N_A}$ are light and $\nu_{N_A+1}, \ldots, \nu_N$ are heavy, but with small mutual square-mass differences within both groups, we can approximate all large square-mass differences as

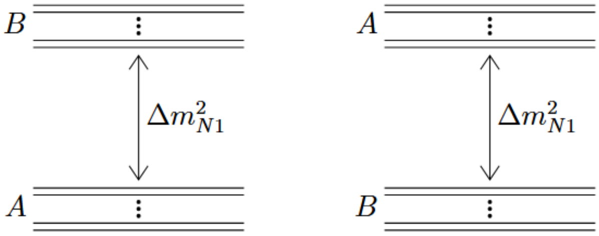

Figure 3.5.1: Schematic description of large Δm^2 dominance between two groups of mass eigenvalues A and B, taken from [GK07].

Δm^2_{N1} and write the probability as

$$P^{\text{eff}}_{\nu_\alpha \to \nu_\beta}(L,E) = \left| \sum_{k \le N_A} U^*_{\alpha k} U_{\beta k} + \exp\left(-i \frac{\Delta m^2_{N1} L}{2E} \right) \sum_{k > N_A} U^*_{\alpha k} U_{\beta k} \right|^2, \tag{3.5.1}$$

where we neglected the phase of the small square-mass differences. Note that this equation only holds for experiments where the length and energy are such that both

$$\frac{|\Delta m^2_{N1}|}{2} \left\langle \frac{L}{E} \right\rangle \sim \pi \tag{3.5.2}$$

and

$$\frac{|\Delta m^2_{kj}|}{2} \left\langle \frac{L}{E} \right\rangle \ll \pi \quad \text{for} \quad k,j \le N_A \quad \text{or} \quad k,j > N_A. \tag{3.5.3}$$

Using unitarity relations of the mixing matrix, one is able to rewrite the transition probabilities in the same form as a two-neutrino mixing scenario with an effective mixing angle, i.e.

$$P^{\text{eff}}_{\nu_\alpha \to \nu_\beta}(L,E) = \sin^2(2\theta^{\text{eff}}_{\alpha\beta}) \sin^2\left(\frac{\Delta m^2_{N1} L}{4E} \right) \quad \text{for} \quad \alpha \neq \beta, \tag{3.5.4}$$

with the effective mixing angle defined such that

$$\sin^2 2\theta^{\text{eff}}_{\alpha\beta} = 4 \left| \sum_k U^*_{\alpha k} U_{\beta k} \right|^2. \tag{3.5.5}$$

The survival probability is given by

$$P^{\text{eff}}_{\nu_\alpha \to \nu_\alpha}(L,E) = 1 - \sin^2 2\theta^{\text{eff}}_{\alpha\alpha} \sin^2\left(\frac{\Delta m^2_{N1} L}{4E} \right), \tag{3.5.6}$$

with an effective mixing angle defined as

$$\sin^2 2\theta^{\text{eff}}_{\alpha\alpha} = 4 \left(\sum_k |U_{\alpha k}|^2 \right) \left(1 - \sum_k |U_{\alpha k}|^2 \right). \tag{3.5.7}$$

If there is only a single independent large squared-mass difference and all other separations are small, the effective mixing angles for transition and survival probabilities respectively reduce to

$$\sin^2 2\theta^{\text{eff}}_{\alpha\beta} = 4|U_{\alpha N}|^2 |U_{\beta N}|^2 \quad \text{and} \quad \sin^2 2\theta^{\text{eff}}_{\alpha\alpha} = 4|U_{\alpha N}|^2 (1 - |U_{\alpha N}|^2). \tag{3.5.8}$$

Note that one is not able to measure CP violation with experiments that are only sensitive to a large Δm^2, as all probabilities are proportional to real values only, and thus can not accommodate a complex phase.

The other interesting limit occurs when there is a squared-mass separation scale which is much smaller than the large separation, commonly called a *active small* Δm^2. In this case, the oscillation in 3.3.10 occurs much slower for the small separation scale, making it effective only on relatively large distances. At such distances, the rapid oscillation induced by the large squared-mass difference will have averaged out, thus allowing only for a precise measurement of the smaller mass difference. We consider three groups of eigenvalues: $\nu_1, \nu_2, \dots \nu_{N_{A_1}} \in A_1, \nu_{A_1+1}, \dots, \nu_{N_A} \in A_2$ and $\nu_{N_A+1}, \dots, \nu_N \in B$, of which the first two groups are respectively separated by a small scale and the third group B is largely separated from them both. The various possible corresponding hierarchies are presented in 3.5.2. One can isolate the mass separation between groups A_1 and A_2 in experiments that are sensitive to $\Delta m^2_{N_A 1}$, so for lengths such that

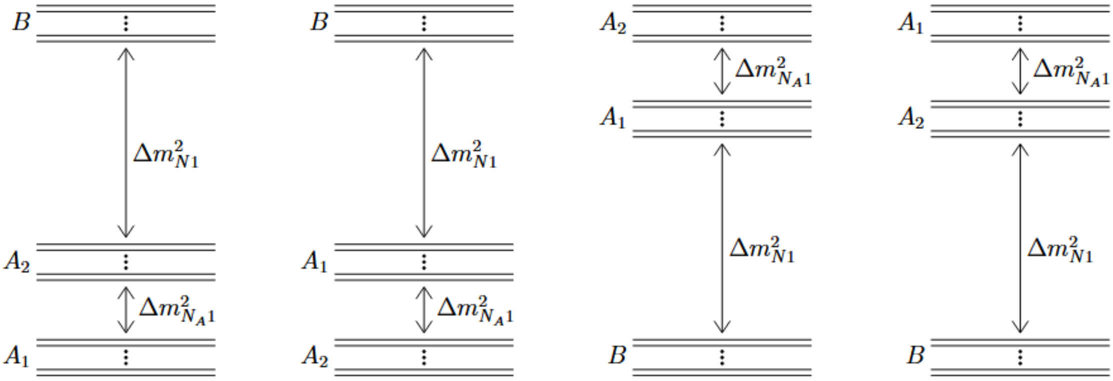

Figure 3.5.2: Schematic description of a active small Δm^2 scenario, with three groups of mass eigenvalues $A_1,\ A_2$ and B, taken from [GK07].

$$\frac{|\Delta m^2_{N_A 1}|}{2}\left\langle\frac{L}{E}\right\rangle \sim \pi, \tag{3.5.9}$$

but for k, j within the same groups we must have

$$\frac{|\Delta m^2_{kj}|}{2}\left\langle\frac{L}{E}\right\rangle \ll \pi \tag{3.5.10}$$

and for k, j in different groups A_i and B

$$\frac{|\Delta m^2_{kj}|}{2}\left\langle\frac{L}{E}\right\rangle \gg \pi. \tag{3.5.11}$$

Note that we do not require that the experiment is sensitive to the smallest mass scale, but that the experiment is sensitive to a unique scale which is much smaller than the largest scale and much larger than the smallest scale. In this case, the survival probability can be written like a two-neutrino scenario, namely

$$P^{\text{eff}}_{\nu_\alpha\to\nu_\alpha}(L,E) = \left(1 - \sum_{k>N_A}|U_{\alpha k}|^2\right)^2 P^{(N_A,1)}_{\nu_\alpha\to\nu_\alpha}(L,E) + \left(\sum_{k>N_A}|U_{\alpha k}|^2\right)^2, \tag{3.5.12}$$

with

$$P^{(N_A,1)}_{\nu_\alpha\to\nu_\alpha}(L,E) = 1 - 4\frac{\left(\sum_{k\le N_{A_1}}|U_{\alpha k}|^2\right)\left(\sum_{k=N_{A_1}+1}^{N_A}|U_{\alpha k}|^2\right)}{\left(\sum_{k=1}^{N_A}|U_{\alpha k}|^2\right)^2}\sin^2\left(\frac{\Delta m^2_{N_A 1}L}{4E}\right). \tag{3.5.13}$$

In terms of an effective mixing angle

$$\sin^2 2\theta^{\text{eff}}_{\alpha\alpha} = 4\frac{\left(\sum_{k\leq N_{A_1}} |U_{\alpha k}|^2\right)\left(\sum_{k=N_{A_1}+1}^{N_A} |U_{\alpha k}|^2\right)}{\left(\sum_{k=1}^{N_A} |U_{\alpha k}|^2\right)^2} \tag{3.5.14}$$

this becomes manifest as

$$P^{(N_A,1)}_{\nu_\alpha\to\nu_\alpha}(L,E) = 1 - \sin^2 2\theta^{\text{eff}}_{\alpha\alpha} \sin^2\left(\frac{\Delta m^2_{N_A 1} L}{4E}\right). \tag{3.5.15}$$

The transition probability has a slightly more complex form, given by

$$\begin{aligned} P^{\text{eff}}_{\nu_\alpha\to\nu_\beta}(L,E) =& 4\left|\sum_{k\leq N_{A_1}} U^*_{\alpha k} U_{\beta k}\right|^2 \sin^2\left(\frac{\Delta m^2_{N_A 1} L}{4E}\right) \\ &+ 4\left(\sum_{j\leq N_{A_1}}\sum_{k>N_A} \mathfrak{Re}\left[U^*_{\alpha k} U_{\beta k} U_{\alpha j} U^*_{\beta j}\right]\right) \sin^2\left(\frac{\Delta m^2_{N_A 1} L}{4E}\right) \\ &+ 2\left(\sum_{j\leq N_{A_1}}\sum_{k>N_A} \mathfrak{Im}\left[U^*_{\alpha k} U_{\beta k} U_{\alpha j} U^*_{\beta j}\right]\right) \sin\left(\frac{\Delta m^2_{N_A 1} L}{2E}\right) + 2\left|\sum_{k>N_A} U^*_{\alpha k} U_{\beta k}\right|^2 . \end{aligned} \tag{3.5.16}$$

The first term has the same form of equation 3.5.4 and describes the mixing of flavour states with neutrinos from the groups A, and the final constant term describes the mixing with neutrinos from group B. The second and third terms describe mixing with both groups, and it is generally not possible to explicitly separate the mixing with various groups due to the phases present in these terms. Although it seems like the expression is almost more complex than the original equation 3.3.10, it should be noted that this formulation only depends on five parameters for n neutrinos. The derivation of the equations above is here omitted, but is laid out pedagogically in chapter 7.8 of [GK07].

3.5.2 3-Neutrino Mixing in Vacuum

In the realistic case of three (active) neutrinos, there are only two independent square-mass differences, Δm^2_{21} and Δm^2_{31}. It has been discussed that experiments measuring short neutrino propagation distances are sensitive to rapid oscillations induced by a large square-mass difference, while long-distance measurements are sensitive to a small separation, if such a distinction is present in the mass ordering. Experimentally, solar neutrino oscillations have indeed measured a small mass difference independent from a larger square-mass difference seen in atmospheric or short baseline (SBL) neutrino experiments, leading to an observed hierarchy [Ada+08; Est+20]

$$\Delta m^2_{\text{SOL}} \ll \Delta m^2_{\text{ATM}}. \tag{3.5.17}$$

By (arbitrarily) labelling the masses as $\Delta m^2_{\text{SOL}} = \Delta m^2_{21}$ and $\Delta m^2_{ATM} = |\Delta m_{31}|^2$, we are able to construct a hierarchy where ν_3 is much heavier than ν_1 and ν_2 called the *normal hierarchy*, or an ordering such that ν_3 is much lighter called the *inverted hierarchy*, both described in figure 3.5.3. Note that both hierarchies accommodate for the large Δm^2 dominance and the active small Δm^2, described in the section above, which allows us to apply the corresponding probability expressions.

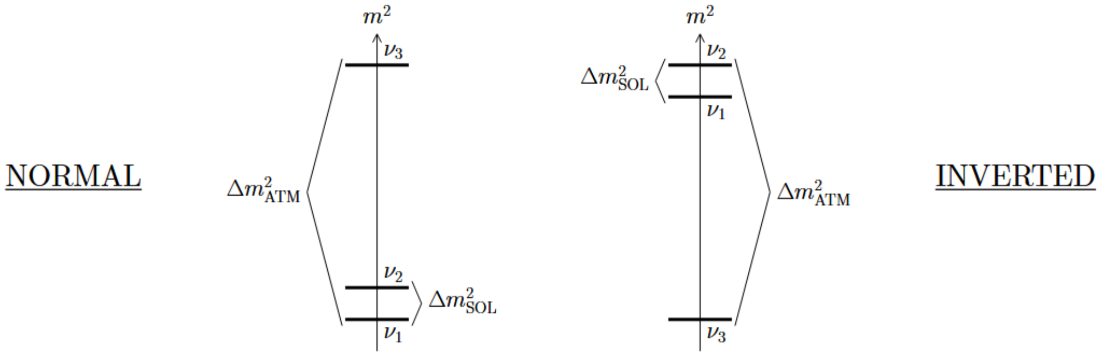

Figure 3.5.3: Schematic representation of the two hierarchies compatible with the measured values of $\Delta m^2_{\rm ATM}$ and $\Delta m^2_{\rm SOL}$ [Est+20; Ada+08]. Image taken from [GK07].

Experiments measuring relatively short propagation distances, like atmospheric experiments measuring energies such that

$$\frac{|\Delta m^2_{31}|}{2}\left\langle \frac{L}{E} \right\rangle \sim \pi \tag{3.5.18}$$

are sensitive only to Δm^2_{31}. This is just the large Δm^2 dominance case with $A = \{\nu_1, \nu_2\}$ and $B = \{\nu_2\}$, so we can effectively measure the oscillations as two-neutrino transition probabilities

$$P^{\rm eff}_{\nu_\alpha\to\nu_\beta}(L,E) = \sin^2(2\theta^{\rm eff}_{\alpha\beta})\sin^2\left(\frac{\Delta m^2_{31}L}{4E}\right), \tag{3.5.19}$$

or survival probabilities

$$P^{\rm eff}_{\nu_\alpha\to\nu_\alpha}(L,E) = 1 - \sin^2(2\theta^{\rm eff}_{\alpha\alpha})\sin^2\left(\frac{\Delta m^2_{31}L}{4E}\right), \tag{3.5.20}$$

with respective effective mixing angles

$$\sin^2 2\theta^{\rm eff}_{\alpha\beta} = 4|U_{\alpha3}|^2|U_{\beta3}|^2 \quad \text{and} \quad \sin^2 2\theta^{\rm eff}_{\alpha\alpha} = 4|U_{\alpha3}|^2(1-|U_{\alpha3}|^2). \tag{3.5.21}$$

On the other hand, through experiments probing longer distances and energies with

$$\frac{|\Delta m^2_{21}|}{2}\left\langle \frac{L}{E} \right\rangle \sim \pi, \tag{3.5.22}$$

one is able to isolate Δm^2_{21}. This is just the active small Δm^2 scenario, with $\nu_1 \in A_1$, $\nu_2 \in A_2$, and $\nu_3 \in B$, so we can again apply our earlier found probabilities. The survival probabilities for both neutrinos and antineutrinos are given by

$$P^{\rm eff}_{\nu_\alpha\to\nu_\alpha}(L,E) = \left(1-|U_{\alpha3}|^2\right)^2 P^{(1,2)}_{\nu_\alpha\to\nu_\alpha}(L,E) + |U_{\alpha3}|^4, \tag{3.5.23}$$

with

$$P^{(1,2)}_{\nu_\alpha\to\nu_\alpha}(L,E) = 1 - \sin^2 2\theta^{\rm eff}_{\alpha\alpha}\sin^2\left(\frac{\Delta m^2_{21}L}{4E}\right) \tag{3.5.24}$$

and the effective mixing angle given as

$$\sin^2 2\theta^{\text{eff}}_{\alpha\alpha} = 4\frac{|U_{\alpha 1}|^2|U_{\alpha 2}|^2}{\left(|U_{\alpha 1}|^2 + |U_{\alpha 2}|^2\right)^2}. \tag{3.5.25}$$

The small active Δm^2 limit transition amplitude is also easily restricted to three flavours, but it is, in reality, never used since solar transition experiments are not able to distinguish between ν_μ and ν_τ, so it will not be given here. The survival probability is, however, very relevant for solar neutrino experiments. If one studies the additional limit where one of the mixing angles, say θ_{13}, is negligibly small, one can even further simplify the probabilities. This limit is called *bilarge mixing*, and is in fact a relevant limit due to the measured smallness of θ_{13} in Daya Bay, at $\sin^2 2\theta_{13} = 0.0833 \pm 0.0022$ [Li24]. A complete list of probabilities is given in [GK07], but for the experiments sensitive to a large Δm^2_{31} one finally finds

$$P^{\text{eff}}_{\nu_\mu \to \nu_\mu}(L, E) = 1 - \sin^2 2\vartheta_{23} \sin^2\left(\frac{\Delta m^2_{31} L}{4E}\right), \tag{3.5.26}$$

$$P^{\text{eff}}_{\nu_\tau \to \nu_\tau}(L, E) = 1 - \sin^2 2\vartheta_{23} \sin^2\left(\frac{\Delta m^2_{31} L}{4E}\right), \tag{3.5.27}$$

$$P^{\text{eff}}_{\nu_\mu \to \nu_\tau}(L, E) = \sin^2 2\vartheta_{23} \sin^2\left(\frac{\Delta m^2_{31} L}{4E}\right), \tag{3.5.28}$$

which are now only dependent on two parameters, and allows for a measurement of ϑ_{23} and Δm^2_{31}. For experiments sensitive only to the small square-mass difference Δm^2_{21}, the probabilities reduce to

$$P^{\text{eff}}_{\nu_\mu \to \nu_\mu}(L, E) = 1 - \frac{1}{2}\sin^2 2\vartheta_{23} - \sin^2 2\vartheta_{12}\, c^4_{23} \sin^2\left(\frac{\Delta m^2_{21} L}{4E}\right), \tag{3.5.29}$$

$$P^{\text{eff}}_{\nu_\tau \to \nu_\tau}(L, E) = 1 - \frac{1}{2}\sin^2 2\vartheta_{23} - \sin^2 2\vartheta_{12}\, s^4_{23} \sin^2\left(\frac{\Delta m^2_{21} L}{4E}\right), \tag{3.5.30}$$

$$P^{\text{eff}}_{\nu_\mu \to \nu_\tau}(L, E) = \frac{1}{2}\sin^2 2\vartheta_{23} - \frac{1}{4}\sin^2 2\vartheta_{12} \sin^2 2\vartheta_{23} \sin^2\left(\frac{\Delta m^2_{21} L}{4E}\right). \tag{3.5.31}$$

Another 3-neutrino phenomenon that is worth mentioning, is that the quartic products in 3.3.10 become all the same up to a sign difference. Defining

$$\mathfrak{Im}[U^*_{\alpha k} U_{\beta k} U_{\alpha j} U^*_{\beta j}] \equiv s_{\alpha\beta;kj} J \tag{3.5.32}$$

with $s_{\alpha\beta;kj} = \pm 1$ and J the Jarlskog invariant, equation 3.3.14 can then be rewritten as

$$\begin{aligned} P_{\nu_\alpha \to \nu_\beta}(L, E) = \delta_{\alpha\beta} &- 4\sum_{k>j} \mathfrak{Re}[U^*_{\alpha k} U_{\beta k} U_{\alpha j} U^*_{\beta j}] \sin^2\left(\frac{\Delta m^2_{kj} L}{4E}\right) \\ &+ 2J \sum_{k>j} s_{\alpha\beta:kj} \sin\left(\frac{\Delta m^2_{kj} L}{2E}\right). \end{aligned} \tag{3.5.33}$$

The CP violating amplitude is then seen to be

$$A^{\text{CP}}_{\alpha\beta}(L, E) = 4J \sum_{k>j} s_{\alpha\beta:kj} \sin\left(\frac{\Delta m^2_{kj} L}{2E}\right), \tag{3.5.34}$$

which also implies that all CP violating amplitudes are equal up to a sign.

3.5.3 3-NEUTRINO MIXING IN MATTER

The neutrino oscillations in matter were discussed in 3.4 and contained two major components: the derivation of the evolution equation leading to 3.4.23, and its solutions for various matter environments. The evolution equation holds for any number of massive neutrinos, but the solutions were only performed for the simple case of two massive states. The general solution to the evolution equation is complicated and is often done numerically, yet for the case of three neutrinos with the limits and hierarchy from figure 3.5.3 we can obtain some useful analytic results. We will first massage the evolution equation to isolate certain parameters, and then we will solve it in the large and small Δm^2 limits.

Recall that the mixing matrix U diagonalizes the square-mass matrix such that $\mathcal{M}^2 = U\mathbb{M}^2U^\dagger$. For a rotation matrix R^{ij} that performs a rotation in the $i-j$ plane, a matrix $D^i(\eta_{ij})$ containing a complex phase $e^{i\eta_{ij}}$ on the i'th component of the diagonal, and a composite matrix

$$W^{ij}(\theta_{ij},\eta_{ij}) = D^i(\eta_{ij})R^{ij}D^{i\dagger}(\eta_{ij}) = D^{j\dagger}(\eta_{ij})R^{ij}D^j(\eta_{ij}),$$

one is able to write the mixing matrix in terms components of the standard parametrization

$$U = R^{23}W^{13}R^{12}. \tag{3.5.35}$$

The rotation matrix R^{23} commutes with the matter potential matrix $\mathbb{A}$, since ν_μ and ν_τ have a similar potential, so we can rewrite the amplitude evolution equation like

$$i\frac{\mathrm{d}}{\mathrm{d}x}\Psi_\alpha = \frac{1}{2E}R^{23}\left(W^{13}R^{12}\mathbb{M}^2R^{12\dagger}W^{13\dagger} + \mathbb{A}\right)R^{23\dagger}\Psi_\alpha. \tag{3.5.36}$$

Performing a basis rotation $\tilde{\Psi} \equiv R^{23^\dagger}\Psi$ we obtain a basis which is neither the flavour nor the mass basis, but for which the evolution equation simplifies to

$$i\frac{\mathrm{d}}{\mathrm{d}x}\tilde{\Psi}_\alpha = \frac{1}{2E}\left(W^{13}R^{12}\mathbb{M}^2R^{12\dagger}W^{13\dagger} + \mathbb{A}\right)\tilde{\Psi}_\alpha. \tag{3.5.37}$$

Note that the evolution equation no longer depends on ϑ_{23}, which implies that it is not affected by the matter, but that the original amplitudes still remain dependent. The equation is now in a form that is suitable for further evaluation.

Consider first the oscillation during short distance propagation, thus being sensitive to the large mass splitting Δm^2_{31}. We find that the square-mass matrix can be approximated by

$$\mathbb{M}^2 \simeq \mathrm{diag}(0, 0, \Delta m^2_{31}), \tag{3.5.38}$$

which implies in particular that it commutes with R^{12}, removing it from the evolution equation. Redefining $\tilde{\Psi}_\alpha \to D^1(-\delta_{13})\tilde{\Psi}_\alpha$, we can also remove the phase matrix in W^{13}, so the new evolution equation becomes

$$i\frac{\mathrm{d}}{\mathrm{d}x}\tilde{\Psi}_\alpha = \frac{1}{2E}\left(R^{13}\mathbb{M}^2R^{13^\dagger} + \mathbb{A}\right)\tilde{\Psi}_\alpha. \tag{3.5.39}$$

Note that the evolution only depends on the mixing angle ϑ_{13}, and that the CP violating phase no longer affects the system. This means, in particular, that also for matter oscillations the experiments only sensitive to one square-mass difference can not measure CP violation. We can write out the equation in full form,

$$i\frac{\mathrm{d}}{\mathrm{d}x}\begin{pmatrix}\tilde{\psi}_{\alpha 1}\\ \tilde{\psi}_{\alpha 2}\\ \tilde{\psi}_{\alpha 3}\end{pmatrix}=\frac{1}{2E}\begin{pmatrix}s_{13}^2\Delta m_{31}^2+A_{\mathrm{CC}} & 0 & c_{13}s_{13}\Delta m_{31}^2\\ 0 & 0 & 0\\ c_{13}s_{13}\Delta m_{31}^2 & 0 & c_{13}^2\Delta m_{31}^2\end{pmatrix}\begin{pmatrix}\tilde{\psi}_{\alpha 1}\\ \tilde{\psi}_{\alpha 2}\\ \tilde{\psi}_{\alpha 3}\end{pmatrix}, \tag{3.5.40}$$

from which it can be clearly seen that the second amplitude is left unaffected. By excluding this amplitude from the equation, and by removing a common phase as we did for the MSW effect treatment, we obtain

$$i\frac{\mathrm{d}}{\mathrm{d}x}\begin{pmatrix}\tilde{\psi}_{\alpha 1}\\ \tilde{\psi}_{\alpha 3}\end{pmatrix}=\frac{1}{4E}\begin{pmatrix}-\Delta m_{31}^2\cos 2\vartheta_{13}+A_{\mathrm{CC}} & \Delta m_{31}^2\sin 2\vartheta_{13}\\ \Delta m_{31}^2\sin 2\vartheta_{13} & \Delta m_{31}^2\cos 2\vartheta_{13}-A_{\mathrm{CC}}\end{pmatrix}\begin{pmatrix}\tilde{\psi}_{\alpha 1}\\ \tilde{\psi}_{\alpha 3}\end{pmatrix}, \tag{3.5.41}$$

which looks similar to the two neutrino scenario for the 1 – 3 sector. We can now diagonalise the matrix using an effective mixing angle ϑ_{13}^M, with

$$\tan 2\vartheta_{13}^M=\frac{\tan 2\vartheta_{13}}{1-\frac{A_{\mathrm{CC}}}{\Delta m_{31}^2\cos 2\vartheta_{13}}}, \tag{3.5.42}$$

which contains a resonance at

$$A_{\mathrm{CC}}^R=\Delta m_{31}^2\cos 2\vartheta_{13}, \tag{3.5.43}$$

and an effective squared-mass difference

$$\Delta m_{M31}^2=\sqrt{(\Delta m_{31}^2\cos 2\vartheta_{13}-A_{\mathrm{CC}})^2+(\Delta m_{31}^2\sin 2\vartheta_{31})^2}. \tag{3.5.44}$$

The treatment of rapidly varying matter densities, or smoothly varying matter densities in general, is not very relevant for the short propagation length assumption, so it will be omitted here. A somewhat more relevant approximation on earth is the *slab approximation*, treating matter as separate slabs of different but constant matter density, of which a discussion can be found in Chapter 9.4 of [GK07]. The probabilities for a constant matter density are still relevant, however, and we will treat this setting now. Defining R_M^{ij} as a rotation in the $i-j$ plane using the effective mixing angle, and the effective square-mass differences $m_{M3}^2=\Delta m_{M32}^2$, $m_{M1}^2=\Delta m_{M21}^2$, the results from the section on large Δm^2 dominance give

$$\begin{aligned}P_{\nu_\alpha\to\nu_\beta}^{\mathrm{eff}}=&4U_{\mathrm{M}\alpha 3}^2U_{\mathrm{M}\beta 3}^2S_{31}^2-4U_{\mathrm{M}\alpha 1}U_{\mathrm{M}\beta 1}U_{\mathrm{M}\alpha 2}U_{\mathrm{M}\beta 2}S_1^2\\ &-4U_{\mathrm{M}\alpha 2}U_{\mathrm{M}\beta 2}U_{\mathrm{M}\alpha 3}U_{\mathrm{M}\beta 3}(S_3^2-S_{31}^2),\end{aligned} \tag{3.5.45}$$

$$\begin{aligned}P_{\nu_\alpha\to\nu_\alpha}^{\mathrm{eff}}=&1-4U_{\mathrm{M}\alpha 3}^2(1-U_{\mathrm{M}\alpha 3}^2)S_{31}^2-4U_{\mathrm{M}\alpha 1}U_{\mathrm{M}\alpha 2}S_1^2\\ &-4U_{M\alpha 2}^2U_{M\alpha 3}^2(S_3^2-S_{31}^2),\end{aligned} \tag{3.5.46}$$

where

$$S_1^2\equiv\sin^2\left(\frac{\Delta m_{M1}^2L}{4E}\right),\quad S_3^2\equiv\sin^2\left(\frac{m_{M3}^2L}{4E}\right),\quad S_{31}^2\equiv\sin^2\left(\frac{\Delta m_{M31}^2L}{4E}\right). \tag{3.5.47}$$

When $U_{M\alpha 2}=0$, which holds for the electron, the probabilities reduce to the two-neutrino scenario form, but with the effective mixing angle depending on the matter mixing angle:

$$P_{\nu_e\to\nu_e}^{\mathrm{eff}}=1-\sin^2 2\vartheta_{ee}^{\mathrm{eff}}S_{31}^2,\quad P_{\nu_e\to\nu_\beta}^{\mathrm{eff}}=\sin^2 2\vartheta_{e\beta}^{\mathrm{eff}}S_{31}^2\quad(\beta=\mu,\tau), \tag{3.5.48}$$

with

$$\sin^2 2\vartheta_{ee}^{\text{eff}} = \sin^2 2\vartheta_{13}^{M}, \tag{3.5.49}$$

$$\sin^2 2\vartheta_{e\mu}^{\text{eff}} = \sin^2 2\vartheta_{23} \sin^2 \vartheta_{13}^{M}, \tag{3.5.50}$$

$$\sin^2 2\vartheta_{e\tau}^{\text{eff}} = \sin^2 2\vartheta_{23} \cos^2 \vartheta_{13}^{M}. \tag{3.5.51}$$

There is a distinct feature of the resonance found for the 1-3 sector, equation 3.5.43. Since A_{CC} is positive, we can only have a resonance if the right-hand side is also positive. Since it was found that the mixing angle θ_{13} is significantly smaller than the other angles, at $\sin^2 2\theta_{13} = 0.0833 \pm 0.0022$ [Li24], we can say that $\cos 2\vartheta_{13}$ is positive. This implies then that the observation of a resonance for neutrinos travelling through matter would correspond to an observation of $\Delta m_{31}^2 > 0$ and thus that neutrino masses are ordered according to the normal hierarchy. Conversely, if we find a resonance for antineutrinos travelling through normal matter, we must have $\Delta m_{31}^2 < 0$, corresponding to the inverted hierarchy.

For the case of a small active Δm_{21}^2 we can repeat the same procedure to arrive at the evolution equation

$$i\frac{\mathrm{d}}{\mathrm{d}x}\hat{\Psi}_\alpha = \frac{1}{2E}(R^{12}\mathbb{M}^2 R^{12^\dagger} + W^{13^\dagger}\mathbb{A}W^{13})\hat{\Psi} \equiv \frac{1}{2E}\hat{\mathbb{M}}^2\hat{\Psi}_\alpha, \tag{3.5.52}$$

where $\hat{\Psi}_\alpha = W^{13^\dagger} R^{23^\dagger}\Psi_\alpha$. The explicit expression of $\hat{\mathbb{M}}^2$ is given by

$$\hat{\mathbb{M}}^2 = \begin{pmatrix} s_{12}^2\Delta m_{21}^2 + c_{13}^2 A_{\text{CC}} & c_{12}s_{12}\Delta m_{21}^2 & -c_{13}s_{13}e^{-i\delta_{13}}A_{\text{CC}} \\ c_{12}s_{12}\Delta m_{21}^2 & c_{12}^2\Delta m_{21}^2 & 0 \\ -c_{13}s_{13}e^{i\delta_{13}}A_{\text{CC}} & 0 & \Delta m_{31}^2 + s_{13}^2 A_{\text{CC}} \end{pmatrix}. \tag{3.5.53}$$

Since $\Delta m_{31}^2 \gg \Delta m_{21}^2$, the heaviest eigenvalue of $\hat{\mathbb{M}}^2$ can be approximated as $\hat{m}_{M3}^2 = \Delta m_{31}^2$. This implies that the amplitude evolution of $\hat{\psi}_{\alpha 3}$ is approximately decoupled from the rest of the amplitudes. Its contribution to the probability will be only proportional to the elements of the mixing matrix, as the oscillatory term will average out, i.e.

$$P_{\nu_\alpha\to\nu_\beta}^{\text{eff}}(x) \supset |U_{\alpha 3}|^2|U_{\beta 3}|^2. \tag{3.5.54}$$

The evolution of the other amplitudes can thus be described independently using the top-left 2×2 block of the matrix, which after the removal of a common phase looks like

$$\hat{\mathbb{M}}_{2\times 2}^2 = \frac{1}{2}\begin{pmatrix} -\cos 2\vartheta_{12}\Delta m_{21}^2 + c_{13}^2 A_{\text{CC}} & \sin 2\vartheta_{12}\Delta m_{21}^2 \\ \sin 2\vartheta_{21}\Delta m_{21}^2 & \cos 2\vartheta_{12}\Delta m_{21}^2 - c_{13}^2 A_{\text{CC}} \end{pmatrix}. \tag{3.5.55}$$

Solving the evolution equation in the limit of decoupling now becomes equal to section 3.4.3, and we find the effective mixing angle

$$\tan 2\vartheta_{12}^{M} = \frac{\tan 2\vartheta_{12}}{1 - \frac{\cos^2\vartheta_{13}A_{\text{CC}}}{\cos 2\vartheta_{12}\Delta m^2}} \tag{3.5.56}$$

with a resonance at

$$\cos^2\vartheta_{13}A_{\text{CC}}^{R} = \cos 2\vartheta_{12}\Delta m_{21}^2. \tag{3.5.57}$$

The eigenvalues of the new matrix are

$$\hat{m}_{M2,1}^2 = \frac{1}{2}\left(\Delta m_{21}^2 + \cos^2\vartheta_{13}A_{\text{CC}} \pm \Delta m_{M21}^2\right), \tag{3.5.58}$$

with

$$\Delta m^2_{M21} = \sqrt{(\Delta m^2_{21} \cos 2\vartheta_{21} - \cos^2 \vartheta_{13} A_{\mathrm{CC}})^2 + (\Delta m^2_{21} \sin 2\vartheta_{21})^2}. \tag{3.5.59}$$

The electron survival probability of the full system becomes a well-used equation,

$$P^{\mathrm{eff}}_{\nu_e \to \nu_e}(x) = (1 - |U_{e3}|^2)^2 P^{(1,2)}_{\nu_e \to \nu_e}(x) + |U_{e3}|^2, \tag{3.5.60}$$

with $P^{(1,2)}_{\nu_e \to \nu_e}$ being the pure 2×2 survival probability, discussed in section 3.4.3.

4

Neutrinos Beyond the Standard Model

The neutrino oscillations and their experimental confirmations form potent evidence that neutrinos are massive, yet they bring with them the question of why neutrino masses are so small. A satisfying mass mechanism should not only introduce neutrino masses, but also contain a mechanism to explain their size with respect to the other fermions. This implies that one naturally looks beyond the simple extensions of the standard model with right-handed neutrinos and unexplained tiny Yukawa couplings, into richer theories. The first part of this chapter is devoted to developing the tools necessary to study such theories, which we will then apply in the part thereafter.

4.1 DIRAC AND MAJORANA MASSES

As we have seen in section 2.1.1, the double cover of the Lorentz group, $\mathrm{SL}(2,\mathbb{C})$, is isomorphic to $SU(2)_L \times SU(2)_R$, of which the fundamental representations are $2 \otimes 1$ and $1 \otimes 2$, respectively working on left-chiral and right-chiral two-component complex vectors, called Weyl spinors. Since these Weyl spinors are considered the fundamental building blocks of a theory with explicit chiral structure, we have used them to describe the matter content of the Standard Model. If we want to use the Weyl spinors to add mass terms in the Lagrangian, we must couple them in such a way that their product is a scalar, which is done by combining a right-chiral and a left-chiral spinor. The two ways we can do so will be discussed now.

4.1.1 DIRAC SPINORS

In the Standard Model, the weak interaction is the only interaction that differentiates between the chiral structures. Since the typical relevant scales are of the order $\mathcal{O}(100)\mathrm{GeV}$, it is for many cases useful to work with fields which present representations of both parity and Lorentz transformations. Such fields, called Dirac fields, were used to describe QED and were considered the proper way to describe fermions before the discovery of parity violation in the weak sector. The structure of this field can be written explicitly as a four-component complex spinor, called a Dirac spinor, defined as

$$\Psi_D = \begin{pmatrix} \psi_L \\ \psi_R \end{pmatrix}, \tag{4.1.1}$$

where $\psi_{L,R}$ are independent Weyl spinors. From this definition one is able to isolate the chiral components using the projection operators $P_{L,R}$, through $\Psi_{L,R} = P_{L,R}\Psi$, with $P_{L,R} = \frac{1}{2}(1 \mp \gamma^5)$, with

$$\Psi_L = \begin{pmatrix} \psi_L \\ 0 \end{pmatrix}, \qquad \Psi_R = \begin{pmatrix} 0 \\ \psi_R \end{pmatrix}. \tag{4.1.2}$$

A Dirac mass is a mass term of the form

$$\mathcal{L} \supset -m_D \bar{\Psi}_D \Psi_D = -m_D \Psi_D^\dagger \gamma^0 \Psi_D \tag{4.1.3}$$

$$= -m_D(\psi_L^\dagger \psi_R + \psi_R^\dagger \psi_L). \tag{4.1.4}$$

This is the type of mass term that is typically introduced for fermions, coupling, for example, an $\bar{e}_L$ with an e_R, and which requires the Higgs mechanism to respect invariance under the gauge group $SU(2)_L$. One can see that such a mass term for the neutrinos would require the existence of a neutral right-handed counterpart.

4.1.2 Majorana Spinors

For a single Weyl spinor, one is also able to write a four-component spinor with both left and right constituents, called a Majorana spinor, as

$$\Psi_M = \begin{pmatrix} \psi_L \\ i\sigma^2 \psi_L^* \end{pmatrix}, \qquad \text{or} \quad \Psi_M = \begin{pmatrix} -i\sigma^2 \psi_R^* \\ \psi_R \end{pmatrix}, \tag{4.1.5}$$

were charge conjugation is applied to form $\psi_L \to i\sigma^2 \psi_L^*$ and ψ_R equivalently. Note that the Majorana spinor has only two complex degrees of freedom, despite its four-component form, and that a Majorana spinor is its own charge conjugate,

$$\Psi_M = \Psi_M^c. \tag{4.1.6}$$

This condition, $\Psi = \Psi^c$, can be interpreted as a generalized reality condition. A Dirac spinor transforms under a complex representation of the Lorentz group, so imposing $\Psi = \Psi^*$ is not Lorentz invariant in general. However, the Majorana condition remains invariant under Lorentz transformations, because it relates the left-handed spinor ψ_L to its conjugate via $i\sigma^2 \psi_L^*$, which transforms as a right-handed spinor. This ensures that the full four-component Majorana spinor transforms covariantly, and allows us to interpret Majorana spinors as real solutions to the spinor field equations, in analogy with real vs complex scalar fields.

A Majorana mass term for a Majorana spinor containing ψ_L can be written as

$$\mathcal{L} \supset -\frac{1}{2} m_M \bar{\Psi}_M \Psi_M = -\frac{1}{2} m_M \Psi_M^\dagger \gamma^0 \Psi_M \tag{4.1.7}$$

$$= -\frac{1}{2} m_M \left(\psi_L^T C \psi_L + \psi_L^\dagger C^\dagger \psi_L^* \right), \tag{4.1.8}$$

where $C = -i\sigma^2$ acts as the charge conjugation matrix in two-component notation. An equivalent expression holds for a Majorana spinor built from a right-handed Weyl spinor ψ_R, in which case the mass term becomes

$$\mathcal{L} \supset -\frac{1}{2} m_M \left(\psi_R^T C \psi_R + \psi_R^\dagger C^\dagger \psi_R^* \right). \tag{4.1.9}$$

The distinction between the two Majorana mass terms becomes significant when we include the gauge invariance condition for $SU(2)_L$. The first spinor defined in 4.1.5 is built from two fields that transform as gauge doublets, while the second one contains two gauge singlets. This has the consequence that the Majorana mass term 4.1.7 is not gauge invariant. In order to add a gauge invariant Majorana term for an $SU(2)_L$ gauge doublet like ℓ_L, we should thus attempt to use the Higgs mechanism, like we did for the other fermions, only now we should add two Higgs terms, one for each doublet. This can not be done in a renormalizable way, since the energy dimension of such an operator, called the Weinberg operator, would be one too high. This can be seen from the explicit form

$$\mathcal{O}_5 = \frac{1}{\Lambda}\left(\overline{\ell^c_L}\cdot\tilde{\Phi}\right)\left(\tilde{\Phi}^T\cdot\ell_L\right), \tag{4.1.10}$$

where ℓ_L is the left-handed lepton doublet, $\tilde{\Phi} = i\sigma^2\Phi^*$ is the conjugate Higgs doublet, and Λ is a mass scale that parametrizes the suppression of this dimension-five operator. After electroweak symmetry breaking, this operator induces a Majorana mass term for the active neutrinos,

$$\mathcal{L}^{\text{eff}}_{\nu,\text{mass}} = -\frac{v^2}{2\Lambda}\nu_L^T C\nu_L + \text{h.c.}, \tag{4.1.11}$$

where v is the vacuum expectation value of the Higgs field. There are also more unorthodox ways to introduce gauge-invariant left-handed Majorana mass terms, such as through the vacuum expectation value of an $SU(2)_L$ Higgs triplet, radiative mechanisms where masses arise at loop-level, or higher-dimensional operators involving extended scalar sectors. For a comprehensive review of such models, see [Cai+17].

For the Majorana spinor containing $SU(2)_L$ singlets, the story is simpler, as the mass term 4.1.9 is already gauge invariant. Since such a term for right-handed neutrinos would be allowed according to the gauge symmetries, spacetime symmetries, and is renormalizable, the principles we use in our model building should persuade us to add it to our Lagrangian, if we decide to include the right handed-neutrino.

4.1.3 DIRAC AND MAJORANA MASSES FOR NEUTRINOS

In order to add mass to the neutrinos, we can either introduce Majorana terms directly for the $SU(2)_L$ doublets ℓ_L, for example, through the Weinberg operator, or we can add right-handed neutrino singlets. Due to their lack of interaction, these hypothesised right-handed neutrinos are called sterile neutrinos, or passive neutrinos. Throughout literature, including in this paper, the term sterile neutrino is used interchangeably with right-handed neutrino, passive neutrino, or sometimes they are simply referred to as a gauge singlet. The original neutrinos, i.e. ν_e, ν_μ and ν_τ will be called either active neutrinos or left-handed neutrinos. We will now introduce the most general form of the Lagrangian with neutrino masses, and then we will review some specific examples.

Although one would be inclined to add one sterile neutrino for each of the three active neutrinos, the most general case extends the Standard Model matter content by n sterile neutrinos, N_R. Following the previous section, in terms of a 3-vector of active flavour neutrinos ν_L and an n-vector of sterile neutrinos N_R, this gives rise to mass terms

$\bar{\nu}_L m_A \nu^c_L$, where m_A is a 3×3 Majorana mass matrix for the active neutrinos,
$\bar{\nu}_L m_D N_R$, where m_D is a $3 \times n$ Dirac mass matrix, and
$\overline{N^c_R} m_S N_R$, where m_S is a $n \times n$ Majorana mass matrix for sterile neutrinos.

All together, this can be summed up in the Lagrangian component

$$\begin{aligned}\mathcal{L} \supset &-\frac{1}{2}\begin{pmatrix}\bar{\nu}_L & \overline{N}^c_R\end{pmatrix}\begin{pmatrix}m_A & m_D \\ m_D^T & m_S\end{pmatrix}\begin{pmatrix}\nu^c_L \\ N_R\end{pmatrix} + \text{h.c.} \qquad (4.1.12)\\ = &-\frac{1}{2}\begin{pmatrix}\bar{\nu}_L & \overline{N}^c_R\end{pmatrix} M \begin{pmatrix}\nu^c_L \\ N_R\end{pmatrix} + \text{h.c.}, \qquad (4.1.13)\end{aligned}$$

where c denotes charge conjugation, and M is a $3 + n \times 3 + n$ mass matrix. The Dirac mass matrix is in general neither diagonal, hermitian, nor even symmetric, just as in the quark sector. The Majorana matrices, although not necessarily hermitian, must be symmetric, since we are contracting a field with its own conjugate. The sterile Majorana components, m_S, can be taken to be diagonal through a regular basis transformation. The general task is to diagonalize this matrix for a specific model, meaning a given number of neutrinos with varying mass terms. We will discuss the various structures of the mass matrix now.

Pure Dirac

In this scenario, we introduce n sterile neutrinos and assume no Majorana mass terms. The resulting mass matrix takes the form

$$M = \begin{pmatrix}0 & m_D \\ m_D^T & 0\end{pmatrix}. \qquad (4.1.14)$$

For $n = 3$, this setup mirrors the structure of the quark sector in terms of flavour mixing. Similarly, diagonalization proceeds in two steps: first, the full matrix is block-diagonalized into Dirac pairs, and then the Dirac mass matrix m_D is diagonalized via a bi-unitary transformation, as in the quark case. In general, the matrix m_D is not symmetric, i.e., $m_D \neq m_D^T$, and may not even be square if $n \neq 3$. To block-diagonalize M, in principle, we perform a singular value decomposition (SVD) of m_D, which yields a diagonal matrix of positive singular values regardless of its shape. The unitary matrices from the SVD simultaneously diagonalize the Dirac blocks and appear in the leptonic mixing matrix. Explicitly, if $m_D = S_{(\nu)} D T^\dagger_{(\nu)}$, then the PMNS matrix is constructed as $U_{\text{PMNS}} = S^\dagger_{(\nu)} S_{(\ell^-)}$, with $S_{(\ell^-)}$ coming from the diagonalization of the charged lepton mass matrix. We will rely on the fact that such a decomposition always exists in the process of diagonalization.

The eigenvalues and eigenstates corresponding to this diagonalization determine the properties of the massive neutrino states. To see this explicitly, we look at the $1 + 1$ neutrino case, where a pure Dirac scenario would yield the diagonalisation

$$\begin{aligned}-2\mathcal{L} \supset &\begin{pmatrix}\bar{\nu}_L & \overline{N}^c_R\end{pmatrix}\begin{pmatrix}0 & m_D \\ m_D & 0\end{pmatrix}\begin{pmatrix}\nu^c_L \\ N_R\end{pmatrix} + \text{h.c.}\\ = &\begin{pmatrix}\bar{\nu}_L & \overline{N}^c_R\end{pmatrix}\begin{pmatrix}1 & 1 \\ 1 & -1\end{pmatrix}\begin{pmatrix}m_D & 0 \\ 0 & -m_D\end{pmatrix}\begin{pmatrix}1 & 1 \\ 1 & -1\end{pmatrix}\begin{pmatrix}\nu^c_L \\ N_R\end{pmatrix} + \text{h.c.}\\ = &\begin{pmatrix}\bar{\nu}_{1L} & \bar{\nu}_{2R}\end{pmatrix}\begin{pmatrix}m_D & 0 \\ 0 & -m_D\end{pmatrix}\begin{pmatrix}\nu_{1R} \\ \nu_{2R}\end{pmatrix} + \text{h.c.} \qquad (4.1.15)\end{aligned}$$

with the mass eigenstates

$$\bar{\nu}_{1L} = \frac{1}{\sqrt{2}}(\bar{\nu}_L + \bar{N}^c_R), \quad \nu_{1R} = \frac{1}{\sqrt{2}}(\nu^c_L + N_R), \tag{4.1.16}$$

$$\bar{\nu}_{2L} = \frac{1}{\sqrt{2}}(\bar{\nu}_L - \bar{N}^c_R), \quad \nu_{2R} = \frac{1}{\sqrt{2}}(\nu^c_L - N_R), \tag{4.1.17}$$

corresponding to eigenvalues $m_\pm = \pm m_D$. Note here that the fact that the two mass eigenstates have the same eigenvalue, as is the case for the quarks, explicitly ensures that there are no Majorana terms present. The cancellation of the Majorana terms is seen explicitly by expanding back into the original fields

$$\begin{aligned} \mathcal{L} \supset & +\frac{m_D}{2}\left(\bar{\nu}_L\nu^c_L + \bar{\nu}_L N_R + \overline{N}^c_R\nu^c_L + \overline{N}^c_R N_R\right) && (4.1.18) \\ & -\frac{m_D}{2}\left(\bar{\nu}_L\nu^c_L - \bar{\nu}_L N_R - \overline{N}^c_R\nu^c_L + \overline{N}^c_R N_R\right) \\ = & +\frac{m_D}{2}(\bar{\nu}_L N_R + \overline{N}^c_R\nu^c_L). && (4.1.19) \end{aligned}$$

This means in particular that any non-degeneracy in mass is directly linked to Majorana terms, and thus to lepton number violation (see 4.1.4).

In the $3+3$ case, for S and T such that

$$S m_D T^\dagger = m_D^{\text{diag}} = T m_D^\dagger S^\dagger, \tag{4.1.20}$$

we can block-diagonalize our mass matrix as

$$\begin{aligned} M_{\text{diag}} &= \begin{pmatrix} S & T \\ S & -T \end{pmatrix} \begin{pmatrix} 0 & m_D \\ m_D^T & 0 \end{pmatrix} \begin{pmatrix} S^\dagger & S^\dagger \\ T^\dagger & -T^\dagger \end{pmatrix} \\ &= \frac{1}{2}\begin{pmatrix} T m_D^\dagger S^\dagger + S m_D V^\dagger & T m_D^T S^\dagger - S m_D T^\dagger \\ -T m_D^T S^\dagger + S m_D T^\dagger & -T m_D^T S^\dagger - S m_D T^\dagger \end{pmatrix} \\ &= \begin{pmatrix} m_D^{\text{diag}} & 0 \\ 0 & -m_D^{\text{diag}} \end{pmatrix}. \end{aligned} \tag{4.1.21}$$

The matrices would then be parametrised, and explicit values of S and T should be determined experimentally.

Pseudo-Dirac models are small Majorana-like perturbations of Dirac models. The mass matrix in the $1+1$ simplification diagonalizes into

$$M = \begin{pmatrix} \varepsilon & m_D \\ m_D & \varepsilon \end{pmatrix} \to M_{\text{diag}} = \begin{pmatrix} m_D + \frac{\varepsilon}{2} & 0 \\ 0 & -m_D + \frac{\varepsilon}{2} \end{pmatrix}, \tag{4.1.22}$$

from which one can now see that Majorana terms like $\varepsilon\bar{\nu}_L\nu^c_L$ appear, as the cancellation in 4.1.18 no longer holds. The direct correlation between the removal of the degeneracy of mass eigenvalues and the appearance of Majorana terms should be noted, and becomes more prominent in cases with dominant Majorana terms.

$1+1$ **Dirac + Majorana**

We now allow both Dirac and Majorana mass terms to be present, and we will illustrate the diagonalization of the corresponding mass matrix in the $1+1$ case. The general mass term for such a system includes both contributions and can be written as

$$\mathcal{L}_{\text{mass}} = \frac{1}{2} \begin{pmatrix} \bar{\nu}_L & \overline{N^c_R} \end{pmatrix} \begin{pmatrix} m_A & m_D \\ m_D & m_S \end{pmatrix} \begin{pmatrix} \nu^c_L \\ N_R \end{pmatrix} + \text{h.c.}, \tag{4.1.23}$$

Due to the Dirac term, the chiral fields ν_L and ν_R do not correspond to mass eigenstates, and we must diagonalize M to identify the physical massive neutrinos. This is achieved through a unitary transformation of the chiral fields:

$$\begin{pmatrix} \bar{\nu}_L \\ \overline{N^c_R} \end{pmatrix} = U n_L, \quad \text{with } n_L = \begin{pmatrix} \nu_{1L} \\ \nu_{2L} \end{pmatrix}, \tag{4.1.24}$$

where ν_{1L} and ν_{2L} are left-handed components of the mass eigenstates. The unitary matrix U is chosen to diagonalize the mass matrix:

$$U^T M U = \text{diag}(m_1, m_2), \tag{4.1.25}$$

with real and non-negative mass eigenvalues m_1 and m_2, which can be computed analytically by solving the characteristic polynomial of M. The mass Lagrangian then becomes

$$\mathcal{L}_{\text{mass}} = \frac{1}{2} n_L^T U^T M U C^\dagger n_L + \text{h.c.} \tag{4.1.26}$$

$$= \frac{1}{2} \sum_{k=1}^{2} m_k \, \nu_{kL}^T C^\dagger \nu_{kL} + \text{h.c.}, \tag{4.1.27}$$

which is a Majorana mass term. We can define the corresponding *Majorana spinors*

$$\nu_k = \nu_{kL} + C\overline{\nu}_{kL}^T = \nu_{kL} + \nu_{kL}^c, \tag{4.1.28}$$

which satisfy the Majorana condition $\nu_k = \nu_k^c$. Thus, the diagonalization of the Dirac + Majorana mass matrix leads to Majorana neutrino eigenstates.

In order to find the eigenvalues in the $1+1$ case we perform basic linear algebra. We define $m_1 \equiv m_+$ and $m_2 \equiv m_-$. Taking the determinant

$$\det \begin{pmatrix} m_A - m_\pm & m_D \\ m_D & m_S - m_\pm \end{pmatrix} = 0 \tag{4.1.29}$$

gives us

$$m_\pm^2 - m_\pm (m_A + m_S) + m_A m_S - m_D^2 = 0, \tag{4.1.30}$$

and thus we find eigenvalues

$$m_\pm = \frac{m_A + m_S \pm \sqrt{m_S^2 + m_A^2 - 2 m_A m_S + 4 m_D^2}}{2}. \tag{4.1.31}$$

It now becomes clear to see that in the Dirac case our eigenvalues become degenerate with $m_\pm = \pm m_D$, while for models with Majorana components the expression is more elaborate, and leads to non-degenerate eigenvalues.

3-generation Dirac + Majorana

We now extend the Dirac + Majorana framework to the realistic case of three active neutrinos and N_s sterile right-handed neutrinos. The fields ν'_e, ν'_μ, and ν'_τ couple to the weak interaction and thus require redefinition in the mass basis, while the sterile fields N_{R_s} are singlets and do not participate in weak interactions.

The full mass Lagrangian can be recast in the form

$$\mathcal{L}_{\text{mass}} = \frac{1}{2}\Psi_L'^T C^\dagger M \Psi_L' + \text{h.c.}, \tag{4.1.32}$$

where we define the extended vector of left-handed fields

$$\Psi_L' \equiv \begin{pmatrix} \nu_L' \\ N_R^c \end{pmatrix}, \qquad \nu_L' = \begin{pmatrix} \nu_{eL}' \\ \nu_{\mu L}' \\ \nu_{\tau L}' \end{pmatrix}, \qquad N_R^c = \begin{pmatrix} N_{R1}^c \\ \vdots \\ N_{RN_s}^c \end{pmatrix}. \tag{4.1.33}$$

Diagonalization is achieved via a unitary transformation

$$\Psi_L' = U n_L, \qquad n_L = \begin{pmatrix} \nu_{1L} \\ \vdots \\ \nu_{NL} \end{pmatrix}, \tag{4.1.34}$$

where $N = 3 + N_s$, and

$$U^T M U = \text{diag}(m_1, \dots, m_N), \tag{4.1.35}$$

with real, non-negative masses m_k. The diagonalized Lagrangian reads

$$\mathcal{L}_{\text{mass}} = \frac{1}{2}\sum_{k=1}^{N} m_k\, \nu_{kL}^T C^\dagger \nu_{kL} + \text{h.c.} \tag{4.1.36}$$

Defining the Majorana fields

$$\nu_k \equiv \nu_{kL} + C\bar{\nu}_{kL}^T, \tag{4.1.37}$$

we see that each mass eigenstate satisfies the Majorana condition $\nu_k = \nu_k^c$, and the theory describes N Majorana neutrinos.

An interesting limit is the *seesaw* limit, in which the sterile Majorana components are taken to be much heavier than the Dirac terms. This scenario will be discussed in section 4.2.

Non-unitarity from Majorana terms

If one has either a non-zero m_A or m_S in addition to the Dirac terms, without restricting them to particular limits, the flavour states can mix with all mass eigenstates in any general way. In particular, this means that the 3×3 block describing the mixing of the active neutrinos with 3 mass eigenstates is no longer unitary, and so the PMNS matrix is no longer unitary. This non-unitarity has several important consequences. First, the charged current weak interaction now couples the flavour eigenstates to a non-orthonormal combination of mass eigenstates. This implies that the mixing matrix appearing in the weak interaction Lagrangian,

$$\mathcal{L}_{\text{int}} \supset \frac{g}{\sqrt{2}}\bar{\ell}_L \gamma^\mu U \nu_{mL} W_\mu^- + \text{h.c.}, \tag{4.1.38}$$

is no longer strictly unitary, and the matrix U must now be interpreted as a rectangular submatrix of a larger unitary matrix involving both active and sterile sectors.

In practical terms, this leads to observable deviations from the Standard Model predictions, such as apparent non-conservation of total lepton number in neutrino scattering and production processes [Ant+06]. Moreover, neutrino oscillation probabilities are modified due to this non-unitarity. These include so-called zero-distance flavour transitions, where a neutrino produced in one flavour can be detected in another even without propagation, which would strongly alter short baseline (SBL) experimental results [Ada+08; Est+20]. Additionally, the violation of unitarity introduces extra CP-violating phases that are not present in the standard three-flavour scenario, leading to new sources of CP asymmetry in neutrino oscillations [Fer+07]. Since the oscillation amplitudes no longer sum to unity, damping effects may also appear if the sterile admixtures are large.

These deviations are constrained by global fits to oscillation data, as well as by precision electroweak measurements. Non-unitary mixing affects the invisible Z boson decay width, universality tests in leptonic decays, and measurements of weak mixing angles, among others. Current bounds indicate that deviations from unitarity must be small, typically at the level of $|\delta U| \lesssim \mathcal{O}(10^{-2})$ [Ble+17; Esc+15], though certain configurations with light sterile neutrinos remain compatible with data.

Active Majorana

Although Dirac masses and sterile Majorana terms can be added in full generality, it is also instructive to consider the effective scenario in which only active Majorana mass terms are present. Such a setup can arise, for instance, as the low-energy limit of a more complete theory in which heavier states have been integrated out, giving rise to the dimension-five Weinberg operator (for a full discussion see section 4.2.1). In the low energy limit, the resulting mass matrix is then a 3×3 complex symmetric matrix acting solely in the active sector. In this minimal extension of the Standard Model, the neutrino mixing matrix is exactly unitary, as the absence of any extra states precludes deviations from unitarity. This simplifies the theoretical framework and aligns well with the current experimental constraints on lepton mixing.

An important consequence of the Majorana nature of active neutrinos is the presence of additional CP-violating phases that cannot be rotated away. For three active Majorana neutrinos, the mixing matrix—still called the Pontecorvo–Maki–Nakagawa–Sakata (PMNS) matrix—depends on three mixing angles and three physical phases: one Dirac-type phase δ and two so-called *Majorana phases*, α_{21} and α_{31}, which arise because rephasing the Majorana fields alters their mass terms. These phases have no analogue in the quark sector. The most conventional parametrization of the PMNS matrix is

$$U_{\text{PMNS}} = \begin{pmatrix} 1 & 0 & 0 \\ 0 & c_{23} & s_{23} \\ 0 & -s_{23} & c_{23} \end{pmatrix} \begin{pmatrix} c_{13} & 0 & s_{13}e^{-i\delta} \\ 0 & 1 & 0 \\ -s_{13}e^{i\delta} & 0 & c_{13} \end{pmatrix} \begin{pmatrix} c_{12} & s_{12} & 0 \\ -s_{12} & c_{12} & 0 \\ 0 & 0 & 1 \end{pmatrix} \begin{pmatrix} 1 & 0 & 0 \\ 0 & e^{i\alpha_{21}/2} & 0 \\ 0 & 0 & e^{i\alpha_{31}/2} \end{pmatrix}, \tag{4.1.39}$$

where $c_{ij} = \cos\theta_{ij}$, $s_{ij} = \sin\theta_{ij}$, and δ, α_{21}, and α_{31} are the physical CP-violating phases. The final diagonal matrix encodes the Majorana phases, which would be unphysical if neutrinos were Dirac particles. As a result, the PMNS matrix for Majorana neutrinos contains six independent parameters, in contrast to four in the Dirac case. So, although the active-only Majorana scenario omits Dirac mass terms and avoids mixing with any sterile states, it is not without physical consequences. Even in this minimal field content, the Majorana mass terms themselves induce non-trivial CP structure.

4.1.4 Lepton Number Violation

In the Standard Model with massless neutrinos, lepton number is an accidental global symmetry associated with the global U(1) phase transformations of the lepton fields. When neutrinos acquire Dirac masses, this symmetry remains intact, and total lepton number is exactly conserved. However, if neutrinos are Majorana particles, this is no longer the case: the Majorana mass term explicitly breaks total lepton number by two units. This breaking is evident from the structure of the Majorana mass term,

$$\mathcal{L}_{\text{mass}} = \frac{1}{2} m \left(\nu_L^T C^\dagger \nu_L + \nu_L^\dagger C \nu_L^* \right) , \tag{4.1.40}$$

which is not invariant under the global phase rotation $\nu_L \to e^{i\phi}\nu_L$. Under such a transformation, the Majorana term transforms as

$$\mathcal{L}_{\text{mass}} \to \frac{1}{2} m \left(e^{2i\phi} \nu_L^T C^\dagger \nu_L + e^{-2i\phi} \nu_L^\dagger C \nu_L^* \right) , \tag{4.1.41}$$

showing explicitly the violation of lepton number by two units ($\Delta L = \pm 2$). This is a direct consequence of the Majorana condition, which identifies neutrinos and antineutrinos as the same particle. Since the lepton number operator assigns opposite charges to particles and antiparticles, this identification renders lepton number non-conserved.

Nevertheless, in the limit where neutrino masses are negligible compared to the energies involved, the theory approximately recovers a conserved effective lepton number. In this regime, neutrinos behave as effectively massless Weyl fermions, and processes involving lepton number violation are highly suppressed. As a result, lepton number is approximately conserved in most weak processes. In order to detect a Majorana mass term, one must search for induced LNV transitions at low energy. The most sensitive and widely studied process of this kind is neutrinoless double beta decay ($0\nu\beta\beta$), in which a nucleus emits two electrons but no neutrinos:

$$(Z, A) \to (Z + 2, A) + 2e^- . \tag{4.1.42}$$

This process violates total lepton number by two units and can only occur if neutrinos are Majorana particles. The rate of this decay is proportional to the square of the effective Majorana mass $m_{\beta\beta}$, which is defined to be a coherent combination of the neutrino mass eigenvalues and mixing parameters, i.e.

$$m_{\beta\beta} = \left| \sum_{i=1}^{3} U_{ei}^2 m_i \right| . \tag{4.1.43}$$

For a full discussion on this effective mass, see section 14.3.1 from [GK07]. The observation of neutrinoless double beta decay would provide direct evidence of lepton number violation and confirm the Majorana nature of neutrinos. Conversely, the absence of such a signal places stringent constraints on the absolute neutrino mass scale and the allowed parameter space of the PMNS matrix. For a current overview of bounds, see [Wor+22b].

4.1.5 Neutrino Oscillations and Majorana Masses

One could wonder if Majorana masses could affect neutrino oscillations in such a way that their presence could be detected using appearance or disappearance experiments. To answer this, one should consider that the contribution of the Majorana term to the PMNS matrix is through a diagonal matrix with complex phases as entries. In vacuum, the oscillation probability in 3.3.10 was proportional to the quartic product

$$\sum_{k,j} U^*_{\alpha k} U_{\beta k} U_{\alpha j} U^*_{\beta j}, \tag{4.1.44}$$

which is a rephasing invariant. Since those are also invariant under the rephasing induced by Majorana terms, vacuum oscillations are not able to detect the origin of the neutrino mass. In matter, the equation governing the transition probabilities is given in 3.4.23. Here too, one can easily see that the additional diagonal matrix of complex phases cancels in the product $U\mathbb{M}^2 U^\dagger$, since $\mathbb{M}$ is diagonal, so matter oscillations are also not affected by Majorana phases. One can state that oscillation experiments are not able to detect whether a neutrino is Majorana or not.

4.2 SEESAW MASS MECHANISMS

The models described above are general classifications of the large number of more detailed variations on how to explicitly introduce such mass terms. We mentioned earlier, however, that a good explanation for active neutrino masses should not only explain their existence but also their small magnitude with respect to the other fermion masses. Since the charged fermions only have Dirac-like mass terms, the requirement of naturalness for the magnitude of neutrino masses holds only for their Dirac components, i.e. $||m_D^{\text{charged fermions}}|| \sim ||m_D^{\text{neutrinos}}||$. For the Majorana-like masses, there is no reason to expect a magnitude off the same scale, so one can generally expect them to be much larger or much smaller. There are various models that introduce naturally-sized Dirac terms in combination with BSM particles in such a way that both very light and very heavy states appear in the mass basis. Such mechanisms are called seesaw mechanisms and are generally considered the most promising models for a realistic description. We will briefly present how mass terms arise as an effective field theory (EFT), and then we will discuss the more important seesaw variants in the following paragraphs.

4.2.1 THE WEINBERG OPERATOR AND THE EFT APPROACH

The essence of seesaw mechanisms is that the lightness of neutrinos can be explained by the heaviness of new physics. We saw that Dirac and Sterile Majorana terms induce non-unitarity in U_{PMNS}, and that experimental results point to an almost unitary mixing matrix. This means that the dominant component of natural neutrinomasses should be active Majorana, and should thus be effectively generated by the Weinberg operator that we introduced in section 4.1.2,

$$\mathcal{O}_5 = \frac{1}{\Lambda} \left(\overline{\ell^c_L} \cdot \tilde{\Phi} \right) \left(\tilde{\Phi}^T \cdot \ell_L \right), \tag{4.2.1}$$

where ℓ_L is the left-handed lepton doublet, $\tilde{\Phi} = i\sigma^2 \Phi^*$ is the conjugate Higgs doublet, and Λ is a mass scale that parametrizes the suppression of this dimension-five operator. The Weinberg operator is the lowest-dimension operator that can generate Majorana terms, but is nevertheless non-renormalizable, and thus cannot be present in a complete theory. One is, however, able to describe a theory in such a way that for low energies an effective Weinberg operator is generated while keeping the full theory renormalizable, similarly to how the low energy limit of the weak interaction can be described using the non-renormalizable Fermi theory. Such a complete high-energy theory is formally called a UV completion, and the low-energy theories are the effective (field) theories. The UV completions contain new heavy matter content, which in the low energy limit becomes static (i.e. the kinetic term vanishes) and can be integrated out using the resulting equations of motion. The effective theory then acquires operators of various dimensions, including higher than $d = 4$, which remain useful as a description up to an energy scale Λ, typically related to the mass and coupling of the heavy particles.

The popular view of the Standard Model is that it is an EFT of some higher unknown UV completion, which has either the same symmetries as the SM, or has additional symmetric structure that is broken into the symmetry structure of the SM at low energies. If the UV completion indeed contains additional matter content, the EFT should also generate higher-dimensional operators with the matter content and symmetry group of the SM. The full low-energy theory of the UV completion of the SM is called the SMEFT, and contains all possible operators for the SM gauge structure. The SMEFT Lagrangian can be written as

$$\mathcal{L}_{\text{SMEFT}} = \mathcal{L}_{\text{SM}} + \frac{1}{\Lambda}\sum_i \mathcal{C}_i^5 \hat{O}_i^5 + \frac{1}{\Lambda^2}\sum_i \mathcal{C}_i^6 \hat{O}_i^6 + \dots \tag{4.2.2}$$

$$= \mathcal{L}_{\text{SM}} + \sum_{d=5} \frac{1}{\Lambda^{d-4}} \sum_i \mathcal{C}_i^d \hat{O}_i^d, \tag{4.2.3}$$

where $\mathcal{C}_i$ are the dimensionless coefficients, called Wilson coefficients, and $\hat{O}_i^d$ are the operators of dimension d. If one decides to introduce certain higher-dimensional operators, the next step is to understand the running of the Wilson coefficients, i.e., one must derive and solve the renormalization group equations (RGEs) for the new theory. Then, one is able to compute the amplitudes belonging to the novel operators and match any observed strengths at the electroweak scale with the predictions of the UV theory. The matching process will be omitted here, however. The only dimension five operator that respects the gauge groups of the SM is the Weinberg operator. For 6 dimensions, one finds 59 independent operators for one flavour [Grz+10], and 2499 operators taking all flavour indices into account [Alo+14]. Note that due to the Λ^{4-d} suppression, the higher-dimensional operators become less and less relevant when the momenta are far below the scale of Λ. Each operator induces new measurable interactions to the Standard Model, and by posing numerical constraints on the interaction, and thus on the Wilson coefficients, one is able to extract information on any matter content and the energy scale corresponding to the UV completion. Applying this to the generation of low-E active Majorana neutrinos, we find various ways to generate the Weinberg operator at low energies by adding heavy matter content. If we want to remain renormalizable, only three of them are considered minimal, i.e., introducing only one extra matter representation and its corresponding interactions. These models are called the minimal seesaw models, classified by Schechter & Valle [SV80], introducing either

- A fermion singlet (Type I),
- A scalar $SU(2)_L$ triplet (Type II),
- A spin-$\frac{1}{2}$ $SU(2)_L$ triplet (Type III).

These seesaw models correspond to concrete yet basic UV-complete theories, each predicting distinct new particles and interactions that may be accessible at high-energy experiments or via precision low-energy observables. As such, they form the most popular theoretically motivated extensions of the Standard Model neutrino sector. Beyond the minimal completions, a variety of more exotic possibilities exist. For instance, by introducing two exotic fields instead of one—a scalar quadruplet with quantum numbers $(1, 4, -\frac{1}{2})$ and a fermion quintuplet $(1, 5, 0)$—one can construct a higher-dimensional version of the seesaw mechanism. In such scenarios, the smallness of neutrino masses comes from a combination of effects: a suppressed induced VEV for the larger scalar multiplet, and mixing with a heavy fermionic state. The example from before, introducing a scalar quadruplet and a fermionic quintuplet, also generates active neutrino masses through operators of higher dimension than the Weinberg operator and introduces an effective neutrino mass operator of dimension nine, schematically written as $(LLHH)(H^\dagger H)^2$ [BR20; AM14].

In the following subsections, we will only discuss the three minimal UV completions in detail, beginning with Type I. We will examine their field content, the structure of their interactions, and show how they give rise to the Weinberg operator in the low-energy limit. In particular, we will relate the EFT formalism to the mass matrix approach, especially in the Type I case where the connection is most transparent.

4.2.2 The Type I Seesaw Mechanism

The Type I seesaw mechanism was originally proposed in 1979 by P. Minkowski [Min77], T. Yanagida [Yan79], and independently by M. Gell-Mann, P. Ramond, and R. Slansky [GRS79], as well as by R. N. Mohapatra and G. Senjanović [MS80]. It introduces n sterile neutrinos containing large Majorana mass components, so $||m_S|| \gg ||m_D||$, no active Majorana component, and the Higgs sector is left unaltered. The mass matrix becomes

$$M = \begin{pmatrix} 0 & m_D \\ m_D^T & m_S \end{pmatrix}. \tag{4.2.4}$$

1+1 Type I Seesaw

In the $1+1$ simplification from 4.1.3 we find the eigenvalues of this matrix to be

$$\begin{aligned} m_\pm &= \frac{m_S \pm \sqrt{m_s^2 + 4m_D^2}}{2} && (4.2.5) \\ &= \frac{m_S}{2} \pm \frac{m_s}{2}\left(1 + \frac{2m_D^2}{m_S^2} + \mathcal{O}(m_D^2/m_S^2)^2\right) && (4.2.6) \end{aligned}$$

and thus

$$\begin{aligned} m_+ &\simeq m_S, && (4.2.7) \\ m_- &\simeq -\frac{m_D^2}{m_S}. && (4.2.8) \end{aligned}$$

We see that a large sterile Majorana component induces a severe splitting of the mass eigenvalues into a very heavy state m_+ and a very light state m_-, which is suppressed naturally be the new scale introduced by the sterile component. In order to see to what extent the light states correspond to active states, we must explicitly find the corresponding basis transformation. Since the mass matrix is symmetric, one can diagonalize it through a single rotation matrix,

$$U^T M U = \mathrm{diag}(m_-, m_+), \tag{4.2.9}$$

with

$$U = \begin{pmatrix} \cos\theta & \sin\theta \\ -\sin\theta & \cos\theta \end{pmatrix}, \tag{4.2.10}$$

where the angle is defined by

$$\tan 2\theta = \frac{2m_D}{m_S}. \tag{4.2.11}$$

In the seesaw limit we then find that

$$\tan 2\theta \simeq 2\theta = 2\frac{m_D}{m_S}, \quad \text{and thus } \theta = \frac{m_D}{m_S} \ll 1. \tag{4.2.12}$$

At first-order this induces a mixing matrix

$$\begin{pmatrix} \nu_L^c \\ N_R \end{pmatrix} \simeq \begin{pmatrix} 1 & -\theta \\ \theta & 1 \end{pmatrix} \begin{pmatrix} \nu_{-L} \\ \nu_{+L} \end{pmatrix}, \tag{4.2.13}$$

from which then the full Majorana fields $\nu_\pm \equiv \nu_{\pm L} + (\nu_{\pm L})^c$ are defined. One can see that mixing between the active flavour states and the heavy state is also suppressed by the scale m_S, which allows for this mechanism to simultaneously explain the smallness of the active neutrino masses, while allowing for enough space to conform to unitarity bounds on the PMNS matrix.

Type I Seesaw as an EFT

In order to come back to our use of the SMEFT description, we consider what happens when we add a right-handed heavy neutrino to the Lagrangian, including a sterile Majorana mass and a Dirac mass. At the Lagrangian level, we see

$$\mathcal{L} \supset -y^\nu \left(\overline{N_R}\tilde{\Phi}^\dagger L_L + \overline{L_L}\tilde{\Phi} N_R \right) + \frac{1}{2} m_S \left(N_R^T \mathcal{C}^\dagger N_R + N_R^\dagger \mathcal{C} N_R^* \right), \tag{4.2.14}$$

with a corresponding Dirac mass of $m_\mathrm{D} = y^\nu v/\sqrt{2}$ after electroweak SSB. At energies way below the mass m_S we are able to set the sterile kinetic terms to zero, and therefore obtain the equation of motion

$$\frac{\partial \mathcal{L}}{\partial N_R} = m_S N_R^T \mathcal{C}^\dagger - y^\nu \overline{L_L}\tilde{\Phi} = 0, \tag{4.2.15}$$

which can be rewritten as

$$N_R = -\frac{y^\nu}{m_S}\tilde{\Phi}^\dagger \mathcal{C}\overline{L_L}^T. \tag{4.2.16}$$

If we now add this expression back into the Lagrangian, we get the effective low-energy contribution to the theory

$$\mathcal{L} = -\frac{1}{2}\frac{(y^\nu)^2}{m_S}\left[(L_L^T \tau_2 \Phi)\mathcal{C}^\dagger(\Phi^T \tau_2 L_L) - (\overline{L_L}\tau_2\Phi^*)\mathcal{C}(\Phi^\dagger \tau_2 \overline{L_L}^T) \right]. \tag{4.2.17}$$

This is just the Weinberg operator with $\Lambda = m_S$ and a coefficient

$$\mathcal{C}^5_{\text{Weinberg}} = -\frac{1}{2}(y^\nu)^2.$$

The Lagrangian after electroweak symmetry breaking will then look like

$$\mathcal{L} = \frac{1}{2}\frac{m_D^2}{m_S}\left(\nu_{1L}^T \mathcal{C}^\dagger \nu_{1L} + \nu_{1L}^\dagger \mathcal{C} \nu_{1L}^* \right), \tag{4.2.18}$$

where the removal of the minus sign required the redefinition $\nu_L \to \nu_{1L} = -i\nu_L$. The procedure makes the low-energy effective Majorana term explicit.

3+N$_S$ Type I Seesaw

The diagonalization of the mass matrix was assumed in order to write the general form of the Majorana neutrinos in 4.1.36, which also holds for the seesaw case. The diagonalization itself was not performed, however, so the exact relation between mass eigenvalues in terms of Dirac or Majorana components was not shown for the $3 + N$ case. There are, just as in the pure Dirac case, two steps in the procedure: the block diagonalization, and the further diagonalization of the 3×3 and $N_S \times N_S$ blocks. We will start with the former.

In general, we use a unitary matrix

$$\mathcal{U} = \begin{pmatrix} U & R \\ \tilde{S} & V \end{pmatrix} \tag{4.2.19}$$

in order to diagonalise the matrix as

$$\mathcal{U}^T M \mathcal{U} \simeq \begin{pmatrix} M_{\text{light}} & 0 \\ 0 & M_{\text{heavy}} \end{pmatrix}, \tag{4.2.20}$$

which produces the *exact seesaw formula*

$$U M_{\text{light}} U^T = -R M_{\text{heavy}} R^T. \tag{4.2.21}$$

Next, the seesaw limit in the $N_S > 1$ case is achieved by taking all eigenvalues of m_S to be much heavier than any element of m_D. In this limit we can use a matrix U to block diagonalize M through

$$\mathcal{U} = \begin{pmatrix} 1 - \frac{1}{2} m_D^\dagger (m_S m_S^\dagger)^{-1} m_D & [(m_S)^{-1} m_D]^\dagger \\ -(m_S)^{-1} m_D & 1 - \frac{1}{2} (m_S)^{-1} m_D m_D^\dagger (m_S^\dagger)^{-1} \end{pmatrix} + \mathcal{O}\left(\left(\frac{m_D}{m_S}\right)^3 \right), \tag{4.2.22}$$

following [**Schechter:1982**]. The expression for the heavy and light matrices are

$$M_{\text{light}} \simeq -m_D^T (m_R)^{-1} m_D \quad \text{and} \quad M_{\text{heavy}} \simeq m_S, \tag{4.2.23}$$

which is called the *approximate seesaw formula*, and follows from approximating $R \simeq m_D m_S^{-1} V$ and $M_{\text{heavy}} = V^{-1} m_s (V^{-1})^T$. The matrices M_{light} and M_{heavy} can now be diagonalized to find explicit eigenvalues.

This next step requires more information on the actual form of m_S and m_D, as there are many scenarios that fit the seesaw requirements. One can generally fine-tune the sterile masses to get the light neutrino masses as one wishes, yet we are mostly interested in more general cases, and we will discuss the quadratic and the linear type I seesaw in some more detail. If we take all the sterile masses to be of the same order Λ, describing the energy scale of new physics, we can write

$$m_S = \Lambda \, \mathbb{I}_{3\times 3}, \tag{4.2.24}$$

which induces a light neutrino matrix

$$M_{\text{light}} = -\frac{1}{\Lambda} m_D^T m_D. \tag{4.2.25}$$

The eigenvalues are then just the eigenvalues of the square of the Dirac matrix suppressed by a large scale. The proportionality of the massive neutrinos takes on the proportionality of the squares of the Dirac eigenvalues, i.e.,

$$m_1 : m_2 : m_3 = m_{D1}^2 : m_{D2}^2 : m_{D3}^2, \tag{4.2.26}$$

from which the model obtains its name. Another possibility is specific for $N_s = 3$, for which we can take m_S and m_D of the same form, but with a difference in energy scale. In particular, if we consider a sterile scale Λ_S and a Dirac scale Λ_D, an interesting scenario occurs when we take

$$m_S = \frac{\Lambda_S}{\Lambda_D} m_D, \tag{4.2.27}$$

which induces a light neutrino matrix

$$M_{\text{light}} \simeq -\frac{\Lambda_D}{\Lambda_S} m_D, \tag{4.2.28}$$

so the eigenvalues will be just those of the Dirac matrix, but rescaled accordingly. The proportionality of the light eigenvalues will be that of the Dirac matrix, however, so it is clear to see that the model derives its name from the relation

$$m_1 : m_2 : m_3 = m_{D1} : m_{D2} : m_{D3}. \tag{4.2.29}$$

The diagonalization process for a Majorana matrix depends, of course, on its specific values, yet some general properties derived from its symmetric complex form are worth mentioning. One can diagonalize m_S as

$$(V_L^\nu)^T m_S V_L^\nu = M_{\text{diag}}, \quad \text{with} \quad M_{\text{diag}}^{ij} = \delta^{ij} m_i, \quad (i,j = 1, \ldots, N_s), \tag{4.2.30}$$

where m_i are real and positive and V_L^ν is unitary (for a proof, see Section 6.7.1 of [GK07]). The exact eigenvalues turn out to be solutions of the equation

$$\begin{pmatrix} \mathfrak{Re}[m_S] & -\mathfrak{Im}[m_S] \\ -\mathfrak{Im}[m_S] & -\mathfrak{Re}[m_S] \end{pmatrix} \begin{pmatrix} \mathfrak{Re}[v^{(j)}] \\ \mathfrak{Im}[v^{(j)}] \end{pmatrix} = m_j \begin{pmatrix} \mathfrak{Re}[v^{(j)}] \\ \mathfrak{Im}[v^{(j)}] \end{pmatrix}, \tag{4.2.31}$$

where $v^{(j)}$ are the eigenvectors of m_S corresponding to m_j. The eigenvalues are thus also eigenvalues of the real symmetric matrix

$$\mathfrak{M} = \begin{pmatrix} \mathfrak{Re}[m_S] & -\mathfrak{Im}[m_S] \\ -\mathfrak{Im}[m_S] & -\mathfrak{Re}[m_S] \end{pmatrix}. \tag{4.2.32}$$

The real eigenvalue problem can be solved numerically, which means that one is able to always compute the heavy neutrino states whenever the seesaw mechanism is in place, as we then have $m_S \simeq M_{\text{heavy}}$. The eigenvectors are then just the columns of V_L^ν, allowing us to obtain the complete diagonalization.

Parametrizations

The parametrization of U_{PMNS} was given in 4.1.39 for a unitary matrix and an active Majorana mass matrix, inducing two Majorana phases. This parametrization serves well at low energies when the new physics is integrated out through the seesaw mechanism, but it is not complete for all mass scales of m_S. It would be more favourable to find a parametrization of the full mass matrix in terms of observable parameters such that lower mass sterile contributions could be studied in accessible parameter space. The amount of required parameters heavily depends on the nature of the particles and the amount of particles introduced, and becomes more elaborate for larger systems. The case that has been studied quite well is the minimal seesaw model (MSM), which introduces two sterile neutrinos in order to account for the two mass differences measured in atmospheric and solar oscillation experiments (see Section 3.5). In such a scenario one, is able to parametrize the mass matrix in terms of 11 parameters, generally (but not exclusively) taken as

- 5 oscillation parameters, $\vartheta_{12}, \vartheta_{13}, \vartheta_{23}$ often still present the form of U_{PMNS}, Δm_{31}^2 and Δm_{21}^2,
- 2 complex phases: the original δ_{CP} in U_{PMNS} and a Majorana phase σ,

- 2 sterile masses M_1 and M_2,
- 2 varying parameters.

We will mention the most common parametrization, called the Casas Ibarra (CI) parametrization after its creators [CI01], and then a brief overview of different parameters in different schemes.

Since for the seesaw model we take the active Majorana mass matrix to be zero, and we are allowed to rotate the sterile neutrinos into a basis such that m_R becomes real and diagonal, only the Dirac mass matrix truly needs a further parametrization. Most schemes, in particular CI, work in the approximate seesaw formula 4.2.23, for which the Dirac matrix can be written as

$$m_D \simeq iU_{\text{PMNS}}\sqrt{M_{\text{light}}}\; R\; \sqrt{M_{\text{heavy}}}. \tag{4.2.33}$$

The CI parametrization introduces the matrix R above, which is an orthogonal 3×2 matrix that satisfies $RR^T = \text{diag}(0, 1, 1)$ for the normal hierarchy, or $RR^T = \text{diag}(1, 1, 0)$ in the inverted hierarchy. Such a matrix can be parametrized using a complex number $\omega = |\omega|e^{i\arg(\omega)}$ through

$$\begin{pmatrix} 0 & 0 \\ \cos\omega & -\sin\omega \\ \xi\sin\omega & \xi\cos\omega \end{pmatrix} \text{ for NH,} \quad \text{or} \quad \begin{pmatrix} \cos\omega & -\sin\omega \\ \xi\sin\omega & \xi\cos\omega \\ 0 & 0 \end{pmatrix} \text{ for IH,} \tag{4.2.34}$$

where $\xi = \pm 1$. This allows one to explicitly write the components of m_D in terms of the parameters encoded in U_{PMNS} and the additional parameters:

$$(m_D)_{\alpha 1} \simeq \begin{cases} +i\sqrt{M_1}\left((U_{\text{PMNS}})_{\alpha 2}\sqrt{m_2}\cos\omega + \xi(U_{\text{PMNS}})_{\alpha 3}\sqrt{m_3}\sin\omega\right) & \text{(NH)} \\ +i\sqrt{M_1}\left((U_{\text{PMNS}})_{\alpha 1}\sqrt{m_1}\cos\omega + \xi(U_{\text{PMNS}})_{\alpha 2}\sqrt{m_2}\sin\omega\right) & \text{(IH)} \end{cases} \tag{4.2.35}$$

$$(m_D)_{\alpha 2} \simeq \begin{cases} -i\sqrt{M_2}\left((U_{\text{PMNS}})_{\alpha 2}\sqrt{m_2}\sin\omega - \xi(U_{\text{PMNS}})_{\alpha 3}\sqrt{m_3}\cos\omega\right) & \text{(NH)} \\ -i\sqrt{M_2}\left((U_{\text{PMNS}})_{\alpha 1}\sqrt{m_1}\sin\omega - \xi(U_{\text{PMNS}})_{\alpha 2}\sqrt{m_2}\cos\omega\right) & \text{(IH)} \end{cases} \tag{4.2.36}$$

where α runs over e, μ and τ. Aside from the well-used CI parametrization there are other parametrizations useful for specific scenarios. An overview is given in table 4.1, taken from [CHZ25]. For a modern overview of the various explicit parametrizations consider consulting Appendix A of [CHZ25].

Parametrization	11 independent parameters of MSM
EMSM [CHZ25]	$m_2,\ m_3(m_1),\ \theta_{12},\ \theta_{13},\ \theta_{23},\ \delta_{CP},\ \sigma,\ M_1,\ M_2,\ \theta_{14},\ \delta_{14}$
Casas–Ibarra [CI01]	$m_2,\ m_3(m_1),\ \theta_{12},\ \theta_{13},\ \theta_{23},\ \delta_{CP},\ \sigma,\ M_1,\ M_2,\ \lvert\omega\rvert,\ \arg\omega$
Natural Reconstruction [XZ11a]	$m_2,\ m_3(m_1),\ \theta_{12},\ \theta_{13},\ \theta_{23},\ \delta_{CP},\ \sigma,\ M_1,\ M_2,\ \lvert a_1\rvert,\ \arg a_1$
Blennow–Fernandez-Martinez [BF11]	$m_2,\ m_3(m_1),\ \theta_{12},\ \theta_{13},\ \theta_{23},\ \delta_{CP},\ \sigma,\ M_1,\ M_2,\ \theta_y,\ \theta_z(\theta_x)$
Modified Casas–Ibarra–Ross[Ell+02]	$m_2,\ m_3(m_1),\ \theta_{12},\ \theta_{13},\ \theta_{23},\ \delta_{CP},\ \sigma,\ \lvert P_{13}\rvert,\ \lvert P_{23}\rvert,\ \lvert P_{12}\rvert,\ \arg P_{12}$
Bi-Unitary [XZ20]	$m_2,\ m_3(m_1),\ M_1,\ M_2,\ \theta_1,\ \theta_2,\ \theta_3,\ \delta_L,\ \gamma_L,\ \theta_R,\ \gamma_R$
Vector Representation [BFS19]	$m_2,\ m_3(m_1),\ M_1,\ M_2,\ u_{e1},\ u_{\mu 1},\ \lvert u_{e2}\rvert,\ \lvert u_{\mu 2}\rvert,$ $\arg u_{e2},\ \arg u_{\mu 2},\ \arg u_{\tau 2}$

Table 4.1: Parametrizations and their 11 independent parameters in minimal sterile neutrino models (MSM), taken from [CHZ25]. m3 (m1) denotes the NH (or IH) scenario. One is able to rewrite the masses in terms of the mass differences.

4.2.3 Type II

The Type II seesaw mechanism offers an alternative path to generate small active neutrino masses, replacing the heavy sterile Majorana neutrinos of the Type I scenario with an $SU(2)_L$ scalar triplet Δ carrying hypercharge $Y = +2$ [MW80; SV80; LSW81]. The Yukawa interaction and scalar potential of the form

$$-\mathcal{L} \supset y_\Delta \, \ell_L^T C i\sigma_2 \Delta \, \ell_L \; - \; \mu \, \Phi^T i\sigma_2 \, \Delta \, \Phi \; + \; \text{h.c.}, \tag{4.2.37}$$

leads to a direct Majorana mass term for the active neutrinos once the neutral component of the triplet acquires a VEV, $\langle \Delta^0 \rangle \equiv v_\Delta$. This VEV is induced via the scalar potential term $\mu H^T i\sigma_2 \Delta H$, resulting in an effective mass

$$m_\nu = y_\Delta \frac{\mu v^2}{M_\Delta^2}, \tag{4.2.38}$$

where $v \simeq 246\,\text{GeV}$ is the electroweak VEV, M_Δ is the mass of the triplet scalar, and μ is a dimensionful coupling. Under the assumption $\mu \sim M_\Delta$ and $M_\Delta \gg v$, the active neutrino masses are naturally suppressed. This construction can also be understood as a minimal way of generating the effective Weinberg operator at tree-level using only scalar exotics. In fact, among the three standard seesaw mechanisms, Type II is unique in relying solely on scalar fields, with the triplet Δ playing the central role. The required couplings involve exactly two interaction vertices: one with the lepton bilinear and one with a pair of Higgs fields, putting bounds on the Wilson coefficients and the scale of new physics. The parameter space is, so far, not saturated [Ant+19].

4.2.4 Type III

The Type III seesaw mechanism introduces one or more fermionic triplets Σ transforming as adjoints under $SU(2)_L$ and carrying zero hypercharge [Foo+89]. These are vector-like fermions of the form

$$\Sigma = \begin{pmatrix} \Sigma^0/\sqrt{2} & \Sigma^+ \\ \Sigma^- & -\Sigma^0/\sqrt{2} \end{pmatrix}, \tag{4.2.39}$$

and couple to the Standard Model lepton doublets through a Yukawa interaction

$$\mathcal{L} \supset -y_T \, \bar{\ell}_L \, \Sigma \, \tilde{\Phi} + \text{h.c.}, \tag{4.2.40}$$

where $\tilde{\Phi} = i\sigma_2 \Phi^*$ is the conjugate Higgs doublet, and y_T is the corresponding Yukawa coupling. After electroweak symmetry breaking, the Higgs again acquires a VEV, and again generates an effective Majorana mass for the active neutrinos,

$$m_\nu = -y_T^T M_T^{-1} \, y_T \, v^2. \tag{4.2.41}$$

Here, M_T is the Majorana mass of the triplet fermions, and v is the Higgs VEV. As in the Type I case, at least two triplets are required to explain the two observed neutrino mass splittings and three triplets are required to produce three massive light neutrinos.

Unlike the gauge-singlet right-handed neutrinos of the Type I model, the fermion triplets in this construction are charged under $SU(2)_L$, and therefore participate in electroweak gauge interactions. This implies that the presence of these triplets could be measured directly, leading again to constrains [GKK19].

4.2.5 INVERSE SEESAW

The inverse seesaw mechanism [MV86; Moh86; WW83] adds sterile neutrino fields, but avoids the requirement of them being extremely heavy. In addition to the right-handed neutrinos N_R, it introduces a second set of left-handed sterile states X_L, which are also singlets under the SM gauge group. The mass matrix in the (ν_L, N_R^c, X_L) basis reads

$$M = \begin{pmatrix} 0 & m_D^T & 0 \\ m_D & m_S & \mu_D \\ 0 & \mu_D^T & \mu_X \end{pmatrix}, \tag{4.2.42}$$

where m_D and μ_D are Dirac mass terms, and m_S and μ_X are Majorana. The defining feature is that μ_X explicitly breaks lepton number, and is assumed to be small.

In the limit μ_X, $m_S \ll m_D \ll \mu_D$, one obtains the light neutrino mass matrix

$$m_\nu \simeq m_D^T (\mu_D^{-1})^T \mu_X \mu_D^{-1} m_D, \tag{4.2.43}$$

so the suppression of m_ν is now tied to small lepton number violation rather than to a high seesaw scale. In contrast to the standard type I seesaw, the active–sterile mixing $m_D^T \mu_D^{-1}$ can be sizeable, which makes the model more sensitive to direct experimental probes.

4.2.6 THE νSMEFT

The models above generally described the introduction of heavy fields such that the matter content of the EFT remained similar to that of the SM, thus being compatible with the SMEFT. Since the mass scale of the hypothetical right-handed neutrino does not, due to its feeble interaction, necessarily need to be extremely high, it is useful to understand what the introduction of a right-handed neutrino at SM energy scales might induce. The full expansion of the SMEFT with the addition of a right-handed neutrino that is not yet integrated out is called the νSMEFT, which is described by the Lagrangian

$$\begin{aligned} \mathcal{L}_{\nu\text{SMEFT}} =& \mathcal{L}_{\text{SM}} + \overline{N}_R i \not{\partial} N_R - (Y_\nu \bar{\ell}_L \tilde{H} N_R + \frac{1}{2} \overline{N}_R^c m_S N_R) \\ & + \frac{1}{\Lambda} \sum_i \mathcal{C}_i^5 \hat{O}_i^5 + \frac{1}{\Lambda^2} \sum_i \mathcal{C}_i^6 \hat{O}_i^6 + \dots \end{aligned} \tag{4.2.44}$$

$$\begin{aligned} =& \mathcal{L}_{\text{SM}} + \overline{N}_R i \not{\partial} N_R - (Y_\nu \bar{\ell}_L \tilde{H} N_R + \frac{1}{2} \overline{N}_R^c m_S N_R) \\ & + \sum_{d=5} \frac{1}{\Lambda^{d-4}} \sum_i \mathcal{C}_i^d \hat{O}_i^d . \end{aligned} \tag{4.2.45}$$

In this case the Weinberg operator is no longer the unique dimension 5 operator, but we also generate a magnetic moment and a dimension 5 coupling with two Higgs doublet, correcting the sterile Majorana mass, i.e.

$$\mathcal{L}^{(5)} = \frac{C_5}{\Lambda} \varepsilon_{kl} \varepsilon_{mn} \overline{L_k^c} L_m H_l H_n + \frac{C_{\nu B}^R}{\Lambda} \overline{\nu_R^c} \sigma^{\mu\nu} \nu_R B_{\mu\nu} + \frac{C_{\nu H}}{\Lambda} \overline{\nu_R^c} \nu_R H^\dagger H, \tag{4.2.46}$$

with C denoting the Wilson coefficients, L a left-handed doublet, H the Higgs doublet and $B_{\mu\nu}$ the field strength tensor of the $U(1)_Y$ gauge boson. In dimension six the extra operators are taken from [Fuy+24] and are presented in table 4.2. Through the νSMEFT many tree-level processes emerge that can affect the

$\psi^2 H^3\ (+H.c.)$		$\psi^2 H^2 D$		$\psi^2 HX\,(+H.c.)$	
$\mathcal{O}_{L\nu H}$	$(\bar{L}\,N_R)\,\widetilde{H}\,(H^\dagger H)$	$\mathcal{O}_{H\nu}$ $\mathcal{O}_{H\nu e}$	$(\overline{\nu_R}\gamma^\mu \nu_R)\,(H^\dagger i\overleftrightarrow{D}_\mu H)$ $(\overline{N}_R\gamma^\mu e)(\tilde{H}^\dagger\, iD_\mu H)$	$\mathcal{O}_{\nu B}$ $\mathcal{O}^*_{\nu W}$	$(\bar{L}\sigma_{\mu\nu}\nu_R)\,\widetilde{H}\,B^{\mu\nu}$ $(\bar{L}\sigma_{\mu\nu}N_R)\tau^I\tilde{H}W^{I\mu\nu}$
$(\bar{R}R)(\bar{R}R)$		$(\bar{L}R)(\bar{R}L)$		$(\bar{L}R)(\bar{L}R)\ (+H.c.)$	
$\mathcal{O}_{\nu\nu}$	$(\overline{N_R}\gamma^\mu N_R)(\overline{N_R}\gamma_\mu N_R)$	$\mathcal{O}_{L\nu}$	$(\bar{L}\gamma^\mu L)(\bar{N}_R\gamma_\mu N_R)$	$\mathcal{O}_{L\nu Le}$	$(\bar{L}_i N_R)\,\varepsilon^{ij}(\bar{L}_j e)$
$\mathcal{O}_{e\nu}$	$(\bar{e}\gamma^\mu e)(\overline{N}_R\gamma_\mu N_R)$	$\mathcal{O}_{Q\nu}$	$(\bar{Q}\gamma^\mu Q)(\overline{N}_R\gamma_\mu N_R)$	$\mathcal{O}_{L\nu Qd}$	$(\bar{L}^i N_R)\varepsilon^{ij}(\bar{Q}^j d)$
$\mathcal{O}_{u\nu}$	$(\bar{u}\gamma^\mu u)(\overline{N}_R\gamma_\mu N_R)$			$\mathcal{O}^{(3)}_{L\nu Qd}$	$(\bar{L}^i\sigma^{\mu\nu}N_R)\varepsilon^{ij}(\bar{Q}^j\sigma_{\mu\nu}d)$
$\mathcal{O}_{d\nu}$	$(\bar{d}\gamma^\mu d)(\bar{N}_R\gamma_\mu N_R)$				
$\mathcal{O}_{du\nu e}$	$(\bar{d}\gamma^\mu u)(\overline{N}_R\gamma_\mu e)$			$\mathcal{O}_{Qu\nu L}$	$(\bar{Q}^i u)(\overline{N}_R L^i)$

Table 4.2: Dimension-6 νSMEFT operators, classified by field content, from [Fuy+24]: *col. 1:* two fermions plus three Higgses; *col. 2:* two fermions, two Higgses and a derivative; *col. 3:* dipole-type operators ($X = B,\ W$), and Hermitian conjugates; *col. 4:* four-fermion operators of various chiralities. Operators marked with a $*$ in col. 3 and col. 4 feed into the neutrino dipole at one loop.

production and decay channels of N_R, thereby allowing for more freedom under experimental constraints. For a derivation of the renormalization group equations, the running of the Wilson coefficients and the low energy matching, see [Fuy+24].

5

The Dodelson–Widrow Mechanism

The type I, II, and III seesaw mechanism can, with the appropriate values, all reproduce low-energy theories that are compatible with unitarity constraints in the active neutrino sector [PR16]. Extending the Standard Model, however, even if minimally, should be done with caution. It would be much more convincing if the addition of a certain particle also predicted further behaviour that could be measured directly or indirectly, for example, through cosmological consequences. Even better would be if the addition also solved one of the shortcomings of the standard model described in section 2.4. In this light, a natural question when adding matter is, of course, if that matter could be a suitable candidate for the missing dark matter. Also, the various seesaw models above are ideally reproduced by a BSM extension that is natural and minimal from a particle physics point of view. From here, it is arguably even more natural to include a right-handed sterile counterpart for the neutrino (through the type I seesaw mechanism) than to leave the Standard Model as it is. This favours the type I seesaw mechanism over the other types, which would still leave the question open of why there is no right-handed neutrino. We saw that due to its neutrality under all gauge interactions, the small mixing angle and large mass, the introduction of such a sterile neutrino will not be easily detectable through direct searches. Its feeble interaction also has an advantage, however, as it allows for a possible feebly interacting, stable yet heavy dark matter candidate. For this reason, the sterile neutrino has received much attention as possible dark matter, more so than the scalar and fermionic triplets of the type II and III mechanism, and it is this sterile DM candidate that the rest of the thesis is devoted to. Dodelson and Widrow were the first to give a quantitative estimate of the amount of dark matter that could be produced using non-resonant active-to-sterile oscillations in the early universe through a 1+1 model of the type I seesaw mechanism [DW94b]. Due to its success, this so-called Dodelson-Widrow (DW) mechanism has been studied further, modified, and generalised to accommodate for some of the subtleties in the early universe. Resonant-based production was proposed by Shi and Fuller in 1999 [SF99], and also remains a well-studied mechanism. For a modern review, consider reading [Aba17]. In this section, we will reproduce the DW mechanism both in its original form, that is, using relations from a 1+1 simplification, and from a modern perspective, exploiting the scenario of large Δm^2 dominance from section 3.5. First, the Boltzmann equations will be reproduced, then they will be solved for a varying mixing angle, and finally, the resulting sterile neutrino population will be confronted with cosmological bounds.

Both in this section and in the next, some heavy derivations are encountered. To preserve readability, we have opted to dedicate various appendices to the most general and longest of such derivations, which will be referenced accordingly in the text.

5.1 Sterile Neutrino Boltzmann Equations

The starting point in modelling the early universe dynamics of sterile neutrino production lies in the simplification of the Boltzmann equations. For a sterile neutrino distribution $f_s = f_s(p,t)$ our starting point is

$$\mathbb{L}[f_s] = \mathbb{C}[f_s], \tag{5.1.1}$$

and it is the goal to turn both sides into workable expressions. For an FLRW universe, the left-hand side can be rewritten, after some simple manipulation, as

$$\mathbb{L}[f_S] = \frac{\mathrm{d}}{\mathrm{d}\lambda} f_s = \left(\frac{\mathrm{d}x^\alpha}{\mathrm{d}\lambda}\frac{\partial}{\partial x^\alpha} - \frac{\mathrm{d}p^\alpha}{\mathrm{d}\lambda}\frac{\partial}{\partial p^\alpha}\right) f_s \tag{5.1.2}$$

$$= \left(P^\alpha \partial_\alpha - \Gamma^\alpha_{\beta\gamma} P^\beta P^\gamma \frac{\partial}{\partial P^\alpha}\right) f_s \tag{5.1.3}$$

$$= \left(E\partial_t - a(t)\dot{a}(t)\delta_{ij}P^i P^j \frac{\partial}{\partial E}\right) f_s \tag{5.1.4}$$

$$= \left(E\partial_t - H(t)\delta_{ij}P^i P^j a^2(t) \frac{\partial}{\partial E}\right) f_s \tag{5.1.5}$$

$$= \left(E\partial_t - Hp^2 \frac{\partial}{\partial E}\right) f_s \tag{5.1.6}$$

$$= p\left(\partial_t - Hp\frac{\partial}{\partial p}\right) f_s, \tag{5.1.7}$$

where the last equation uses the approximation $E^2 p^2$, with $p^2 \delta_{ij} P^i P^j a^2(t)$ the three-momentum. Formally yet intuitively, this statement implies that the convective derivative of f_s along a geodesic equals the collision integral.

The right-hand side of the Boltzmann equation describes the effect of all microscopic interactions on the evolution of the phase-space distribution. In its most general form, the collision functional for a particle species with momentum p_1^μ is written as

$$C[f_1] = \frac{1}{2E_1} \sum_{\text{processes}} \int \prod_{i=2}^{n} \frac{\mathrm{d}^3 p_i}{(2\pi)^3\, 2E_i}\, (2\pi)^4\, \delta^{(4)}\left(\sum_{\text{in}} p - \sum_{\text{out}} p\right) \left|\mathcal{M}\right|^2 \mathcal{F}[f], \tag{5.1.8}$$

where:

- The sum runs over all possible scattering, decay, or production processes in which the species participates;
- $|\mathcal{M}|^2$ is the squared, spin-summed matrix element for the given process;
- The statistical factor $\mathcal{F}[f]$ describes gain and loss for a particular process:

$$\mathcal{F}[f] \;=\; \prod_{\text{out}} [f_{\text{out}}] \prod_{\text{in}} (1 \pm f_{\text{in}}) \;-\; \prod_{\text{in}} [f_{\text{in}}] \prod_{\text{out}} (1 \pm f_{\text{out}}), \tag{R2}$$

with the upper sign for bosons and the lower sign for fermions. The first term represents gain from processes producing the momentum state p_1, while the second term represents loss from processes depleting it. The

$(1 \pm f)$ factors implement Bose enhancement or Pauli blocking.

The relevant process in our case describes the conversion of an active neutrino into a sterile neutrino, in which the interaction rate of the active neutrino is determined by the thermal bath in the early universe, and the conversion is additionally proportional to the oscillation probability at the time of interaction. Following Appendix B, we perform the integrals over the final states of equation 5.1.8 to define the interaction rate, so that our Boltzmann equation becomes

$$\begin{aligned}\left(\partial_t - Hp\frac{\partial}{\partial p}\right)f_S = \sum_i \int & \mathrm{d}^3p'_a \; \Gamma_i(p'_a, p) f_a(p'_a, t)[1 - f_s(p,t)] \\ & - \int \mathrm{d}^3p'_a \; \Gamma_i(p'_a, p) f_s(p,t)[1 - f_a(p'_a, t)],\end{aligned} \tag{5.1.9}$$

where $f_a(p'_a, t)$ represents the active neutrino distribution and $\Gamma_i(p'_a, p)$ is the differential rate kernel. In order to further turn this into a usable equation, we make the following approximations:

1. For a given channel, the kernel $\Gamma_i(p'_a, p)$ is taken to be isotropic, which is well-justified in a homogeneous and isotropic background.
2. $\Gamma_i(p'_a, p)$ is taken to be conservative, meaning that the energy of the final scattered sterile neutrino is similar to that of an initial active neutrino at a local scale. Although the motivation behind this assumption is mostly computational simplicity, the validity of this assumption has been analysed in [**Dolgov_2002**], and it was shown to make of little quantitive difference.
3. Fermi-blocking is taken to be negligible, i.e. $f_i \ll 1$.

With these assumptions, one obtains

$$\left(\partial_t - Hp\frac{\partial}{\partial p}\right)f_s(p,t) \simeq \Gamma(\nu_a \to \nu_s; p, t)\, [f_a(p,t) - f_s(p,t)]\,, \tag{5.1.10}$$

with

$$\Gamma(\nu_a \to \nu_s; p, t) \simeq \frac{1}{2}\Gamma_a(p,t)\langle P_m(\nu_a \to \nu_s; p, t)\rangle \tag{5.1.11}$$

denoting the effective conversion rate from active to sterile neutrinos, where Γ_a is the total scattering rate of the active neutrino species with the thermal bath, $\langle P_m \rangle$ is the in-medium (thermally) averaged oscillation probability, and the factor of 1/2 arises from averaging over spin states [Th092; St087b]. Intuitively, one can understand the rate as proportional to the decoherent interaction rate of the active neutrino (the "measurement" rate) and the probability that such a decoherent interaction results in a sterile neutrino, which is just the oscillation probability at the time of interaction. If one takes the sterile neutrino to be much heavier than the active neutrinos, a mixing scenario similar to that of the large Δm^2-dominance occurs, and we can use the effective probability from equation 3.5.4 to write

$$\begin{aligned}\Gamma(\nu_a \to \nu_s; p, t) &\simeq \frac{1}{2}\Gamma_a(p,t)\langle P_m(\nu_a \to \nu_s; p, t)\rangle & (5.1.12)\\ &= \frac{1}{2}\Gamma_a(p,t)\left\langle \sin^2\left(\frac{\Delta m^2 L}{4E}\right)\right\rangle \sin^2(2\theta_M(p,t)) & (5.1.13)\\ &= \frac{1}{4}\Gamma_a(p,t)\sin^2(2\theta_M(p,t)). & (5.1.14)\end{aligned}$$

5.1.1 Rates and Angles from Thermal Field Theory

In the description of the interactions between the neutrinos and the thermal bath, effects such as finite temperature and finite density should be taken into consideration, requiring a treatment using thermal field theory. These contributions then become important not only in the rate Γ_a, but also in the potential that enters the effective mixing angle. We will not fully reproduce such derivations, but rather take them from reviews such as [Aba17]. We will, however, briefly describe how and why the various terms emerge in the effective mixing angle and then apply them using the cited results.

The starting point is again the fact that, in a medium, the neutrino dispersion relation is modified from its vacuum form. The forward scattering of neutrinos off the background particles adds a correction to the energy,

$$E \;\rightarrow\; E + V(p, T, \mu), \tag{5.1.15}$$

which acts as an effective matter potential. Physically, this term describes the coherent effect of the medium on the neutrino's propagation, analogous to the effect of the charged weak current on the propagation of electron neutrinos in the sun. In the mixing-angle denominator, this real shift appears as $(1 - \frac{V}{\cos 2\vartheta\Delta})^2$. In addition, interactions with the medium also lead to an *imaginary* correction to the dispersion relation,

$$E \;\rightarrow\; E + V(p, T, \mu) \;-\; i\,\frac{\Gamma_a(p, T)}{2}, \tag{5.1.16}$$

whose origin is the finite lifetime of a neutrino state in the medium due to scattering and absorption. This imaginary part describes decoherent interactions which "collapse" the wave packet, and similarly modifies the mixing-angle denominator as

$$\left|1 - \frac{V + i\Gamma_a/2}{\cos 2\vartheta\Delta}\right|^2 = \left(\frac{\Gamma^2/4}{\cos^2 2\vartheta\Delta^2} + \left(1 - \frac{V}{\cos 2\vartheta\Delta}\right)^2\right). \tag{5.1.17}$$

The extra term of Γ_a^2 in the denominator is called the damping term, and can be understood as a quantum Zeno effect. If the mean time before a decoherent interaction (i.e., a measurement) of the neutrino with the background is much shorter than the time required to build up any significant oscillation probability, the state collapses without producing a sterile neutrino. To properly account for this damping, one should recompute the effective mixing angle $\theta_M(p, t)$ through the QKEs, as done in [Sto87b; FV97; BLL00; VW00; LVW00]. We will consider the regimes in which the damping term is relevant or negligible after discussing the thermal potential and the active neutrino interaction rate in section 5.1.2.

Coming back to our manipulation of the Boltzmann equation, we insert the expression for the effective mixing angle in matter from section 3.5. Using formula 3.5.43 for the resonance corresponding to a large mass splitting, we can rewrite

$$\sin^2(2\vartheta_M) = \frac{\tan^2(2\vartheta_M)}{1+\tan^2(2\vartheta_M)} = \frac{\sin^2(2\vartheta)}{\sin^2(2\vartheta) + (\cos(2\vartheta) - \frac{2EV+i\Gamma_a/2}{\Delta m^2})^2} \tag{5.1.18}$$

$$= \frac{\frac{\Delta m^2}{4p^2}\sin^2(2\vartheta)}{\frac{\Delta m^2}{4p^2}\sin^2(2\vartheta) + \Gamma_a^2/4 + [\frac{\Delta m^2}{2p}\cos(2\vartheta) - V]^2} \tag{5.1.19}$$

$$= \frac{\Delta^2 \sin^2(2\vartheta)}{\Delta^2\sin^2(2\vartheta) + \Gamma_a^2/4 + [\Delta\cos(2\vartheta) - V_{\mathrm{T}} - V_D]^2}, \tag{5.1.20}$$

where $\Delta \equiv \Delta(p) = \frac{\Delta m}{2p}$, $V_{\mathrm{T}} = V_T(p, T)$ is the finite temperature contribution to the potential and $V_D = V_D(p, T)$ is the potential arising from finite density effects. Including this in the Boltzmann equation while defining the quantum damping term as $D(p) \equiv \Gamma_a(p)/2$ leads to the familiar form

$$\begin{aligned}\left(\partial_t - Hp\frac{\partial}{\partial p}\right)f_s(p,t) =& \frac{\Gamma_a(p)}{4}\frac{\Delta^2(p)\sin^2 2\vartheta}{\Delta^2(p)\sin^2 2\vartheta + D^2(p) + [\Delta(p)\cos 2\vartheta - V]^2} \\ &\times \left[f_a(p,t) - f_s(p,t)\right].\end{aligned} \tag{5.1.21}$$

The Boltzmann equation derived above is valid for oscillations between any set of neutrino states with a large mass splitting (relative to the mass differences of states within the group) and for any generic isotropic potential. It is this equation that often forms the starting point of calculations involving modified rates and potentials, as will be seen in Section 6.

5.1.2 NOTES ON THE POTENTIALS

The potentials in the equation above arise from forward scattering interactions with background particles in the early universe medium, corresponding to the real part of the active neutrino self-energy in the medium. The loop diagrams for this self-energy contain propagators for the background particles, which are replaced by their thermal versions, incorporating the statistical distributions of the medium. Finite density effects appear when these thermal propagators are traced over asymmetric particle–antiparticle populations, while purely thermal contributions arise from symmetric equilibrium distributions. Figure 5.1.1 illustrates the lowest-order diagrams contributing to the forward-scattering potential. The density potential is given by

$$V_D = \sqrt{2}G_F\begin{cases} 2(n_{\nu_e} - n_{\bar\nu_e}) + (n_{\nu_\mu} - n_{\bar\nu_\mu}) + (n_{\nu_\tau} - n_{\bar\nu_\tau}) + (n_e^- - n_{e^+}) - \frac{n_n}{2} & \text{for } \nu_e \rightleftharpoons \nu_s, \\ (n_{\nu_e} - n_{\bar\nu_e}) + 2(n_{\nu_\mu} - n_{\bar\nu_\mu}) + (n_{\nu_\tau} - n_{\bar\nu_\tau}) - \frac{n_n}{2} & \text{for } \nu_\mu \rightleftharpoons \nu_s, \\ (n_{\nu_e} - n_{\bar\nu_e}) + (n_{\nu_\mu} - n_{\bar\nu_\mu}) + 2(n_{\nu_\tau} - n_{\bar\nu_\tau}) - \frac{n_n}{2} & \text{for } \nu_\tau \rightleftharpoons \nu_s. \end{cases}$$

from which the proportionality to lepton asymmetries is easily read. Although the case of an initial lepton number is interesting and can lead to useful resonances for sterile neutrino production, studied primarily in [SF99] and refined in [AFP01], it is not the aim of this research and will therefore be neglected from now on. The thermal potential has positive contributions from both leptons and anti-leptons, and its contribution for a flavour α is given by

$$V_T(p) = -\frac{8\sqrt{2}G_F p}{3m_Z^2}\left[\left(\langle E_{\nu_\alpha}\rangle n_{\nu_\alpha} + \langle E_{\bar\nu_\alpha}\rangle n_{\bar\nu_\alpha}\right) + \left(\langle E_\alpha\rangle n_\alpha + \langle E_{\bar\alpha}\rangle n_{\bar\alpha}\right)\right], \tag{5.1.22}$$

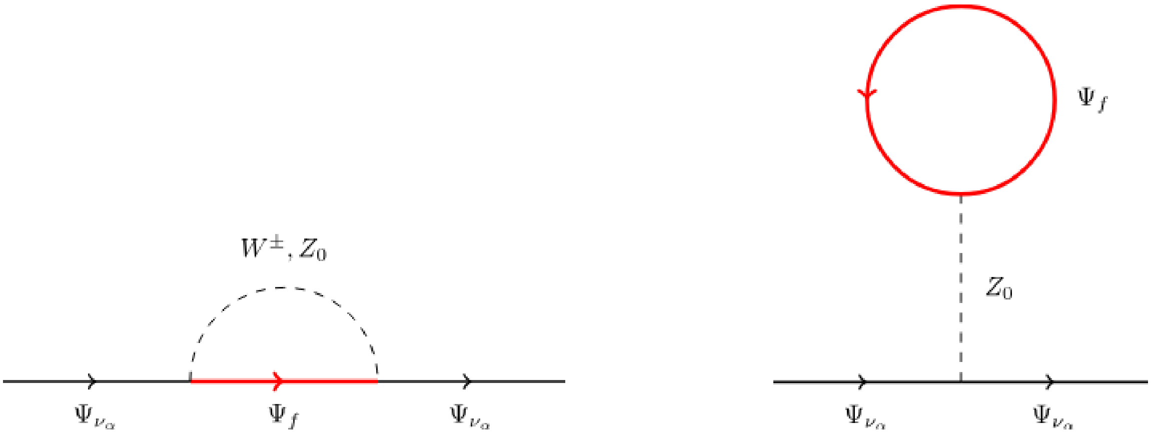

Figure 5.1.1: Lowest order contributions to a propagating active neutrino's self energy. Red lines are thermal propagators. From [Aba17].

which, for a symmetric lepton vs anti-lepton scenario, can be reduced to

$$V_T(p) = -\frac{16\sqrt{2}G_F p}{3m_Z^2}\left[\left(\langle E_{\nu_\alpha}\rangle n_{\nu_\alpha} + \langle E_\alpha\rangle n_\alpha\right)\right]. \tag{5.1.23}$$

Since the number density of non-relativistic particles like τ is exponentially suppressed, they will not contribute to the potential. The muon becomes non-relativistic at around $\mathcal{O}(100\text{MeV})$, so in the early universe its contributions should be modelled with caution. For the electron neutrino, the potential is given by [AFP01; Kel+20] as

$$V_T = -3.72\, G_{\mathrm{F}}\, p\, T^4 \left(\frac{1}{m_Z^2} + \frac{2}{m_W^2}\right). \tag{5.1.24}$$

The collision or interaction rate through W and Z bosons is given up to first order, for electron neutrinos and muon or tau neutrinos respectively, by [AFP01]

$$\Gamma_a(p) = \begin{cases} 1.27 G_{\mathrm{F}}^2\, p\, T^4 & \text{for } \nu_e, \\ 0.92 G_{\mathrm{F}}^2\, p\, T^4 & \text{for } \nu_\mu, \quad \nu_\tau. \end{cases} \tag{5.1.25}$$

For contributions up to two-loop diagrams in various epochs of the early universe, one is referred to the tabulated values of the supplementary material of [ASL07]. From the rate described above, we are able to discuss the contribution of the damping term in equation 5.1.21. As we see that the full term is of the same order of magnitude as the interaction rate squared, and that the interaction rate is of similar order of the thermal potential, we are inclined to say that the damping term is non-negligible. One should take into account, however, that the potential enters in the Boltzmann equation with an additional power of Δ, and so one must evaluate the relation between Δ and $\Gamma(p)$ in order to evaluate the relevance of the damping term. For a sterile neutrino with $m_s > 10\text{keV}$ at temperatures around $\mathcal{O}(10^2\text{MeV})$, one finds that the omission of the damping term is easily justified, since

$$\Delta m^2 \simeq 10^{-10}\text{GeV}^2 \gg \Gamma_a p \simeq G_F^2 T^4 p^2 = \mathcal{O}(10^{-16}\text{GeV}^2), \tag{5.1.26}$$

while such an assumption is no longer valid as T approaches 1GeV. One should note that no potential term is added for the sterile neutrinos, as we expect no interactions in this sector. A modification of such a condition can lead to fruitful results and will be investigated later [AV24].

To obtain our final form of the Boltzmann equation, we recall that neutrinos are not produced in any sort of other fundamental interaction so we can set the initial distribution to zero and consider only terms related to oscillations. Additionally, there is an important distinction between the oscillation of active into sterile neutrinos versus sterile into active oscillations, as for oscillations back into active neutrinos a quantum measurement is practically never performed for a small f_s, and any potential scattering with the heavy neutrino state through its tiny active component becomes coherent. Beyond tree-level, the decay from sterile neutrinos back into active neutrinos does occur, but on a timescale much larger than the production era [Wol81]. This means that for the collision term, we must only account for the production of sterile neutrinos, and can neglect the negative term of f_s in the Boltzmann equations. Applying this and neglecting the damping term and lepton potential, one obtains the relation

$$\left(\partial_t - Hp\frac{\partial}{\partial p}\right) f_S(p,t) = \frac{\Gamma_a(p)}{4}\sin^2(2\vartheta_{\text{eff}}(p,T))\, f_a(p,t), \tag{5.1.27}$$

where

$$\sin^2 2\vartheta_{\text{eff}} = \frac{\Delta^2(p)\sin^2 2\vartheta}{\Delta^2(p)\sin^2 2\vartheta + [\Delta(p)\cos 2\vartheta - V_T]^2} \tag{5.1.28}$$

which is to be valid in the sub- GeV region. A final comment concerns the form of $f_a(p,t)$. If we assume the active neutrinos to be in thermal equilibrium, which is relevant in the production epoch as we expect $T \gg T^{\nu}_{\text{freeze-out}} \sim \mathcal{O}(1)\text{MeV}$, we can describe the active distribution function by

$$f_A(E,t) = \frac{1}{e^{E/T}+1} \simeq \frac{1}{e^{p/T}+1}. \tag{5.1.29}$$

The task is now to solve the above equation.

5.2 SOLVING THE EQUATION

For the sole purpose of calculating the DM abundance, the evolution of various momentum modes does not need to remain resolved, but only knowledge of the number density evolution is required. For this reason, we integrate both sides of the equation over momentum phase space to get

$$\dot{n}_s + 3Hn_s = n_a\gamma, \tag{5.2.1}$$

where

$$\gamma = \frac{1}{n_a}\int \frac{d^3p}{2(2\pi)^3}\sin^2(2\theta_{\text{eff}}(p,T))\Gamma_a(p,T) f_a, \tag{5.2.2}$$

and the number density is given by

$$n_i = \frac{g}{(2\pi)^3}\int d^3p\, f_i, \tag{5.2.3}$$

with for neutrinos the internal degrees of freedom being $g = 2$. In order to understand the development of the abundance better, we express our equations in terms of the ratio $r = \frac{n_s}{n_a}$ and rewrite

$$\dot{n}_S + 3Hn_s = n_a\gamma \tag{5.2.4}$$

$$\frac{\dot{a}}{a}\frac{dn_s}{d\ln a} + 3Hn_s = n_a\gamma \tag{5.2.5}$$

$$\frac{\frac{dn_s}{d\ln a}}{n_a} + 3r = \frac{\gamma}{H} \tag{5.2.6}$$

$$\frac{dr}{d\ln a} + r\frac{\frac{dn_a}{d\ln a}}{n_a} + 3r = \frac{\gamma}{H} \tag{5.2.7}$$

$$\frac{dr}{d\ln a} + r\frac{d\ln(T^3)}{d\ln a} + 3r = \frac{\gamma}{H} \tag{5.2.8}$$

$$\frac{dr}{d\ln a} - r\frac{d\ln g_*}{d\ln a} - \cancel{3r\frac{d\ln a}{d\ln a} + 3r} = \frac{\gamma}{H}, \tag{5.2.9}$$

where we used that $g_* a^3 T^3 =$ constant, and so $n_a \propto T^3 \propto g_*^{-1}a^{-3}$, which leads to

$$\frac{dr}{d\ln a} = \frac{\gamma}{H} + r\frac{d\ln g_*}{d\ln a}. \tag{5.2.10}$$

Especially after the quark-hadron transition g_* stays approximately constant and so the amount of sterile neutrinos is mostly determined by the development of the ratio γ/H. In order to understand the production, we must therefore understand the expression for the rate given in 5.2.2.

The proportion γ/H can be rewritten, using $H^{-1} = \frac{M_{\mathrm{Pl}}}{1.66\sqrt{g_*}T^2}$ and by defining $s_\vartheta \equiv \sin 2\vartheta$, $c_\vartheta \equiv \cos 2\vartheta$ and $\Gamma_a \equiv 0.92\ G_F^2 p\, T^4$, as

$$\begin{aligned}
\frac{\gamma}{H} &= \frac{1}{\sqrt{g_*}}\frac{M_{\mathrm{Pl}}}{1.66}\frac{1}{2n_aT^2}\int_0^\infty \frac{\mathrm{d}^3p}{(2\pi)^3}\sin^2 2\vartheta_{\mathrm{eff}}\Gamma_a(p,T)f_a && (5.2.11)\\
&= 0.28\frac{M_{\mathrm{Pl}}G_{\mathrm{F}}^2}{\sqrt{g_*}}\frac{1}{n_aT^2}\frac{1}{(2\pi)^3}\int_0^\infty \mathrm{d}^3p\,\frac{\Delta^2 s_\vartheta^2}{s_\vartheta^2 + [\Delta c_\vartheta - V_T]^2}pT^4 f_a && (5.2.12)\\
&= \frac{0.28}{3\zeta(3)}\frac{M_{\mathrm{Pl}}G_{\mathrm{F}}^2}{\sqrt{g_*}}\frac{s_\vartheta^2}{T}\frac{1}{4\pi}\int_0^\infty \mathrm{d}^3p\,\frac{p}{s_\vartheta^2 + [c_\vartheta + \frac{-V_T}{\Delta}]^2}f_a, && (5.2.13)
\end{aligned}$$

where we inserted $n_a = \frac{3\zeta(3)}{2\pi^2}T^3$. Next, we will insert our definition for

$$V_T = -1.37\cdot 10^2\ G_{\mathrm{F}}^2 p\, T^4,$$

and in an attempt to improve readability we approximate $\cos 2\vartheta \simeq 1$ and neglect the sine term in the denominator, i.e. $c_\vartheta \simeq 1,\ s_\vartheta^2 + 1 \simeq 1$.

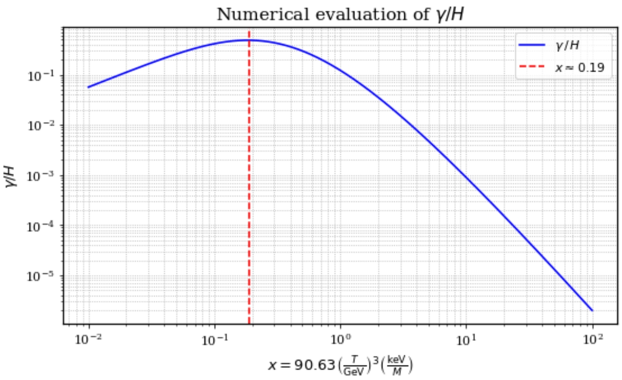

Figure 5.2.1: Numerical evaluation of $\frac{\gamma}{H}$ with a constant $g_* = 10.8$, leading to maximum in relative production at $x \simeq 0.19$.

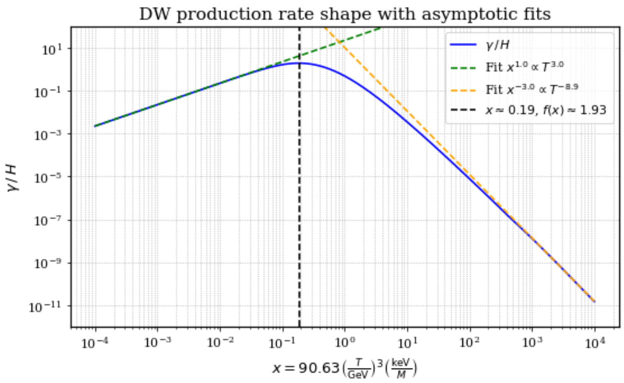

Figure 5.2.2: DW production rate with asymptotic fits, the low T regime scaling like $\sim T^3$ and the high T regime scaling like $\sim T^{-9}$.

Although the integral is almost ready to be performed numerically at this point, it is good practice to define the integral in terms of dimensionless variables. To this extent, we define $y \equiv p/T$ and $x \equiv c\left(\frac{T}{\mathrm{GeV}}\right)^3\left(\frac{m_S}{\mathrm{keV}}\right)^{-1}$ with $c^2 \equiv 2.74 \cdot 10^2 G_\mathrm{F}^2(\mathrm{GeV})^6/(\mathrm{keV})^2 \simeq (90.63)^2$, such that it will cancel nicely. Plugging our new definitions into the integral yields

$$= \frac{0.28}{3\zeta(3)}\frac{M_\mathrm{Pl}G_\mathrm{F}^2}{\sqrt{g_*}}s_\vartheta^2 T^3 \int_0^\infty \mathrm{d}y \frac{y^3}{[1+\frac{2.74\cdot 10^2 G_\mathrm{F}^2 T^6 y^2}{\Delta m^2}]}\frac{1}{e^y+1}$$

$$= \frac{0.28}{3\zeta(3)}\frac{M_\mathrm{Pl}G_\mathrm{F}^2}{\sqrt{g_*}}s_\vartheta^2 \frac{m_s\,\mathrm{GeV}^3}{\mathrm{keV}c} x \int_0^\infty \mathrm{d}y \frac{y^3}{(e^y+1)[1+\frac{2.74\cdot 10^2 G_\mathrm{F}^2(\,\mathrm{GeV})^6 x^2 y^2}{c^2(\mathrm{keV})^2}]^2} \tag{5.2.14}$$

$$= \frac{0.28}{3\zeta(3)}\frac{M_\mathrm{Pl}G_\mathrm{F}^2}{c}\frac{10^{-7}}{\sqrt{10.8}}\left(\frac{\sin^2 2\vartheta}{10^{-8}}\right)\left(\frac{10.8}{g_*}\right)^{1/2}\left(\frac{m_s}{10\mathrm{keV}}\right)\underbrace{x\int_0^\infty \mathrm{d}y \frac{y^3}{(e^y+1)(1+x^2y^2)^2}}_{\equiv I(x)} \tag{5.2.15}$$

$$\simeq \frac{9.31}{90.63}\left(\frac{\sin^2 2\vartheta}{10^{-8}}\right)\left(\frac{10.8}{g_*}\right)^{1/2}\left(\frac{m_s}{10\mathrm{keV}}\right)I(x), \tag{5.2.16}$$

where the interaction rate is taken to have contributions from both electrons and muons, according to equation 5.1.25. The normalised rate γ/H measures the production rate of sterile neutrinos relative to the expansion of the universe, so a value of $\gamma/H \sim 1$ implies that sterile neutrinos are efficiently produced via oscillations with active neutrinos during that epoch. The integration over $y = p/T$ sums over the momentum dependence of this rate, weighed by the thermal distribution of active neutrinos. The integral itself is not easily done analytically and is performed numerically using Python, as described in some more detail in Appendix C.1. Taking $g_* = 10.8$, $\sin^2 2\vartheta = 10^{-8}$ and $m_s = 10\mathrm{keV}$, one finds that γ/H has a maximum at $x \simeq 0.19$, or $T_\mathrm{max} \simeq 128\ \mathrm{MeV}\ (m_S/\mathrm{keV})^{\frac{1}{3}}$, as can be seen from figure 5.2.1. Furthermore, one is able to extract the asymptotic scaling behaviour by fitting the numerical result in the regions $x \ll 1$ and $x \gg 1$, corresponding respectively to low and high temperature limits. The resulting fit shows that $\gamma/H \propto x \sim T^3$ for $x \lesssim 0.01$, while for $x \gtrsim 1$ one obtains $\gamma/H \propto x^{-3} \sim T^{-9}$. The fits in 5.2.2 were obtained via linear regression in log-log space over the respective domains, and the code is available in Appendix C.1. It thus becomes clear that there is only a limited temperature range in which production through the DW mechanism becomes close to efficient. At temperatures much above or below $\mathcal{O}(100\mathrm{MeV})$, a strong suppression takes place, which is even without considering the additional suppression from the damping term.

While the integrated evolution equation for the number density provides insight into the total abundance of sterile neutrinos, it does not retain any information about how these particles are distributed in momentum. This distinction becomes important when considering physical effects that are sensitive to the detailed shape of the distribution function, such as the free-streaming behaviour of sterile neutrinos and their impact on structure formation. Moreover, the oscillation and production rates themselves depend on energy, so different modes will have different oscillation probabilities, and thus we cannot draw strong conclusions on the phase-space distribution just from the number density. To describe the full evolution of the distribution, we therefore require a treatment that resolves the full momentum dependence. This is a fairly tedious task, but by assuming that the effective number of relativistic degrees of freedom g_* remains approximately constant during the production epoch, it becomes possible to severely simplify the relevant equations analytically. Starting from the original equation 5.1.27, we will use the identity

$$T\left(\frac{\partial f_S}{\partial T}\right)_E + E\left(\frac{\partial f_S}{\partial E}\right)_T = T\left(\frac{\partial f_S}{\partial T}\right)_{E/T} \tag{5.2.17}$$

to rewrite

$$\partial_t f_S - HE\frac{\partial}{\partial E}f_S = \left[\frac{1}{4}\sin^2(2\vartheta_{\mathrm{eff}})\Gamma_a\right]f_A \tag{5.2.18}$$

$$-H\left(T\frac{\partial f_S}{\partial T}\bigg|_E + E\frac{\partial f_S}{\partial E}\bigg|_T\right) = \left[\frac{1}{4}\sin^2(2\vartheta_{\mathrm{eff}})\Gamma_a\right]f_A \tag{5.2.19}$$

$$-\frac{\partial}{\partial T}\left(\frac{f_S}{f_A}\right)\bigg|_{p/T} = \frac{1}{4}\frac{\alpha s_\vartheta^2}{\sqrt{g_*}}\frac{pT}{[1-\frac{V_T}{\Delta}]^2}, \tag{5.2.20}$$

where in the last equation we defined $\alpha \equiv \frac{0.92 M_{\mathrm{Pl}} G_{\mathrm{F}}^2}{1.66}$, we used that $HT = 1.66\sqrt{g_*}T^3/M_{\mathrm{Pl}}$ and that for a constant g_*

$$\frac{\partial}{\partial T}\left(\frac{f_S}{f_A}\right)_{(y=p/T)} = \frac{1}{f_A}\left(\frac{\partial f_S}{\partial T}\right)_y - \frac{f_S}{f_A^2}\left(\frac{\partial f_A(y)}{\partial T}\right)_y = \frac{1}{f_A}\left(\frac{\partial f_S}{\partial T}\right)_y. \tag{5.2.21}$$

Again changing the variables from T to x and y and integrating both sides gives

$$\frac{f_S}{f_A} = \frac{1}{4}\frac{\alpha s_\vartheta^2}{\sqrt{g_*}}\int_T^\infty \mathrm{d}T'\frac{pT'}{[1+x^2y'^2]^2} \tag{5.2.22}$$

$$= \frac{1}{4}\frac{\alpha s_\vartheta^2}{\sqrt{g_*}}\int_T^\infty \mathrm{d}T'\frac{yT'^2}{[1+x^2y'^2]^2} \tag{5.2.23}$$

$$= \frac{1}{4}\frac{\alpha s_\vartheta^2}{\sqrt{g_*}}\frac{\mathrm{GeV}^3}{\mathrm{keV}}\frac{m_s}{3c}y\int_x^\infty \mathrm{d}x'\frac{1}{[1+x'^2y^2]^2} \tag{5.2.24}$$

$$= \frac{1}{12}\frac{\alpha\,\mathrm{GeV}^3}{\sqrt{10.8}c}10^{-7}\left(\frac{m_s}{10\mathrm{keV}}\right)\left(\frac{\sin^2(2\vartheta)}{10^{-8}}\right)\left(\frac{10.8}{g_*}\right)^{1/2}y\int_x^\infty \mathrm{d}x'\frac{1}{[1+x'^2y^2]^2} \tag{5.2.25}$$

$$\simeq 0.062\left(\frac{m_s}{10\mathrm{keV}}\right)\left(\frac{\sin^2(2\vartheta)}{10^{-8}}\right)\left(\frac{10.8}{g_*}\right)^{1/2}y\int_x^\infty \mathrm{d}x'\frac{1}{[1+x'^2y^2]^2} \tag{5.2.26}$$

The ratio f_S/f_A, even after computing the integral, remains a complex function depending on x and y. This is to be expected, as the dynamics in the early universe are such that production varies along with temperature, and additionally, because oscillation probabilities depend on varying momentum. In figures 5.2.1 and 5.2.2 we saw, however, that most of the production of sterile neutrinos occurs at a temperature slightly above

100MeV, and that afterwards the production decreases sharply. Well below this value, production due to oscillations effectively ceases and the sterile distribution freezes in. Below the active neutrino freeze-out temperature at around $\sim$ 1MeV, the ratio will no longer change either. This motivates us to study the integral of the limit $T \ll T_{\max}$, taking $x \to 0$, and to interpret the resulting distribution as final. The expression becomes a standard integral if we change variables from $x \to u = xy$, $dx \to \frac{1}{y}du$, and gives

$$\int_{x=0}^{\infty} \mathrm{d}x' \frac{1}{[1+x'^2y^2]^2} = \frac{\pi}{4y}. \tag{5.2.27}$$

Accounting for this numerical factor then leads to a final ratio of

$$\frac{f_S}{f_A} = 0.049\left(\frac{m_s}{10\mathrm{keV}}\right)\left(\frac{\sin^2(2\vartheta)}{10^{-8}}\right)\left(\frac{10.8}{g_*}\right)^{1/2}, \tag{5.2.28}$$

which is just a constant depending on the sterile mass and the mixing angle, and in particular, no longer has any momentum dependence. This implies that the final sterile distribution mimics a thermal active neutrino distribution, which allows us to construct resulting energy densities and cosmological values directly from the active neutrino sector values.

5.3 DW STERILE NEUTRINOS AS DARK MATTER

From equation 5.2.28 the computation of the energy density is a straightforward matter of rewriting

$$\frac{\Omega_s}{\Omega_a} = \frac{m_s n_s}{m_a n_a} = \frac{m_s f_s}{m_a f_a} \tag{5.3.1}$$

into

$$\begin{aligned}
\Omega_s &= \frac{\Omega_a}{m_a} m_s \frac{f_s}{f_a} && (5.3.2)\\
&= \frac{1}{92h^2\mathrm{eV}} 10\mathrm{keV} \cdot 0.049\left(\frac{m_s}{10\mathrm{keV}}\right)^2\left(\frac{\sin^2(2\vartheta)}{10^{-8}}\right)\left(\frac{10.8}{g_*}\right)^{1/2} && (5.3.3)\\
&\simeq 10.87\left(\frac{m_s}{10\mathrm{keV}}\right)^2\left(\frac{\sin^2(2\vartheta)}{10^{-8}}\right)\left(\frac{10.8}{g_*}\right)^{1/2}, && (5.3.4)
\end{aligned}$$

and so

$$\frac{\Omega_s}{0.26} = 0.418\left(\frac{m_s}{\mathrm{keV}}\right)^2\left(\frac{\sin^2(2\vartheta)}{10^{-8}}\right)\left(\frac{10.8}{g_*}\right)^{1/2}. \tag{5.3.5}$$

The DW mechanism is thus easily able to produce the full dark matter energy density with reasonable mass and mixing angle values. Tuning the parameters to a value of $\Omega_s/0.26 = 1$ gives a line in parameter space commonly known as the Dodelson-Widrow line. The DW contour lines for various fractions of the total dark matter is given in figure 5.3.1.

Above, we presented the expression for the energy density for a general mass and mixing angle. If one probes a pure 1+1 seesaw model, however, a relation between ϑ and m_s is naturally induced, as was described in 4.2.12. Although this scenario is not considered to be realistic, it is worth mentioning since it was the original model used by Dodelson and Widrow in [DW94b], and it is a hypothetical way to obtain information about the

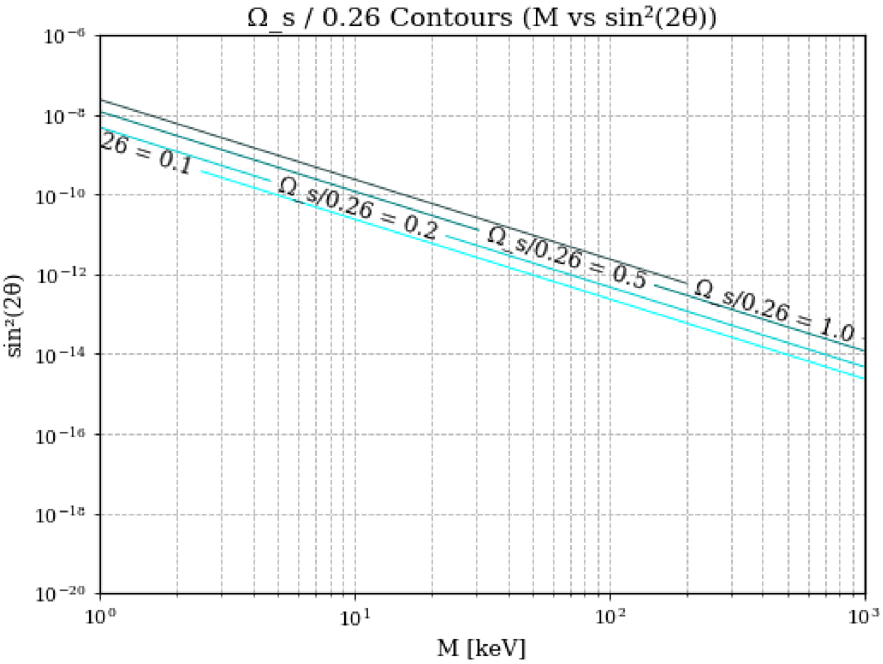

Figure 5.3.1: Dodelson–Widrow line for various fractions of $\frac{\Omega_s}{0.26}$, plotted in the parameters space of $\sin^2 2\vartheta$ and the sterile neutrino mass in units of keV.

Dirac component of the neutrino mass matrix, m_D. Using

$$\sin^2 2\vartheta \simeq 4\vartheta^2 \simeq 4\frac{m_D^2}{m_s^2}, \tag{5.3.6}$$

one can see that the mass of the sterile neutrino is cancelled out in the energy density, leaving only the relation

$$\frac{\Omega_s}{0.26} = 4 \cdot 41.81\left(\frac{m_D^2}{\mathrm{eV}^2}\right)\left(\frac{10.8}{g_*}\right)^{1/2} \simeq 1.67\left(\frac{m_D}{10^{-1}\mathrm{eV}}\right)^2\left(\frac{10.8}{g_*}\right)^{1/2}. \tag{5.3.7}$$

Note in particular that there is only one parameter, m_D, so requiring sterile neutrinos to be all dark matter puts a precise prediction on m_D, and through bounds on m_ν also on m_s. As mentioned, this is not considered to be relevant due to the oversimplification and the exclusion of such values in parameters space.

5.3.1 X-Ray Constraints

Although gauge singlets ν_R are not coupled to any gauge bosons, we saw that the heavy mass eigenstate ν_4 obtains a small fractional component of a weak eigenstate. It is through this component that the heavy state can undergo radiative decay through the weak interaction, thus putting bounds on the ν_4 dark matter candidacy. Such modes were first worked out by Shrock [Shr74] and Pal and Wolfenstein [PW82b]. The decay channels are given in figure 5.3.2. The constraints due to these decays are twofold: first of all, the general lifetime of ν_4 must be long enough to explain dark matter in various epochs of the universe and not spoil production, for which all decay channels are relevant; secondly, measurements or non-measurements of photon by-products of the first two channels can put direct bounds on sterile neutrino abundances. The

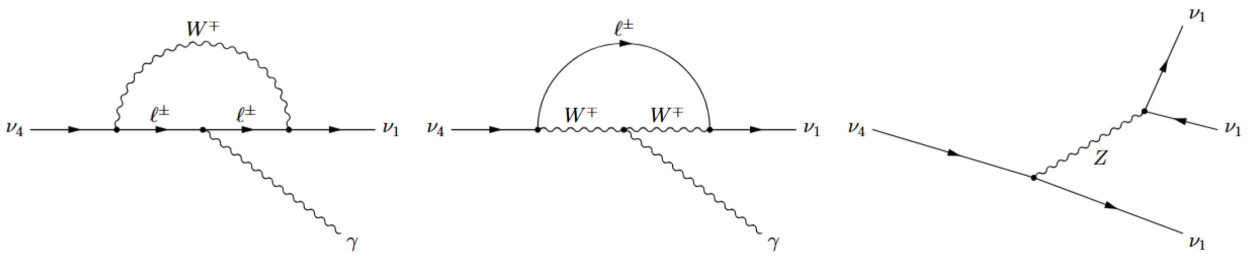

Figure 5.3.2: Diagrammatic representations of heavy neutrino decay channels, taken from [Kop21].

photonic decay rates from the first two diagrams are given by [Kop21; Shr74; LS77; MS77; PW82a; Shr82]

$$\Gamma(\nu_4 \to \nu_a \gamma)^{\mathrm{D}} = \frac{9\alpha_{\mathrm{em}} G_F^2 m_4^5}{512\pi^4} \sum_{j=1,2,3} \left(1 - \frac{m_j^2}{m_4^2}\right)^3 \left(1 + \frac{m_j^2}{m_4^2}\right) \left| \sum_{\alpha=e,\mu,\tau} \left(1 - \frac{m_\alpha^2}{2M_W^2}\right) U_{\alpha 4} U_{\alpha j}^* \right|^2$$
$$\simeq 0.683 \times 10^{-30}\,\mathrm{s}^{-1} \times \left(\frac{\sin^2 2\theta}{10^{-8}}\right) \times \left(\frac{m_4}{\mathrm{keV}}\right)^5 \tag{5.3.8}$$

in the case of Dirac neutrinos, and [PW82a; XZ11b]

$$\Gamma(\nu_4 \to \nu_a \gamma)^{\mathrm{M}} = \frac{9\alpha_{\mathrm{em}} G_F^2 m_4^5}{256\pi^4} \sum_{j=1,2,3} \left(1 - \frac{m_j^2}{m_4^2}\right)^3 \times \tag{5.3.9}$$
$$\left\{ \left(1 + \frac{m_j^2}{m_4^2}\right)^2 \left[\sum_{\alpha=e,\mu,\tau} \left(1 - \frac{m_\alpha^2}{2M_W^2}\right) \mathrm{Im}(U_{\alpha 4} U_{\alpha j}^*) \right]^2 \right.$$
$$\left. + \left(1 - \frac{m_j^2}{m_4^2}\right)^2 \left[\sum_{\alpha=e,\mu,\tau} \left(1 - \frac{m_\alpha^2}{2M_W^2}\right) \mathrm{Re}(U_{\alpha 4} U_{\alpha j}^*) \right]^2 \right\}$$
$$\simeq 1.36 \times 10^{-30}\,\mathrm{s}^{-1} \times \left(\frac{\sin^2 2\theta}{10-8}\right) \times \left(\frac{m_4}{\mathrm{keV}}\right)^5 \tag{5.3.10}$$

for Majorana neutrinos, where m_j represent the mass eigenstates and m_α the flavour eigenstates. The difference in Dirac vs Majorana rates is due to the fact that for Majorana neutrinos both $W^\pm \ell^\mp$ loops contribute, while for Dirac (anti-) neutrinos only $W^{+(-)} \ell^{-(+)}$ is present.

The rates above estimate the lifetime of a sterile neutrino to be of the order $\tau \propto \mathcal{O}(10^{30}\mathrm{s})$, which is much larger than the age of the universe, as is required for a viable DM candidate. We can thus safely conclude that the radiative decay does not spoil stability or production.

The constraints from photon (non-)measurements, on the other hand, are quite harsh, and we will take some time to investigate their effects on the DW line (see figure 5.3.3). The emitted photons are expected to lie in the keV range, and could thus be detectable by X-ray telescopes. Given $m_4 \gg m_1$ we get kinematically, from $p_4^2 = (p_1^\mu + k_\gamma^\mu)^2$, that the photon energy

$$E_\gamma = \frac{m_4}{2} + \mathcal{O}(m_1) = \frac{m_4}{2} + \mathcal{O}(\mathrm{eV}),$$

so for an $\mathcal{O}(10 \text{ keV})$ sterile neutrino we expect the emission of 5 keV photons from high DM-density areas. The peculiar velocity of each sterile neutrino induces a Doppler broadening of the spectrum coming from, for example, centres of galaxies or galaxy clusters. The decay rate in 5.3.10 is of importance for the intensity of a potential signal, so the predicted signal is also dependent on $\sin^2 2\vartheta$ and m_s. Although the lifetime of the sterile neutrinos is large for the expected ranges of $\sin^2 2\vartheta$ and m_s, the fields of view of X-ray telescopes like *Chandra* or *XMM-Newton* contain around 10^{78} particles, so one expects a signal from a $10^{15}M_\odot$ cluster to be around $10^{48}\mathrm{s}^{-1}$ [Aba17]. The first constraint by the diffuse X-ray background was performed by Drees and Wright [Dre00], and was strengthened by Dolgov [DH02]. The first estimates for rates from dark matter halos from galaxies and clusters together with search proposals, came from [AFT01]. Since then, many sources have been studied as a follow-up, including the cosmic X-ray background [Boy+06a], clusters [C R+06], dwarf galaxies [Boy+06b; LKB09; LK12; LK10], the Andromeda galaxy [CZN12] and the Milky Way [RHP06]. The most stringent constraints have been derived from deep X-ray studies of nearby galaxies and clusters. In particular, the *Chandra* analysis of the Andromeda galaxy by Horiuchi *et al.* [Hor+14] currently provides one of the tightest bounds on the parameter space. Comparable limits are obtained from stacked observations of dwarf spheroidal galaxies [MNE14], while Perseus cluster data from *Suzaku* extend the reach to somewhat higher sterile neutrino masses [Tam+15]. At even higher energies, complementary constraints arise from the full-sky *Fermi* GBM measurements [Ng+15] and INTEGRAL/SPI observations of the Galactic halo [Boy+08]. Together, these searches consistently find no statistically significant unidentified emission lines and instead provide upper limits on the decay flux across a wide mass range. A plot combining the various constraints is presented in figure 5.3.3, taken from [Aba17]. As can be seen, the combined X-ray bounds completely rule out the Dodelson-Widrow line parameter space.

5.3.2 Cosmological Constraints

Aside from X-ray production, a sterile neutrino dark matter population would have effects on various aspects from standard cosmological theory, such as high redshift structure formation, the matter power spectrum, and Local Group density profiles. If dark matter were to be fully thermal or partially thermal, results from the active neutrino species could be generalised to the sterile sector, only considering the effect of a different mass. The most dominant effect would be the suppression of clustering below the free streaming scale, which for neutrinos takes the form

$$\lambda_{\text{FS}} = \int \frac{v(t)\mathrm{d}t}{a(t)} \simeq 1.2\,\text{Mpc}\left(\frac{\text{keV}}{m_\nu}\right)\left(\frac{\langle p/T\rangle}{3.15}\right), \tag{5.3.11}$$

where the relation $\langle p/T\rangle \simeq 3.15$ holds for a thermalised Fermi gas. For non-thermal dark matter, a full momentum-resolved treatment using a numerical Boltzmann solver is required.

For sterile neutrinos, there are two well-understood cases, namely the case of fully thermalised dark matter and the case of an idealised Dodelson-Widrow scenario, meaning that the canonical oscillation-based production is the only contribution to the sterile distribution. The masses in the two idealised models are related by [Vie+05]

$$m_{\text{DW, ideal}} \simeq 4.46\,\text{keV}\left(\frac{m_{\text{thermal}}}{1\,\text{keV}}\right)\left(\frac{0.12}{\Omega_{\nu_s}h^2}\right). \tag{5.3.12}$$

If production peaks too close to the quark-hadron transition, one can expect a deviation from this relation, as the DW distribution will lie further away from an ideal case due to effects of varying relevant degrees of freedom. This would lead to a cooling of the spectrum by up to 20% [Aba06], and should be studied, leaving the momenta resolved.

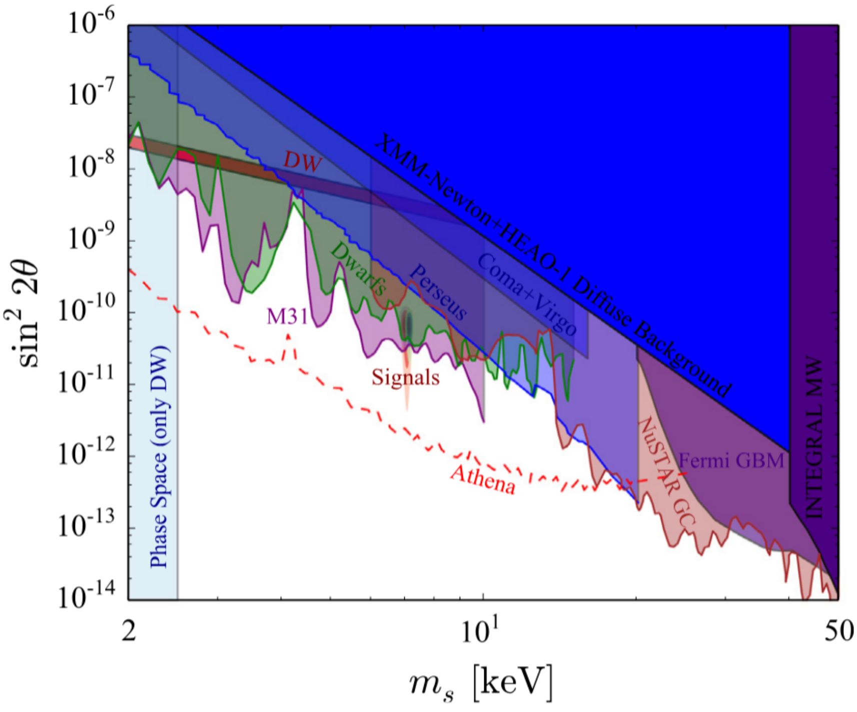

Figure 5.3.3: Taken from [Aba17]. The allowed parameter space for sterile neutrino dark matter, assuming it accounts for the entire dark matter abundance, is displayed. At the lowest masses and energies, the most constraining bounds arise from *Chandra* X-ray observations of M31 [Hor+14] and stacked dwarf spheroidal galaxies [MNE14]. Limits from the diffuse cosmic X-ray background [Boy+06a] and individual clusters such as Coma and Virgo [C R+06] are also shown. Moving to higher energies, constraints from the *Fermi* GBM [Ng+15] and INTEGRAL/SPI [Boy+08] become relevant. The vertical exclusion line reflects the case where the Dodelson–Widrow mechanism accounts for all of the dark matter, which is now ruled out; however, DW production can still contribute a subdominant fraction. Finally, the forecasted sensitivity of the upcoming *Athena* X-ray telescope [NM16] is included for comparison.

The current most precise way to study small scales of the matter power spectrum is by looking at the clustering of intergalactic gas. Measuring along the line of sight, one can use the Lyman-α absorption lines in the spectrum of high redshift quasars, also called the Lyman-α forest [Vie+05; Aba06] [Sch16; CHD99; McD+06; Sel+06; Vie+08; Vie+06; Vie+13; Bau+16]. The strongest constraints place limits of $m_{\mathrm{thermal}} \geq 5.3$ keV corresponding to an ideal DW mass of $m_{\mathrm{DW,\,ideal}} \geq 41$ keV at 2σ [Irš+17]. Additionally, from high redshift structure formation derived from galaxy number counts [BHO01] or CMB optical depth [Sch+14], one is able to introduce additional limits of $m_{\mathrm{thermal}} \geq 2.5$ keV at 2σ [Men+17]. Finally, the density profiles of galaxies exclude high DM clustering around galactic nuclei, introducing a required free-streaming length corresponding to a mass of $m_{\mathrm{thermal}} \simeq 2$ keV [And+13; Lov+12]. Besides modern X-ray bounds, it is clear that the canonical Dodelson-Widrow mechanism is not compatible with cosmological constraints either, if sterile neutrinos are to make up all of the dark matter.

6

Self-Interactions

Despite the simple and natural nature of sterile neutrino production through the Dodelson–Widrow mechanism, we have seen that the parameter space is ruled out for the canonical setup. In order to have sterile neutrinos be the full dark matter component, several new ideas have been proposed that evade X-ray bounds and cosmological constraints. The commonality of these ideas is the addition of an interaction that modifies the interaction rate, the potential and collision term in the sterile Boltzmann equation 5.1.21 leading to different production rates and epochs, and sometimes to different sterile neutrino decay products. Among the more minimalistic ones are self-interactions between active neutrinos [Gou+20b; Kel+20; Ben+22], self-interactions among sterile neutrinos [JF19; Bri+23a; Bri+23b; AV24], and sterile-active interactions [Bri+21], but also more elaborate models adding additional SM singlets [MNS14; MT15; PK08] or dark entropy producing models [HV17] have been studied. It is the aim of this chapter to expose the effects and results from neutrino self-interactions on the sterile population.

6.1 STERILE SELF-INTERACTIONS THROUGH SCALARS

The effect of self-interactions in the sterile sector was first proposed in the heavy mediator scenario by [JF19]. The resulting production mechanism, however, requires a strong tuning of the Yukawa coupling, as the dark matter fraction differs several orders of magnitude for an order 10^{-3} change in the coupling. This has led to the study of lighter mediators, first done for specific values by [Bri+21] and then generalised to a wide range of sub GeV mediator masses by [AV24]. It is the latter article that we shall reproduce in this section, taking the Boltzmann equation in 5.1.21 as a starting point.

6.1.1 SETTING UP THE BOLTZMANN EQUATION

The self-interactions are considered to be mediated by a real scalar ϕ with a mass m_ϕ. In order to simplify our calculations, we treat the sterile neutrinos as relativistic, so we set the scalar mass to be larger than the sterile mass by an order of magnitude, $m_\phi > 10 \ m_s$. Although the exact choice of a lower bound is somewhat arbitrary, this allows us to work safely within the relativistic regime. The scalar is taken to be a singlet under the gauge groups of the Standard Model, so one can add an interaction term to the Lagrangian as

$$\mathcal{L}_{\text{int}} = y_s \bar{\nu}_s \nu_s \phi. \tag{6.1.1}$$

Due to this new interaction term, a few processes are introduced, namely

1. $\nu_s \nu_s \leftrightarrow \phi$

2. $\nu_s\nu_s \leftrightarrow \nu_s\nu_s$

3. $\nu_s\nu_s \leftrightarrow \phi\phi$,

represented in figure 6.1.1. This modifies our Boltzmann equations severely. Note that alongside pure dark-sector interactions, these processes open up new regimes for oscillation based production as the decoherent interaction rate is enhanced, also boosting the damping factor. Additionally, the dispersion relation of sterile neutrinos gets modified, changing the relative potential between the active and sterile neutrinos, affecting the mixing angle. The goal then is to study each modified term and set up new Boltzmann equations. The set of equations that we will try to derive consists of the number density and the energy density equations, in particular, the right-hand sides of

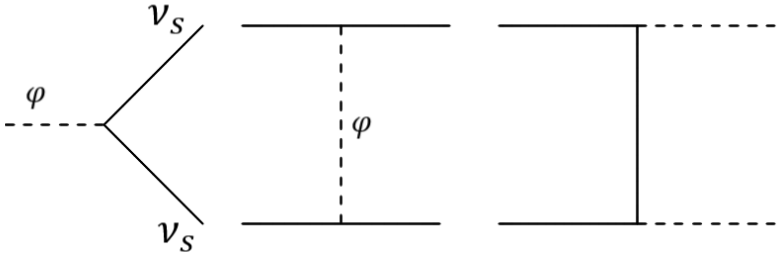

Figure 6.1.1: Processes introduced by scalar-mediated self-interactions in the sterile neutrino sector. Note that not all channels are described; only various initial and final products. Due to the Majorana nature of the sterile neutrinos, the s- and u-channel have a relative minus sign with respect to the t—channel.

$$\dot{n}(t) + 3Hn(t) = \mathcal{C}_n \tag{6.1.2}$$
$$\dot{\rho}(t) + 4H\rho(t) = \mathcal{C}_\rho. \tag{6.1.3}$$

To be able to derive any terms integrated over the distribution functions, however, we must have some information on the distribution functions of ν_s and ϕ themselves. If we assume that the number density of the neutrinos is low and that momentum exchange within the sterile sector is efficient, we can treat the population as a dilute interacting gas, and thus approximate its phase space distribution as Maxwell–Boltzmann,

$$f_s(T_s, p) = e^{(-\frac{p-\mu}{T_s})}, \tag{6.1.4}$$

where μ is the chemical potential and T_s is the temperature of the dark sector. Furthermore, we consider the (inverse) decay from $\phi \leftrightarrow \nu_s\nu_s$ to be efficient enough to uphold chemical equilibrium, so we can take $\mu_\phi = 2\mu_s \equiv 2\mu$ and describe the scalar population by

$$f(T_s, E_\phi) = e^{-\frac{E_\phi - \mu_\phi}{T_s}} = e^{\frac{2\mu_s}{T_s}} e^{-\frac{E_\phi}{T_s}}. \tag{6.1.5}$$

Note in particular that the overall magnitude of f_ϕ is suppressed by a factor $e^{\frac{\mu}{T_s}}$ with respect to f_s. Using these distributions, we are now able to find somewhat workable expressions for the potentials and rates.

Define V_{eff} to be the total potential. As in the previous chapter, we assume no effects of Lepton number asymmetry, and thus V_{eff} only takes contributions from thermal interactions with the plasma. Such contributions now also contain sterile interactions, so we obtain

$$V_{\text{eff}} = V_a^{\text{Th}} - V_s^{\text{Th}}. \tag{6.1.6}$$

Note that the relative minus sign arises similarly as is described in 3.4.15. The active thermal potential is the same as described earlier in 5.1.2, while for the sterile neutrino potential, the thermal contributions are computed in [AV24], given by

$$\begin{aligned} V_s(p) = &-\frac{y^2}{2p^2}\int_0^\infty \frac{\mathrm{d}k}{8\pi^2}\Bigg[\left(\frac{m_\phi^2}{2}\left[\log\left(\frac{m_\phi^2+4kp}{m_\phi^2}\right)+\log\left(\frac{-m_\phi^2}{-m_\phi^2+4kp}\right)\right]-4kp\right)f_s(k) \\ &+\left(\frac{m_\phi^2}{2}\frac{k}{\varepsilon_2}\left[\log\left(\frac{m_\phi^2+2\varepsilon_2 p+2pk}{m_\phi^2+2\varepsilon_2 p-2pk}\right)+\log\left(\frac{m_\phi^2-2\varepsilon_2+2pk}{m_\phi^2+2\varepsilon_2 p-2pk}\right)\right]-\frac{4pk^2}{\varepsilon_2}\right)f_\phi(\varepsilon_2)\Bigg], \end{aligned} \tag{6.1.7}$$

with $\varepsilon_2 = \sqrt{k^2+m_\phi^2}$ and f_ϕ the phase space distribution of the mediator. Since the scalar distribution remains suppressed by an additional factor of $e^{\frac{\mu}{T_s}}$, this can be approximated by just taking the terms proportional to f_s. Although the sterile potential remains fairly painstaking to work with, in the limit where the temperature is much higher or much lower than the mediator mass, the expression reduces to [AV24]

$$V_s(p) = \begin{cases} \frac{y^2}{8p^2}T_s^2 & T_s \gg m_\phi \\ -\frac{7\pi^2 y^2 p T_s^4}{45 m_\phi^4} + \mathcal{O}(m_\phi^{-5}) & T_s \ll m_\phi. \end{cases} \tag{6.1.8}$$

One important aspect to notice about these limits is that somewhere midway the potential changes sign, which is estimated to occur at around $pT_s \simeq m_\phi^2$.

The general expression for the interaction rate of a process $(i+j \;\to\; k+l)$ for which Fermi-blocking is negligible, is given by the phase–space integral

$$\begin{aligned} \Gamma_{ij\to kl}(p_i) &= \frac{1}{2E_i}\int \frac{d^3\mathbf{p}_j}{(2\pi)^3 2E_j}\frac{d^3\mathbf{p}_k}{(2\pi)^3 2E_k}\frac{d^3\mathbf{p}_l}{(2\pi)^3 2E_l} \\ &\qquad \times (2\pi)^4\delta^{(4)}(p_i+p_j-p_k-p_l)\,|\mathcal{M}_{ij\to kl}|^2 f_j(p_j) \qquad (6.1.9) \\ &\simeq \frac{1}{2E_i}\int \mathrm{d}\Pi_j\, f(p_j)\; 4(p_i\cdot p_j)\;\sigma_{ij\to kl} \qquad (6.1.10) \end{aligned}$$

where $|\mathcal{M}|^2$ is the squared scattering amplitude summed over spins and the f_i are distribution functions. For a more complete derivation, consider reading Appendix $A.3$. Using the expressions for the square amplitudes derived in Appendix A,

$$\begin{aligned} |\mathcal{M}|^2_{\nu_s\nu_s\leftrightarrow\nu_s\nu_s} = 8y^4\Bigg[&\frac{s^2}{\left[(s-m_\varphi^2)^2+m_\varphi^2\Gamma_\varphi^2\right]} - \frac{(s^2+st)\,(s-m_\varphi^2)(-t-s-m_\varphi^2)}{\left[(s-m_\varphi^2)^2+m_\varphi^2\Gamma_\varphi^2\right](s+t+m_\varphi^2)^2} \\ &+\frac{t^2}{(t-m_\varphi^2)^2} - \frac{(t^2+st)\,(t-m_\varphi^2)(-t-s-m_\varphi^2)}{(t-m_\varphi^2)^2\,(t+s+m_\varphi^2)^2} \\ &+\frac{(s+t)^2}{(s+t+m_\varphi^2)^2} + \frac{st\,(s-m_\varphi^2)(t-m_\varphi^2)}{\left[(s-m_\varphi^2)^2+m_\varphi^2\Gamma_\varphi^2\right](t-m_\varphi^2)^2}\Bigg] \end{aligned} \tag{6.1.11}$$

and

$$|\mathcal{M}|^2_{\nu_s\nu_s\leftrightarrow\phi\phi} = 4y^4\frac{(s+2t-2m_\phi)^2}{t^2(2m_\phi^2-s-t)}\big(-m_\phi^4+2m_\phi^2 t-t(s+t)\big) \tag{6.1.12}$$

one is able to obtain the cross sections

$$\sigma_{\nu_s\nu_s\to\phi\phi}(s) = \frac{y^4}{4\pi s^2}\left[\frac{6m_\varphi^4 - 4m_\varphi^2 s + s^2}{2m_\varphi^2 - s} 2\ln\left(\frac{\sqrt{s(s-4m_\varphi^2)} - s + 2m_\varphi^2}{\sqrt{s(s-4m_\varphi^2)} + s - 2m_\varphi^2}\right) - 6\sqrt{s(s-4m_\varphi^2)}\right], \quad (6.1.13)$$

and

$$\sigma_{\nu_s\nu_s\to\nu_s\nu_s}(s) = \frac{y^4}{2\pi s^2\left[(m_\varphi^2 - s)^2 + m_\varphi^2\Gamma_\varphi^2\right]}\left[\frac{s\left(5m_\varphi^6 - 9m_\varphi^4 s + 6s^3\right)}{m_\varphi^2 + s}\frac{2\left(5m_\varphi^8 - 9m_\varphi^6 s + 4s^3\right)}{2m_\varphi^2 + s}\ln\left(\frac{m_\varphi^2}{m_\varphi^2 + s}\right)\right]. \quad (6.1.14)$$

Once again, the steps are available in Appendix A, in particular relating to the treatment of Majorana fermions in the spinors. From here, the interaction rates are to be derived. The expressions are too elaborate to treat analytically, so they should be either implemented numerically or they should be approximated. For the sterile rate, there are three relevant regimes:

- very high temperature regime $pT_s \gg m_\phi^2$,
- very low temperature regime $pT_s \ll m_\phi^2$,
- and the resonant intermediate regime where $pT_s \simeq m_\phi^2$.

In these limits, the rates respectively reduce to

$$\frac{3y^4T_s^2}{2\pi^3 p}e^{\left(\frac{\mu_s}{T_s}\right)}, \qquad \frac{20y^4pt_s^4}{\pi^3 m_\phi^4}e^{\left(\frac{\mu_s}{T_s}\right)}, \qquad \text{and} \qquad \frac{y^2T_sm_\phi^2}{2\pi p^2}e^{-\frac{m_\phi^2 0}{4pT_s}+\frac{\mu}{T_s}}. \quad (6.1.15)$$

By combining these expressions for the resonant and the respective high and low temperature regimes, one is able to approximate the rate as the piecewise function from [AV24],

$$\Gamma_{\nu_s\nu_s\leftrightarrow\nu_s\nu_s}(p) = \begin{cases} \frac{3y^4T_s^2}{2\pi^3 p}e^{\left(\frac{\mu_s}{T_s}\right)} + \frac{y^2T_sm_\phi^2}{2\pi p^2}e^{-\frac{m_\phi^2 0}{4pT_s}+\frac{\mu}{T_s}} & pT_s > \frac{3m_\phi^2}{2\sqrt{10}} \\ \frac{20y^4pt_s^4}{\pi^3 m_\phi^4}e^{\left(\frac{\mu_s}{T_s}\right)} + \frac{y^2T_sm_\phi^2}{2\pi p^2}e^{-\frac{m_\phi^2 0}{4pT_s}+\frac{\mu}{T_s}} & pT_s \leq \frac{3m_\phi^2}{2\sqrt{10}} \end{cases}. \quad (6.1.16)$$

The sterile-to-scalar rate is computed numerically.

By applying these statements, we are now ready to tackle the full forms of the collision terms. We classify the collision terms in two categories: terms that insert energy from the visible sector into the dark sector (i.e., oscillation-based production) and terms that describe scattering in the dark sector, so our equations become

$$\dot{n}(t) + 3Hn(t) = C_n^{\nu_a} + C_n^{\phi\phi} \quad (6.1.17)$$
$$\dot{\rho}(t) + 4H\rho(t) = C_\rho^{\nu_a} + C_\rho^{\phi\phi}. \quad (6.1.18)$$

We only need to consider the terms for oscillations based production and the final scalar states, since pure sterile 2-to-2 scattering does not affect the number or energy density and since the process $\nu_s\nu_s \leftrightarrow \phi$ is in chemical equilibrium, so it does not contribute either.

The first term again depends on the interaction rate of the active neutrinos with the thermal bath, but now also obtains contributions from sterile-sterile scattering, so the total rate is increased. The potential and damping terms are modified, so we obtain

$$C_n^{\nu_a} = g_s \int \frac{d^3p}{(2\pi)^3} \frac{\Gamma_t(p)}{4} \frac{\Delta^2(p)\sin^2 2\vartheta}{\Delta^2(p)\sin^2 2\vartheta + D^2(p) + [\Delta(p)\cos 2\vartheta - V_{\text{eff}}]^2} f_a(p,t)$$

where $\Gamma_t = \Gamma_a + \Gamma_{\nu_s\nu_s\to\nu_s\nu_s} + \Gamma_{\nu_s\nu_s\to\phi\phi}$ is the total interaction rate, $D(p) = \frac{\Gamma_t(p)}{2}$, and the effective potential is as defined earlier. Note that the efficiency of the scalar decay induces the scalar term in the total rate. The energy density equation is obtained by integrating over an extra factor of p.

The second term depends only on the 2-to-2 process into scalars, affecting the total number of sterile neutrinos by subsequent decays into 4 neutrinos. A step-by-step derivation is present in Appendix B, but starting from

$$C_n^{\phi\phi} = -\frac{1}{2}\int d\Pi_1 d\Pi_2 d\Pi_3 d\Pi_4 (2\pi)^4 \delta^{(4)}(\dots)\left[f_s f_s |\mathcal{M}_{12\to34}|^2 - f_\phi f_\phi |\mathcal{M}_{34\to12}|^2\right]$$

one can rewrite

$$\begin{aligned} &= -\frac{1}{2}\int d\Pi_1 d\Pi_2 2s\, \sigma_{\nu_s\nu_s\leftrightarrow\phi\phi}(s) f_s^{EQ} f_s^{EQ}\left[\frac{f_s f_s}{f_s^{EQ} f_s^{EQ}} - \frac{f_\phi f_\phi}{f_s^{EQ} f_s^{EQ}}\right] \\ &= -n_s^2\left[1 - \frac{n_s^2}{(n_s^{EQ})^2}\right]\frac{1}{16}\int_{z_{\min}}^{\infty} dz\, z^4 K_1(z)\, \sigma_\varphi(s = z^2T^2), \end{aligned}$$

where we used $z = \frac{\sqrt{s}}{T}$ and K_1, the first-order Bessel function of the second kind, as is conventional and numerically practical for the thermally averaged cross section. In their most general form, the integrated Boltzmann equations describing sterile production including scalar-mediated self-interactions and a dark sector in chemical equilibrium are given by

$$\begin{aligned} \dot{n}(t) + 3Hn(t) = &\frac{g_s}{2}\frac{1}{(2\pi)^2}\int dp\, p^2\Gamma_t(p)\frac{\Delta^2(p)\sin^2 2\vartheta f_a(p,t)}{\Delta^2(p)\sin^2 2\vartheta + D^2(p) + [\Delta(p)\cos 2\vartheta - V_{\text{eff}}]^2} \\ &- n_s^2\left[1 - \frac{n_s^2}{(n_s^{EQ})^2}\right]\frac{1}{16}\int_{z_{\min}}^{\infty} dz\, z^4 K_1(z)\, \sigma_\varphi(s = z^2T^2) \end{aligned} \tag{6.1.19}$$

$$\begin{aligned} \dot{\rho}(t) + 4H\rho(t) = &\frac{g_s}{2}\frac{1}{(2\pi)^2}\int dp\, p^3\Gamma_t(p)\frac{\Delta^2(p)\sin^2 2\vartheta f_a(p,t)}{\Delta^2(p)\sin^2 2\vartheta + D^2(p) + [\Delta(p)\cos 2\vartheta - V_{\text{eff}}]^2} \\ &- n_s^2\left[1 - \frac{n_s^2}{(n_s^{EQ})^2}\right]\frac{T}{16}\int_{z_{\min}}^{\infty} dz\, z^4 K_1(z)\, \sigma_\varphi(s = z^2T^2) \end{aligned} \tag{6.1.20}$$

What now remains is to solve the equations.

6.1.2 LIGHT MEDIATORS

The equations as presented are computable numerically as they are, although the process might be a bit tedious. Motivated, however, by results from [JF19] stating that a heavy scalar mediator solution necessarily requires a fine-tuning of the Yukawa coupling, we will explore the lower mass range in more detail. This allows us to make a few simplifications. Consider the difference in contribution to the interaction rate from the various processes, plotted in figure 6.1.2 for a 1MeV scalar mass and in 6.1.3 for a 1GeV scalar mass, both taken at constant chemical potential and at $T_s = T$. For the lower mass plot, it is clear to see that the rates are

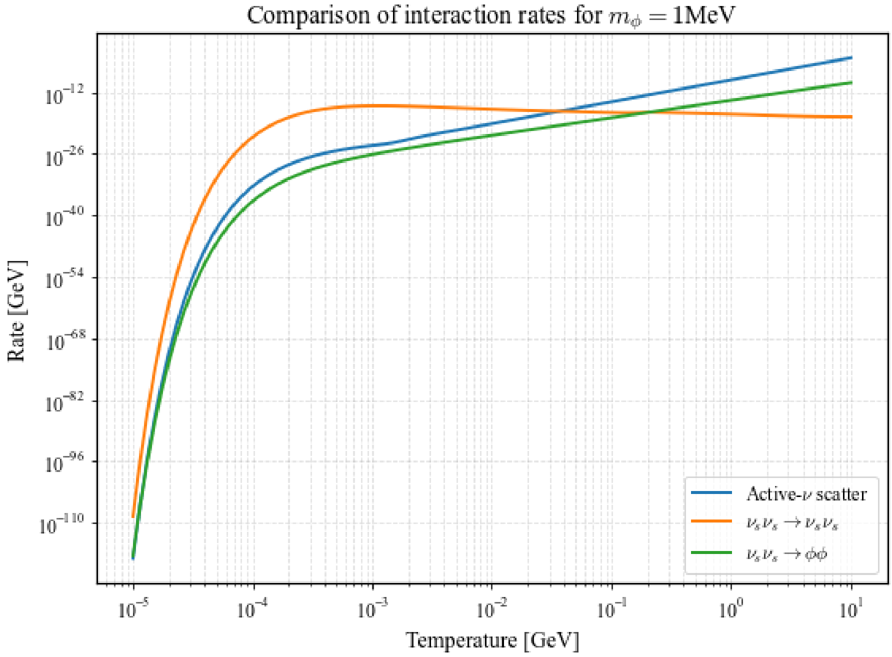

Figure 6.1.2: Interaction rates for a scalar mediator mass of 1 MeV at $T_s = T$ and fixed chemical potential. The plot shows that production is dominated by the SM contribution at high temperatures and by sterile–sterile scattering around 10^{-1} MeV, after which production effectively shuts off.

dominated by two different peaks: the Standard Model interaction rate in the high-temperature regime, and the sterile-sterile scattering at around 10^{-1}MeV, after which all production ceases. For the higher mass range, one sees that at around 100 MeV, both sterile-sterile and SM interactions are prominent. This means, in particular, that for the light mediator scenario one, is able to split the production into two different phases: the pure Dodelson–Widrow regime, and the later sterile production regime. This will allow us to make certain approximations about equations 6.1.19. Physically, what happens is that the DW mechanism produces an initial abundance of scalars and sterile neutrinos, such that the dark sector can obtain chemical equilibrium, after which self-interactions are kick-started that lead to a second production regime once the sector cools down sufficiently. For the heavier mediator case in 6.1.3 the self-interaction production regime is mingled with the DW regime, requiring a full numerical computation of equations 6.1.19.

The approximations we make are as follows:

- we neglect, similarly to the case of a pure DW system, the term in the denominator proportional to $\sin^2 2\vartheta$, and we set $\cos 2\vartheta = 1$.

- we neglect the contribution from $\Gamma_{\phi\phi}$ to the *production* of dark-sector energy density. Note that this only means that we approximate

$$\Gamma_t = \Gamma_a + \Gamma_{\nu_s\nu_s} + \Gamma_{\phi\phi} \to \Gamma_a + \Gamma_{\nu_s\nu_s}, \tag{6.1.21}$$

  and not that we neglect the 2-to-2 process changing sterile number density within the dark sector, i.e. $C^{\phi\phi}$ is still present. The interaction rates in 6.1.2 and 6.1.3 are averaged over f_a, so we have not yet found a reason to neglect the number-changing process.

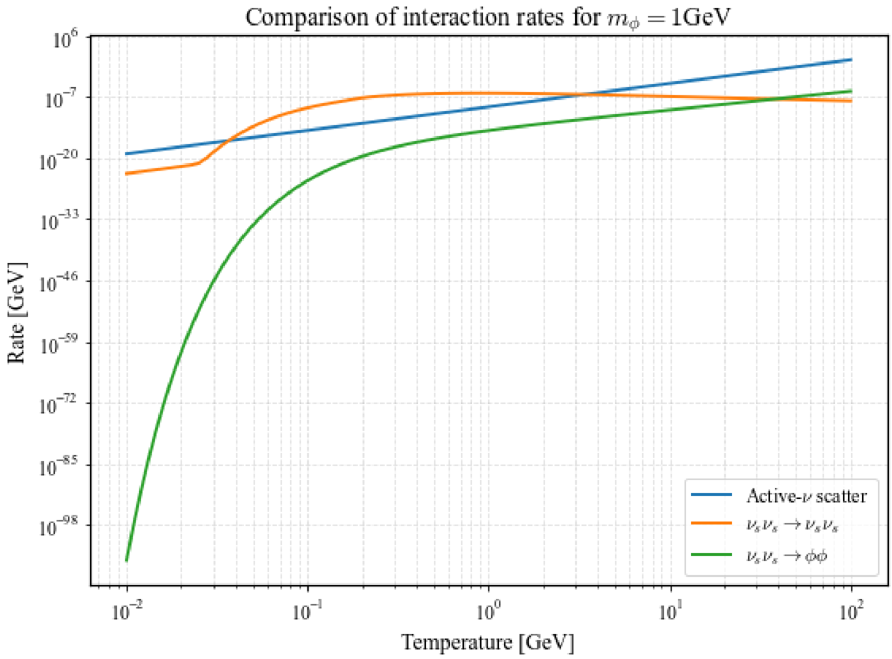

Figure 6.1.3: Interaction rates for a scalar mediator mass of 1 GeV under the same conditions. In this case, SM and sterile–sterile processes both contribute significantly around 100 MeV, so the two production regimes are no longer clearly separated.

One is also able to neglect the damping term and the effective potential with respect to $\Delta(p)$, which would turn the production integrand into the simple form

$$p^2\Gamma_t(p)\sin^2 2\vartheta f_a(p,t).$$

This was done in the original paper by Astros and Vogl, [AV24]. Practically speaking, however, the largest numerical hurdle is $\Gamma_{\phi\phi}$, so despite its simple form, the integrand does not lead to much advantage in our numerical computation. For this reason, we decide to reduce the denominator using only the listed approximations above, and we will compare our full evolution with the simplified case described in [AV24]. We first solve the equations without $\mathcal{C}^{\phi\phi}$, and then the complete system.

For a practical guide to our implementations of the system in python, one is referred to C.2. We rewrite the equations in variables $Y \equiv \frac{n_s}{s}$ and $X \equiv \frac{\rho_s}{\rho_{SM}}$, to find

$$\frac{\mathrm{d}Y}{\mathrm{d}T} = \frac{\mathrm{d}t}{\mathrm{d}T}\frac{1}{s}\mathcal{C}_n^{\nu_a}, \tag{6.1.22}$$

$$\frac{\mathrm{d}X}{\mathrm{d}T} = \frac{\mathrm{d}t}{\mathrm{d}T}\frac{1}{\rho_{SM}}\mathcal{C}_\rho^{\nu_a}, \tag{6.1.23}$$

where s is the entropy density of the visible sector and ρ_{SM} is the energy density of the Standard Model. In practice, one evolves the dimensionless variables $x \equiv \frac{m}{T}$, with m some reference mass, and one integrates over $q \equiv \frac{p}{T}$, as described in the relevant appendix. The results for a scalar of mass $m_\phi = 150$ keV are plotted in figure 6.1.4, where one is clearly able to see the influence of the self-interactions on the final yield, pushing it up by several orders of magnitude. In order to match the required energy density of dark matter, the mixing angle is tuned to $\sin^2 2\vartheta = 1.11 \cdot 10^{-13}$, which is in good agreement with [AV24], justifying their assumption of simplifying the expression for the mixing angle. The scaling of the mixing angle not only affects the final

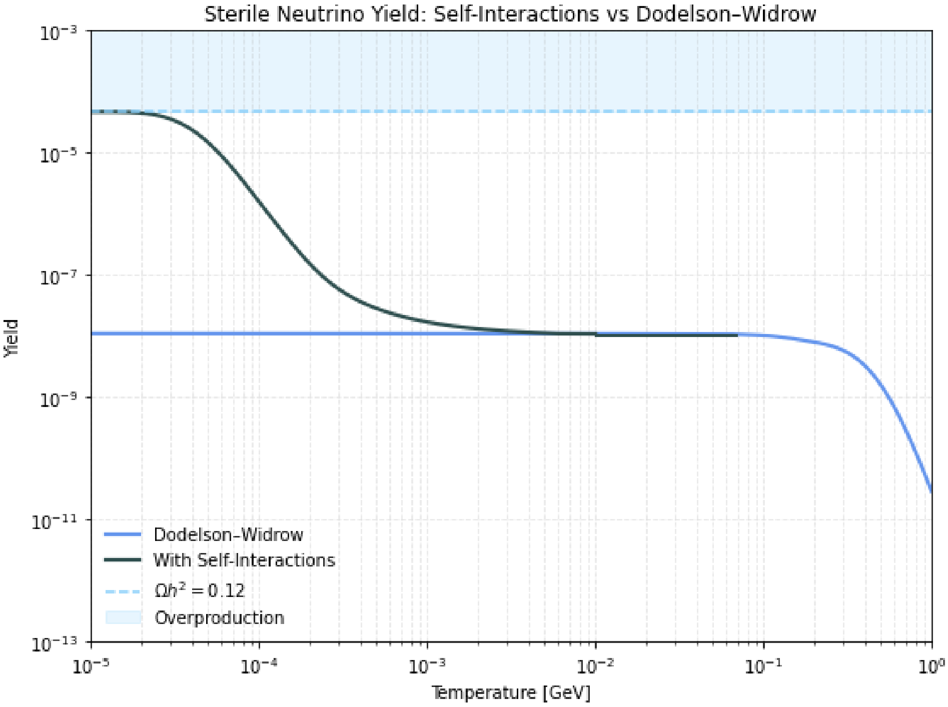

Figure 6.1.4: Sterile neutrino yield for a scalar mediator with mass $m_\phi = 150$ keV and a mixing angle $\sin^2 2\vartheta = 1.11\cdot 10^{-13}$. Number-changing processes are neglected.

yield linearly, but also determines the DW yield and therefore the initial value for the self-interaction yield. The effect of varying the mixing angle is graphed in image 6.1.5.

Next, we add the collision term $\mathcal{C}^{\phi\phi}$ to the numerical system. The process $2\ \nu_s \rightarrow\ 4\ \nu_s$ increases the number of sterile neutrinos while injecting no energy into the dark sector. This implies a cooler dark sector temperature T_s, and thus a different production regime with respect to the standard photon temperature T. The results for a 150 keV scalar mass are plotted in figure 6.1.6, and a few things are to be seen. First, note that there is an amplification of the total yield, which requires an even smaller mixing angle. In order to match the results with [AV24], a mixing angle of $\sin^2 2\vartheta = 2.16 \times 10^{-15}$ and a Yukawa coupling of 9×10^{-4} are used, allowing for a well-corresponding plot. Secondly, we see that the production is not only enhanced but also realised at earlier times or higher temperatures. This is exactly due to the cooling described above, allowing for a small production bump at around 1 MeV. Thirdly, it should be mentioned that more smaller wiggles can also be seen, besides the bump at 1 MeV. These distortions are purely numerical residues of the stiffness of our equations, and should not be assigned any physical value. Finally, we see that in image 6.1.6 the two-peak production approximation is well-justified. Evolving the system from above a GeV, we see a clean overlap between the pure DW scenario and the self-interaction enhanced scenario between 10^{-2} and 1 GeV, meaning that even in the enhanced scenario, only the DW process contributes in this regime. Then, once the DW yield has frozen in, the self-interaction enhanced yield grows further.

6.1.3 INTERMEDIATE MASS RANGE

Next, we will consider the range for m_ϕ where the two production regimes are no longer decoupled. We can fairly intuitively understand that the reason for the decoupling was that the various active vs sterile contributions to equation 6.1.19 became dominant at different temperatures. Reversing this logic, we expect the rates and potentials to be of similar magnitude in this regime, allowing for some useful by-products. In

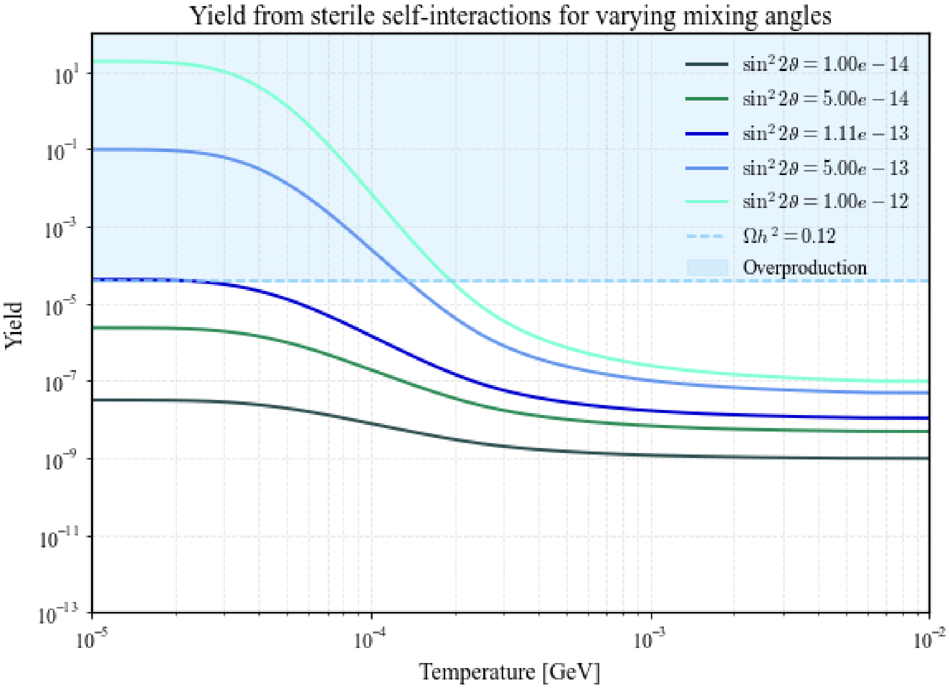

Figure 6.1.5: Effects of the variation of the mixing angle $\sin^2 2\vartheta$ on the final sterile neutrino yield produced by self-interactions given an initial yield from the Dodelson–Widrow mechanism, determined by the same mixing angle.

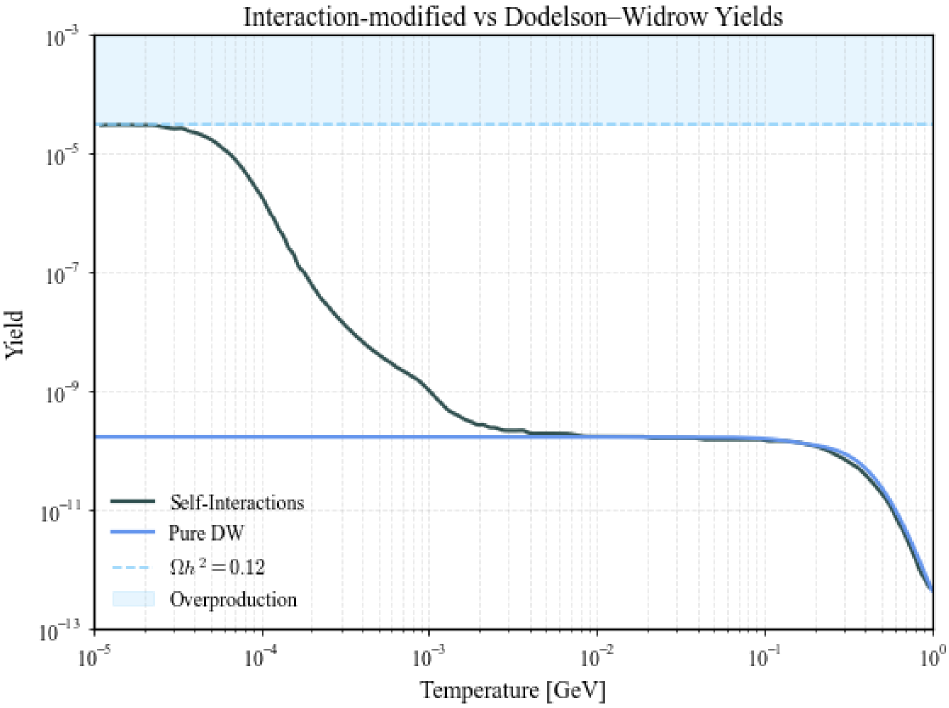

Figure 6.1.6: Sterile neutrino yield including the collision term $\mathcal{C}^{\phi\phi}$ for a scalar mediator mass of 150 keV. The additional $2\nu_s \to 4\nu_s$ process enhances the total production and shifts it to earlier times, producing a small bump around 1 MeV. The comparison with the pure DW case shows that the two-peak production picture remains valid.

particular, looking at the mixing angle

$$\sin^2 2\vartheta_M = \frac{\Delta^2 \sin^2 2\vartheta}{\Delta^2 \sin^2 2\vartheta + [\Delta \cos 2\vartheta - V_a + V_s]^2} \tag{6.1.24}$$

we see that there are a few regimes where resonances can occur similarly to those in the MSW effect of 3.4.3. For this to happen, we must have that the term in the square brackets vanishes, i.e.

$$\Delta \cos 2\vartheta - V_a + V_s \to 0. \tag{6.1.25}$$

This is most easily satisfied for higher temperatures, since there we have $\langle \Delta \rangle_T \simeq \frac{m_s^2}{6T} \ll 1$, such that we must only require V_a to be of the same magnitude as V_s. Using expression 6.1.8 and 5.1.24, one finds that this translates to

$$\rho_s \simeq \frac{31\pi^3 \sqrt{2} G_{\mathrm{F}} m_\phi^4}{y^2} \left[\frac{\rho_{\nu_e} + \rho_{\bar{\nu}_e}}{m_Z^2} + \frac{\rho_e + \rho_{\bar{e}}}{m_W^2} \right]. \tag{6.1.26}$$

Once this condition is satisfied, the resonance can dominate production, leading to the approximate collision term

$$C_n^{\nu_a} \simeq \frac{g_s}{2\pi^2} \int \mathrm{d}p\, p^2 \, \frac{\Delta^2(p) \sin^2 2\vartheta}{\Gamma_t(p)} f_a(p), \tag{6.1.27}$$

where the remaining rate in the denominator arises from the damping term. The resulting Boltzmann equation is now easily computed numerically, and is presented in figure 6.1.7. To allow for comparison with [AV24], we plot the yield using similar values for y and $\sin^2 2\vartheta$. A few things are of relevance for discussion. Firstly, a strong boost of the production is still achieved, allowing for the neutrinos to reach the required en-

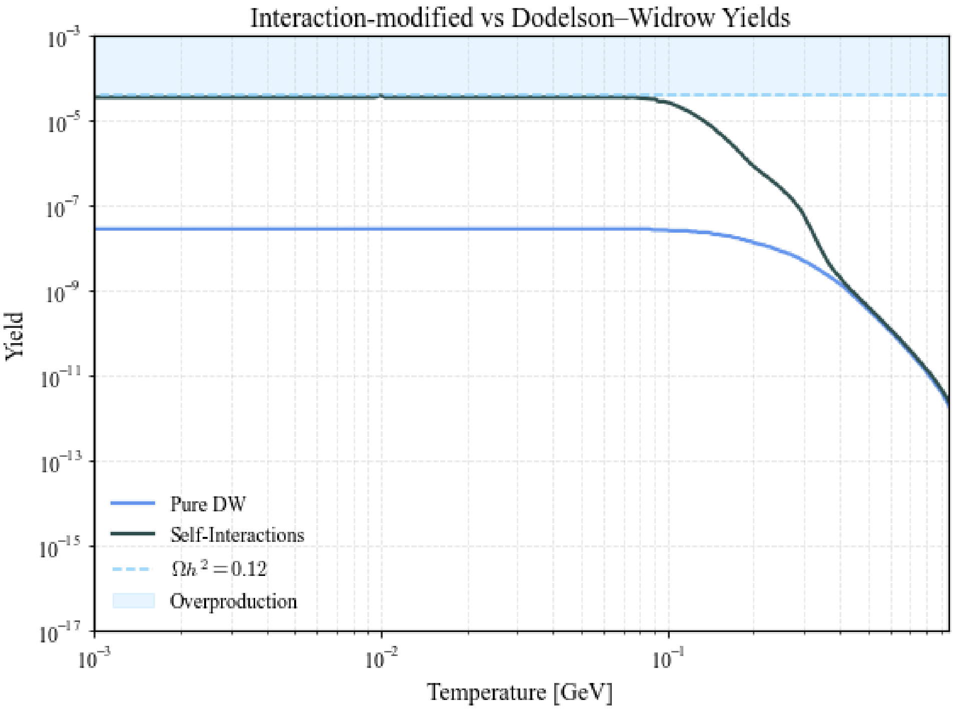

Figure 6.1.7: Sterile neutrino yield in the intermediate mediator mass regime, where active and sterile contributions to the effective potential become comparable and resonant enhancement of the mixing angle can occur. The resulting production overlaps with and departs early from the canonical DW peak, leading to a boosted yield but with weaker amplification than in the fully separated two-epoch scenario.

ergy density. The amplification is not as strong, however, as in the scenario where both production epochs are separated. Secondly, one sees that the production occurs much earlier, departing from the canonical DW mechanism already around the DW production peak.

6.1.4 AVAILABLE PARAMETER SPACE

Now that we understand the evolution of the sterile neutrino population, we are able to examine the final yields under the same cosmological restrictions that excluded the Dodelson–Widrow mechanism. In particular, it is of great interest to see whether or not the lower mixing angle required to produce a yield corresponding to dark matter is able to avoid X-ray constraints. There are no modifications of the decay channel of steriles into photons, so the same X-ray data can be used.

Regarding Lyman-α forest observations, however, some reevaluations should be made. The limits set on sterile neutrino dark matter differ, as the resulting cosmological evolution is slightly different with respect to the Dodelson–Widrow warm-DM bounds discussed in section 5.3.2. In essence, any dark matter with a large velocity dispersion (from being "warm") erases structure below its free-streaming length, suppressing the matter power spectrum on sub-Mpc scales. For thermal WDM, this suppression is conventionally expressed as a bound on its root-mean-square velocity $v_{\rm rms}$ today. In particular, one can write

$$v_{\rm rms} \simeq 0.04 \left(\frac{\Omega h^2}{0.12}\right)^{1/3} \left(\frac{m_{\rm WDM}}{1\,{\rm keV}}\right)^{-4/3} {\rm km/s}, \tag{6.1.28}$$

so that Lyman-α data yield a lower limit on $m_{\rm WDM}$ [Vie+05]. We saw that [Vie+05] found $m_{\rm WDM} \gtrsim 0.55$ keV (2σ) for a fully thermal relic — which corresponds to $m_s \gtrsim 2.0$ keV for Dodelson–Widrow sterile neutrinos — by combining Lyman-α with CMB data. More recent high-resolution studies quoted much stronger bounds: e.g. [Irš+17] report $m_{\rm WDM} \gtrsim 5.3$ keV at 2σ from Lyman-α forest alone, implying $v_{\rm rms} \lesssim 6$ m/s today. Even this, however, is sensitive to astrophysical assumptions. Relaxing those (e.g. about the intergalactic medium temperature) leads to a more conservative limit $m_{\rm WDM} \gtrsim 1.9$ keV [Irš+17], corresponding to $v_{\rm rms} \lesssim 16$ m/s.

The Lyman-α constraints do not depend directly on the active–sterile mixing angle, but they probe the dark matter phase-space distribution required to constitute all of the dark matter. Assuming Maxwell-Boltzmann distributions, this means that the mixing angle enters only in determining the temperature after which the population decouples. To extract the temperature, one equates the sterile neutrino's present-day velocity dispersion (second moment of its distribution) to that of a thermal WDM particle at the Lyman bound, yielding an inequality of the form

$$m_s \gtrsim \frac{\langle p^2\rangle^{1/2}}{v_{\rm rms}} = \frac{1}{v_{\rm rms}} \left(\frac{\int {\rm d}p^3 p^2 f_s(p)}{\int {\rm d}p^3 f_s(p)}\right)^{1/2}, \tag{6.1.29}$$

up to numerical factors [Vie+05]. Applying our assumption of a Maxwell-Boltzmann distribution, treating the equation of state as that of a relativistic perfect fluid, and considering that the distribution only starts redshifting after the yield freezes in, we are able to reduce this to

$$m_s \gtrsim \frac{\sqrt{12}\ T_{s,0}}{v_{\rm rms}} = \frac{\sqrt{12}}{v_{\rm rms}} \left(\frac{T_0}{T_d} T_{s,d}\right), \tag{6.1.30}$$

where T_d marks the time at which the sterile yield freezes in. Since the exact point where the population becomes cosmologically stable can vary slightly as one modifies m_s and $\sin^2 2\vartheta$, one can extract T_s and $T_{s,d}$ for various combinations of m_s and $\sin^2 2\vartheta$. In practice, this is not very difficult, as the expression for T_s in terms of T is known (see equation C.2.9), and the data obtained from sweeping the parameter space will already provide the full yield evolution for the various combinations of parameters. The precise practical implementation behind the extraction is more elaborately discussed in Appendix C.2.3.

Finally, dark matter self-interactions may alter this picture. If sterile neutrinos remain tightly coupled until late times, they no longer behave as free–streaming particles but rather as a fluid. In this regime, the relevant suppression scale is set by the sound horizon, which is reduced by a factor of $1/\sqrt{3}$ relative to the free–streaming length. Consequently, the velocity bound is relaxed by a factor of $3^{-1/4}$. In order to understand when this correction to the Lyman-α bound is necessary, one realizes that the determining factor for when self-interactions decouple is the cross section. We will work either in the limit where we can consider a relativistic decoupling (and can keep our free-streaming bound), or in the limit of a very non-relativistic decoupling. The self–scattering cross section for a Yukawa interaction with coupling y and a heavy mediator φ approaches the constant value

$$\sigma \simeq \frac{2y^4 m_s^2}{\pi m_\varphi^4}, \tag{6.1.31}$$

in the non–relativistic limit. For warm dark matter, it was found that corrections due to self-interactions become relevant only once $\sigma/m_s \lesssim 10^{-5}$ cm^2/g [Ega+21]. Following [AV24], we therefore decide to plot this line in the parameter space of (m_s, y), and we will plot both regimes: the free–streaming Lyman-α bound, corresponding to $m_{\mathrm{WDM}} \simeq 1.9$ keV and $v_{\mathrm{rms}} \simeq 16$ m/s, and the corrected bound, relaxed by $3^{-1/4}$. We will not take the transition region into consideration.

First, consider the $(m_s, \sin^2 2\vartheta)$ parameter space plotted in figure 6.1.8 for the light scalar mediator regime described in section 6.1.2. We used X-ray exclusion data taken from the GitHub page supplementing [Aba17], combined with updated NuSTAR data from [B M+20]. The regions excluded due to Lyman-α bounds are plotted following the above paragraph, where below the dotted blue line we expect a relaxation of the bounds. All points on the plot represent combinations of parameters describing a saturated sterile neutrino dark matter. Lines of constant y have been used to sweep the parameter space, and are plotted too. The parameter space predicted by the canonical Dodelson–Widrow mechanism is also drawn for reference, using the code for the contour plot in Appendix C.1. For small enough mixing angles, namely $\sin^2 2\vartheta \lesssim 10^{-12}$, a sterile neutrino mass range opens up which is currently not excluded by X-ray or Lyman-α bounds, for which the mass would generally exceed 10 keV. The available space is, however, not very extensive and does not leave much wiggle room for the mass. Free-streaming bounds are seen to be responsible for a large part of the excluded sub–10 keV region. In figure 6.1.9, a similar plot is given, only now for a much heavier mediator describing the scenario in section 6.1.3. Since such a mediator strongly reduces the non-relativistic cross section, no corrected Lyman-α bounds are relevant. Similarly as before, all mixing angles larger than $\sin^2 2\vartheta \sim 10^{-12}$ are seen to be excluded by current X-ray bounds. Since the intermediate mass scenario induces a much earlier production and freeze-in of the sterile neutrino population, however, the higher temperature at the end of production brings with it a difference in bounds related to the free-streaming. It is intuitive to see that a larger part of the space describes distributions that freeze out while relativistic, thus being restricted by their free-streaming scale. Another important aspect of the higher-mass mediator is the naturalness of the Yukawa coupling. For this scenario, one is able to have a coupling of order $\mathcal{O}(10^{-2})$ while keeping the mixing angle above $\sin^2 2\vartheta \sim 10^{-14}$.

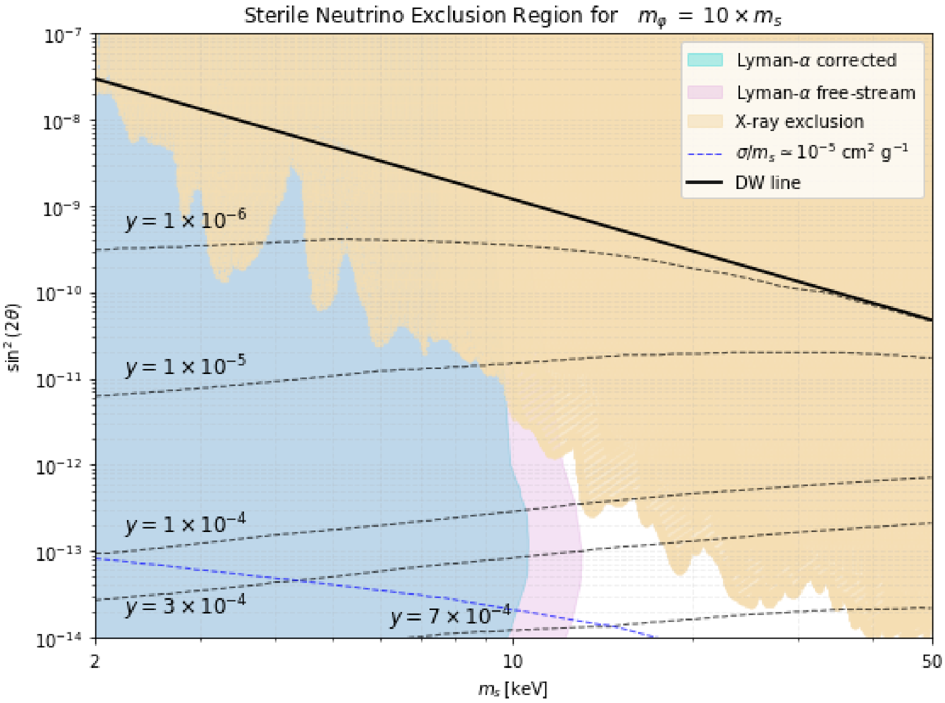

Figure 6.1.8: Parameter-space in the $(m_s, \sin^2 2\vartheta)$ plane for the light scalar mediator scenario. Each point on the plot corresponds to parameters that yield a saturated sterile-neutrino dark-matter abundance ($\Omega_s h^2 \simeq 0.12$) given the production dynamics described in the text. Shaded/hatched exclusion regions are shown as follows: X-ray limits combine the compilation in [Aba17] with the NuSTAR updates of [B M+20]; the Lyman−α free-streaming exclusion corresponds to the conservative thermal WDM bound $m_{\mathrm{WDM}} \simeq 1.9\,\mathrm{keV}$ (equivalently $v_{\mathrm{rms}} \simeq 16\,\mathrm{m/s}$) following [Vie+05; Irš+17]; the dotted blue line indicates the region where late self-interactions can relax the Lyman−α bound by the factor $3^{-1/4}$ discussed in the text (see also [Ega+21]). The canonical Dodelson–Widrow contour is drawn for reference. Lines of constant Yukawa coupling y show how the required coupling varies across the plane. The light-mediator case opens a narrow window at very small mixing angles ($\sin^2 2\vartheta \lesssim 10^{-12}$) and $m_s \gtrsim \mathcal{O}(10\,\mathrm{keV})$ that is not excluded by current X-ray or conservative Lyman−α bounds, but the allowed region is small.

6.2 ACTIVE SELF-INTERACTIONS THROUGH SCALARS

The case of active-neutrino self-interactions is a comparable extension of the Standard Model and probes a distinct region of parameter space. We will discuss active self-interactions here as a useful comparison to the scalar self-interactions considered for sterile neutrinos, but stress that writing a gauge-invariant coupling between a new scalar and two left-handed $SU(2)$ doublets is not minimal in the naive sense. For two left-handed doublets, one must either introduce an $SU(2)_L$ triplet mediator or else generate the interaction through higher-dimensional operators that involve the Higgs doublet; these model choices have different phenomenological consequences. Nevertheless, presenting a brief overview of active-sector self-interactions clarifies the current status of the modified Dodelson–Widrow mechanism and highlights complementary constraints and signals, even where we do not reproduce every derivation in full rigour.

Historically, these interactions were first constrained by measurements of the invisible decay width of the Z boson at the Large Electron-Positron Collider (LEP) [Sch06]. More recently, redshift-dependent cosmological observations and flavour-sensitive laboratory experiments have provided significantly stronger bounds [Ber+18; Est+20]. The implications of such interactions for sterile neutrino production, however, have only been systematically explored in recent works [Gou+20a; An+23; KZ19; Kel+20]. In [Ber+18], a large part of the parameter space was evaluated through cosmological bounds from the $\Lambda-$CDM model by comput-

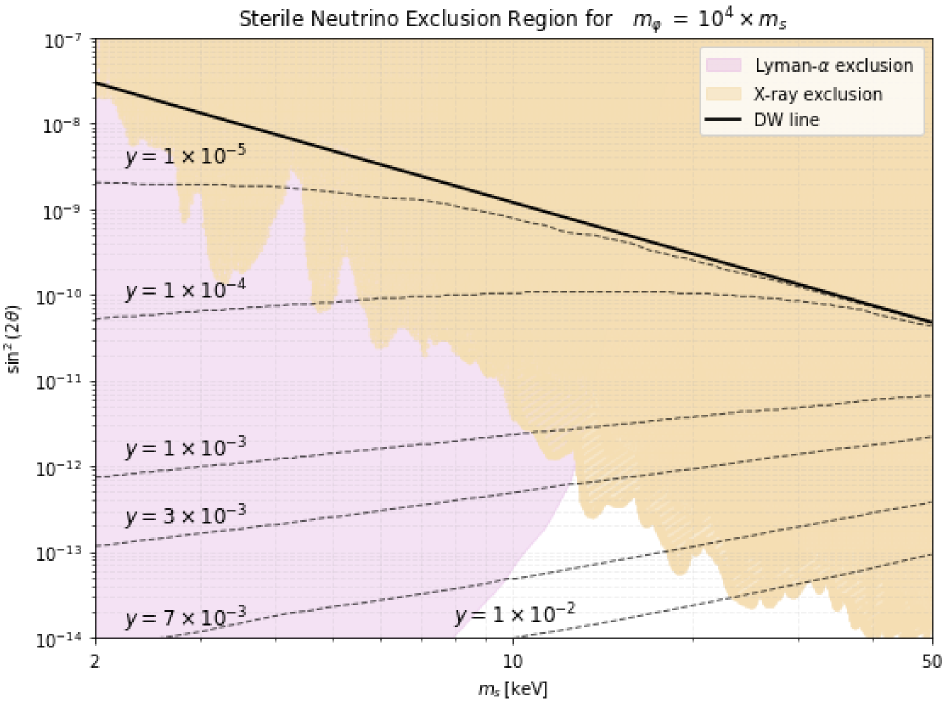

Figure 6.1.9: Parameter-space in the $(m_s, \sin^2 2\vartheta)$ plane for the intermediate scalar mediator scenario . Styling and shading follow figure 6.1.8 (X-ray exclusions from [Aba17; B M+20]; Lyman-α free-streaming bound from [Vie+05; Irš+17]). Because the mediator is heavier, the non-relativistic self-scattering cross section is strongly suppressed and the self-interaction relaxation of the Lyman-α bound is not effective; therefore only the uncorrected free-streaming exclusion is shown. Production in this regime occurs earlier and freeze-in often finishes while the sterile population is still relativistic, so free-streaming constraints exclude a larger fraction of low-mass parameter space. As in the light case, X-ray limits cut away large mixing angles: mixing angles $\gtrsim \mathcal{O}(10^{-12})$ are typically excluded by present X-ray data. The intermediate/heavy mediator scenario, however, allows for more "natural" Yukawa couplings (e.g. $y \sim \mathcal{O}(10^{-2})$) while maintaining very small mixing angles (down to $\sin^2 2\vartheta \sim 10^{-14}$) – a region that is potentially interesting from a model-building perspective.

ing the effect of the sterile neutrino distribution function on the matter power spectrum. A heavy scalar mediator was ruled out at 95%, while the lighter mediators are not excluded, hence we will study the yield produced by only the light-mediator model and compare the production regimes with those of the sterile interaction counterpart. The structure of the text will repeat that of the sterile case: we will set up the Boltzmann equation, solve it, and discuss the parameter space.

6.2.1 SETTING UP THE BOLTZMANN EQUATION

We consider a coupling

$$\mathcal{L}_{\text{int}} = \lambda_\phi \nu_a \nu_a \phi. \tag{6.2.1}$$

The resulting diagrammatic processes are essentially the same as before, only now producing a sterile neutrino in the outgoing legs, i.e. $\nu_a\nu_a \to \nu_a\nu_s$. The process of setting up the Boltzmann equation is somewhat repetitive. First, we must modify our total rate and potential as

$$\Gamma_t = \Gamma_{\text{SM}} + \Gamma_\phi \quad \text{and} \quad V_t = V_{\text{SM}} + V_\phi, \tag{6.2.2}$$

where Γ_ϕ is the interaction rate of active neutrinos through the scalar ϕ, and V_ϕ is the potential entering the modified dispersion relation due to interactions with the scalar. This then similarly leads to a modified mixing angle and equation

$$\frac{\partial f_s}{\partial t} - p\frac{\partial f_s}{\partial p} = \frac{\Gamma_{\mathrm{SM}} + \Gamma_\phi}{4} \sin^2 2\vartheta_{\mathrm{eff}} f_{\nu_a}, \tag{6.2.3}$$

where

$$\sin^2 2\vartheta_{\mathrm{eff}} \simeq \frac{\Delta \sin^2 2\vartheta}{\Delta \sin^2 2\vartheta + \frac{\Gamma_t^2}{4} + [\Delta \cos 2\vartheta - V_t]^2}. \tag{6.2.4}$$

The per-particle rate is again given by

$$\Gamma_\phi(p) = \frac{1}{2E_1} \int \mathrm{d}\Pi_2 \mathrm{d}\Pi_3 \mathrm{d}\Pi_4\, f_{\nu_a}(p_2)(2\pi)^4 \delta^{(4)}(p_1 + p_2 - p_3 - p_4) \left| \mathcal{M}_{\nu_a\nu_a \xrightarrow{\phi} \nu_a\nu_a} \right|^2, \tag{6.2.5}$$

which can be numerically computed using our known Yukawa amplitude for Majorana fermions. In the very heavy limit of m_ϕ, the theory reduces to a Fermi four-point interaction-like theory, and the rate can be expected to scale like

$$\Gamma_\phi \propto \frac{\lambda_\phi^4\, p T^4}{m_\phi^4}. \tag{6.2.6}$$

In the other limit, when m_ϕ is smaller than the typical momentum (i.e., $m_\phi < T$), we can use the narrow width approximation to find

$$\Gamma_\phi(E) \simeq \frac{\lambda_\phi^2 T^2}{16\pi E} \left[\frac{\pi^2}{6} + \mathrm{Li}_2(-e^\omega) + \omega \ln(1 + e^\omega) - \frac{\omega^2}{2} \right], \tag{6.2.7}$$

with

$$\omega = \frac{m_\phi^2}{4ET} \tag{6.2.8}$$

and Li_2 the dilogarithm. For more details, see Appendix A.3.4.

The potential of the neutrino due to interactions with the Standard Model is left unchanged, and the thermal potential due to interactions with the scalar is given by [NR88b; QV95]

$$\begin{aligned} V_\varphi^T(E, T) = \frac{\lambda_\varphi^2}{16\pi^2 E^2} \int_0^\infty dp \Bigg[& \left(\frac{m_\varphi^2 p^2}{\omega} L_1^+(E,p) + \frac{2}{\omega} L_2^+(E,p) - \frac{4Ep^2}{\omega} \right) \frac{1}{e^{\omega/T} - 1} \\ & + \left(\frac{m_\varphi^2}{2} L_1^+(E,p) - 4Ep \right) \frac{1}{e^{p/T} + 1} \Bigg], \end{aligned} \tag{6.2.9}$$

where

$$L_1^+(E,p) = \ln\left(\frac{4pE + m_\varphi^2}{4pE - m_\varphi^2}\right) \text{ , and} \tag{6.2.10}$$

$$L_2^+(E,p) = \ln\left(\frac{(2pE + 2E\omega + m_\varphi^2)(2pE - 2E\omega + m_\varphi^2)}{(-2pE + 2E\omega + m_\varphi^2)(-2pE - 2E\omega + m_\varphi^2)}\right) . \tag{6.2.11}$$

To get an understanding of the potential we plot the Standard Model- and scalar potential together with $\Delta(p)$ in figure 6.2.1 for a typical mode $p \sim T$ and $m_{\nu_s} = 40$ keV. One sees that the regime in which the canonical Dodelson–Widrow mechanism normally occurs is modified by the potential, and the dominance of Δ over the total potential occurs at later times.

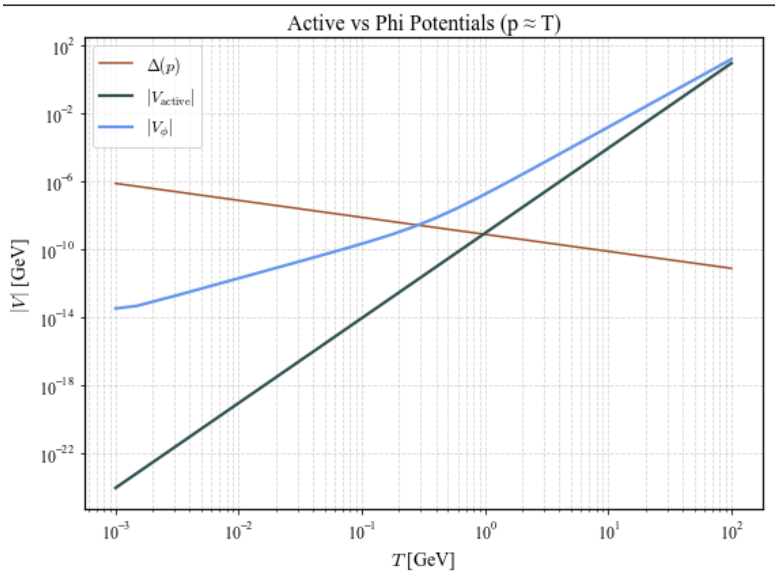

Figure 6.2.1: Comparison of potentials induced by active neutrino interactions with the Standard Model and the scalar mediator for a typical mode $p \sim T$ and a scalar mass $m_\phi = 1$ MeV. For reference, $\Delta(p)$ is also plotted for a sterile neutrino mass of $m_{\nu_s} = 40$ keV.

6.2.2 SOLVING THE BOLTZMANN EQUATION

Since the right-hand side of 6.2.4 does not depend on the sterile distribution itself, the computation of the yield becomes just a matter of integrating over the temperature. In particular, the yield at a given time T is

$$Y(T) = \frac{1}{(2\pi)^2}\int_T^\infty \mathrm{d}T' \frac{1}{HT's(T')}\int_0^\infty \mathrm{d}p\, p^2\, \Gamma_t(p, T') \sin^2 2\vartheta_{\text{eff}} f_{\nu_a}(p, T'). \tag{6.2.12}$$

First, we consider the integrand of the temperature integral as a function of T for a typical mode $p \sim T$, to understand the contribution of the various temperature regimes to the production. Defining

$$\gamma = \frac{1}{(2\pi)^2}\int_0^\infty \mathrm{d}p\, p^2\, \Gamma_t(p, T') \sin^2 2\vartheta_{\text{eff}} f_{\nu_a}(p, T') \tag{6.2.13}$$

we plot the normalized contribution to $\frac{\gamma}{HT}$ in figure 6.2.2a. One immediately sees two points of interest.

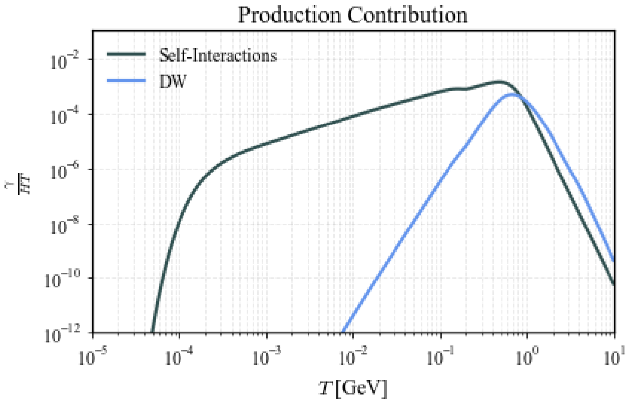

(a) Contribution to the change in number density from self-interactions compared to the canonical mechanism for $\sin^2 2\vartheta = 1 \times 10^{-9}$, $m_{\nu_s} = 40$ keV, $m_\phi = 1$ MeV, and $\lambda_\phi = 10^{-4}$.

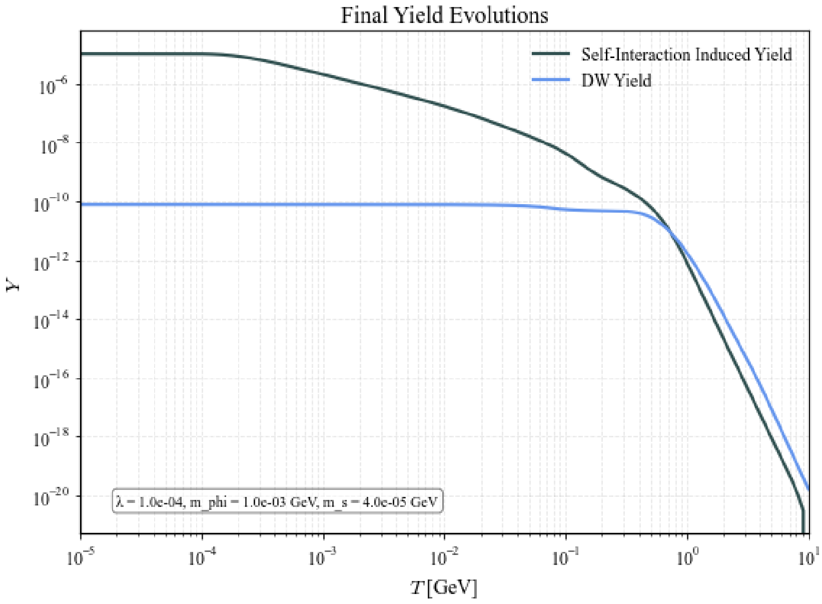

(b) Comparison of yields from self-interaction enhanced production and the canonical setup. The mixing angle is set at $\sin^2 2\vartheta = 5.23 \times 10^{-15}$ to produce the correct relic abundance.

Figure 6.2.2: (a) Rate contributions for self-interactions vs. canonical mechanism. (b) Evolution of yields under the same scenarios.

First, the early phase of the production is slightly damped with respect to DW, which is due to a suppression from the potential. Secondly, the production remains relevant for much longer after DW production ceases. It is this latter aspect that induces a strong boost in production. Turning now to the full computation of the integral we obtain figure 6.2.2b. First, the DW yield is mimicked pretty narrowly, then the scalar interaction rate induces a strong boost departing from DW, before stabilizing around $T \sim 10^{-4}$. The mixing angle is tuned at $\sin^2 2\vartheta = 5.23 \times 10^{-15}$ in order for the sterile neutrino to be the full dark matter energy density for a 40 keV sterile neutrino.

6.2.3 Discussion of the Parameter Space

The parameter space corresponding to this mechanism was analysed in [Gou+20a] using a numerical solver tool called CLASS, which allows one to track the momentum-resolved Boltzmann equations, including most first-order cosmological contributions [Les11]. The process will not be reproduced, but its results will briefly be discussed for completeness.

First of all, notice that the mixing angle required for a 40 keV sterile neutrino dark matter saturation is fairly low with respect to the sterile self-interaction cases, sitting at 5.23×10^{-15}. This is seemingly more easily compatible with constraints from X-ray observations. The results from [Gou+20a] are presented in Figure 6.2.3. The analysis of [Gou+20a] combined the momentum-resolved Boltzmann evolution obtained with CLASS with a range of astrophysical and collider probes in order to carve out the viable regions of parameter space. In particular, the study incorporated constraints from the Milky Way satellite galaxy population, limits on invisible Z-decays, X-ray bounds from sterile neutrino decay lines, and phase-space density limits from dwarf galaxies. The analysis differentiates scenarios with a heavy mediator (their Case A), characterized by $m_\varphi \gtrsim$ GeV and sizeable coupling $\lambda_\varphi \gtrsim \mathcal{O}(0.1)$, are ruled out at high significance. The problem for such cases is the tension between the strong interactions required for efficient sterile neutrino production and the stringent collider limits on such couplings. Scenarios with a light mediator (Cases B and C, depending on the precise value) remain viable, provided the interaction strength is suppressed. Within this regime, sterile

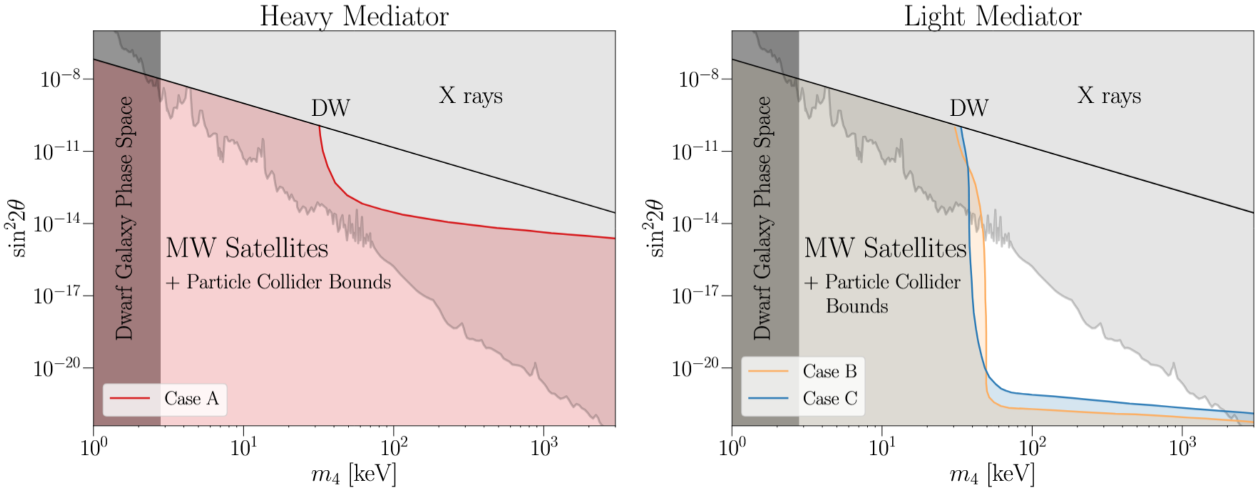

Figure 6.2.3: Sterile neutrino dark matter constraints from [Gou+20a], shown for different mediator mass regimes. The middle panel corresponds to Case A, where production proceeds via a heavy mediator with $m_\varphi \gtrsim$ GeV and sizeable coupling $\lambda_\varphi \gtrsim \mathcal{O}(0.1)$; this region is ruled out at $\gg 95\%$ confidence. The right panel shows Cases B and C, in which production occurs through a light mediator with suppressed couplings. In this scenario, a small triangular region in parameter space remains viable, allowing sterile neutrino dark matter masses between 37 keV and several MeV, depending on the mediator parameters.

neutrino dark matter masses from approximately 37 keV up to several MeV can still be accommodated, as illustrated in Figure 6.2.3.

6.3 STERILE SELF-INTERACTION THROUGH VECTORS

Sterile neutrinos produced via the Dodelson–Widrow mechanism in the presence of self-interactions through scalar mediators, both in the active and sterile case, are able to account for 100% of Dark Matter. Despite this, we have seen that the available parameter space is not superfluous, and might well be pushed backwards by future X-ray experiments. In this light, we might wonder if modified yet similar mechanisms are able to open up more parameter space, in particular by looking for an alternative mediator. In this section, we focus our attention on sterile neutrino production through self-interactions using a spin 1 boson mediator. We will first present a suitable current and calculate the corresponding interaction amplitudes, before we turn to the Boltzmann equations. We will then follow a similar set-up and solution of the equation, after which we present the results in comparison with the scalar mediators.

6.3.1 THE (EFFECTIVE) MODEL

When introducing interactions mediated by a spin-1 boson, a natural first step is to consider a vector current of the form

$$\mathcal{J}_V^\mu = \bar{\nu}_s \gamma^\mu \nu_s. \tag{6.3.1}$$

However, if the fermion in question is a Majorana particle, this current identically vanishes. The reason for this is the Majorana condition $\nu_s = \nu_s^c$, which implies that under charge conjugation the vector current transforms as

$$\bar{\nu}_s \gamma^\mu \nu_s \longrightarrow -\bar{\nu}_s \gamma^\mu \nu_s, \tag{6.3.2}$$

and therefore must be zero. This can be seen explicitly by using the property $\bar{\psi}\gamma^\mu\psi = -\bar{\psi}^c\gamma^\mu\psi^c$, which for $\psi = \psi^c$ enforces

$$\bar{\nu}_s \gamma^\mu \nu_s = 0. \tag{6.3.3}$$

Thus, a pure vector interaction between Majorana fermions and a vector mediator is prohibited by the self-conjugate nature of the field. This can most intuitively be understood by an attempt to gauge such a theory, as one would induce a conserved charge for a particle that is its own antiparticle. To circumvent this, we turn to the axial-vector current, defined as

$$\mathcal{J}_A^\mu = \bar{\nu}_s \gamma^\mu \gamma^5 \nu_s, \tag{6.3.4}$$

which, in contrast to the vector current, does not vanish for Majorana fermions. From the perspective of Lorentz and discrete symmetries, the axial-vector current constitutes the simplest non-trivial bilinear for a neutral Majorana fermion to couple to a spin-1 mediator.

We therefore consider an interaction mediated by a massive vector boson V_μ coupled axially to sterile neutrinos ν_s. At the level of an effective theory, valid below some cutoff scale Λ, the relevant terms in the Lagrangian can be written as

$$\mathcal{L} \supset -\frac{1}{4} V_{\mu\nu} V^{\mu\nu} + \frac{1}{2} m_V^2 V_\mu V^\mu + \bar{\nu}_s i \partial\!\!\!/ \nu_s + g_V \bar{\nu}_s \gamma^\mu \gamma^5 \nu_s \, V_\mu, \tag{6.3.5}$$

where $V_{\mu\nu} = \partial_\mu V_\nu - \partial_\nu V_\mu$ denotes the usual field-strength tensor, m_V is the mediator mass, and g_V is the axial coupling constant. Although this bottom-up construction describes the leading interactions relevant for sterile neutrino self-scattering, from a model-building perspective, embedding Eq. (6.3.5) into a theoretically consistent framework imposes several non-trivial requirements. Nevertheless, the focus of this work follows a bottom-up approach: before attempting to construct a UV completion, we investigate whether such an effective interaction can provide viable phenomenology in the low-energy regime. In particular, we will analyse the scattering amplitudes induced by the axial-vector mediator, determine the corresponding interaction rates in the early Universe, and ultimately assess the impact on sterile neutrino production and dark matter abundance.

We now set out to compute the 2–to–2 sterile neutrino scattering amplitude. Taking the axial vector current from 6.3.4 we are able to reproduce the same S-matrix treatment as in the scalar case (see Appendix A.3), with 2 major differences: the propagator is to be replaced with the vector propagator, introducing an extra factor of $g_{\mu\nu}$, and the bilinears contain a factor of $\gamma_\mu\gamma^5$. At first glance, the axial bilinear is expected to introduce difficulties, as we applied identities for $\bar{u}v$–like bilinears several times, yet looking at the charge conjugation phases in A.1.5 we understand that the same identities hold for the axial case. Additionally, since the metric is symmetric in $\mu \leftrightarrow \nu$, our summation of terms symmetric in $x \leftrightarrow y$ in A is still valid. This implies that the structure of the S-matrix element in A.1.15 is equal, up to the explicit bilinear construction. We therefore find an amplitude similar to A.1.16, namely

$$i\mathcal{M} = ig_V^2\left[\frac{(\bar{v}_1\gamma_\mu\gamma^5u_2)(\bar{u}_3\gamma^\mu\gamma^5v_4)}{s-m_V^2+i\Gamma_V m_V} - \frac{(\bar{u}_4\gamma_\mu\gamma^5u_2)(\bar{u}_3\gamma^\mu\gamma^5u_1)}{t-m_V^2+i\varepsilon} - \frac{(\bar{u}_3\gamma_\mu\gamma^5u_2)(\bar{u}_4\gamma^\mu\gamma^5u_1)}{u-m_V^2+i\varepsilon}\right]. \tag{6.3.6}$$

Taking the spin-averaged square of this amplitude introduces the real differences in energy-dependence with respect to the scalar case. Considering only $\mathcal{M}_{s-\text{channel}}$, for example, the spin-averaged square amplitude leads to a contribution

$$\overline{|\mathcal{M}_s|^2} = \frac{1}{8}\frac{g_V^4}{(s-m_V^2)^2+\Gamma_V^2m_V^2}\mathrm{Tr}[\not{p}_3\gamma_\mu\gamma^5\not{p}_4\gamma_\nu\gamma^5]\mathrm{Tr}[\not{p}_1\gamma^\mu\gamma^5\not{p}_2\gamma^\nu\gamma^5] \tag{6.3.7}$$

$$= \frac{1}{8}\frac{g_V^4}{(s-m_V^2)^2+\Gamma_V^2m_V^2}\mathrm{Tr}[\not{p}_3\gamma_\mu\not{p}_4\gamma_\nu]\mathrm{Tr}[\not{p}_1\gamma^\mu\not{p}_2\gamma^\nu] \tag{6.3.8}$$

$$= \frac{1}{8}\frac{g_V^4}{(s-m_V^2)^2+\Gamma_V^2m_V^2}\mathrm{Tr}[\gamma_\mu\gamma^\alpha\gamma_\nu\gamma^\beta]\mathrm{Tr}[\gamma^\mu\gamma^\gamma\gamma^\nu\gamma^\delta]p_{3\beta}p_{4\alpha}p_{1\delta}p_{2\gamma} \tag{6.3.9}$$

which is then contracted using the familiar trace identities to find

$$= \frac{g_V^4}{(s-m_V^2)^2+\Gamma_V^2m_V^2}(t^2+u^2), \tag{6.3.10}$$

where we see that the dependence is no longer on s^2 but on (t^2+u^2). For the entire amplitude we repeat the process to find

$$\begin{aligned}\overline{|\mathcal{M}_{\nu_s\nu_s\to\nu_s\nu_s}|^2} = \Bigg[&\frac{s^2+2st+2t^2}{(s-m_V^2)^2+\Gamma_V^2m_V^2} + \frac{2s^2+2st+t^2}{(t-m_V^2)^2} + \frac{s^2+t^2}{(s+t+m_V^2)^2}\\ &+ \frac{2s^2}{(m_V^2-t)(m_V^2+s+t)} - \frac{2t^2(s-m_V^2)}{[(s-m_V^2)^2+\Gamma_V^2m_V^2](s+t+m_V^2)}\\ &+ \frac{2(s-m_V^2)(s+t)^2}{[(s-m_V^2)^2+\Gamma_V^2m_V^2](t-m_V^2)}\Bigg],\end{aligned} \tag{6.3.11}$$

where we made use of $s+t+u=0$. Now we can again obtain the cross section by rewriting $t=\frac{s}{2}(\cos\vartheta-1)$, which is the integrated over in Mathematica and divided by $32\pi s$ to find

$$\begin{aligned}\sigma_{\nu_s\nu_s\leftrightarrow\nu_s\nu_s} =& \frac{g_V^4}{24\pi s(s-m_V^2)^2+\Gamma_V^2 m_V^2)}\Bigg[\\ &\frac{m_V^6(4s-2\Gamma_V^2)+3m_V^4 s(s-\Gamma_V^2)-6m_V^2 s^3-s^4}{2m_V^2+s}\ln\left(\frac{m_V^2+s}{m_V^2}\right)\\ &+\frac{s(6m_V^6(\Gamma^2-2s)+m_V^4 s(9\Gamma_V^2+s)+m_V^2 s^2(6\Gamma_V^2+7s)+6s^4)}{m_V^2(m_V^2+s)}\Bigg].\end{aligned} \tag{6.3.12}$$

Next, we set out to obtain an expression for the interaction rate from

$$\Gamma_s(p_1)=\frac{1}{2p_1}\int \mathrm{d}\Pi_2\, f_s(p_2)\; 4(p_1\cdot p_2)\;\sigma_{\nu_s\nu_s\to\nu_s\nu_s}. \tag{6.3.13}$$

First, we simplify the phase space measure to

$$\mathrm{d}^3p_2=p_2^2\mathrm{d}\,p_2\;\mathrm{d}\Omega=p_2^2\;\mathrm{d}p_2\;\mathrm{d}\phi\;\mathrm{d}(\cos\beta)=(2\pi)\,p_2^2\;\mathrm{d}p_2\;\mathrm{d}(\cos\beta), \tag{6.3.14}$$

where we denote β as the angle between p_1 and p_2 in the lab frame. Then, using $\frac{s}{2}=p_1p_2(1-\cos\beta)$, we find that

$$\mathrm{d}(\cos\beta)=-\frac{\mathrm{d}s}{2p_1p_2}, \tag{6.3.15}$$

which allows us to write

$$\begin{aligned}\Gamma_s(p_1)&=\frac{1}{16\pi^2p_1}\int_0^\infty \mathrm{d}p_2p_2f_s(p_2)\int_{-1}^{1}\mathrm{d}\cos\beta\;4\,(p_1\cdot p_2)\sigma(s)\\ &=\frac{1}{16\pi^2\,p_1^2}\int_0^\infty \mathrm{d}p_2f_s(p_2)\int_0^{4p_1p_2}\mathrm{d}s\;s\sigma(s).\end{aligned} \tag{6.3.16}$$

To give some feeling for this expression, we consider $f_s(p_2)$ to be a Maxwell-Boltzmann equation with temperature T_s and chemical potential μ, and plot the normalized rate $g_V^{-4}e^{-\frac{\mu}{T_s}}\;\Gamma_s(p_1)$ for a typical mode $p_2\sim T_s$ in figure 6.3.1.

6.3.2 LIGHT MEDIATOR BOLTZMANN EQUATIONS

Besides the rate, the full modified Boltzmann equation requires the computation of V_s and an expression for the distribution function $f_s(p)$. For the same arguments as before, we take f_s to be well approximated by a Maxwell-Boltzmann distribution at temperature T_s and chemical potential μ, so only the thermal computation of V_s remains. Given the similarities with the scalar mediator of section 6.1.1, however, we can avoid the exact computation of V_s by working in the light mediator limit. The argument is similar to that in the scalar case: for a typical mode, $p\sim T$, we expect the potential to scale like $V_s\propto T$ whenever $T\gg m_V$. In the regime below ~ 80 GeV, however, the Standard Model potential scales like T^5, and thus dominates the total potential. This means that the canonical DW set-up dominates. Once we get to the low temperature regime, we can imagine a similar or stronger contribution coming from the sterile potential. Recall, though, that the potential enters the denominator of the expression for the effective mixing angle as

$$[\Delta-V_{\text{eff}}]^2, \tag{6.3.17}$$

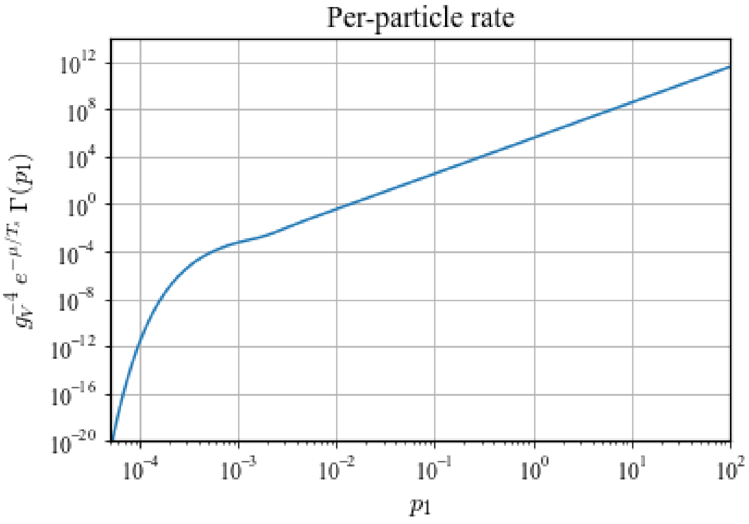

Figure 6.3.1: Normalized sterile–sterile scattering rate for a Maxwell–Boltzmann mode $p_2 \sim T_s$, plotted as $g_V^{-4} e^{-\mu/T_s}\, \Gamma_s(p_1)$ for a vector mediator of mass $m_V = 150\ \mathrm{keV}$. The rate was computed assuming a sterile distribution $f_s(p) \propto \exp[-(E_p - \mu)/T_s]$ and is shown as a function of the probe momentum p_1 (in units of T_s). The plotted normalization factor removes the explicit g_V^4 and chemical-potential dependence so that the shape and p–dependence of the collision kernel are clear.

and that $\Delta \propto 1/T$. For the low temperature limit this means that we can approximate that term as Δ, allowing us again to find two separate regimes

- $T \gg m_V$, where the Dodelson Widrow mechanism is active,
- $T \lesssim m_V$, where the Boltzmann equation becomes

$$\frac{\mathrm{d}f_s}{\mathrm{d}t} \simeq \frac{\Gamma_s + \Gamma_a}{4} \sin^2 2\vartheta\, f_a. \tag{6.3.18}$$

The latter case is analogous to the scenario in 6.1.1, only now with a modified rate Γ_s. Since the numerical results from the full evolution of the Boltzmann equation in 6.1.1 corresponded very closely to the fully simplified equation, used in [AV24], we conclude that such an assumption is in place as long as the production regimes are equally well-separated.

6.3.3 SOLVING THE BOLTZMANN EQUATIONS

Equation 6.3.18 has contributions from the active and from the sterile rate. The former is very well understood by now and shall not be discussed, while the latter has a more unfriendly structure coming from T_s and e^{μ/T_s}. We first integrate over the phase-space of the particle with momentum p_1 to find the number density equation

$$\begin{aligned} \dot{n}_s + 3Hn_s &= g \int \frac{\mathrm{d}^3 p_1}{(2\pi)^3} \frac{\Gamma_s}{4} \sin^2 2\vartheta\, f_a(p_1) \\ &= \frac{1}{4(4\pi)^4} e^{\frac{\mu}{T_s}} \int \mathrm{d}p_1 \frac{1}{e^{p_1/T_s} + 1} \int \mathrm{d}p_2 e^{\frac{-p_2}{T_s}} J(4\, p_1 p_2), \end{aligned} \tag{6.3.19}$$

where we defined $J(u)$ to be the integral

$$J(u) \equiv \int_0^u \mathrm{d}s\, s\sigma(s). \tag{6.3.20}$$

The latter definition is especially useful for practical purposes, as the function can be precomputed numerically, and then interpolated in order to avoid very deeply nested numerical integrations in the final expression. Using

$$T_s = \frac{\rho_s}{3n_s} \tag{6.3.21}$$

and

$$e^{\frac{\mu}{T_s}} = \frac{n_s}{n_S^{eq}} = 2\pi^3 \frac{n_s}{T_s^3} \tag{6.3.22}$$

we can express the entire equation in terms of ρ_s, n_s and T. This leads to the system of equations

$$n_s' = \frac{3n_s}{T} - \frac{1}{HT}\frac{27}{32\pi}\frac{n_s^4}{\rho_s^3}\int_0^\infty \mathrm{d}p_1 \frac{1}{e^{p_1/T}+1}\int_0^\infty \mathrm{d}p_2 e^{\frac{-3p_2 n_s}{\rho_s}} J(4p_1p_2). \tag{6.3.23}$$

$$\rho_s' = \frac{4\rho_s}{T} - \frac{1}{HT}\frac{27}{32\pi}\frac{n_s^4}{\rho_s^3}\int_0^\infty \mathrm{d}p_1 \frac{p_1}{e^{p_1/T}+1}\int_0^\infty \mathrm{d}p_2 e^{\frac{-3p_2 n_s}{\rho_s}} J(4p_1p_2). \tag{6.3.24}$$

With the appropriate variable redefinitions, this system can be solved numerically, using initial conditions from Dodelson–Widrow production. For more information about the practical strategies applied, one is referred to Appendix C.3.

In order to remain well below the DW peak production temperature, we solve the system for a spin-1 boson mediator with mass $m_V = 150$ keV. To allow for comparison with our earlier systems, we choose the coupling g_V to be of the same size of the typical Yukawa coupling from section 6.1.2, i.e. $g_V = 2 \times 10^{-4}$. We plot the resulting yield evolution in figure 6.3.2, where we tuned $\sin^2 2\vartheta = 4.86 \times 10^{-14}$ to produce a final yield that is able to account for 100% of dark matter exactly. In order to understand how the scenario compares to a scalar mediator, we overlap both yield evolution in figure 6.3.3. For the latter plot, we choose $\sin^2 2\vartheta = 1.11 \times 10^{-13}$, so that the scalar-mediated system is able to produce 100% of the dark matter fraction.

The boost in sterile neutrino production is seen to be very substantial, allowing for the mixing angle to be even lower than in the scalar case for a similar mass. The main reason for this seems to be a wider production temperature range rather than a sharper production growth. For a similar mediator mass and coupling strength, the production starts earlier, which might bring our assumption of decoupled production regimes in danger. To ensure safety, it would then be required to solve the full system of equations.

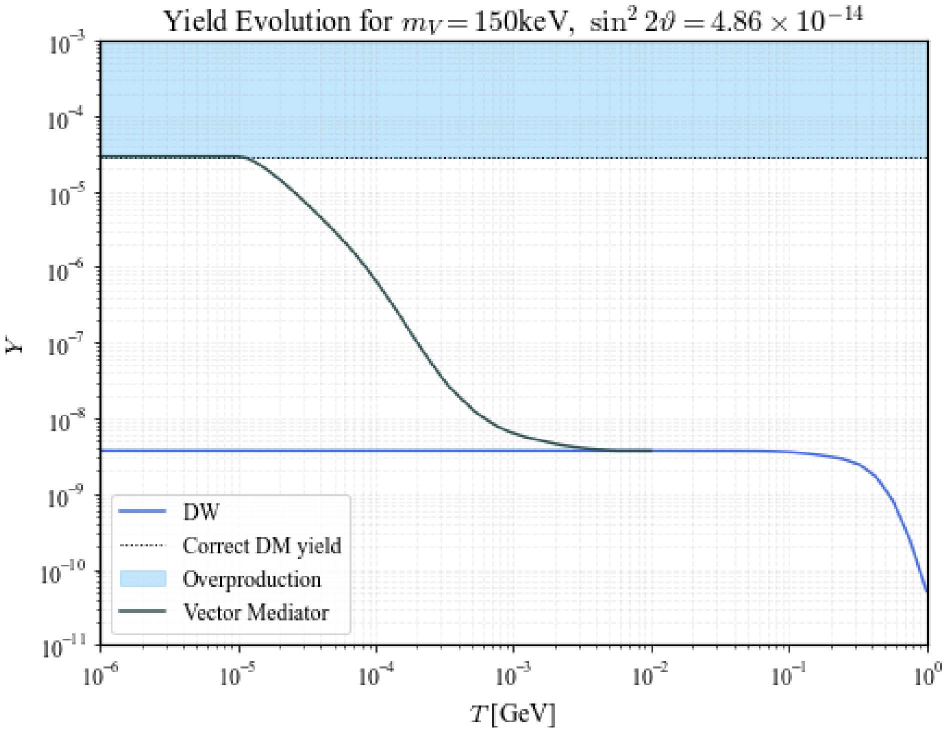

Figure 6.3.2: Yield evolution $Y_s \equiv n_s/s$ for a spin-1 (vector) mediator with mass $m_V = 150$ keV and a sterile neutrino of mass $m_s = 40$ keV. The parameters are the coupling $g_V = 2 \times 10^{-4}$ and mixing angle tuned to $\sin^2 2\vartheta = 4.86 \times 10^{-14}$ so that the final yield equals the observed dark-matter abundance. Production begins earlier than in the scalar case and proceeds over a wider temperature range, producing a substantial enhancement of the final abundance for the chosen parameters.

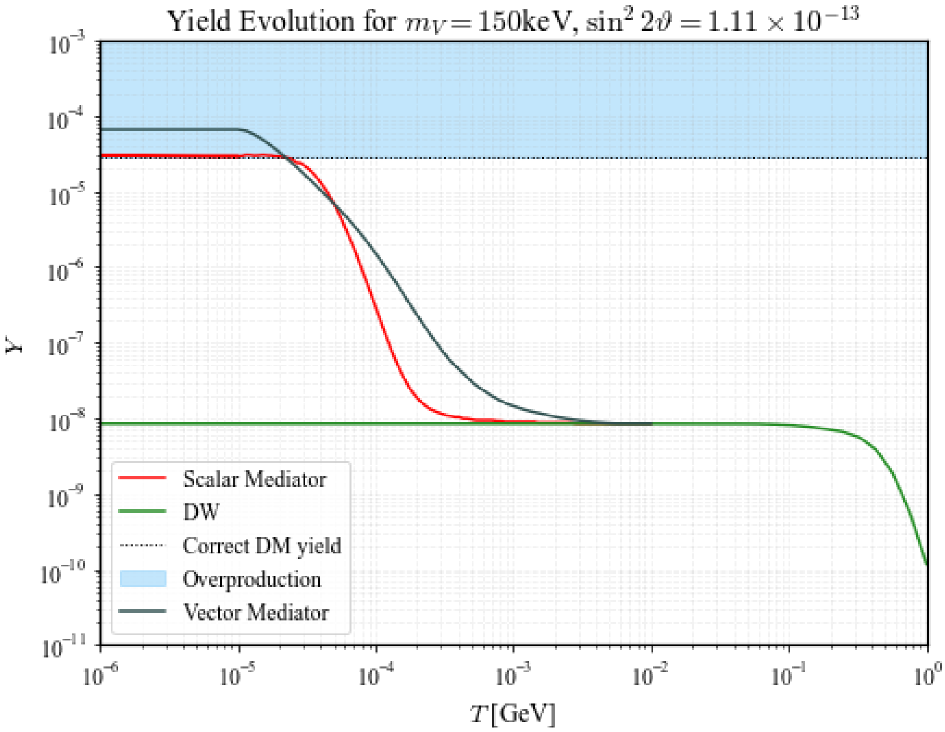

Figure 6.3.3: Comparison of yield evolutions for a spin-1 (vector) mediator and a scalar mediator both with mass $m_{V,\,\phi} = 150\ \mathrm{keV}$. Parameters used: coupling $g_V = y = 2 \times 10^{-4}$ and mixing angle tuned to $\sin^2 2\vartheta = 1.11 \times 10^{-13}$ so that the final scalar yield equals the observed dark-matter abundance for a 15 keV sterile neutrino. One sees that for the same parameters, a vector mediator tends to overproduce dark matter.

7

Conclusions

Due to the inherently neutral characteristics that define a gauge singlet, the sterile (or right-handed) neutrino forms an appealing candidate for dark matter. The production of such a dark matter population through neutrino oscillations was suggested by Dodelson and Widrow [DW94b], allowing for certain combinations of the sterile neutrino mass m_s and the active-sterile mixing angle $\sin^2 2\vartheta$ to saturate the dark matter energy density. The required mixing angles were too high, however, to be compliant with X-ray constraints, as a sufficiently high mixing angle allows for a measurable production of such rays coming from radiative decay channels [Aba17; B M+20].

In order to avoid these radiative decay constraints, several modified production mechanisms were suggested, typically enhancing neutrino interactions by adding couplings to new dark sector particles in either the active or sterile sector. The more minimal approaches saw the addition of self-interactions between active neutrinos [Gou+20b; Kel+20; Ben+22], self-interactions among sterile neutrinos [JF19; Bri+21; AV24], and sterile–active interactions [Bri+21]. Increasingly elaborate models introduced additional SM singlets [MNS14; MT15; PK08] or invoked dark entropy production [HV17].

This thesis first laid the foundational knowledge in Chapters 2, 3 and 4, then reproduced both the original Dodelson–Widrow mechanism (Chapter 5) and the sterile self-interaction modified set-up, where the mediator was taken to be a scalar, following [AV24] (Chapter 6.1). The parameters were swept over to find combinations of the sterile mass m_s, the mixing angle $\sin^2 2\vartheta$ and the Yukawa coupling y that produced the required dark matter yield for both the case of a light scalar ($10\, m_s = m_\phi \lesssim 1$ MeV) and an intermediately heavy mediator ($10^4\, m_s = m_\phi \lesssim 1$ GeV). The yields were computed by deriving the relevant modified terms in the integrated set of Boltzmann equations, which could then be solved numerically. In agreement with the reproduced article [AV24], the system allows for a sufficiently small mixing angle such that parameter space compatible with X-ray and cosmological (Lyman-α) bounds is opened up. The newly opened up parameter space, plotted in Figures 6.1.8 and 6.1.9, was, however, not enormous. Then an intuition was given to active-active scalar self-interactions in Chapter 6.2 by describing results from most recent literature [Gou+20a]. A comparison of the parameter space with the sterile counterpart was made, and it was seen that the sterile sector allowed for some more freedom in the mass and mixing angle, although different methods were used in the construction of the space.

Finally, in 6.3, we newly introduced a spin-1 boson coupling axially to the sterile neutrinos, inducing vector-mediated self-interactions. To simplify matters, we worked in the scenario where the vector mass was much smaller than the momentum of the typical mode, allowing for the Boltzmann equation in 6.3.18. We derived the corresponding amplitudes and rates, and were able to solve the consequent Boltzmann equations numerically. The sterile neutrino production epoch was seen to initiate sooner and cease later than in the scalar mediated case, leading to a stronger enhancement of the final dark matter yield. This allows for the mixing angle to be as low as $\sin^2 2\vartheta = \mathcal{O}(10^{-14})$, two orders lower than in the scalar case, for the same coupling strength and mass. Such mixing angles are comparable in size to the active self-interaction case, but have the benefit of not further disturbing the active sector, being therefore less sensitive to cosmological and particle accelerator bounds. The earlier initiation of production might, however, bring the light vector limit assumption in danger, so a complete assessment of the Boltzmann equation would be favourable. A full evaluation of the parameter space is yet to be performed, however, and is a clear next step forward for the continuation of this research. This would require the numerical evaluation of the complete set of equations, and also requires a computation of the thermal potential induced by the vector interactions onto the sterile neutrinos.

A

Calculation of Amplitudes and Rates

There are several expressions in section 6.1.1 that we will derive in more detail, namely the spin-averaged squared amplitudes, the cross sections and the interaction rates for sterile neutrinos.

A.1 AMPLITUDES

The process of obtaining S-matrix matrix elements when dealing with Majorana fermions is somewhat more involved with respect to Dirac fermions, and deserves some attention. In most literature one finds an intuitive description based on Feynman diagrams, but to further convince the reader of the correct form we have decided to also include the S-matrix elements derived using Wick's theorem. The reason behind additional terms and diagrams can be best understood from considering the free solution of Majorana fermions and its conjugate,

$$\psi = \frac{1}{(2\pi)^3} \int \frac{\mathrm{d}^3 k}{\sqrt{2E}} \sum_r \left(a_{k,s} u_{k,s} e^{-ik\cdot x} + a^\dagger_{k,s} v_{k,s} e^{ik\cdot x} \right) \tag{A.1.1}$$

$$\overline{\psi} = \frac{1}{(2\pi)^3} \int \frac{\mathrm{d}^3 k}{\sqrt{2E}} \sum_r \left(a_{k,s} \overline{v}_{k,s} e^{-ik\cdot x} + a^\dagger_{k,s} \overline{u}_{k,s} e^{ik\cdot x} \right), \tag{A.1.2}$$

where one can see that only one set of creation and annihilation operators is used. This implies that there are more non-trivial contributions when contracting final and initial states with interpolating fields. The respective signs between channels can be understood from the terms involving an odd number of permutations. We first give a list of bilinear identities which are used in simplifying the expressions, and then we thoroughly evaluate both fermionic and scalar final state amplitudes.

A.1.1 IDENTITIES FOR 4-COMPONENT SPINORS

We make repeated use of the bilinear identities obtained from the charge-conjugation properties of the Dirac matrices and the defining relation between u- and v-spinors (see [DHM10]). These identities follow algebraically from

$$v(p,s) = C\,\overline{u(p,s)}^{\,T}, \qquad \overline{v}(p,s) = -\,u(p,s)^T C^{-1}, \tag{A.1.3}$$

together with the similarity relation

$$C^{-1}\Gamma C \;=\; \eta_C^{\Gamma}\,\Gamma^{T}, \tag{A.1.4}$$

with

$$\eta_C^{\Gamma} = \begin{cases} +1, & \Gamma = 1,\; \gamma_5,\; \gamma_\mu\gamma_5, \\ -1, & \Gamma = \gamma_\mu,\; \sigma_{\mu\nu},\; \sigma_{\mu\nu}\gamma_5 \end{cases} \tag{A.1.5}$$

where $\eta_C^{\Gamma} = \pm 1$ is the charge-conjugation phase for the Dirac matrix Γ. From these relations one obtains the general transposition/charge-conjugation formulae, e.g.

$$\bar{u}(p_1,s_1)\,\Gamma\,u(p_2,s_2) \;=\; -\,\eta_C^{\Gamma}\,\bar{v}(p_2,s_2)\,\Gamma\,v(p_1,s_1), \tag{A.1.6}$$

and similarly for mixed $\bar{u}\Gamma v$ bilinears. In particular, for $\Gamma = 1$ and $\Gamma = \gamma^\mu$ (using $\eta_C^{1} = +1,\ \eta_C^{\gamma^\mu} = -1$) one obtains the useful identities

$$\bar{v}(p_1,s_1)\,v(p_2,s_2) \;=\; -\,\bar{u}(p_2,s_2)\,u(p_1,s_1), \tag{A.1.7}$$

$$\bar{v}(p_1,s_1)\,\gamma^\mu\,v(p_2,s_2) \;=\; \bar{u}(p_2,s_2)\,\gamma^\mu\,u(p_1,s_1). \tag{A.1.8}$$

For Majorana fermions the field satisfies $\psi = \psi^c = C\bar{\psi}^T$, so particle and antiparticle spinor wave-functions are identified and the above relations become especially useful: one may freely replace v-spinors by the charge conjugates of u-spinors (and vice versa).

From now on we will denote

$$u_1 \equiv u(p_1,s_1), \quad u_2 \equiv u(p_2,s_2), \quad \text{etc.}, \tag{A.1.9}$$

to compactify any further derivations.

A.1.2 OBTAINING $-i\mathcal{M}_{\nu_s\nu_s\to\nu_s\nu_s}$

We consider the $2\nu_s \leftrightarrow 2\nu_s$ matrix element mediated by a scalar propagator, arising from

$$\mathcal{L}_{\text{int}} = y\;\bar{\nu}_s\nu_s\,\phi. \tag{A.1.10}$$

We define the initial and final states to be

$$|\,i\,\rangle = \sqrt{2E_2}\sqrt{2E_1}a_2^\dagger a_1^\dagger|\,0\,\rangle \tag{A.1.11}$$

$$|f\rangle = \sqrt{2E_3}\sqrt{2E_4}a_3^\dagger a_4^\dagger|\,0\,\rangle, \tag{A.1.12}$$

and we let

$$\mathcal{A}_{fi}^{\overbracket{\phi\phi}} = \langle f|S^{(2)\overbracket{\phi\phi}}|\,i\,\rangle \tag{A.1.13}$$

denote the contribution to the second order matrix element coming from the scalar propagator. Above we have defined

$$a_i \equiv a(p_i,s_i), \tag{A.1.14}$$

and we will continue using this notation. Since the initial and final states consist of creation and annihilation operators of the same kind, the combinatorics of contracting interpolating and asymptotic fields becomes more extensive. We find

$$\begin{aligned}
\mathcal{A}_{fi}^{\overset{\sqcap}{\phi\phi}} &= \frac{i}{2!}(-iy)^2 \int \mathrm{d}^4x\mathrm{d}^4y \int \frac{\mathrm{d}^4k}{(2\pi)^4}\frac{e^{-ik(x-y)}}{k^2-m^2+i\varepsilon}\langle f| : (\bar{\psi}\psi)_x(\bar{\psi}\psi)_y : | i \rangle \\
&= -iy^2\frac{1}{2!}\int \mathrm{d}^4x\mathrm{d}^4y \int \frac{\mathrm{d}^4k}{(2\pi)^4}\frac{e^{-ik(x-y)}}{k^2-m^2+i\varepsilon}\langle f|2 : (\bar{\psi}_+\psi_+)_x(\bar{\psi}_-\psi_-)_y : \\
&+ (\bar{\psi}_+\psi_-)_x(\bar{\psi}_+\psi_-)_y : + : (\bar{\psi}_-\psi_+)_x(\bar{\psi}_-\psi_+)_y : +2 : (\bar{\psi}_+\psi_-)(\bar{\psi}_-\psi_+) : | i \rangle \\
&= -iy^2 \int \mathrm{d}^4x\mathrm{d}^4y \int \frac{\mathrm{d}^4k}{(2\pi)^4}\frac{e^{-ik(x-y)}}{k^2-m^2+i\varepsilon}\int \frac{\mathrm{d}^3k_1\cdots\mathrm{d}^3k_4}{(2\pi)^{12}}\frac{\sqrt{2^4E_1\cdots E_4}}{\sqrt{2^4E_{k_1}\cdots E_{k_4}}} \\
&\times \langle\, 0 \,|\, a_4a_3(2 : a_{k_1}a_{k_2}a_{k_3}^{\dagger}a_{k_4}^{\dagger} : \bar{v}_{k_1}u_{k_2}e^{-ix(k_1+k_2)}\bar{u}_{k_3}v_{k_4}e^{iy(k_3+k_4)} \\
&+ : a_{k_1}a_{k_2}^{\dagger}a_{k_3}a_{k_4}^{\dagger} : \bar{v}_{k_1}v_{k_2}e^{-ix(k1-k2)}\bar{v}_{k_3}v_{k_4}e^{-iy(k_3-k_4)} \\
&+ : a_{k_1}^{\dagger}a_{k_2}a_{k_3}^{\dagger}a_{k_4} : \bar{u}_{k_1}u_{k_2}e^{-ix(k_2-k_1)}\bar{u}_{k_3}u_{k_4}e^{-iy(k_4-k_3)} \\
&+ 2 : a_{k_1}a_{k_2}^{\dagger}a_{k_3}^{\dagger}a_{k_4} : \bar{v}_{k_1}v_{k_2}e^{-ix(k_1-k_2)}\bar{u}_{k_3}u_{k_4}e^{-iy(k_4-k_3)})a_2^{\dagger}a_1^{\dagger} \,|\, 0 \,\rangle .
\end{aligned}$$

From the commutation relations we find four separate contractions for every term over which we should average, namely

$$\begin{aligned}
\mathcal{A}_{fi}^{\overset{\sqcap}{\phi\phi}} &= -iy^2\frac{1}{8}\int \mathrm{d}^4x\mathrm{d}^4y \int \frac{\mathrm{d}^4k}{(2\pi)^4}\frac{e^{-ik(x-y)}}{k^2-m^2+i\varepsilon}\int \mathrm{d}^3k_1\cdots\mathrm{d}^3k_4\frac{\sqrt{2^4E_1\cdots E_4}}{\sqrt{2^4E_{k_1}\cdots E_{k_4}}} \\
&\times \Bigg(2\,\bar{v}_{k_1}u_{k_2}\bar{u}_{k_3}v_{k_4}e^{-ix(k_1+k_2)}e^{iy(k_3+k_4)}\Big[\delta(p_3-k_3)\delta(p_4-k_4)-\delta(p_3-k_4)\delta(p_4-k_4)\Big] \\
&\cdot \Big[\delta(p_1-k_1)\delta(p_2-k_2)-\delta(p_1-k_2)\delta(p_2-k_1)\Big] && \text{(A)} \\
&+ \bar{v}_{k_1}v_{k_2}\bar{v}_{k_3}v_{k_4}e^{-ix(k_1-k_2)}e^{iy(k_4-k_3)}\Big[\delta(p_3-k_2)\delta(p_4-k_4)-\delta(p_3-k_4)\delta(p_4-k_2)\Big] \\
&\cdot \Big[\delta(p_1-k_1)\delta(p_2-k_3)-\delta(p_1-k_3)\delta(p_2-k_1)\Big] && \text{(B)} \\
&+ \bar{u}_{k_1}u_{k_2}\bar{u}_{k_3}u_{k_4}e^{-ix(k_2-k_1)}e^{iy(k_3-k_4)}\Big[\delta(p_3-k_1)\delta(p_4-k_3)-\delta(p_3-k_3)\delta(p_4-k_1)\Big] \\
&\cdot \Big[\delta(p_1-k_4)\delta(p_2-k_2)-\delta(p_1-k_2)\delta(p_2-k_4)\Big] && \text{(C)} \\
&+ 2\bar{v}_{k_1}v_{k_2}\bar{u}_{k_3}u_{k_4}e^{-ix(k_1-k_2)}e^{iy(k_3-k_4)}\Big[\delta(p_3-k_2)\delta(p_4-k_3)-\delta(p_3-k_3)\delta(p_4-k_2)\Big] \\
&\cdot \Big[\delta(p_1-k_1)\delta(p_2-k_4)-\delta(p_1-k_4)\delta(p_2-k_1)\Big]\Bigg) && \text{(D)}
\end{aligned}$$

We will now compute term (A) in some detail, explicitly showing the Majorana fermionic relations that are applied, after which we pass more rapidly through terms (B), (C) and (D). Expanding the delta products and cancelling them with the integrals over $\mathrm{d}k_i$, the normalization terms cancel and one gets

$$
\begin{aligned}
(\mathrm{A}) = -iy^2\frac{1}{8}\int \mathrm{d}^4x\mathrm{d}^4y \int \frac{\mathrm{d}^4k}{(2\pi)^4}\frac{e^{-ik(x-y)}}{k^2-m^2+i\varepsilon}2\Big(&\bar{v}_1u_2\bar{u}_3v_4 - \bar{v}_2u_2\bar{u}_3v_4 \\
&- \bar{v}_1u_2\bar{u}_4v_3 + \bar{v}_2u_1\bar{u}_4v_3\Big)e^{-ix(p_1+p_2)}e^{iy(p_3+p_4)}.
\end{aligned}
$$

We now use the identities $-\bar{v}_2u_1 = \bar{v}_1u_2$ and $-\bar{u}_4v_3 = \bar{u}_3v_4$ to work towards our final expression.

$$
\begin{aligned}
(\mathrm{A}) &= -iy^2\frac{1}{8}\int \mathrm{d}^4x\mathrm{d}^4y \int \frac{\mathrm{d}^4k}{(2\pi)^4}\frac{8\,\bar{v}_1u_2\bar{u}_3v_4}{k^2-m^2+i\varepsilon}e^{-ix(k+p_1+p_2)}e^{iy(k+p_3+p_4)} \\
&= -iy^2(2\pi)^4\delta^{(4)}(p_1+p_2-p_3-p_4)\frac{\bar{v}_1u_2\bar{u}_3v_4}{s-m^2+i\varepsilon}
\end{aligned}
$$

From (B) we a $t-$ and $u-$channel contribution, for which we use $\bar{v}_1v_3\bar{v}_2v_4 = \bar{u}_4u_2\bar{u}_3u_1$ and an equivalent $(3-4)$permutation respectively to obtain

$$
(\mathrm{B}) = -iy^2\frac{1}{8}(2\pi)^4\delta^{(4)}(\ldots)\left(\frac{2\,\bar{u}_3u_2\bar{u}_4u_1}{u-m^2+i\varepsilon} - \frac{2\,\bar{u}_4u_2\bar{u}_3u_1}{t-m^2+i\varepsilon}\right).
$$

In similar fashion

$$
(\mathrm{C}) = -iy^2\frac{1}{8}(2\pi)^4\delta^{(4)}(\ldots)\left(\frac{2\,\bar{u}_3u_2\bar{u}_4u_1}{u-m^2+i\varepsilon} - \frac{2\,\bar{u}_4u_2\bar{u}_3u_1}{t-m^2+i\varepsilon}\right)
$$

and

$$
(\mathrm{D}) = -iy^2\frac{1}{8}(2\pi)^4\delta^{(4)}(\ldots)\left(\frac{4\,\bar{u}_3u_2\bar{u}_4u_1}{u-m^2+i\varepsilon} - \frac{4\,\bar{u}_4u_2\bar{u}_3u_1}{t-m^2+i\varepsilon}\right).
$$

All together this results in the amplitude

$$
\begin{aligned}
\mathcal{A}_{fi}^{\overset{\sqcap}{\phi\phi}} &= (\mathrm{A}) + (\mathrm{B}) + (\mathrm{C}) + (\mathrm{D}) \\
&= -\,iy^2(2\pi)^4\delta^{(4)}(\ldots)\left(\frac{\bar{v}_1u_2\bar{u}_3v_4}{s-m^2+i\varepsilon} - \frac{\bar{u}_4u_2\bar{u}_3u_1}{t-m^2+i\varepsilon} + \frac{2\,\bar{u}_3u_2\bar{u}_4u_1}{u-m^2+i\varepsilon}\right),
\end{aligned}
$$

and so

$$
-i\mathcal{M} = i\,y^2\left(\frac{\bar{v}_1u_2\bar{u}_3v_4}{s-m^2+i\varepsilon} - \frac{\bar{u}_4u_2\bar{u}_3u_1}{t-m^2+i\varepsilon} + \frac{\bar{u}_3u_2\bar{u}_4u_1}{u-m^2+i\varepsilon}\right). \tag{A.1.15}
$$

We should be wary, however, using the given $s-$channel propagator due to the finite lifetime of the scalar mediator which can become relevant around energies s. We should therefore replace the propagator with the Breit-Wigner propagators, i.e.

$$
-i\mathcal{M} = i\,y^2\left(\frac{\bar{v}_1u_2\bar{u}_3v_4}{s-m^2+im\Gamma_\phi} - \frac{\bar{u}_4u_2\bar{u}_3u_1}{t-m^2+i\varepsilon} + \frac{\bar{u}_3u_2\bar{u}_4u_1}{u-m^2+i\varepsilon}\right). \tag{A.1.16}
$$

A.1.3 $\overline{|\mathcal{M}_{\nu_s\nu_s\to\nu_s\nu_s}|}^2$

Defining the various terms of A.1.16 as their respective channel contribution, we write

$$\begin{aligned} |\mathcal{M}_{\int\int\to\int\int}|^2 &= |\mathcal{M}_s - \mathcal{M}_t + \mathcal{M}_u|^2 \\ &= |\mathcal{M}_s|^2 + |\mathcal{M}_t|^2 + |\mathcal{M}_u|^2 + 2\mathfrak{Re}\mathcal{M}_s\mathcal{M}_u - 2\mathfrak{Re}\mathcal{M}_s\mathcal{M}_t - 2\mathfrak{Re}\mathcal{M}_t\mathcal{M}_u \end{aligned}$$

The first three terms yield

$$\begin{aligned} \overline{|\mathcal{M}_s|}^2 &= 2y^4\left[\frac{\bar{v}_1u_2\bar{u}_3v_4\bar{v}_4u_3\bar{u}_2v_1}{(s-m^2)^2+m^2\Gamma_\phi^2}\right] \\ &= 2y^4\left[\frac{\mathrm{Tr}[\not{p}_1\not{p}_2]\mathrm{Tr}[\not{p}_3\not{p}_4]}{(s-m^2)^2+m^2\Gamma_\phi^2}\right] \\ &= 8y^4\frac{s^2}{(s-m^2)^2+m^2\Gamma_\phi^2} \end{aligned}$$

and similarly

$$\begin{aligned} \overline{|\mathcal{M}_t|}^2 &= 8y^4\frac{t^2}{(t-m^2)^2} \\ \overline{|\mathcal{M}_u|}^2 &= 8y^2\frac{(s+t)^2}{(s+t+m^2)^2}, \end{aligned}$$

where we used that for relativistic initial and final states $s+t+u = 0$. The real part of the cross term involves the removal of the imaginary component of the Breit-Wigner propagator, for which we multiply by its complex conjugate in both the numerator and denominator so that we can isolate the real part of the numerator, i.e.

$$\begin{aligned} 2\mathfrak{Re}\mathcal{M}_s\mathcal{M}_u &= \frac{2y^4[(s-m^2)]}{[(s-m^2)^2+m^2\Gamma_\phi^2][-s-t-m^2]}\bar{v}_1u_2\bar{u}_3v_4\bar{u}_1u_4\bar{u}_2u_3 && \text{(A.1.17)} \\ &= -\frac{2y^4[(s-m^2)]}{[(s-m^2)^2+m^2\Gamma_\phi^2][-s-t-m^2]}\mathrm{Tr}[\not{p}_1\not{p}_3\not{p}_4\not{p}_2] && \text{(A.1.18)} \\ &= -\frac{8y^4[(s-m^2)]}{[(s-m^2)^2+m^2\Gamma_\phi^2][-s-t-m^2]}(s^2+st), && \text{(A.1.19)} \end{aligned}$$

where the sign-change is induced by a spinor bilinear identity, and $u = -s-t$ lead to the (s^2+st) term. Similarly we find, for the other cross terms, we get trace contribution

$$\mathrm{Tr}[\not{p}_1\not{p}_3\not{p}_2\not{p}_4] \text{ and } \mathrm{Tr}[\not{p}_1\not{p}_2\not{p}_3\not{p}_4] \tag{A.1.20}$$

leading respectively to

$$\begin{aligned} 2\mathfrak{Re}\mathcal{M}_t\mathcal{M}_u &= -\frac{8y^4(t^2+ts)}{(t-m^2)(-t-s-m^2)} \\ -2\mathfrak{Re}\mathcal{M}_s\mathcal{M}_t &= -\frac{8y^4((s-m^2)st)}{[(s-m^2)^2+m^2\Gamma_\phi^2][t-m^2]}. \end{aligned}$$

Summing the terms and leaving only squared terms in the denominator then leads to

$$
\begin{aligned}
|\mathcal{M}|^2_{\nu_s\nu_s\leftrightarrow\nu_s\nu_s} = 8y^4 \Bigg[& \frac{s^2}{\left[(s-m_\varphi^2)^2+m_\varphi^2\Gamma_\varphi^2\right]} - \frac{(s^2+st)\,(s-m_\varphi^2)(-t-s-m_\varphi^2)}{\left[(s-m_\varphi^2)^2+m_\varphi^2\Gamma_\varphi^2\right]\,(s+t+m_\varphi^2)^2} \\
& + \frac{t^2}{(t-m_\varphi^2)^2} - \frac{(t^2+st)\,(t-m_\varphi^2)(-t-s-m_\varphi^2)}{(t-m_\varphi^2)^2\,(t+s+m_\varphi^2)^2} \\
& + \frac{(s+t)^2}{(s+t+m_\varphi^2)^2} + \frac{st\,(s-m_\varphi^2)(t-m_\varphi^2)}{\left[(s-m_\varphi^2)^2+m_\varphi^2\Gamma_\varphi^2\right]\,(t-m_\varphi^2)^2}\Bigg].
\end{aligned}
\tag{A.1.21}
$$

For good practice, the amplitude has also been evaluated in Mathematica using the Feyncalc package. We will briefly show the main definitions and stepts of the code. Following a similar path as in the manual calculation, we define

```
Ms = (-I y)^2*
   SpinorVBar[p1, 0].SpinorU[p2, 0] *(I/(s - MS^2 + I* MS*MS2))*
   SpinorUBar[p3, 0].SpinorV[p4, 0];

Mt = (-I y)^2*SpinorVBar[p2, 0].SpinorV[p4, 0]*(I/(t - MS^2))*
   SpinorUBar[p3, 0].SpinorU[p1, 0];

Mu = (-I y)^2*SpinorVBar[p2, 0].SpinorV[p3, 0]*(I/(u - MS^2))*
   SpinorUBar[p4, 0].SpinorU[p1, 0];
```

and compute terms one by one, i.e.

```
    Mscc = FermionSpinSum[Ms*ComplexConjugate[Ms]] // DiracSimplify //
   FullSimplify ;
MsccMandel = ExpandScalarProduct[Mscc] // Contract

crossST =
  2* Re[ FermionSpinSum[Ms*ComplexConjugate[Mt]]] // DiracSimplify //
   FullSimplify;

crossSTMandel =
 ExpandScalarProduct[crossST] /. {u -> -s - t} // Contract //
    Simplify // ComplexExpand // Simplify
```

We then compute the full term and find the desired result.

```
    In[48]:
MsqManual =
 4/2 * 4 y^4 *( (MsccMandel + MtccMandel + MuccMandel +
     crossSTMandel - crossSUMandel - crossTUMandel ) /. {4 y^4 -> 1,
    y^4 -> 1/4} )

Out[48]= 8 y^4 (
-((t (s+t))/((MS^2-t) (MS^2+s+t)))
+(s+t)^2/(MS^2+s+t)^2+
t^2/(MS^2-t)^2
+(s t (MS^2-s))/((MS^2-t) (MS^4+MS^2 (MS2^2-2 s)+s^2))
-(s (MS^2-s) (s+t))/((MS^4+MS^2 (MS2^2-2 s)+s^2) (MS^2+s+t))
+s^2/(MS^4+MS^2 (MS2^2-2 s)+s^2))
```

A.1.4 OBTAINING $-i\mathcal{M}_{\nu_s\nu_s\to\phi\phi}$

The S-matrix computation of the two-to-two scattering into scalars is less extensive, since initial and final states are different. Defining

$$\phi = \frac{1}{(2\pi)^3}\int \frac{\mathrm{d}^3k}{\sqrt{(2E)}}\left(b_k e^{-ik\cdot x} + b_k^\dagger e^{ik\cdot x}\right) \tag{A.1.22}$$

and

$$\begin{aligned} |\, i\,\rangle &= \sqrt{2E_2 2E_1}\, a_2^\dagger a_1^\dagger |\, 0\,\rangle \\ |f\rangle &= \sqrt{2E_3 2E_4}\, b_3^\dagger b_4^\dagger |\, 0\,\rangle, \end{aligned}$$

we find

$$\begin{aligned} \mathcal{A}_{fi}^{\overset{\sqcap}{\nu_s\nu_s}} =& \frac{iy^2}{2!}\int \mathrm{d}^4x\mathrm{d}^4y \int \frac{\mathrm{d}^4k}{(2\pi)^4}\frac{e^{-ik\cdot(x-y)}}{k^2-m^2+i\varepsilon}\langle f|\Big(\\ &(\not{k}+m) : [(\bar{\psi}_+ + \bar{\psi}_-)\phi_-]_x[(\psi_+ + \psi_-)\phi_-]_y : \\ &+ (-\not{k}+m) : [(\psi_+ + \psi_-)\phi_-]_x[(\bar{\psi}_+ + \bar{\psi}_-)\phi_-]_y : \Big)|\, i\,\rangle \\ =& \frac{iy^2}{2!}\int \mathrm{d}^4x\mathrm{d}^4y \int \frac{\mathrm{d}^4k}{(2\pi)^4}\frac{e^{-ik\cdot(x-y)}}{k^2-m^2+i\varepsilon}\int \frac{\mathrm{d}^4k_1\cdots\mathrm{d}^4k_4}{(2\pi)^{12}}\frac{\sqrt{2^4E_1\cdots E_4}}{\sqrt{2^4E_{k_1}\cdots E_{k_4}}}\langle\, 0\,|\Big(\\ &(\not{k}+m)b_3b_4b_{k_3}^\dagger b_{k_4}^\dagger e^{ik_3x+ik_4y}a_{k_1}\bar{v}_{k_1}e^{-ik_1x}a_{k_2}u_{k_2}e^{-ik_2y} \\ &(-\not{k}+m)b_3b_4b_{k_3}^\dagger b_{k_4}^\dagger e^{ik_3x+ik_4y}a_{k_1}u_{k_1}e^{-ik_1x}a_{k_2}\bar{v}_{k_2}e^{-ik_2y}\Big)|\, 0\,\rangle. \end{aligned}$$

Contracting the operators, executing the deltas, setting $m = 0$, and rearranging $\bar{v}_1u_2 = -u_1\bar{v}_2$ leads to

$$\begin{aligned} &= \frac{iy^2}{2}\int \mathrm{d}^4x\mathrm{d}^4y\int \mathrm{d}^4k\frac{\not{k}}{k^2+i\varepsilon}\Big(\\ &e^{-ix(k-(p_3-p_1)}e^{iy(k-(p_2-p_4))} + e^{-ix(k-(p_3-p_2)}e^{iy(k-(p_1-p_4))}\Big) \\ &= \frac{iy^2}{2}(2\pi)^4\int \mathrm{d}^4k\frac{\not{k}}{k^2+i\varepsilon}\Big(\delta^{(4)}(k-(p_3-p_1))\delta^{(4)}(k-(p_2-p_4)) \\ &+ \delta^{(4)}(k-(p_3-p_2))\delta^{(4)}(k-(p_1-p_4))\Big)\bar{v}_1u_2 \\ &= -i\frac{y^2}{2}\bar{v}_2\left[\frac{\not{p}_1-\not{p}_3}{t+i\varepsilon} - \frac{\not{p}_1-\not{p}_4}{u+i\varepsilon}\right]u_1. \end{aligned}$$

A.1.5 $\overline{|\mathcal{M}_{\nu_s\nu_s\to\phi\phi}|}^2$

From the expression above we again find two squared channels and a cross term. Summing the spins cancels the factor 1/2, and the contraction $\sum \bar{v}_2 u_1 \bar{u}_1 v_2$ is present in all contributions, so that

$$\begin{aligned}
\overline{|\mathcal{M}|}^2 &= |\mathcal{M}_t|^2 + |\mathcal{M}_u|^2 - 2\mathfrak{Re}\mathcal{M}_t\mathcal{M}_u \qquad \text{(A.1.23)}\\
&= y^4\left[\frac{1}{t^2}\not{p}_2(\not{p}_1 - \not{p}_3)\not{p}_1(\not{p}_1 - \not{p}_3) + \frac{1}{u^2}\not{p}_2(\not{p}_1 - \not{p}_4)\not{p}_1(\not{p}_1 - \not{p}_4) - \frac{1}{tu}\not{p}_2(\not{p}_3 - \not{p}_3)\not{p}_1(\not{p}_1 - \not{p}_4)\right]\\
&= y^4\mathrm{Tr}[\gamma^\mu\gamma^\nu\gamma^\rho\gamma^\sigma]\left[\frac{1}{t^2}(p_{2\mu}p_{1\nu}p_{1\rho}p_{1\sigma} - p_{2\mu}p_{3\nu}p_{1\rho}p_{1\sigma} - p_{2\mu}p_{1\nu}p_{1\rho}p_{3\sigma} + p_{2\mu}p_{3\nu}p_{1\rho}p_{3\sigma})\right.\\
&\qquad \left. + \frac{1}{u^2}(3 \leftrightarrow 4)_{\mu\nu\rho\sigma} - \frac{2}{tu}(p_{2\mu}p_{1\nu}p_{1\rho}p_{1\sigma} - p_{2\mu}p_{3\nu}p_{1\rho}p_{1\sigma} - (3 \leftrightarrow 4)_{\mu\nu\rho\sigma})\right]\\
&= 4y^4\left(\eta^{\mu\nu}\eta^{\rho\sigma} - \eta^{\mu\rho}\eta^{\nu\sigma} + \eta^{\mu\sigma}\eta^{\nu\rho}\right)\Big[\ \dots\Big]\\
&= 4y^4\left[\frac{1}{t^2}\big(- m_\phi^4 + 2tm_\phi^2 - t^2 + sm_\phi^2 - st - sm_\phi^2\big) + \frac{1}{(2m_\phi^2 - s - t)^2}\big(- m_\phi^4 + 2tm_\phi^2 - t^2 - st\big)\right.\\
&\qquad \left. - \frac{1}{t(m_\phi^2 - s - t)}\big(2m_\phi^4 + 2t^2 - 4m_\phi^2 t + 2st\big)\right]\\
&= 4y^4\frac{(s + 2t - 2m_\phi)^2}{t^2(2m_\phi^2 - s - t)}\big(- m_\phi^4 + 2m_\phi^2 t - t(s + t)\big) \qquad \text{(A.1.24)}
\end{aligned}$$

A.2 CROSS SECTIONS

For a two-to-two process with equal outgoing masses one is able to compute the cross section in the centre of mass frame as

$$\begin{aligned}
\sigma_{\nu_s\nu_s\to kk} &= \int \mathrm{d}\Pi_3\mathrm{d}\Pi_4(2\pi)^4\delta^{(4)}(p_1 + p_2 - p_3 - p_4)\frac{\overline{|\mathcal{M}_{\nu_s\nu_s\to kk}|}^2}{4p_1\cdot p_2} \qquad \text{(A.2.1)}\\
&= \frac{1}{64\pi^2 s}\int \mathrm{d}\Omega\frac{|\vec{p}'|}{|\vec{p}|}\overline{|\mathcal{M}_{\nu_s\nu_s\to kk}|}^2 \qquad \text{(A.2.2)}\\
&= \frac{1}{32\pi s}\int \mathrm{d}\cos\vartheta\frac{|\vec{p}'|}{|\vec{p}|}\overline{|\mathcal{M}_{\nu_s\nu_s\to kk}|}^2, \qquad \text{(A.2.3)}
\end{aligned}$$

where $\mathrm{d}\Pi_i = \frac{\mathrm{d}^3p}{(2\pi)^3 2E_i}$, $|\vec{p}'| = \frac{1}{2\sqrt{s}}[s^2 - 4sm_k^2]^{\frac{1}{2}}$ is the outgoing 3-momentum, and $|\vec{p}|$ the incoming momentum. Note that for massless final and initial states the outgoing and incoming momenta simplify. In our case we integrate over $|\mathcal{M}_{\nu_s\nu_s\to\nu_s\nu_s}|^2$ and $|\mathcal{M}_{\nu_s\nu_s\to\phi\phi}|^2$. have written all spin-averaged squared amplitudes in terms of Mandelstam variables s and t only, so rewriting t in terms of s, outgoing masses, and $\cos\vartheta$ allows us to perform the integration. One easily computes, for scalar and neutrino final states respectively,

$$t = \begin{cases} (m_\phi^2 - \frac{s}{2}) - \sqrt{s(s - 4m_\phi^2)}\cos\vartheta & \to \phi\phi, \\ -\frac{s}{2} + \frac{s}{2}\cos\vartheta & \to \nu_s\nu_s. \end{cases} \qquad \text{(A.2.4)}$$

Although the integrals could be done manually using partial fraction decomposition, we opt to use Mathematica to find

$$\sigma_{\nu_s\nu_s\to\phi\phi}(s) = \frac{y^4}{4\pi s^2}\left[\frac{6m_\varphi^4 - 4m_\varphi^2 s + s^2}{2m_\varphi^2 - s} 2\ln\left(\frac{\sqrt{s(s-4m_\varphi^2)} - s + 2m_\varphi^2}{\sqrt{s(s-4m_\varphi^2)} + s - 2m_\varphi^2}\right) - 6\sqrt{s(s-4m_\varphi^2)}\right], \qquad \text{(A.2.5)}$$

and

$$\sigma_{\nu_s\nu_s\to\nu_s\nu_s}(s) = \frac{y^4}{2\pi s^2\left[(m_\varphi^2 - s)^2 + m_\varphi^2\Gamma_\varphi^2\right]}\left[\frac{s\left(5m_\varphi^6 - 9m_\varphi^4 s + 6s^3\right)}{m_\varphi^2 + s}\frac{2\left(5m_\varphi^8 - 9m_\varphi^6 s + 4s^3\right)}{2m_\varphi^2 + s}\ln\left(\frac{m_\varphi^2}{m_\varphi^2 + s}\right)\right]. \qquad \text{(A.2.6)}$$

A.3 RATES

The most general starting point for the interaction rate of a process

$$i + j \ \to\ k + l$$

is given by the phase–space integral

$$\begin{aligned}\Gamma_{ij\to kl}(p_i) &= \frac{1}{2E_i}\int \frac{d^3\mathbf{p}_j}{(2\pi)^3 2E_j}\frac{d^3\mathbf{p}_k}{(2\pi)^3 2E_k}\frac{d^3\mathbf{p}_l}{(2\pi)^3 2E_l} \\ &\qquad \times (2\pi)^4\delta^{(4)}(p_i + p_j - p_k - p_l)\,|\mathcal{M}_{ij\to kl}|^2 f_j(p_j)\,[1 \pm f_k][1 \pm f_l], &\text{(A.3.1)} \\ &\simeq \frac{1}{2E_i}\int \mathrm{d}\Pi_j\, f(p_j)\; 4(p_i\cdot p_j)\;\sigma_{ij\to kl} &\text{(A.3.2)}\end{aligned}$$

where $|\mathcal{M}|^2$ is the squared scattering amplitude summed over spins, the f_i are distribution functions, and the final–state statistical factors account for Pauli blocking ($-$) or Bose enhancement ($+$). The last equation becomes exact if we set $[1 \pm f_k] = 1$.

For practical purposes, one often integrates over initial distributions as well, as we will see in B, yielding the thermally averaged rate

$$\langle\Gamma_{ij\to kl}\rangle = \frac{1}{n_i n_j}\int d\Pi_i d\Pi_j d\Pi_k d\Pi_l\,(2\pi)^4\delta^{(4)}(p_i + p_j - p_k - p_l)|\mathcal{M}|^2 f_i f_j, \qquad \text{(A.3.3)}$$

with $d\Pi_i \equiv \frac{d^3\mathbf{p}_i}{(2\pi)^3 2E_i}$ and n_i the number density.

A.3.1 STERILE-STERILE INTERACTION RATES VIA SCALAR MEDIATORS

Consider first the case of sterile–sterile interactions through oscillations, as described in figure A.3.1. Since a light neutrino eigenstate collapses into a sterile state, it is the distribution of the light neutrino (i.e., predominantly active) that determines the momentum p_1. One thus trades one of the sterile distribution functions f_s for an active distribution f_a multiplied by the conversion probability:

$$f_s(p,t) \ \longrightarrow\ f_a(p,t)\,P(\nu_a \to \nu_s; p, t). \qquad \text{(A.3.4)}$$

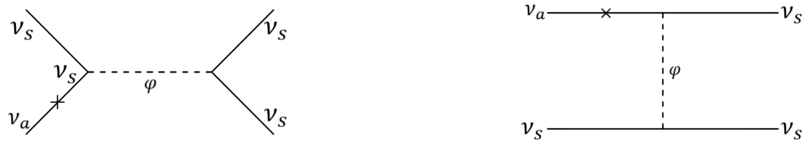

Figure A.3.1: Contributions to sterile neutrino production induced by the 2-to-2 scattering of sterile neutrinos and the oscillation of an active into a sterile neutrino.

The rate, not yet integrated over the initial active distribution, is computed by

$$\Gamma_{\nu_s\nu_s\to\nu_s\nu_s}(p_1) = \frac{1}{2E_1}\int \mathrm{d}\Pi_2\, f(p_2)\; 4(p_1\cdot p_2)\; \sigma_{\nu_s\nu_s\to\nu_s\nu_s}, \tag{A.3.5}$$

which, if we consider f_s as a Maxwell-Boltzmann distribution with chemical potential μ and temperature T_s, can be approximated as [AV24]

$$\Gamma_{\nu_s\nu_s\leftrightarrow\nu_s\nu_s}(p_1) = e^{\mu/T_s}\times\begin{cases} \frac{3y^4T_s^2}{2\pi^3 p_1} + \frac{y^2 T_s m_\phi^2}{2\pi p_1^2} e^{-\frac{m_\phi^2}{4p_1T_s}} & p_1T_s > \frac{3m_\phi^2}{2\sqrt{10}} \\ \frac{20y^4 p_1 T_s^4}{3\pi^3 m_\phi^4} + \frac{y^2 T_s m_\phi^2}{2\pi p_1^2} e^{-\frac{m_\phi^2}{4p_1T_s}} & p_1T_s \leq \frac{3m_\phi^2}{2\sqrt{10}}. \end{cases} \tag{A.3.6}$$

For scatterings of active neutrinos with the thermal plasma (electrons, positrons, other neutrinos, etc), the appropriate interaction rate cannot be computed from vacuum amplitudes alone. Medium effects from finite temperature and density modify both propagators and interaction vertices. This requires the use of thermal field theory, which resums forward–scattering diagrams into effective self–energies. The net effect is that both the interaction rate Γ_a and the potential V entering oscillation dynamics are dressed by the medium, as discussed in Section 5.1.2.

For purely sterile scatterings mediated by a new boson φ, no thermal resummation is needed, since sterile neutrinos do not participate in Standard Model interactions. The rate is the same as above, only now the averaging can be done with a sterile state too. The other relevant 2-to-2 scattering process involves final states $\to 2\phi$, also diagrammatically represented below. The scattering into scalars has no easy analytic expression, but should be computed numerically.

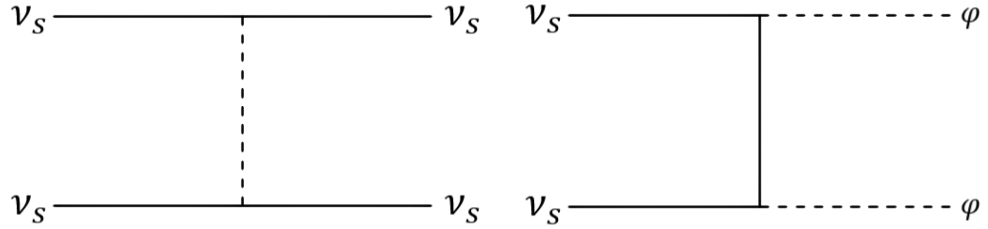

Figure A.3.2: 2-to-2 scattering into sterile and scalar final states.

A.3.2 INTERACTION RATES AND THERMAL AVERAGING

It is customary to define the thermally averaged cross section times velocity as

$$\langle \sigma v \rangle = \langle \Gamma(ij \to k\ell) \rangle = \int \mathrm{d}\Pi \, \frac{\Gamma(ij \to k\ell; p)}{n_i^{eq} n_j^{eq}}, \tag{A.3.7}$$

with n_i^{eq} the equilibrium number density, which is often the effective rate that enters into Boltzmann equations. By factoring out the chemical potential from the integral and using the equilibrium densities for known distributions, we can reduce this average to known expressions. For Maxwell–Boltzmann statistics, the equilibrium density takes the form

$$n_i^{\mathrm{eq}} = g_i \, \frac{m_i^2 T}{2\pi^2} K_2\left(\frac{m_i}{T}\right), \tag{A.3.8}$$

where K_ν are the modified Bessel functions of the second kind. These special functions naturally appear because integrals over the relativistic phase space reduce to combinations of $K_\nu(z)$ after angular integration.

Gondolo and Gelmini [GG91] then derived a particularly useful representation of the thermal average:

$$\langle \sigma v \rangle = \frac{1}{8\, m_i^2 m_j^2 T K_2\left(\frac{m_i}{T}\right) K_2\left(\frac{m_j}{T}\right)} \int_{s_{\min}}^{\infty} ds \, \lambda(s, m_i^2, m_j^2) \, \frac{K_1(\sqrt{s}/T)}{\sqrt{s}} \, \sigma(s), \tag{A.3.9}$$

with $s_{\min} = (m_i + m_j)^2$ and λ the Källén function

$$\lambda(s, m_i^2, m_j^2) = [s - (m_i + m_j)^2][s - (m_i - m_j)^2]. \tag{A.3.10}$$

The K_1–factor weights the cross section at $\sqrt{s}$ against the thermal distribution of incoming states, and exponentially suppresses large $\sqrt{s} \gg T$.

A.3.3 MOMENTS OF SCALAR FINAL STATES

As an explicit example useful for our system, consider massless incoming fermions annihilating into scalars of mass M_φ. Define $z = \sqrt{s}/T$, so that the threshold corresponds to $z_{\min} = 2M_\varphi/T$.

NUMBER PRODUCTION RATE. The standard thermally averaged cross section reads

$$\langle \sigma v \rangle = \frac{1}{16} \int_{z_{\min}}^{\infty} dz \, z^4 K_1(z) \, \sigma_\varphi(s = z^2 T^2). \tag{A.3.11}$$

Here the prefactor $1/16$ arises from phase-space normalization for two massless incoming states.

ENERGY-WEIGHTED RATE. Often one requires not just the number production, but also the rate at which *energy* is injected into the final states. This corresponds to the first energy moment,

$$\langle (E_1 + E_2) \, \sigma v \rangle = \frac{T}{16} \int_{z_{\min}}^{\infty} dz \, z^5 K_1(z) \, \sigma_\varphi(s = z^2 T^2). \tag{A.3.12}$$

The extra factor of z reflects the additional weight by the total incoming energy $\sqrt{s} = zT$.

In practice these expressions can be evaluated numerically to fairly high precision, and are therefore used as the components for scattering and production rates in our Boltzmann system, see Appendix B.

A.3.4 ACTIVE–ACTIVE INTERACTION RATES

The complete formal expression for active–active rates is no different than its sterile counterpart, only differing in the relevant distribution functions. Let us focus on the light limit, in particular the regime where typical momenta are larger than the scalar mass, such that the scalar can be produced on-shell. In this situation the dominant contribution to neutrino self-interactions arises from the process

$$\nu_a \nu_a \longleftrightarrow \phi \longleftrightarrow \nu_a \nu_a, \tag{A.3.13}$$

mediated by an intermediate real ϕ. The corresponding cross section is strongly enhanced near the resonance at $s = m_\phi^2$, which we will exploit by taking it as the only contribution. To make this enhancement explicit, we start from the general expression for the s-channel contribution:

$$\sigma(\nu_a \nu_a \to \nu_a \nu_a) = \frac{\lambda_\phi^4 s}{8\pi \left[(s - m_\phi^2)^2 + m_\phi^2 \gamma_\phi^2 \right]}, \tag{A.3.14}$$

where γ_ϕ denotes the decay width of the scalar. For a scalar decaying to two neutrinos through the same Yukawa coupling, this width is given by

$$\gamma_\phi = \frac{\lambda_\phi^2 m_\phi}{8\pi}. \tag{A.3.15}$$

In the narrow-width approximation, the Breit–Wigner propagator simplifies according to

$$\frac{1}{(s - m_\phi^2)^2 + m_\phi^2 \gamma_\phi^2} \longrightarrow \frac{\pi}{m_\phi \gamma_\phi} \, \delta(s - m_\phi^2), \tag{A.3.16}$$

which can be applied to the the cross section to give

$$\sigma_{\text{NWA}}(\nu_a \nu_a \to \nu_a \nu_a) = \frac{\lambda_\phi^4 s}{8\pi} \cdot \frac{\pi}{m_\phi \gamma_\phi} \, \delta(s - m_\phi^2). \tag{A.3.17}$$

Substituting the expression for γ_ϕ, we find that the combination of factors reduces the coupling dependence to λ_ϕ^2:

$$\sigma_{\text{NWA}} = \frac{\lambda_\phi^2 s}{m_\phi^2} \, \delta(s - m_\phi^2). \tag{A.3.18}$$

The interaction rate for a neutrino of energy E scattering with a thermal background of active neutrinos is computed by integrating this cross section over the Fermi–Dirac distribution of targets:

$$\Gamma_\phi(E) = \int \frac{d^3 p_{\text{tar}}}{(2\pi)^3} f_\nu(p_{\text{tar}}) \, \sigma_{\text{NWA}}(s), \tag{A.3.19}$$

where

$$s = 2EE_{\text{tar}}(1 - \cos\theta). \tag{A.3.20}$$

Performing the phase-space integral using the delta yields a rate that scales as

$$\Gamma_\phi(E) \simeq \frac{\lambda_\phi^2 T^2}{16\pi E}\left[\frac{\pi^2}{6} + \mathrm{Li}_2(-e^\omega) + \omega \ln(1+e^\omega) - \frac{\omega^2}{2}\right], \tag{A.3.21}$$

where

$$\omega = \frac{m_\phi^2}{4ET}. \tag{A.3.22}$$

The polylogarithmic terms arise from the averaging over Fermi–Dirac distributions.

A.3.5 STERILE-STERILE INTERACTION RATES FOR VECTOR MEDIATORS

Start from the standard collision-to-rate relation (per particle with momentum p_1):

$$\Gamma(p_1) = \frac{1}{2E_1}\int d\Pi_2\, f_2(p_2)\; 4(p_1\cdot p_2)\; \sigma\big(s = (p_1+p_2)^2\big). \tag{A.3.23}$$

For massless particles $E_i = p_i$. Evaluate the phase-space measure for particle 2:

$$d\Pi_2 = \frac{d^3\mathbf{p}_2}{(2\pi)^3 2p_2} = \frac{p_2^2 dp_2\, d\cos\beta\, d\varphi}{(2\pi)^3 2p_2} = \frac{p_2\, dp_2\, d\cos\beta\, d\varphi}{2(2\pi)^3},$$

where β is the angle between $\mathbf{p}_1$ and $\mathbf{p}_2$. Insert into (A.3.23) and integrate over $\varphi \in [0, 2\pi]$:

$$\Gamma(p_1) = \frac{1}{2p_1}\int_0^\infty dp_2 \int_{-1}^{1} d\cos\beta\, \frac{p_2}{2(2\pi)^3}\,(2\pi)\, f_2(p_2)\; 4(p_1\cdot p_2)\,\sigma(s) \tag{A.3.24}$$

$$= \frac{1}{2p_1}\cdot\frac{1}{(2\pi)^2}\int_0^\infty dp_2\; p_2 f_2(p_2) \int_{-1}^{1} d\cos\beta\; 2s\,\sigma(s), \qquad s = 2p_1p_2(1-\cos\beta). \tag{A.3.25}$$

Change integration variable $\cos\beta \mapsto s$ for fixed p_1, p_2:

$$s = 2p_1p_2(1-\cos\beta), \qquad d\cos\beta = -\frac{ds}{2p_1p_2}, \quad s \in [0, 4p_1p_2].$$

Hence

$$\int_{-1}^{1} d\cos\beta\; 2s\,\sigma(s) = \int_0^{4p_1p_2} \frac{ds}{2p_1p_2}\; 2s\,\sigma(s) = \frac{1}{p_1p_2}\int_0^{4p_1p_2} ds\; s\,\sigma(s).$$

Plugging back we obtain

$$\Gamma(p_1) = \frac{1}{2p_1}\cdot\frac{1}{(2\pi)^2}\int_0^\infty dp_2\; p_2 f_2(p_2)\cdot\frac{1}{p_1p_2}\int_0^{4p_1p_2} ds\; s\,\sigma(s) \tag{A.3.26}$$

$$= \frac{1}{4(2\pi)^2 p_1^2}\int_0^\infty dp_2\, f_2(p_2)\underbrace{\int_0^{4p_1p_2} ds\; s\,\sigma(s)}_{=K(4p_1p_2)}. \tag{A.3.27}$$

Using $(2\pi)^2 = 4\pi^2$ we may rewrite

$$\boxed{\Gamma(p_1) \;=\; \frac{1}{16\pi^2\, p_1^2} \int_0^\infty dp_2\, f_2(p_2)\; K\big(4p_1p_2\big).} \tag{A.3.28}$$

B

Calculation of Scalar Mediator Collision Terms

Using our definitions for the rates and cross sections we are able to find explicit expressions for the collision terms of the integrated Boltzmann equations. Before we do so, however, we first consider the various processes to be taken into consideration. We classify our terms into two kinds: processes that transfer energy from the visible sector into the dark sector, i.e. oscillation-based production processes, and scattering processes within the dark sector.

The first class is described by a collision term C^{ν_a}, integrated over the active distribution function and proportional to the mixing angle. This term will be similar to the Dodelson–Widrow case, only now also containing oscillation through self-interactions.

The second class describes two processes: the (inverse) decay $\phi \leftrightarrow \nu_s\nu_s$, and the two-to-two scattering $\phi\phi \leftrightarrow \nu_s\nu_s$. The former can be neglected, since we approximated our dark-sector distribution functions to be in chemical equilibrium with one another, i.e. $\mu_\phi = 2\mu_s$. The latter, named $C^{\phi\phi}$ will be derived in this section.

As stated in equation 5.1.8, the starting point for the momentum-resolved collision term is given by

$$C[f_1] = \frac{1}{2E_1} \sum_{\text{processes}} \int \prod_{i=2}^{n} \frac{\mathrm{d}^3 p_i}{(2\pi)^3\, 2E_i}\, (2\pi)^4\, \delta^{(4)}\left(\sum_{\text{in}} p - \sum_{\text{out}} p\right) \left|\mathcal{M}\right|^2 \mathcal{F}[f]. \tag{B.0.1}$$

Since we will be using integrated equations, we perform the integration over $\frac{d^3p_1}{(2\pi)^3}$ to write

$$\mathcal{C}_n = \sum_{\text{processes}} \int \prod_{i=1}^{4} \mathrm{d}\Pi_i (2\pi)^4\, \delta^{(4)}\left(\sum_{\text{in}} p - \sum_{\text{out}} p\right) \left|\mathcal{M}\right|^2 \mathcal{F}[f]. \tag{B.0.2}$$

for the number density, and over $\frac{d^3p_1p_1}{(2\pi)^3}$

$$\mathcal{C}_\rho = \sum_{\text{processes}} \int \prod_{i=1}^{4} \mathrm{d}\Pi_i\, p_1\, (2\pi)^4\, \delta^{(4)}\left(\sum_{\text{in}} p - \sum_{\text{out}} p\right) \left|\mathcal{M}\right|^2 \mathcal{F}[f]. \tag{B.0.3}$$

for the energy density. Note that the integration over the various moments is due to a similar integration being performed on the left-hand side of the Botlzmann equation:

$$n = \frac{g_s}{2\pi^2} \int dp p^2 f(p), \qquad \rho = \frac{g_s}{2\pi^3} \int dp p^2 f(p). \tag{B.0.4}$$

As described in the main text, we assume Fermi-blocking to be negligible and the early universe to isotropic, such that we can integrate over the magnitude of the momentum and take $[1 \pm f] = 1$.

B.0.1 OSCILLATION-BASED PROCESSES

We can now derive all contributions from the thermal bath and sterile tree-level interaction induced production

$$\begin{aligned}
\mathcal{C}_n^{\nu_a} &= \frac{g_s}{2} \int \prod_{i=1}^{4} \mathrm{d}\Pi_i \, p_1 \, (2\pi)^4 \, \delta^{(4)}(\ldots) \, \left|\mathcal{M}_{\nu_s\nu_s\leftrightarrow\nu_s\nu_a}\right|^2 [-f_s f_s + f_s f_a] \\
&\quad + \frac{g_s}{2} \int \prod_{i=1}^{4} \mathrm{d}\Pi_i \, p_1 \, (2\pi)^4 \, \delta^{(4)}(\ldots) \, \left|\mathcal{M}_{\nu_\phi\nu_\phi\leftrightarrow\nu_s\nu_a}\right|^2 [-f_\phi f_\phi + f_s f_a] \\
&\quad + \sum_{\text{processes}} g_s \int \prod_{i=1}^{n} \mathrm{d}\Pi_i \, p_1 \, (2\pi)^4 \, \delta^{(4)}(\ldots) \, \left|\mathcal{M}_{\nu_s\nu_s\leftrightarrow\nu_s\nu_a}\right|^2 [-f_s + f_a] \cdot f_1^{\text{bath}} \cdots f_n^{\text{bath}} \\
&\simeq \frac{g_s}{2} \int \prod_{i=1}^{4} \mathrm{d}\Pi_i \, p_1 \, (2\pi)^4 \, \delta^{(4)}(\ldots) \, \left|\mathcal{M}_{\nu_s\nu_s\leftrightarrow\nu_s\nu_a}\right|^2 f_s f_a \\
&\quad + \frac{g_s}{2} \int \prod_{i=1}^{4} \mathrm{d}\Pi_i \, p_1 \, (2\pi)^4 \, \delta^{(4)}(\ldots) \, \left|\mathcal{M}_{\nu_\phi\nu_\phi\leftrightarrow\nu_s\nu_a}\right|^2 f_s f_a \\
&\quad + \frac{g_s}{2} \int \frac{d^3 p_1}{(2\pi)^3} \Gamma^{\text{bath}}_{\nu_a\to\nu_s}(p_1) f_a(p_1) \\
&= \frac{g_s}{2} \int \mathrm{d}\Pi_1 \overbrace{\int \mathrm{d}\Pi_2 \mathrm{d}\Pi_3 \mathrm{d}\Pi_4 \delta^{(4)}(\ldots) \, \left|\mathcal{M}_{\nu_s\nu_s\leftrightarrow\nu_s\nu_s}\right|^2 f_s(p_2)}^{\Gamma_{\nu_s\nu_s\to\nu_s\nu_s}} f_a(p_1) \langle P(\nu_a \to \nu_s; p)\rangle \\
&\quad + \text{“}\phi\text{”} \\
&\quad + \frac{g_s}{2} \frac{1}{2\pi^2} \int \mathrm{d}p p^2 \Gamma_a \langle P(\nu_a \to \nu_s; p)\rangle \\
&= \frac{g_s}{2} \frac{1}{(2\pi)^2} \int \mathrm{d}p \, p^2 \left(\Gamma_{2\nu_s\leftrightarrow 2\phi}(p, T_s) + \Gamma_a(p, T) + \Gamma_{2\nu_s\leftrightarrow 2\nu_s}(p, T_s) \right) \sin^2 2\vartheta_{\text{eff}} \, f_a(p, T).
\end{aligned} \tag{B.0.5}$$

For the energy equation, we similarly get

$$\mathcal{C}_\rho^{\nu_a} = \frac{g_s}{2} \frac{1}{(2\pi)^2} \int \mathrm{d}p \, p^3 \left(\Gamma_{2\nu_s\leftrightarrow 2\phi}(p, T_s) + \Gamma_a(p, T) + \Gamma_{2\nu_s\leftrightarrow 2\nu_s}(p, T_s) \right) \sin^2 2\vartheta_{\text{eff}} \, f_a(p, T). \tag{B.0.6}$$

B.0.2 Two-to-two Scattering

For the scattering process,

$$
\begin{aligned}
\mathcal{C}_n^{\phi\phi} &= -\frac{1}{2}\int \mathrm{d}\Pi_1\mathrm{d}\Pi_2\mathrm{d}\Pi_3\mathrm{d}\Pi_4(2\pi)^4\delta^{(4)}(\ldots)\left[f_sf_s|\mathcal{M}_{12\to 34}|^2 - f_\phi f_\phi|\mathcal{M}_{34\to 12}|^2\right] \\
&= -\frac{1}{2}\int \mathrm{d}\Pi_1\mathrm{d}\Pi_2\; 2s\int \mathrm{d}\Pi_3\mathrm{d}\Pi_4(2\pi)^4\delta^{(4)}(\ldots)\frac{|\mathcal{M}_{\nu_s\nu_s\leftrightarrow\phi\phi}|^2}{2s}\left[f_sf_s - f_\phi f_\phi\right] \\
&= -\int \mathrm{d}\Pi_1\mathrm{d}\Pi_2 s\;\sigma_{\nu_s\nu_s\leftrightarrow\phi\phi}(s)\left[f_sf_s - f_\phi f_\phi\right] \\
&= -\int \mathrm{d}\Pi_1\mathrm{d}\Pi_2 s\;\sigma_{\nu_s\nu_s\leftrightarrow\phi\phi}(s)f_s^{EQ}f_s^{EQ}\left[\frac{f_sf_s}{f_s^{EQ}f_s^{EQ}} - \frac{f_\phi f_\phi}{f_s^{EQ}f_s^{EQ}}\right] \\
&= -\int \mathrm{d}\Pi_1\mathrm{d}\Pi_2 s\;\sigma_{\nu_s\nu_s\leftrightarrow\phi\phi}(s)f_s^{EQ}f_s^{EQ}\left[\frac{n_s^2}{(n_s^{EQ})^2} - \frac{n_s^4}{(n_s^{EQ})^4}\right] \\
&= -n_s^2\left[1-\frac{n_s^2}{(n_s^{EQ})^2}\right]\frac{\int \mathrm{d}\Pi_1\mathrm{d}\Pi_2 s\;\sigma_{\nu_s\nu_s\leftrightarrow\phi\phi}(s)f_s^{EQ}f_s^{EQ}}{(n_s^{EQ})^2} \\
&= -n_s^2\left[1-\frac{n_s^2}{(n_s^{EQ})^2}\right]\langle\sigma v\rangle \\
\mathcal{C}_n^{\phi\phi} &= -n_s^2\left[1-\frac{n_s^2}{(n_s^{EQ})^2}\right]\frac{1}{16}\int_{z_{\min}}^{\infty} dz\; z^4K_1(z)\,\sigma_\varphi(s=z^2T^2). \qquad \text{(B.0.7)}
\end{aligned}
$$

Similarly again for the energy equation, one obtains

$$
\begin{aligned}
\mathcal{C}_n^{\phi\phi} &= -n_s^2\left[1-\frac{n_s^2}{(n_s^{EQ})^2}\right]\langle(E_1+E_2)\,\sigma v\rangle \\
&= -n_s^2\left[1-\frac{n_s^2}{(n_s^{EQ})^2}\right]\frac{T}{16}\int_{z_{\min}}^{\infty} dz\; z^5K_1(z)\,\sigma_\varphi(s=z^2T^2). \qquad \text{(B.0.8)}
\end{aligned}
$$

C

Description of Numerical Code

The numerical efforts performed in this thesis consist of evaluating the integral in equation 5.2.15 and solving the differential equations presented in section 6. We will outline the strategies used for both.

C.1 Dodelson-Widrow Integration

The numerical evaluation of the integral in equation 5.2.15 using python is a fairly straightforward task, making use of built-in functions from scipy.integrate. Despite its simplicity we show parts of the code anyway such that our values can be used to reproduce our exact findings.

First one defines the integrand and performs the integration over dimensionless variable y:

```
# Define the integrand
def integrand(y, x):
   return y**3 / ((1 + (x**2) * y**2)**2 * (np.exp(y) + 1))

# Define the full function f(x)
def f(x):
   integral, _ = quad(integrand, 0, np.inf, args=(x,), epsabs=1e-10, epsrel=1e-10)
   return x * integral
```

Next, values of y and their corresponding integrated results are tabulated.

```

# Generate 2000 logarithmically spaced x-values from 1/100 to 100
x_vals = np.logspace(-2, 2, 2000)
f_vals = np.array([f(x) for x in x_vals])
```

The resulting plot is found in 5.2.1.

The regression is then performed using the built-in function linregress from scipy.stats. The same integral as before is performed over a broader range, after which two separate fits are made for the low and high values of the logarithm of x. The resulting plot is found in 5.2.2.

```
# Generate x values and compute f(x)
x_vals = np.logspace(-4, 4, 10000)
f_vals = np.array([f(x) for x in x_vals])
```

```

# Evaluate f(x) at x = 0.19
x_peak = 0.19
f_peak = f(x_peak)


# Log-log fit in low-x range (x ~ 10^-2 to 10^-1)
mask_low = (x_vals >= 1e-4) & (x_vals <= 1e-2)
logx_low = np.log10(x_vals[mask_low])
logf_low = np.log10(f_vals[mask_low])
slope_low, intercept_low, *_ = linregress(logx_low, logf_low)
fit_low = 10**intercept_low * x_vals**slope_low

# Log-log fit in high-x range (x ~ 10^0 to 10^2)
mask_high = (x_vals >= 1e3) & (x_vals <= 1e4)
logx_high = np.log10(x_vals[mask_high])
logf_high = np.log10(f_vals[mask_high])
slope_high, intercept_high, *_ = linregress(logx_high, logf_high)
fit_high = 10**intercept_high * x_vals**slope_high
```

C.2 Solving the Scalar Mediator Differential Equations

In all of the following scenarios the system is implemented numerically following the same general strategy. The system of equations described in 6.1.19 is expressed in dimensionful variables, which is generally unfavourable for numerical applications. Additionally, the evolving variable T spans various orders of magnitude, requiring either a loss of resolution in the low temperature range or a terrible efficiency in the high temperature range. In order to solve both problems we express our system fully in terms of the logarithms of dimensionless variables. The chosen variables are

$$Y \equiv \frac{n_s}{s(T)} \tag{C.2.1}$$

$$X \equiv \frac{\rho_s}{\rho_{SM}} \tag{C.2.2}$$

$$x \equiv \frac{m}{T}, \tag{C.2.3}$$

where m is some arbitrary reference mass. Furthermore, we perform our momentum-integrals over dimensionless quantity

$$q \equiv \frac{p}{T}. \tag{C.2.4}$$

For ease in computation we will implement all terms as python functions not only in these variables, but also as functions of m_ϕ, $\sin^2 2\vartheta$ and y, the Yukawa coupling. Our system of equation then looks something like

$$\frac{\mathrm{d}\log Y}{\mathrm{d}\log x} = -\frac{m}{x}\frac{1}{Y}\frac{\mathrm{d}t}{\mathrm{d}T}\frac{1}{s}\left[\mathcal{C}_n^{\nu_a} + \mathcal{C}_n^{\phi\phi}\right], \tag{C.2.5}$$

$$\frac{\mathrm{d}\log X}{\mathrm{d}\log x} = -\frac{m}{x}\frac{1}{X}\frac{\mathrm{d}t}{\mathrm{d}T}\frac{1}{\rho_{SM}}\left[\mathcal{C}_\rho^{\nu_a} + \mathcal{C}_\rho^{\phi\phi}\right]. \tag{C.2.6}$$

The terms in front of the collision terms are all functions of T, which are easily evaluated using $T = m/x$. For the exact evolution of T throughout the early universe we use the formula obtain by **[Laine_2015]**,

$$\frac{3}{2}\sqrt{\frac{5}{\pi^3}}\frac{M_{\mathrm{Pl}}}{T^3}\frac{\mathrm{d}T}{\mathrm{d}t} = -\frac{\sqrt{g_{\mathrm{eff}}(T)}h_{\mathrm{eff}}(T)}{i_{\mathrm{eff}}(T)}, \tag{C.2.7}$$

and the tabulated values from the corresponding supplemental material.

Considering, for example, the collision term $\mathcal{C}$, we find not much trouble in turning this into an expression of our new variables. The thermally averaged cross section is already integrated over dimensionless $z = \frac{\sqrt{s}}{T}$, which will now be integrated over $z = \frac{x\sqrt{s}}{m}$. In practice, this integral will be evaluated using an interpolated function, as we will see in section C.2.2, reducing the appearance of numerical signatures. The factor n_s^2 is converted using $n_s = Ys$, leaving us only with the term $[1 - \left(\frac{n_s}{n_s^{\mathrm{eq}}}\right)^2]$. This is evaluated using

$$\frac{n_s}{n_s^{\mathrm{eq}}} = Y\frac{s}{n_s^{\mathrm{eq}}} = \frac{2}{g_s}\frac{\pi^4}{45}g_{*s}(m/x)\ Y\frac{T^3}{T_s^3}, \tag{C.2.8}$$

and using

$$\frac{T_s}{T} = \frac{X}{4Y}\frac{g_*(\frac{m}{x})}{g_{*s}(\frac{m}{x})}. \tag{C.2.9}$$

In general the process repeats itself in this way, using T_s and $e^{\frac{\mu}{T_s}} = \frac{n_s}{n_s^{eq}}$ from the formulas above to rewrite everything in new variables. One should, however, be careful of numerical instabilities arising from evaluating very small or very large numbers that are non-physical. In particular we find that the piecewise function describing sterile interaction rate,

$$\Gamma_{\nu_s\nu_s\leftrightarrow\nu_s\nu_s}(p_1) = e^{\mu/T_s} \times \begin{cases} \frac{3y^4T_s^2}{2\pi^3p_1} + \frac{y^2T_sm_\phi^2}{2\pi p_1^2}e^{-\frac{m_\phi^2}{4p_1T_s}} & p_1T_s > \frac{3m_\phi^2}{2\sqrt{10}} \\ \frac{20y^4p_1T_s^4}{3\pi^3m_\phi^4} + \frac{y^2T_sm_\phi^2}{2\pi p_1^2}e^{-\frac{m_\phi^2}{4p_1T_s}} & p_1T_s \le \frac{3m_\phi^2}{2\sqrt{10}} \end{cases}, \tag{C.2.10}$$

introduces instabilities due to its factors of T_s which induce large powers of $\frac{(X)^n}{(Y)^m}$ which are later cancelled by inverse powers coming from $e^{\frac{\mu}{T_s}}$. We therefore opt to rewrite

$$\begin{split}\Gamma_{\nu_s\nu_s\leftrightarrow\nu_s\nu_s}(X, Y, q, x) = \frac{\pi^4}{90}\times \\ \begin{cases} \frac{3y^4}{2\pi^3}\frac{(4Yg_{*s})^2}{(Xg_*)}\frac{m}{qx} + \frac{y^2m_\phi^2}{2\pi}\frac{(4Yg_{*s})^3}{(Xg_*)^2}\frac{x}{q^2m}\exp[-\frac{m_\phi^2x^2}{4m^2q}\frac{(4Yg_{*s})}{(Xg_*)}] & \frac{qm^2}{x^2}\frac{X}{4Y}\frac{g_*}{g_{*s}} > \frac{3m_\phi^2}{2\sqrt{10}} \\ \frac{20y^4}{3\pi^3m_\phi^4}(Xg_*)q\left(\frac{m}{x}\right)^5 + \frac{y^2m_\phi^2}{2\pi}\frac{(4Yg_{*s})^3}{(Xg_*)^2}\frac{x}{q^2m}\exp[-\frac{m_\phi^2x^2}{4m^2q}\frac{(4Yg_{*s})}{(Xg_*)}] & \frac{qm^2}{x^2}\frac{X}{4Y}\frac{g_*}{g_{*s}} \le \frac{3m_\phi^2}{2\sqrt{10}}. \end{cases}\end{split} \tag{C.2.11}$$

Besides these peculiarities the implementation into python is straightforward, and only requires the standard diligence. The potentials are dealt with somewhat more easily, as the sterile potential depends only on one argument and is numerically computed individually, and the active potential is a simple function of p and T. We will now turn to the code.

C.2.1 Light Mediator Limit

We will not present the entire code, as it would be too lengthy, but we will provide the general structure and the central function that solves the differential equation. The code below is valid for both light and intermediate mass ranges of the mediating scalar, only one should take the appropriate initial conditions. In the intermediate mass case, the initial conditions are taken to be extremely low but non-zero, say 10^{-25}, in order to prevent numerical distortions. The overall division is as follows:

1. Import modules
2. Define constants
3. Define distribution functions
4. Define the functions for interactions rates and potentials
5. Build the collision integrals
6. Build the full system of equations
7. Solve the system
8. Cache and plot results.

Using the earlier mentioned rate

```python
   def piecewise_rate_term(X, Y, x, mref, mphi, q):

   x_term = X * dof(mref/x)
   y_term = 4*Y * dofs(mref/x)

   treshold = 3 * mphi**2 / ( 2 * np.sqrt(10))
   query = q * mref**2/x**2 * x_term/y_term

   a = 3 * y**4 /(2* np.pi**3)
   b = 20*y**4/(3*np.pi**3 * mphi**4)
   c = y**2 * mphi**2 / (2* np.pi)

   resonance = c * y_term**3/x_term**2 * x/(q**2 * mref) * np.exp(-mphi**2 * x**2 *
       y_term /(4*mref**2 * q * x_term))

   if query > treshold:
      return a * y_term**2 / x_term * mref/(q*x) + resonance
   else:
      return b * x_term * q * (mref/x)**5 + resonance
```

we define the component of the collision term proportional to the sterile rate,

```python
def sterile_integral_Y(X, Y, x, mref, mphi):

   def sterile_integrand_Y(X, Y, x, mref, mphi, q):

      numerator = q**2 * fa(q) * piecewise_rate_term(X, Y, x, mref, mphi, q) * delta(
          mphi, x, q)
      denominator = full_rate(X, Y, x, mref, mphi, q)**2/4 + (delta(mphi, x, q) -
          pot_active(x, mref, q) + pot_sterile(q*x/mref))

      return

   integral , _ = quad(lambda q: sterile_integrand_Y(X, Y, x, mref, mphi, q), 0, 30)

   return integral
```

and similarly for the energy density collision term, only with an extra factor of q. Note that the integration over q is only performed up to $p = 30T$. Using these building blocks, we are able to define the full equations

```
def dlogYdlogx(X, Y, x, mref, mphi):

   first_numerical_factor = 3/2 * Mpl/1.66 * 45/(np.pi * (2*np.pi)**3) * gspinNu/2 *
       sint**2 * .92 * fermiC**2
   first_dof_term = np.sqrt(dof(mref/x))/i_eff(mref/x)
   first_normalization = 1/Y * mref**3/x**3
   first_integral = integral_active_Y

   first_term = first_numerical_factor * first_dof_term * first_normalization *
       first_integral



   second_numerical_factor = 3/2 * 1/16 * Mpl/1.66 * gspinNu/2 * sint**2
   second_dof_term = np.sqrt(dof(mref/x))/i_eff(mref/x)
   second_normalization = 1/Y * x**2/mref**2
   second_integral = sterile_integral_Y(X, Y, x, mref, mphi)

   second_term = second_numerical_factor * second_dof_term * second_normalization *
       second_integral



   return second_term

def dlogXdlogx(X, Y, x, mref, mphi):

   first_numerical_factor = 9/2 * Mpl/1.66 * 45/(np.pi * (2*np.pi)**3) * gspinNu/2 *
       sint**2 * .92 * fermiC**2
   first_dof_term = dofs(mref/x)/(i_eff(mref/x)*np.sqrt(dof(mref/x)))
   first_normalization = 1/X * mref**3/x**3
   first_integral = integral_active_X

   first_term = first_numerical_factor * first_dof_term * first_normalization *
       first_integral



   second_numerical_factor = 9/2 * 1/16 * Mpl/1.66 * gspinNu/2 * sint**2
   second_dof_term = dofs(mref/x)/(i_eff(mref/x)*np.sqrt(dof(mref/x)))
   second_normalization = 1/X * x**2/mref**2
   second_integral = sterile_integral_X(X, Y, x, mref, mphi)
   second_term = second_numerical_factor * second_dof_term * second_normalization *
       second_integral


   return second_term
```

These can now be solved using the built-in *solve_ivp* function from *scipy.integrate*,

```
   # ---- system for solve_ivp ----
def rhs(logx, vars, mref, mphi):
   X, Y = vars
   x = np.exp(logx) # we evolve in log(x) for stability
   dY = dlogYdlogx(X, Y, x, mref, mphi)
   dX = dlogXdlogx(X, Y, x, mref, mphi)
   return [dX, dY]

# ---- values and initial conditions ----
mref = 1e-3
mphi = 1.5e-4
T0 = 0.1
x0 = mref/T0
logx0 = np.log(x0)

# compute Y0, X0 from your collision integrals
Y0 = collision_integral_DW_n(T0)
X0 = collision_integral_DW_E(T0)
y0 = [X0, Y0]

# ---- integration range ----
logx_span = (logx0, np.log(1e2)) # evolve up to T=1e-5

sol = solve_ivp(rhs, logx_span, y0, args=(mref, mphi),
           method="Radau", rtol=1e-8, atol=1e-12, max_step=0.01)
```

Since the system is quite stiff, it is recommended to use either *Radau* of *BDF* as a solving method.

C.2.2 INCLUDING NUMBER CHANGING PROCESSES

The integrals over the cross sections involving logarithms are a frequent source of numerical instability around the lower integration bounds. We therefore decide to interpolate the results and use that in the final system of equations,

```
   z_upper=np.inf

   scalarT = np.atleast_1d(T).astype(float)
   out = np.zeros_like(scalarT)

   for i, Ti in enumerate(scalarT):
      zmin = 2.0 * MS / Ti
      if zmin >= z_upper:
         out[i] = 0.0
         continue

      def integrand(z):
         s = (z * Ti)**2
         return z**4 * k1(z) * sigma_phi(s, MS)

      val, err = quad(integrand, zmin, z_upper, limit=200)
      out[i] = 0.0625 * val # 1/16 * integral

   return out if out.size > 1 else float(out)

def make_thermal_interpolators(mphi, T_min=1e-6, T_max=1e3, n_points=300):
   z_upper = 200.0
   T_grid = np.logspace(np.log10(T_min), np.log10(T_max), n_points)

   sigma_v_vals = np.zeros_like(T_grid)
   sigma_vE_vals = np.zeros_like(T_grid)

   for i, Ti in enumerate(T_grid):
      zmin = 2.0 * mphi / Ti
      if zmin < z_upper:
         # σ< v>
         def integrand_sigma(z):
            s = (z * Ti)**2
            return z**4 * k1(z) * sigma_phi(s, mphi)
         val_sigma, _ = quad(integrand_sigma, zmin, z_upper, limit=200)
         sigma_v_vals[i] = 0.0625 * val_sigma # 1/16 factor

         # <(E1+E2) σv>
         def integrand_sigmaE(z):
            s = (z * Ti)**2
            return z**5 * k1(z) * sigma_phi(s, mphi)
         val_sigmaE, _ = quad(integrand_sigmaE, zmin, z_upper, limit=200)
         sigma_vE_vals[i] = (Ti / 16.0) * val_sigmaE

      # If zmin >= z_upper, both are 0 (already inited as zeros)

   # Make log-log interpolators for stability
   sigma_v_interp = interp1d(
      np.log(T_grid), np.log(sigma_v_vals + 1e-300),
      kind='linear', bounds_error=False, fill_value=-np.inf
   )
   sigma_vE_interp = interp1d(
      np.log(T_grid), np.log(sigma_vE_vals + 1e-300),
      kind='linear', bounds_error=False, fill_value=-np.inf
   )

   # Return callable functions that take T and return the interpolated values
   def sigma_v_func(T):
      return np.exp(sigma_v_interp(np.log(T)))
   def sigma_vE_func(T):
      return np.exp(sigma_vE_interp(np.log(T)))

   return sigma_v_func, sigma_vE_func
```

Solving the code looks no different from before, only with the additional term on the right hand side.

C.2.3 Scanning the Parameter Space

Once the initial value problem solver function is defined the parameter space sweep in the two limits is becomes mostly a matter of patience, as the numerical integration is to be performed some thousand times. This has been performed for the scalar mediator. Since this produces perhaps the most important plot of this thesis, we describe and present the full code and strategy.

There are four variables which are relevant, $\sin^2 2\vartheta$, the coupling y, m_s and m_ϕ. In order to reduce the number of variables to 3, such that a 2D pot of solutions can be made, one has two “easy”options: either we set the mediator mass to a constant, or we set the mediator mass to a multiple of m_s. In order to stay in the regime of massless sterile neutrinos, it is favoured to take m_ϕ as a multiple of m_s so that we can sweep m_s over a larger range. We then make a list of $y-$values for which we solve the function in order to generate the contour plot, and then we are ready to sweep. In practice, we define a wrapper function for the solver, and set up a grid for m_s and $\sin^2 2\vartheta$.

```
def run_solver(sint, MS, msterile, y, x_init, x_final, X_init=1.0, Y_init=1e-20):

   def rhs(logx, vars, sint, MS, msterile, y):
      X, Y = vars
      x = np.exp(logx) # we evolve in log(x) for stability
      dX = dlogXdlogx(X, Y, x, sint, MS, msterile, y)
      dY = dlogYdlogx(X, Y, x, sint, MS, msterile, y)
      return [dX, dY]

   # Initial conditions in log-space
   logx_span = [np.log(x_init), np.log(x_final)]
   y0 = [np.log(X_init), np.log(Y_init)]

   # Solve IVP
   sol = solve_ivp(rhs, logx_span, y0, args=(sint, MS, msterile, y),
               dense_output=True, rtol=1e-6, atol=1e-9)

   x_vals = np.exp(sol.t)
   X_vals = np.exp(sol.y[0])
   Y_vals = np.exp(sol.y[1])

   return x_vals, X_vals, Y_vals

msterile_grid = np.logspace(np.log10(2e-3), np.log10(5e-2), 100) # [GeV]
sint_grid = np.logspace(-15, -10, 100) # sin^2 θ
y_grid = np.logspace(-7, -2, 6) # Yukawa couplings
```

We then define a target for the yield, such that we wind the correct energy density. Also, we want to find the temperature at which production ceases for the computation of the Lyman-α bounds. For this we define a function that returns that temperature of the yield Y_T that is the last yield value such that $|Y_T - Y_{\mathrm{final}}| > \Delta Y$, which we can set for precision.

```
def Y_target(msterile):
   """
   Compute the target yield for given sterile mass [GeV]:
   Y = (Omega_DM * rho_crit/h^2) / (m * s_today)
   """
   return (Omega_DM_h2 * rho_crit_h2) / (msterile * s_entropy_today)

# Freeze-in deviation threshold
delta_Y_fraction = 1e-10 # extremely strict stabilization criterion

def find_freeze_in(x_vals, Y_vals, X_vals, delta_frac=1e-2):
   Y_final = Y_vals[-1]
   deviation = np.abs(Y_vals - Y_final)
   mask = deviation > delta_frac * Y_final

   if not np.any(mask):
      return x_vals[-1], X_vals[-1] # fully stabilized from the start

   idx = np.where(mask)[0][-1] # last val above threshold
   return x_vals[idx], X_vals[idx]
```

We are now ready to create a for-loop running over our grid.

```
outfile = "parameter_scan.csv"
with open(outfile, "w", newline="") as f:
   writer = csv.writer(f)
   writer.writerow(["msterile[GeV]", "MS[GeV]", "sin^2(theta)", "y",
             "Y_final", "Y_target", "x_d(GeV)", "X_d"])

for msterile in msterile_grid:
   MS = 10.0 * msterile
   Y_ref = Y_target(msterile)
   for sint in sint_grid:
      for y in y_grid:
         try:
            # Solve system
            x_vals, X_vals, Y_vals = run_solver(sint, MS, msterile, y,
                                   x_init=100.0, x_final=0.01)

            Y_final = Y_vals[-1]

            # Skip unphysical or failed runs
            if np.isnan(Y_final) or Y_final < 1e-30:
               continue

            # Freeze-in point
            x_d, X_d = find_freeze_in(x_vals, Y_vals, X_vals,
                                    delta_frac=delta_Y_fraction)

            # Log results
            with open(outfile, "a", newline="") as f:
                writer = csv.writer(f)
                writer.writerow([msterile, MS, sint, y,
                                 Y_final, Y_ref, x_d, X_d])

        except RuntimeError:
            continue
```

Note that the output produces, aside from the parameters required to produce the general plot, also the temperature x_d and the energy density X_D at the production halt. Y_d is taken as $Y_{\rm final}$. This allows us to produce the conditions for Lyman-α bounds through equation 6.1.30.

C.3 SOLVING THE VECTOR MEDIATOR DIFFERENTIAL EQUATIONS

We provide a similar outline of the strategy and code used to evaluate the yield evolution from the scenario presented in equation 6.3.23. First we discuss the manipulation of the integrals.

C.3.1 VARIABLE REDEFINITIONS

We consider a process $1 + 2 \to 3 + 4$ with massless particles and the following definitions for distribution functions and cosmological functions:

- The kernel
  $$K(z) \equiv \int_0^z ds\, s\, \sigma(s) \qquad (z \geq 0),$$
  which frequently appears after the angular integration.

- Distributions:
  $$f_a(p_1) = \frac{1}{e^{p_1/T} + 1} \qquad \text{(Fermi–Dirac for species } a\text{)},$$
  and the target (species 2) taken Maxwell–Boltzmann (MB) at temperature T_s with chemical potential μ:
  $$f_2(p_2) = e^{\mu/T_s}\, e^{-p_2/T_s}.$$

- The SM thermodynamic quantities:
  $$\rho_{\rm SM} = \frac{\pi^2}{30} g_*(T)\, T^4, \qquad s_{\rm SM} = \frac{2\pi^2}{45} g_{*s}(T)\, T^3.$$

- The new-sector parameters:
  $$X \equiv \frac{\rho_s}{\rho_{\rm SM}}, \qquad Y \equiv \frac{n_s}{s_{\rm SM}}.$$
  We will also use $x \equiv m/T$ and $x_s \equiv m/T_s$ where m is a convenient mass scale for nondimensionalisation.

The production rate density (per physical volume) from integrating over the p_1 population with degeneracy g_s and mixing suppression $\sin^2 2\vartheta$ is

$$R \equiv s_{\rm SM} \ \ \dot{Y} = \frac{g_s \sin^2 2\vartheta}{4} \int \frac{d^3\mathbf{p}_1}{(2\pi)^3} f_a(p_1)\ \Gamma(p_1).$$

Inserting (A.3.28) and using $d^3\mathbf{p}_1 = 4\pi p_1^2 dp_1$ gives

$$R = \frac{g_s \sin^2 2\vartheta}{4} \int \frac{4\pi p_1^2 dp_1}{(2\pi)^3} f_a(p_1)\ \frac{1}{16\pi^2 p_1^2} \int_0^\infty dp_2 f_2(p_2)\, K(4p_1p_2) \tag{C.3.1}$$

$$= \frac{g_s \sin^2 2\vartheta}{4} \cdot \frac{4\pi}{(2\pi)^3} \cdot \frac{1}{16\pi^2} \int_0^\infty dp_1 f_a(p_1) \int_0^\infty dp_2 f_2(p_2)\, K(4p_1p_2). \tag{C.3.2}$$

We then collect numerical factors $\frac{g_s \sin^2 2\vartheta}{4} \cdot \frac{4\pi}{(2\pi)^3} \cdot \frac{1}{16\pi^2} = \frac{g_s \sin^2 2\vartheta}{128\pi^4}$, so that

$$R = \frac{g_s \sin^2 2\vartheta}{128\pi^4} \int_0^\infty dp_1 f_a(p_1) \int_0^\infty dp_2 f_2(p_2)\ K(4p_1p_2). \tag{C.3.3}$$

Now we move to the dimensionless set of variables

$$y \equiv \frac{p_1}{T}, \qquad y_s \equiv \frac{p_2}{T_s}.$$

Then $dp_1 = T dy,\ dp_2 = T_s\, dy_s, f_a(p_1) = \frac{1}{e^y+1}, f_2(p_2) = e^{\mu/T_s} e^{-y_s}$. Therefore

$$R = \frac{g_s \sin^2 2\vartheta}{128\pi^4}\ TT_s\ e^{\mu/T_s} \int_0^\infty \frac{dy}{e^y+1} \int_0^\infty dy_s\, e^{-y_s}\ K\big(4TT_s\, y\, y_s\big). \tag{C.3.4}$$

Next we aim to express T_s and e^{μ/T_s} in terms of X, Y, where we use the relations

$$\rho_{\rm s} = X\rho_{\rm SM}(T), \qquad n_{\rm s} = Y s_{\rm SM}(T).$$

Assuming the new-sector particles are massless MB with $\rho_{\rm new}/n_{\rm new} = 3T_s$ (MB relation), we have

$$3T_s = \frac{\rho_{\rm new}}{n_{\rm new}} = \frac{X\rho_{\rm SM}}{Y s_{\rm SM}} = \frac{X}{Y} \cdot \frac{\frac{\pi^2}{30} g_*(T) T^4}{\frac{2\pi^2}{45} g_{*s}(T) T^3} = \frac{X}{Y} \cdot \frac{3}{4} \cdot \frac{g_*(T)}{g_{*s}(T)}\, T.$$

Hence

$$\boxed{T_s \ = \ \frac{X}{4Y} \frac{g_*(T)}{g_{*s}(T)}\, T} \tag{C.3.5}$$

and therefore

$$x_s \equiv \frac{m}{T_s} \ = \ x \cdot \frac{Y}{X}\, 4\frac{g_{*s}}{g_*}, \qquad (x \equiv m/T). \tag{C.3.6}$$

Next, we express the MB fugacity factor e^{μ/T_s} in terms of X and Y. The MB equilibrium number density at temperature T_s is (massless)

$$n_{\rm eq}(T_s) = \frac{g_2}{\pi^2} T_s^3.$$

Since the actual number density is $n_{\text{new}} = Y s_{\text{SM}}(T)$, we have

$$e^{\mu/T_s} = \frac{n_{\text{new}}}{n_{\text{eq}}(T_s)} = \frac{Y s_{\text{SM}}(T)}{(g_2/\pi^2)T_s^3} = Y\frac{(2\pi^2/45)g_{*s}T^3}{(g_2/\pi^2)T_s^3}.$$

Using T/T_s from (C.3.5) and simplifying gives

$$\boxed{e^{\mu/T_s} = \frac{128\pi^4}{45}\,\frac{g_{*s}^4}{g_2 g_*^3}\,\frac{Y^4}{X^3}\;.} \tag{C.3.7}$$

(One may check the powers: $T/T_s \sim (4Y/X)(g_{*s}/g_*)$, cubing yields $(4^3)(Y^3/X^3)(g_{*s}^3/g_*^3)$ and with the prefactors the numerical factor is $(2\pi^2/45)\pi^2 4^3 = 128\pi^4/45$.)

We are now ready to combine everything to set up the full system of equation in our new variables, which will be done in log-space for general internal degrees of freedom g_2, g_s. We have

$$\frac{d\ln Y}{dt} = \frac{R}{s_{\text{SM}}Y}.$$

Insert expression (C.3.4) for R, the SM entropy $s_{\text{SM}} = (2\pi^2/45)g_{*s}T^3$, and the fugacity (C.3.7). After algebraic simplification (collecting numerical constants carefully), one obtains

$$\frac{d\ln Y}{dt} = \frac{g_s\,\sin^2 2\vartheta}{8\pi^2}\,\frac{g_{*s}^2}{g_2 g_*^2}\,\frac{Y^2}{X^2}\,\frac{x}{m}\int_0^\infty \frac{dy}{e^y+1}\int_0^\infty dy_s\,e^{-y_s}\,K\!\left(\frac{m^2 y y_s}{x^2}\,\frac{X}{Y}\,\frac{g_*}{g_{*s}}\right). \tag{C.3.8}$$

Since for us both distribution functions describe Majorana particle populations, we can set

$$g_2 = g_s.$$

Then the explicit degeneracy factor g_s/g_2 cancels, and (C.3.8) becomes:

$$\boxed{\frac{d\ln Y}{dt} = \frac{\sin^2 2\vartheta}{8\pi^2}\left(\frac{g_{*s}}{g_*}\right)^2\frac{Y^2}{X^2}\,\frac{x}{m}\int_0^\infty \frac{dy}{e^y+1}\int_0^\infty dy_s\,e^{-y_s}\,K\!\left(\frac{m^2 y y_s}{x^2}\,\frac{X}{Y}\,\frac{g_*}{g_{*s}}\right)} \tag{C.3.9}$$

This is almost the compact form we use for numerics, only lacking the evolved variable to be converted to $\log x.x \equiv m/T$ satisfies

$$\frac{d\ln x}{dt} = \frac{d}{dt}(\ln m - \ln T) = -\frac{d\ln T}{dt}.$$

During radiation domination (and adiabatic expansion) one has $T \propto 1/a$ so $d\ln T/dt = -H$, thus

$$\frac{d\ln x}{dt} = H$$

and therefore

$$\boxed{\frac{d\ln Y}{d\ln x} = \frac{1}{H}\,\frac{d\ln Y}{dt}.} \tag{C.3.10}$$

The energy equation is derived similarly, yielding

$$\boxed{\frac{d\log X}{d\log x} = \frac{\sin^2 2\vartheta}{6\pi^2}\frac{M_{\rm Pl}}{1.66}\frac{1}{\sqrt{g_*}}\left(\frac{g_{*s}}{g_*}\frac{Y}{X}\right)^3\frac{x^3}{m^3}\int_0^\infty\frac{dy\,y}{e^y+1}\int_0^\infty dy_s\,e^{-y_s}\,K\!\left(\frac{m^2\,y\,y_s}{x^2}\frac{X}{Y}\frac{g_*}{g_{*s}}\right)}, \qquad (C.3.11)$$

where the factor $\frac{1}{H}$ is included.

C.3.2 CODING CONSIDERATIONS

Solving the integrals and system of equations is done in exactly the same manner as in the case of the scalar mediator. The only non-triviality that changes in this system is the modification of the piecewise rate into the numerical integral over the kernel. In order to prevent radical computation times, we precompute and interpolate the integrals for several values for the coupling strength g_V and the mass m_V. This is displayed below.

```
def sigma(s, g, M, Gamma):
   """Cross section σ(s) for given s (scalar)."""
   if s <= 0:
      return 0.0

   num_common = (M**6 * (4*s - 2*Gamma**2)
              + 3*M**4 * s * (s - Gamma**2)
              - 6*M**2 * s**3 - s**4)
   num3 = (6*M**6 * (Gamma**2 - 2*s)
         + M**4 * s * (9*Gamma**2 + s)
         + M**2 * s**2 * (6*Gamma**2 + 7*s)
         + 6*s**4)

   term1 = -6*np.log(M**2) * num_common / (2*M**2 + s)
   term2 = 6*np.log(M**2 + s) * num_common / (2*M**2 + s)
   term3 = s * num3 / (M**2 * (M**2 + s))

   numerator = g**4 * (term1 + term2 + term3)
   denominator = (24*np.pi * s**2
               * (M**4 + M**2*(Gamma**2 - 2*s) + s**2))
   return numerator / denominator

def compute_J_grid(g, M, u_grid, u_cutoff=1e-12):
   """Compute J(u) for given g and u grid with cutoff at small u."""
   Gamma = g**2 / (8 * np.pi * M)
   J_vals = []

   for u in u_grid:
      if u < u_cutoff:
         J_vals.append(1e-40) # or small constant if preferred
      else:
         res, _ = integrate.quad(lambda s: s * sigma(s, g, M, Gamma),
                           0, u, limit=200)
         J_vals.append(res)
```

```
    return np.array(J_vals)

def precompute_J_list(u_min=1e-20, u_max=1e10, num_points=1000, plot=False, u_cutoff=1e
    -12):
    """
    Precompute J(u) for all g in g_list with cutoff for small u.
    Returns: list of interp1d objects (log-log interpolation).
    """
    u_grid = np.logspace(np.log10(u_min), np.log10(u_max), num_points)
    interpolators = []

    for g in g_list:
        J_vals = compute_J_grid(g, mV, u_grid, u_cutoff=u_cutoff)

        # Optional: enforce monotonic growth for stability
        J_vals = np.maximum.accumulate(J_vals)

        interp_func = interp1d(u_grid, J_vals, kind='linear',
                                bounds_error=False,
                                fill_value=(J_vals[0], J_vals[-1]))
        interpolators.append(interp_func)

    return interpolators
```

This function can then be imported and called in the main system.

Bibliography

[Bec96] Henri Becquerel. “Sur les radiations émises par phosphorescence; Sur les radiations invisibles émises par les corps phosphorescents”. In: *Comptes Rendus de l’Académie des Sciences* 122 (1896). (24 février 1896), p. 420.

[CC98] Pierre Curie and Marie Curie. “Sur une substance nouvelle radio-active, contenue dans la pechblende”. In: *Comptes Rendus de l’Académie des Sciences* 127 (1898), pp. 175–178.

[Rut99] Ernest Rutherford. “Uranium radiation and the electrical conduction produced by it”. In: *Philosophical Magazine* 47.284 (1899), pp. 109–163.

[Vil00] Paul Villard. “Sur la réflexion et la réfraction des rayons cathodiques et des rayons déviables du radium”. In: *Comptes Rendus de l’Académie des Sciences* 130 (1900), pp. 1010–1012.

[CC02] Pierre Curie and Marie Curie. “Sur la charge électrique des particules émises par les substances radioactives”. In: *Comptes Rendus de l’Académie des Sciences* 134 (1902), pp. 85–87.

[EW27] C. D. Ellis and W. A. Wooster. “The Average Energy of Disintegration of Radium E”. In: *Proceedings of the Royal Society A* 117 (1927), pp. 109–123.

[Pau30] Wolfgang Pauli. *Letter to the Tübingen conference*. Unpublished letter proposing the neutrino, December 4, 1930. 1930.

[Per33] Jean Perrin. “La spectroscopie des électrons de désintégration”. In: *Annales de Physique* 10 (1933), pp. 401–419.

[Zwi33] F. Zwicky. “Die Rotverschiebung von extragalaktischen Nebeln”. In: *Helv. Phys. Acta* 6 (1933), pp. 110–127.

[BP34] Hans Bethe and Rudolf Peierls. “The Neutrino”. In: *Nature* 133 (1934), p. 532. DOI: 10.1038/133532a0.

[Fer34a] Enrico Fermi. “Tentativo di una teoria dell’emissione dei raggi beta”. In: *Il Nuovo Cimento* 11.1 (1934), pp. 1–19.

[Fer34b] Enrico Fermi. “Versuch einer Theorie der β-Strahlen. I”. In: *Zeitschrift für Physik* 88 (1934), pp. 161–177. DOI: 10.1007/BF01351864.

[Pau34] Wolfgang Pauli. “Discussion du Rapport de M. Heisenberg”. French. In: *Structures et propriétés des noyaux atomiques. Rapports et discussions du septième Conseil de Physique tenu à Bruxelles du 22 au 29 octobre 1933*. Institut International de Physique Solvay. Paris: Gauthier-Villars, 1934, pp. 324–325, 214–215.

[Zwi37] F. Zwicky. “On the Masses of Nebulae and of Clusters of Nebulae”. In: *Astrophys. J.* 86 (1937), p. 217. DOI: 10.1086/143864.

[Pon46] Bruno Pontecorvo. “Inverse beta processes and nonconservation of lepton charge”. In: *Chalk River Report PD-205 (unpublished)* (1946). Reprinted in J. Phys. Conf. Ser. 335 (2011) 012052.

[ABG48] R.A. Alpher, H. Bethe, and G. Gamow. “The Origin of Chemical Elements”. In: *Phys. Rev.* 73 (1948), pp. 803–804. DOI: 10.1103/PhysRev.73.803.

[GP55] M. Gell-Mann and A. Pais. “Behavior of neutral particles under charge conjugation”. In: *Phys. Rev.* 97 (1955), pp. 1387–1389.

[Cow+56] C. L. Cowan et al. “Detection of the Free Neutrino: A Confirmation”. In: *Science* 124 (1956), pp. 103–104. DOI: `10.1126/science.124.3212.103`.

[LY56] T.D. Lee and C.N. Yang. “Question of Parity Conservation in Weak Interactions”. In: *Phys. Rev.* 104 (1956), pp. 254–258. DOI: `10.1103/PhysRev.104.254`.

[LY57] T.D. Lee and C.N. Yang. “Parity Nonconservation and a Two-Component Theory of the Neutrino”. In: *Phys. Rev.* 105 (1957), pp. 1671–1675. DOI: `10.1103/PhysRev.105.1671`.

[MS57] R. E. Marshak and E. C. G. Sudarshan. “The Structure of Weak Interactions”. In: *Proc. Padua Conf.* (1957).

[Pon57a] Bruno Pontecorvo. “Inverse beta processes and nonconservation of lepton charge”. In: *Zh. Eksp. Teor. Fiz.* 33 (1957), p. 549.

[Pon57b] Bruno Pontecorvo. “Mesonium and anti-mesonium”. In: *Sov. Phys. JETP* 6 (1957), p. 429.

[Wu+57] C.S. Wu et al. “Experimental Test of Parity Conservation in Beta Decay”. In: *Phys. Rev.* 105 (1957), pp. 1413–1415. DOI: `10.1103/PhysRev.105.1413`.

[FG58] R. P. Feynman and M. Gell-Mann. “Theory of Fermi interaction”. In: *Phys. Rev.* 109 (1958), pp. 193–198.

[GGS58] M. Goldhaber, L. Grodzins, and A.W. Sunyar. “Helicity of Neutrinos”. In: *Phys. Rev.* 109 (1958), pp. 1015–1017. DOI: `10.1103/PhysRev.109.1015`.

[Pon59] B. Pontecorvo. “Neutrino Experiments and the Problem of Conservation of Leptonic Charge”. In: *Sov. Phys. JETP* 9 (1959), pp. 1148–1150.

[Sch60] M. Schwartz. “Feasibility of Using High Energy Neutrinos to Study the Weak Interactions”. In: *Phys. Rev. Lett.* 4 (1960), pp. 306–307. DOI: `10.1103/PhysRevLett.4.306`.

[Gla61] S. L. Glashow. “Partial-symmetries of weak interactions”. In: *Nucl. Phys.* 22 (1961), pp. 579–588.

[Dan+62] G. Danby et al. “Observation of High-Energy Neutrino Reactions and the Existence of Two Kinds of Neutrinos”. In: *Phys. Rev. Lett.* 9 (1962), pp. 36–44. DOI: `10.1103/PhysRevLett.9.36`.

[MNS62] Ziro Maki, Masami Nakagawa, and Shoichi Sakata. “Remarks on the Unified Model of Elementary Particles”. In: *Prog. Theor. Phys.* 28 (1962), pp. 870–880.

[Bah+63] J.N. Bahcall et al. “Solar neutrino flux”. In: *Astrophys. J.* 137 (1963), pp. 344–346. DOI: `10.1086/147513`.

[EB64] François Englert and Robert Brout. “Broken Symmetry and the Mass of Gauge Vector Mesons”. In: *Phys. Rev. Lett.* 13 (1964), pp. 321–323.

[GHK64] Gerald S. Guralnik, C. R. Hagen, and T. W. B. Kibble. “Global Conservation Laws and Massless Particles”. In: *Phys. Rev. Lett.* 13 (1964), pp. 585–587.

[Hig64a] Peter W. Higgs. “Broken symmetries and the masses of gauge bosons”. In: *Phys. Rev. Lett.* 13 (1964), pp. 508–509.

[Hig64b] Peter W. Higgs. “Broken symmetries, massless particles and gauge fields”. In: *Phys. Lett.* 12 (1964), pp. 132–133.

[Fel+66] J.E. Felten et al. “Cosmology from X-ray Astronomy”. In: *Astrophys. J.* 146 (1966), p. 955. DOI: `10.1086/148972`.

[Hig66] Peter W. Higgs. "Spontaneous symmetry breakdown without massless bosons". In: *Phys. Rev.* 145 (1966), pp. 1156–1163.

[Sak67] A.D. Sakharov. "Violation of CP Invariance, C Asymmetry, and Baryon Asymmetry of the Universe". Russian. In: *Pisma Zh. Eksp. Teor. Fiz.* 5 (1967). [JETP Lett. 5 (1967) 24–27], pp. 32–35. URL: `https://inspirehep.net/literature/51139`.

[Wei67] S. Weinberg. "A Model of Leptons". In: *Phys. Rev. Lett.* 19 (1967), pp. 1264–1266.

[Pon68a] B. Pontecorvo. "Neutrino experiments and the problem of conservation of leptonic charge". In: *Sov. Phys. JETP* 26 (1968), pp. 984–988.

[Pon68b] Bruno Pontecorvo. "Neutrino Experiments and the Problem of Conservation of Leptonic Charge". In: *Sov. Phys. JETP* 26 (1968), pp. 984–988.

[GP69a] V. N. Gribov and B. Pontecorvo. "Neutrino astronomy and lepton charge". In: *Phys. Lett. B* 28 (1969), pp. 493–496.

[GP69b] V. N. Gribov and B. Pontecorvo. "Neutrino astronomy and lepton charge". In: *Phys. Lett. B* 28 (1969), pp. 493–496.

[GIM70] S. L. Glashow, J. Iliopoulos, and L. Maiani. "Weak Interactions with Lepton-Hadron Symmetry". In: *Phys. Rev. D* 2 (7 Oct. 1970), pp. 1285–1292. DOI: `10.1103/PhysRevD.2.1285`. URL: `https://link.aps.org/doi/10.1103/PhysRevD.2.1285`.

[RF70] V.C. Rubin and W.K. Ford. "Rotation of the Andromeda Nebula from a Spectroscopic Survey of Emission Regions". In: *Astrophys. J.* 159 (1970), p. 379. DOI: `10.1086/150317`.

[t H71] Gerard 't Hooft. "Renormalizable Lagrangians for massive Yang-Mills fields". In: *Nucl. Phys. B* 35 (1971), pp. 167–188.

[tV72] Gerard 't Hooft and M. J. G. Veltman. "Regularization and Renormalization of Gauge Fields". In: *Nucl. Phys. B* 44 (1972), pp. 189–213.

[Has+73a] F. J. Hasert et al. "Observation of neutrino-like interactions without muon or electron in the Gargamelle neutrino experiment". In: *Phys. Lett. B* 46 (1973), pp. 138–140.

[Has+73b] F. J. Hasert et al. "Search for elastic muon-neutrino electron scattering". In: *Phys. Lett. B* 47 (1973), pp. 469–472.

[Has73a] F. J. et al. Hasert. "Observation of neutrino-like interactions without muon or electron in the Gargamelle neutrino experiment". In: *Phys. Lett. B* 46 (1973), pp. 138–140.

[Has73b] F. J. et al. Hasert. "Search for Elastic Muon-Neutrino Electron Scattering". In: *Phys. Lett. B* 46 (1973), pp. 121–124.

[Bal74] C. et al. Baltay. "Observation of Weak Neutral Current Interactions at Fermilab". In: *Phys. Rev. Lett.* 32 (1974), pp. 1456–1459.

[Bie74] J. K. Bienlein. "Review of neutrino interactions". In: *Phys. Rept.* 12 (1974), pp. 75–123.

[BNL74] BNL. "Discovery of the charm quark". In: (1974). J/ψ discovery in 1974 at BNL and SLAC.

[Has+74] F. J. Hasert et al. "Observation of neutrino-like interactions without muon or electron". In: *Nucl. Phys. B* 73 (1974), pp. 1–22.

[Shr74] R. Shrock. "Decay Lo → $\nu l \gamma$ in gauge theories of weak and electromagnetic interactions". In: *Phys. Rev. D* 9 (1974), p. 743. DOI: `10.1103/PhysRevD.9.743`.

[t H76] G. 't Hooft. "Symmetry Breaking Through Bell–Jackiw Anomalies". In: *Phys. Rev. Lett.* 37 (1976), pp. 8–11. DOI: `10.1103/PhysRevLett.37.8`.

[BP76a] S. M. Bilenky and B. Pontecorvo. "Lepton mixing and neutrino oscillations". In: *Phys. Lett. B* 61.3 (1976), pp. 248–250.

[BP76b] S. M. Bilenky and B. Pontecorvo. "The quark-lepton analogy and neutrino oscillations". In: *Yad. Fiz.* 24 (1976), pp. 603–608.

[ES76] S. Eliezer and A. R. Swift. "Exploration of neutrino mass using a three-flavor formalism". In: *Nucl. Phys. B* 105 (1976), pp. 45–60.

[FM76] H. Fritzsch and P. Minkowski. "Vector-like weak currents, massive neutrinos, and neutrino beam oscillations". In: *Phys. Lett. B* 62 (1976), pp. 72–76.

[LS77] B. W. Lee and R. E. Shrock. "Natural Suppression of Symmetry Violation in Gauge Theories: Muon - Lepton and Electron Lepton Number Nonconservation". In: *Phys. Rev. D* 16 (1977), p. 1444. DOI: `10.1103/PhysRevD.16.1444`.

[MS77] W. Marciano and A. Sanda. "Exotic Decays of the Muon and Heavy Leptons in Gauge Theories". In: *Phys. Lett. B* 67 (1977), p. 303. DOI: `10.1016/0370-2693(77)90377-X`.

[Min77] P. Minkowski. "mu → e gamma at a rate of one out of 1-billion muon decays?" In: *Phys. Lett. B* 67 (1977), pp. 421–428. DOI: `10.1016/0370-2693(77)90435-X`.

[PQ77a] R.D. Peccei and H.R. Quinn. "CP Conservation in the Presence of Instantons". In: *Phys. Rev. Lett.* 38 (1977), pp. 1440–1443. DOI: `10.1103/PhysRevLett.38.1440`.

[PQ77b] R.D. Peccei and H.R. Quinn. "CP Conservation in the Presence of Instantons". In: *Phys. Rev. Lett.* 38 (1977), pp. 1440–1443. DOI: `10.1103/PhysRevLett.38.1440`.

[Vel77] M. J. G. Veltman. "Limit on mass differences in the Weinberg model". In: *Nucl. Phys. B* 123 (1977), pp. 89–99.

[BP78] S. M. Bilenky and B. Pontecorvo. "The Quark-Lepton Analogy and the Muonic Charge". In: *Phys. Rept.* 41 (1978), pp. 225–261.

[Wei78] S. Weinberg. "A New Light Boson?" In: *Phys. Rev. Lett.* 40 (1978), pp. 223–226. DOI: `10.1103/PhysRevLett.40.223`.

[Wol78] L. Wolfenstein. "Neutrino Oscillations in Matter". In: *Phys. Rev. D* 17 (1978), pp. 2369–2374. DOI: `10.1103/PhysRevD.17.2369`.

[Cre+79] R.J. Crewther et al. "Chiral Estimate of the Electric Dipole Moment of the Neutron in Quantum Chromodynamics". In: *Phys. Lett. B* 88 (1979), pp. 123–127. DOI: `10.1016/0370-2693(79)90128-X`.

[GRS79] M. Gell-Mann, P. Ramond, and R. Slansky. "Complex spinors and unified theories". In: *Supergravity*. Ed. by P. van Nieuwenhuizen and D.Z. Freedman. North Holland, 1979, pp. 315–321.

[Yan79] T. Yanagida. "Horizontal gauge symmetry and masses of neutrinos". In: *Proceedings: Workshop on the Unified Theories and the Baryon Number in the Universe*. KEK-79-18. 1979, pp. 95–99.

[MW80] M. Magg and C. Wetterich. "Neutrino Mass Problem and Gauge Hierarchy". In: *Phys. Lett. B* 94 (1980), pp. 61–64. DOI: `10.1016/0370-2693(80)90825-4`.

[MS80] R.N. Mohapatra and G. Senjanović. "Neutrino Mass and Spontaneous Parity Nonconservation". In: *Phys. Rev. Lett.* 44 (1980), pp. 912–915. DOI: `10.1103/PhysRevLett.44.912`.

[SV80] J. Schechter and J. W. F. Valle. "Neutrino masses in SU(2) x U(1) theories". In: *Phys. Rev. D* 22 (1980), p. 2227. DOI: `10.1103/PhysRevD.22.2227`.

[LSW81] G. Lazarides, Q. Shafi, and C. Wetterich. "Proton Lifetime and Fermion Masses in an SO(10) Model". In: *Nucl. Phys. B* 181 (1981), pp. 287–300. DOI: `10.1016/0550-3213(81)90354-0`.

[Wol81] Lincoln Wolfenstein. "CP properties of Majorana neutrinos and double beta decay". In: *Physics Letters B* 107.1 (1981), pp. 77–79. ISSN: 0370-2693. DOI: `https://doi.org/10.1016/0370-2693(81)91151-5`. URL: `https://www.sciencedirect.com/science/article/pii/0370269381911515`.

[PW82a] P. B. Pal and L. Wolfenstein. "Radiative Decays of Massive Neutrinos". In: *Phys. Rev. D* 25 (1982), p. 766. DOI: `10.1103/PhysRevD.25.766`.

[PW82b] Palash B. Pal and Lincoln Wolfenstein. "Radiative decays of massive neutrinos". In: *Physical Review D* 25.4 (1982), pp. 766–773. DOI: `10.1103/PhysRevD.25.766`. URL: `https://doi.org/10.1103/PhysRevD.25.766`.

[Pee82] P.J.E. Peebles. "Large-Scale Background Temperature and Mass Fluctuations Due to Scale-Invariant Primeval Perturbations". In: *Astrophys. J. Lett.* 263 (1982), pp. L1–L5. DOI: `10.1086/183911`.

[Shr82] R. E. Shrock. "Electromagnetic Properties and Decays of Dirac and Majorana Neutrinos in a General Class of Gauge Theories". In: *Nucl. Phys. B* 206 (1982), p. 359. DOI: `10.1016/0550-3213(82)90273-5`.

[Mil83] M. Milgrom. "A modification of the Newtonian dynamics as a possible alternative to the hidden mass hypothesis". In: *Astrophys. J.* 270 (1983), pp. 365–370. DOI: `10.1086/161130`.

[UA183] UA1. "Experimental observation of *W* and *Z* bosons". In: (1983). UA1 and UA2 Collaborations at CERN, discovered W and Z bosons in 1983.

[WW83] D. Wyler and L. Wolfenstein. "Massless Neutrinos in Left-Right Symmetric Models". In: *Nucl. Phys. B* 218 (1983), p. 205. DOI: `10.1016/0550-3213(83)90482-0`.

[Blu+84] G.R. Blumenthal et al. "Formation of Galaxies and Large-Scale Structure with Cold Dark Matter". In: *Nature* 311 (1984), pp. 517–525. DOI: `10.1038/311517a0`.

[KRS85] V. A. Kuzmin, V. A. Rubakov, and M. E. Shaposhnikov. "On the Anomalous Electroweak Baryon Number Nonconservation in the Early Universe". In: *Phys. Lett. B* 155 (1985), pp. 36–42. DOI: `10.1016/0370-2693(85)91028-7`.

[MS85] S.P. Mikheev and A.Yu. Smirnov. "Resonance Amplification of Oscillations in Matter and Solar Neutrino Spectroscopy". In: *Sov. J. Nucl. Phys.* 42 (1985), pp. 913–917.

[FY86] M. Fukugita and T. Yanagida. "Baryogenesis Without Grand Unification". In: *Phys. Lett. B* 174 (1986), pp. 45–47. DOI: `10.1016/0370-2693(86)91126-3`.

[Hax86] W.C. Haxton. "Adiabatic conversion of solar neutrinos". In: *Phys. Rev. Lett.* 57 (1986), pp. 1271–1274. DOI: `10.1103/PhysRevLett.57.1271`.

[Hol86] B. Holdom. "Two U(1)'s and Epsilon Charge Shifts". In: *Phys. Lett. B* 166 (1986), pp. 196–198. DOI: `10.1016/0370-2693(86)91377-8`.

[MS86] S.P. Mikheev and A.Yu. Smirnov. "Resonant amplification of neutrino oscillations in matter and solar-neutrino spectroscopy". In: *Nuovo Cim. C* 9 (1986), pp. 17–26. DOI: `10.1007/BF02508049`.

[Moh86] R. N. Mohapatra. "Mechanism for Understanding Small Neutrino Mass in Superstring Theories". In: *Phys. Rev. Lett.* 56 (1986), p. 561. DOI: `10.1103/PhysRevLett.56.561`.

[MV86] R. N. Mohapatra and J. W. F. Valle. “Neutrino Mass and Baryon Number Nonconservation in Superstring Models”. In: *Phys. Rev. D* 34 (1986), p. 1642. DOI: `10.1103/PhysRevD.34.1642`.

[Sto87a] L. Stodolsky. “On the treatment of neutrino oscillations in a medium”. In: *Phys. Rev. D* 36 (1987), pp. 2273–2279. DOI: `10.1103/PhysRevD.36.2273`.

[Sto87b] L. Stodolsky. “On the Treatment of Neutrino Oscillations in a Thermal Environment”. In: *Phys. Rev. D* 36 (1987), p. 2273.

[Wei87] S. Weinberg. “Anthropic Bound on the Cosmological Constant”. In: *Phys. Rev. Lett.* 59 (1987), pp. 2607–2610. DOI: `10.1103/PhysRevLett.59.2607`.

[BU88] J.N. Bahcall and R.K. Ulrich. “Solar Models, Neutrino Experiments, and Helioseismology”. In: *Rev. Mod. Phys.* 60 (1988), pp. 297–372. DOI: `10.1103/RevModPhys.60.297`.

[NR88a] D. Notzold and G. Raffelt. “Neutrino Dispersion at Finite Temperature and Density”. In: *Nucl. Phys. B* 307 (1988), pp. 924–936. DOI: `10.1016/0550-3213(88)90113-7`.

[NR88b] Dirk Nötzold and Georg Raffelt. “Neutrino dispersion at finite temperature and density”. In: *Nuclear Physics B* 307.4 (1988), pp. 924–936. ISSN: 0550-3213. DOI: `https://doi.org/10.1016/0550-3213(88)90113-7`. URL: `https://www.sciencedirect.com/science/article/pii/0550321388901137`.

[Foo+89] R. Foot et al. “Seesaw Neutrino Masses Induced by a Triplet of Leptons”. In: *Z. Phys. C* 44 (1989), p. 441. DOI: `10.1007/BF01415558`.

[Wei89] S. Weinberg. “The Cosmological Constant Problem”. In: *Rev. Mod. Phys.* 61 (1989), pp. 1–23. DOI: `10.1103/RevModPhys.61.1`.

[GG91] Paolo Gondolo and Graciela Gelmini. “Cosmic abundances of stable particles: Improved analysis”. In: *Nuclear Physics B* 360.1 (1991), pp. 145–179. ISSN: 0550-3213. DOI: `https://doi.org/10.1016/0550-3213(91)90438-4`. URL: `https://www.sciencedirect.com/science/article/pii/0550321391904384`.

[Sak91] A.D. Sakharov. “Violation of CP invariance, C asymmetry, and baryon asymmetry of the universe”. In: *Sov. Phys. Usp.* 34.5 (1991). Originally published in ZhETF Pis’ma 5, 32–35 (1967), pp. 392–393. DOI: `10.1070/PU1991v034n05ABEH002497`. URL: `https://doi.org/10.1070/PU1991v034n05ABEH002497`.

[Tho92] M. J. Thomson. “Damping of quantum coherence by elastic and inelastic processes”. In: *Phys. Rev. A* 45 (4 Feb. 1992), pp. 2243–2249. DOI: `10.1103/PhysRevA.45.2243`. URL: `https://link.aps.org/doi/10.1103/PhysRevA.45.2243`.

[DW94a] S. Dodelson and L.M. Widrow. “Sterile Neutrinos as Dark Matter”. In: *Phys. Rev. Lett.* 72 (1994), pp. 17–20. DOI: `10.1103/PhysRevLett.72.17`. arXiv: `hep-ph/9303287`.

[DW94b] Scott Dodelson and Lawrence M. Widrow. “Sterile-neutrinos as dark matter”. In: *Phys. Rev. Lett.* 72 (1994), pp. 17–20. DOI: `10.1103/PhysRevLett.72.17`. arXiv: `hep-ph/9303287`.

[CDF95] CDF. “Observation of the top quark”. In: (1995). CDF and DØ Collaborations at Fermilab, 1995.

[QV95] C. Quimbay and S. Vargas-Castrillón. “Fermionic dispersion relations in the standard model at finite temperature”. In: *Nuclear Physics B* 451.1 (1995), pp. 265–302. ISSN: 0550-3213. DOI: `https://doi.org/10.1016/0550-3213(95)00298-7`. URL: `https://www.sciencedirect.com/science/article/pii/0550321395002987`.

[JKG96] G. Jungman, M. Kamionkowski, and K. Griest. “Supersymmetric Dark Matter”. In: *Phys. Rept.* 267 (1996), pp. 195–373. DOI: `10.1016/0370-1573(95)00058-5`. arXiv: `hep-ph/9506380`.

[FV97] R. Foot and R. R. Volkas. “Studies of neutrino asymmetries generated by ordinary–sterile neutrino oscillations in the early universe and implications for big bang nucleosynthesis bounds”. In: *Phys. Rev. D* 55 (1997), p. 5147.

[BKS98] J.N. Bahcall, P.I. Krastev, and A.Yu. Smirnov. “Where do we stand with solar neutrino oscillations?” In: *Phys. Rev. D* 58 (1998), p. 096016. DOI: `10.1103/PhysRevD.58.096016`. arXiv: `hep-ph/9807216`.

[Cle+98] B.T. Cleveland et al. “Measurement of the solar electron neutrino flux with the Homestake chlorine detector”. In: *Astrophys. J.* 496 (1998), pp. 505–526. DOI: `10.1086/305343`.

[Fuk+98] Y. Fukuda et al. “Evidence for oscillation of atmospheric neutrinos”. In: *Phys. Rev. Lett.* 81 (1998), pp. 1562–1567. DOI: `10.1103/PhysRevLett.81.1562`. arXiv: `hep-ex/9807003`.

[Mat98] M. Mateo. “Dwarf Galaxies of the Local Group”. In: *Ann. Rev. Astron. Astrophys.* 36 (1998), pp. 435–506. DOI: `10.1146/annurev.astro.36.1.435`.

[Abd+99] J.N. Abdurashitov et al. “Measurement of the solar neutrino capture rate by the Russian-American gallium solar neutrino experiment during one half of the 22 year solar cycle”. In: *Phys. Rev. C* 60 (1999), p. 055801. DOI: `10.1103/PhysRevC.60.055801`. arXiv: `astro-ph/9907113`.

[CHD99] Rupert A. C. Croft, Wayne Hu, and Romeel Davé. “Cosmological Limits on the Neutrino Mass from the<mml:math xmlns:mml=”http://www.w3.org/1998/Math/MathML” display=”inline”>< In: *Physical Review Letters* 83.6 (1999), pp. 1092–1095. ISSN: 1079-7114. DOI: `10.1103/physrevlett.83.1092`. URL: `http://dx.doi.org/10.1103/PhysRevLett.83.1092`.

[Ham+99] W. Hampel et al. “GALLEX solar neutrino observations: Results for GALLEX IV”. In: *Phys. Lett. B* 447 (1999), pp. 127–133. DOI: `10.1016/S0370-2693(98)01579-2`.

[SF99] Xiangdong Shi and George M. Fuller. “New Dark Matter Candidate: Nonthermal Sterile Neutrinos”. In: *Phys. Rev. Lett.* 82 (14 Apr. 1999), pp. 2832–2835. DOI: `10.1103/PhysRevLett.82.2832`. URL: `https://link.aps.org/doi/10.1103/PhysRevLett.82.2832`.

[BLL00] P. Di Bari, P. Lipari, and M. Lusignoli. “Active–sterile neutrino oscillations in the early universe and the atmospheric neutrino anomaly”. In: *Int. J. Mod. Phys. A* 15 (2000), p. 2289.

[BP00] R. Bousso and J. Polchinski. “Quantization of four form fluxes and dynamical neutralization of the cosmological constant”. In: *JHEP* 06 (2000), p. 006. DOI: `10.1088/1126-6708/2000/06/006`. arXiv: `hep-th/0004134`.

[Dre00] Manuel Drees. “Comment on ”A New Dark Matter Candidate: Non-thermal Sterile Neutrinos””. In: *arXiv* hep-ph/0003127 (2000). arXiv: `hep-ph/0003127`. URL: `https://arxiv.org/abs/hep-ph/0003127`.

[LVW00] K. S. M. Lee, R. R. Volkas, and Y. Y. Y. Wong. “Sterile neutrino asymmetry generation via active–sterile oscillations: An analytic approach”. In: *Phys. Rev. D* 62 (2000), p. 093025.

[VW00] R. R. Volkas and Y. Y. Y. Wong. “Relic neutrino asymmetries”. In: *Phys. Rev. D* 62 (2000), p. 093024.

[AFP01] Kevork Abazajian, George M. Fuller, and Mitesh Patel. “Sterile neutrino hot, warm, and cold dark matter”. In: *Physical Review D* 64.2 (2001). ISSN: 1089-4918. DOI: `10.1103/physrevd.64.023501`. URL: `http://dx.doi.org/10.1103/PhysRevD.64.023501`.

[AFT01] Kevork N. Abazajian, George M. Fuller, and Wallace H. Tucker. “Direct Detection of Warm Dark Matter in the X-Ray”. In: *The Astrophysical Journal* 562.2 (2001), pp. 593–604. DOI: 10.1086/323851. arXiv: astro-ph/0106002 [astro-ph]. URL: https://arxiv.org/abs/astro-ph/0106002.

[BHO01] Rennan Barkana, Zoltan Haiman, and Jeremiah P. Ostriker. “Constraints on Warm Dark Matter from Cosmological Reionization”. In: *The Astrophysical Journal* 558.2 (2001), pp. 482–496. ISSN: 1538-4357. DOI: 10.1086/322393. URL: http://dx.doi.org/10.1086/322393.

[CI01] J. A. Casas and A. Ibarra. “Oscillating neutrinos and $\mu \to e\gamma$”. In: *Nucl. Phys. B* 618 (2001), pp. 171–204. DOI: 10.1016/S0550-3213(01)00475-8. arXiv: hep-ph/0103065.

[Fuk+01] S. Fukuda et al. “Solar 8B and hep Neutrino Measurements from 1258 Days of Super-Kamiokande Data”. In: *Phys. Rev. Lett.* 86 (2001), pp. 5651–5655. DOI: 10.1103/PhysRevLett.86.5651. arXiv: hep-ex/0103032.

[SR01] Y. Sofue and V. Rubin. “Rotation Curves of Spiral Galaxies”. In: *Ann. Rev. Astron. Astrophys.* 39 (2001), pp. 137–174. DOI: 10.1146/annurev.astro.39.1.137. arXiv: astro-ph/0010594.

[Ahm+02] Q.R. Ahmad et al. “Direct evidence for neutrino flavor transformation from neutral current interactions in the Sudbury Neutrino Observatory”. In: *Phys. Rev. Lett.* 89 (2002), p. 011301. DOI: 10.1103/PhysRevLett.89.011301. arXiv: nucl-ex/0204008.

[BGP02] J.N. Bahcall, M.C. Gonzalez-Garcia, and C. Pena-Garay. “Solar neutrinos before and after KamLAND”. In: *JHEP* 07 (2002), p. 054. DOI: 10.1088/1126-6708/2002/07/054. arXiv: hep-ph/0204314.

[DH02] A. D. Dolgov and S. H. Hansen. “Massive Sterile Neutrinos as Warm Dark Matter”. In: *Astroparticle Physics* 16.4 (2002), pp. 339–344. DOI: 10.1016/S0927-6505(01)00149-4. arXiv: hep-ph/0009083 [hep-ph]. URL: https://arxiv.org/abs/hep-ph/0009083.

[Ell+02] John Ellis et al. “A New Parametrization of the Seesaw Mechanism and Applications in Supersymmetric Models”. In: *Phys. Rev. D* 66 (2002), p. 115013. DOI: 10.1103/PhysRevD.66.115013.

[Dou03] M.R. Douglas. “The Statistics of string / M theory vacua”. In: *JHEP* 05 (2003), p. 046. DOI: 10.1088/1126-6708/2003/05/046. arXiv: hep-th/0303194.

[Sus03] L. Susskind. “The Anthropic landscape of string theory”. In: *In: Universe or Multiverse? (ed. B. Carr)* (2003). arXiv: hep-th/0302219.

[Bek04] J.D. Bekenstein. “Relativistic gravitation theory for the modified Newtonian dynamics paradigm”. In: *Phys. Rev. D* 70 (2004), p. 083509. DOI: 10.1103/PhysRevD.70.083509. arXiv: astro-ph/0403694.

[Eid+04] S. Eidelman et al. “Review of Particle Physics”. In: *Physics Letters B* 592.1 (2004). Review of Particle Physics, pp. 1–5. ISSN: 0370-2693. DOI: https://doi.org/10.1016/j.physletb.2004.06.001. URL: https://www.sciencedirect.com/science/article/pii/S0370269304007579.

[BHS05] G. Bertone, D. Hooper, and J. Silk. “Particle Dark Matter: Evidence, Candidates and Constraints”. In: *Phys. Rept.* 405 (2005), pp. 279–390. DOI: 10.1016/j.physrep.2004.08.031. arXiv: hep-ph/0404175.

[Vie+05] Matteo Viel et al. “Constraining warm dark matter candidates including sterile neutrinos and light gravitinos with WMAP and the Lyman-<mml:math xmlns:mml=”http://www.w3.org/1998/Math/
display=”inline”><mml:mi>α</mml:mi></mml:math>forest”. In: *Physical Review D* 71.6 (2005). ISSN: 1550-2368. DOI: 10.1103/physrevd.71.063534. URL: http://dx.doi.org/10.1103/PhysRevD.71.063534.

[Aba06] Kevork Abazajian. “Linear cosmological structure limits on warm dark matter”. In: *Physical Review D* 73.6 (2006). ISSN: 1550-2368. DOI: 10.1103/physrevd.73.063513. URL: http://dx.doi.org/10.1103/PhysRevD.73.063513.

[Ant+06] Stefan Antusch et al. “Unitarity of the Leptonic Mixing Matrix”. In: *JHEP* 10 (2006), p. 084. DOI: 10.1088/1126-6708/2006/10/084. eprint: hep-ph/0607020.

[Bak+06] C.A. Baker et al. “An Improved experimental limit on the electric dipole moment of the neutron”. In: *Phys. Rev. Lett.* 97 (2006), p. 131801. DOI: 10.1103/PhysRevLett.97.131801. arXiv: hep-ex/0602020.

[Boy+06a] Andrey Boyarsky et al. “Constraints on sterile neutrino as a dark matter candidate from the diffuse X-ray background”. In: *Monthly Notices of the Royal Astronomical Society* 370 (2006), pp. 213–218. DOI: 10.1111/j.1365-2966.2006.10458.x. arXiv: astro-ph/0512509 [astro-ph]. URL: https://arxiv.org/abs/astro-ph/0512509.

[Boy+06b] Andrey Boyarsky et al. “Where to find a dark matter sterile neutrino?” In: *Physical Review Letters* 97 (2006), p. 261302. DOI: 10.1103/PhysRevLett.97.261302. arXiv: astro-ph/0603660 [astro-ph]. URL: https://arxiv.org/abs/astro-ph/0603660.

[BCG+06] Marusa Bradac, Douglas Clowe, Anthony Gonzalez, et al. “Strong and Weak Lensing United III: Measuring the Mass Distribution of the Merging Galaxy Cluster 1E0657-56”. In: *Astrophys. J.* 652 (2006), pp. 937–947. arXiv: astro-ph/0608408.

[C R+06] C. R. Watson et al. “Direct x-ray constraints on sterile neutrino warm dark matter”. In: *Phys. Rev. D* 74 (2006), p. 033009. DOI: 10.1103/PhysRevD.74.033009.

[Cas06] Diego Casadei. *Searches for Cosmic Antimatter*. 2006. arXiv: astro-ph/0405417 [astro-ph]. URL: https://arxiv.org/abs/astro-ph/0405417.

[Clo+06] Douglas Clowe et al. “A direct empirical proof of the existence of dark matter”. In: *Astrophys. J. Lett.* 648 (2006), pp. L109–L113. arXiv: astro-ph/0608407.

[McD+06] Patrick McDonald et al. “The Lyα forest power spectrum from the Sloan Digital Sky Survey”. In: *Astrophysical Journal Supplement Series* 163.1 (2006), pp. 80–109. DOI: 10.1086/444361. arXiv: astro-ph/0407377 [astro-ph]. URL: https://arxiv.org/abs/astro-ph/0407377.

[Mes06] M. D. Messier. *Review of Neutrino Oscllations Experiments*. 2006. arXiv: hep-ex/0606013 [hep-ex]. URL: https://arxiv.org/abs/hep-ex/0606013.

[Pol06] J. Polchinski. “The Cosmological Constant and the String Landscape”. In: *hep-th/0603249* (2006). arXiv: hep-th/0603249.

[RHP06] Signe Riemer-Sørensen, Steen H. Hansen, and Kristian Pedersen. “Sterile neutrinos in the Milky Way: Observational constraints”. In: *The Astrophysical Journal* 644 (2006), pp. L33–L36. DOI: 10.1086/505869. arXiv: astro-ph/0603661 [astro-ph]. URL: https://arxiv.org/abs/astro-ph/0603661.

[Sch06] Schael. “Precision electroweak measurements on the Z resonance”. In: *Physics Reports* 427.5 (2006), pp. 257–454. ISSN: 0370-1573. DOI: `https://doi.org/10.1016/j.physrep.2005.12.006`. URL: `https://www.sciencedirect.com/science/article/pii/S0370157305005119`.

[Sel+06] Uroš Seljak et al. “Can sterile neutrinos be the dark matter?” In: *Physical Review Letters* 97 (2006), p. 191303. DOI: `10.1103/PhysRevLett.97.191303`. arXiv: `astro-ph/0602430 [astro-ph]`. URL: `https://arxiv.org/abs/astro-ph/0602430`.

[Vie+06] Matteo Viel et al. “Can sterile neutrinos be ruled out as warm dark matter candidates?” In: *Physical Review Letters* 97 (2006), p. 071301. DOI: `10.1103/PhysRevLett.97.071301`. arXiv: `astro-ph/0605706 [astro-ph]`. URL: `https://arxiv.org/abs/astro-ph/0605706`.

[VKF+06] A. Vikhlinin, A. Kravtsov, W. Forman, et al. “Chandra Sample of Nearby Relaxed Galaxy Clusters: Mass, Gas Fraction, and Mass-Temperature Relation”. In: *Astrophys. J.* 640 (2006), pp. 691–709. DOI: `10.1086/500288`. arXiv: `astro-ph/0507092`.

[ASL07] Takehiko Asaka, Mikhail Shaposhnikov, and Mikko Laine. “Lightest sterile neutrino abundance within theνMSM”. In: *Journal of High Energy Physics* 2007.01 (2007), pp. 091–091. ISSN: 1029-8479. DOI: `10.1088/1126-6708/2007/01/091`. URL: `http://dx.doi.org/10.1088/1126-6708/2007/01/091`.

[Fer+07] Enrique Fernandez-Martinez et al. “CP-violation from non-unitary leptonic mixing”. In: *Phys. Lett. B* 649 (2007), pp. 427–435. DOI: `10.1016/j.physletb.2007.03.069`. eprint: `hep-ph/0703098`.

[GK07] Carlo Giunti and Chung W. Kim. *Fundamentals of Neutrino Physics and Astrophysics*. Oxford, UK: Oxford University Press, 2007. ISBN: 9780198508717.

[Ada+08] P. Adamson et al. “Measurement of Neutrino Oscillations with the MINOS Detectors in the NuMI Beam”. In: *Phys. Rev. Lett.* 101 (2008), p. 131802. DOI: `10.1103/PhysRevLett.101.131802`. arXiv: `0806.2237`.

[Boy+08] Andrey Boyarsky et al. “Constraining DM properties with SPI”. In: *Monthly Notices of the Royal Astronomical Society* 387 (2008), pp. 1345–1350. DOI: `10.1111/j.1365-2966.2008.13003.x`. arXiv: `0710.4922 [astro-ph]`. URL: `https://arxiv.org/abs/0710.4922`.

[HFG08] D. Hanneke, S. Fogwell, and G. Gabrielse. “New Measurement of the Electron Magnetic Moment and the Fine Structure Constant”. In: *Phys. Rev. Lett.* 100 (2008), p. 120801. DOI: `10.1103/PhysRevLett.100.120801`. arXiv: `0801.1134 [physics.atom-ph]`.

[PK08] Kalliopi Petraki and Alexander Kusenko. “Dark-matter sterile neutrinos in models with a gauge singlet in the Higgs sector”. In: *Physical Review D* 77.6 (2008). ISSN: 1550-2368. DOI: `10.1103/physrevd.77.065014`. URL: `http://dx.doi.org/10.1103/PhysRevD.77.065014`.

[Vie+08] Matteo Viel et al. “How cold is cold dark matter? Small–scales constraints from the flux power spectrum of the high–redshift Lyman–α forest”. In: *Physical Review Letters* 100.4 (2008), p. 041304. DOI: `10.1103/PhysRevLett.100.041304`. arXiv: `0709.0131 [astro-ph]`. URL: `https://arxiv.org/abs/0709.0131`.

[LKB09] Michael Loewenstein, Alexander Kusenko, and Peter L. Biermann. “New limits on sterile neutrinos from Suzaku observations of the Ursa Minor dwarf spheroidal galaxy”. In: *The Astrophysical Journal* 700.1 (2009), pp. 426–435. DOI: `10.1088/0004-637X/700/1/426`. arXiv: `0812.2710 [astro-ph]`. URL: `https://arxiv.org/abs/0812.2710`.

[WMO+09] M.G. Walker, M. Mateo, E.W. Olszewski, et al. “A Universal Mass Profile for Dwarf Spheroidal Galaxies”. In: *Astrophys. J.* 704 (2009), pp. 1274–1287. DOI: `10.1088/0004-637X/704/2/1274`. arXiv: `0906.0341`.

[Ber10] G. Bertone. *Particle Dark Matter: Observations, Models and Searches*. Cambridge Univ. Press, 2010. DOI: `10.1017/CBO9780511770739`.

[DHM10] Herbi K. Dreiner, Howard E. Haber, and Stephen P. Martin. “Two-component spinor techniques and Feynman rules for quantum field theory and supersymmetry”. In: *Physics Reports* 494.1–2 (2010), pp. 1–196. ISSN: 0370-1573. DOI: `10.1016/j.physrep.2010.05.002`. URL: `http://dx.doi.org/10.1016/j.physrep.2010.05.002`.

[Grz+10] B. Grzadkowski et al. “Dimension-Six Terms in the Standard Model Lagrangian”. In: *JHEP* 10 (2010), p. 085. DOI: `10.1007/JHEP10(2010)085`. arXiv: `1008.4884 [hep-ph]`.

[LK10] Michael Loewenstein and Alexander Kusenko. “Dark matter search using Chandra observations of Willman 1, and a spectral feature consistent with a decay line of a 5 keV sterile neutrino”. In: *The Astrophysical Journal* 714.1 (2010), pp. 652–662. DOI: `10.1088/0004-637X/714/1/652`. arXiv: `0912.0552 [astro-ph.CO]`. URL: `https://arxiv.org/abs/0912.0552`.

[BF11] Mattias Blennow and Enrique Fernandez-Martinez. “Parametrization of seesaw models and light sterile neutrinos”. In: *JHEP* 07 (2011), p. 096. DOI: `10.1007/JHEP07(2011)096`. arXiv: `1105.5936 [hep-ph]`.

[Les11] Julien Lesgourgues. *The Cosmic Linear Anisotropy Solving System (CLASS) I: Overview*. 2011. arXiv: `1104.2932 [astro-ph.IM]`. URL: `https://arxiv.org/abs/1104.2932`.

[XZ11a] Z. Xing and S. Zhou. *Neutrinos in Particle Physics, Astronomy and Cosmology*. Advanced Topics in Science and Technology in China. Springer Berlin Heidelberg, 2011. ISBN: 9783642175602.

[XZ11b] Z. Xing and S. Zhou. *Neutrinos in Particle Physics, Astronomy and Cosmology*. Advanced Topics in Science and Technology in China. Springer Berlin Heidelberg, 2011. ISBN: 9783642175602.

[Aad+12] G. Aad et al. “Observation of a new particle in the search for the Standard Model Higgs boson with the ATLAS detector at the LHC”. In: *Physics Letters B* 716.1 (Sept. 2012), pp. 1–29. ISSN: 0370-2693. DOI: `10.1016/j.physletb.2012.08.020`. URL: `http://dx.doi.org/10.1016/j.physletb.2012.08.020`.

[CZN12] C. R. Watson, Z. Li, and N. K. Polley. “Constraining Sterile Neutrino Warm Dark Matter with Chandra Observations of the Andromeda Galaxy”. In: *JCAP* 07 (2012), p. 030. DOI: `10.1088/1475-7516/2012/07/030`. eprint: `1111.4217`.

[FM12] B. Famaey and S. McGaugh. “Modified Newtonian Dynamics (MOND): Observational Phenomenology and Relativistic Extensions”. In: *Living Rev. Relativ.* 15 (2012), p. 10. DOI: `10.12942/lrr-2012-10`. arXiv: `1112.3960`.

[LK12] Michael Loewenstein and Alexander Kusenko. “Dark matter search using XMM-Newton observations of Willman 1”. In: *The Astrophysical Journal* 751.2 (2012), p. 82. DOI: `10.1088/0004-637X/751/2/82`. arXiv: `1203.5229 [astro-ph.CO]`. URL: `https://arxiv.org/abs/1203.5229`.

[Lov+12] Mark R. Lovell et al. “The haloes of bright satellite galaxies in a warm dark matter universe: Satellite galaxies in WDM”. In: *Monthly Notices of the Royal Astronomical Society* 420.3 (2012), pp. 2318–2324. ISSN: 0035-8711. DOI: `10.1111/j.1365-2966.2011.20200.x`. URL: `http://dx.doi.org/10.1111/j.1365-2966.2011.20200.x`.

[Mar12] J. Martin. "Everything You Always Wanted To Know About The Cosmological Constant Problem (But Were Afraid To Ask)". In: *Comptes Rendus Physique* 13 (2012), pp. 566–665. DOI: `10.1016/j.crhy.2012.04.008`. arXiv: `1205.3365`.

[And+13] Donnino Anderhalden et al. "Hints on the nature of dark matter from the properties of Milky Way satellites". In: *Journal of Cosmology and Astroparticle Physics* 2013.03 (2013), pp. 014–014. ISSN: 1475-7516. DOI: `10.1088/1475-7516/2013/03/014`. URL: `http://dx.doi.org/10.1088/1475-7516/2013/03/014`.

[Vie+13] Matteo Viel et al. "Warm dark matter as a solution to the small scale crisis: new constraints from high redshift Lyman-α forest data". In: *Physical Review D* 88.4 (2013), p. 043502. DOI: `10.1103/PhysRevD.88.043502`. arXiv: `1306.2314 [astro-ph.CO]`. URL: `https://arxiv.org/abs/1306.2314`.

[AM14] Amine Ahriche and Kristian L. McDonald. "The Social and Realistic Aspects of Dimension-9 Seesaw Models". In: *Phys. Rev. D* 89 (2014), p. 095007. DOI: `10.1103/PhysRevD.89.095007`. arXiv: `1401.00000 [hep-ph]`.

[Alo+14] Rodrigo Alonso et al. "The Effective Field Theory of the Standard Model: Extended with Right-Handed Neutrinos". In: *JHEP* 04 (2014), p. 159. DOI: `10.1007/JHEP04(2014)159`. arXiv: `1312.2014 [hep-ph]`.

[Hor+14] Shunsaku Horiuchi et al. "Sterile neutrino dark matter bounds from galaxies of the Local Group". In: *Physical Review D* 89.2 (2014), p. 025017. DOI: `10.1103/PhysRevD.89.025017`. arXiv: `1311.0282 [astro-ph.CO]`. URL: `https://arxiv.org/abs/1311.0282`.

[MNE14] Dmitry Malyshev, Andrii Neronov, and Daniel Eckert. "Constraints on 3.55 keV line emission from stacked observations of dwarf spheroidal galaxies". In: *Physical Review D* 90.10 (2014), p. 103506. DOI: `10.1103/PhysRevD.90.103506`. arXiv: `1408.3531 [astro-ph.CO]`. URL: `https://arxiv.org/abs/1408.3531`.

[MNS14] Alexander Merle, Viviana Niro, and Daniel Schmidt. "New production mechanism for keV sterile neutrino Dark Matter by decays of frozen-in scalars". In: *Journal of Cosmology and Astroparticle Physics* 2014.03 (2014), pp. 028–028. ISSN: 1475-7516. DOI: `10.1088/1475-7516/2014/03/028`. URL: `http://dx.doi.org/10.1088/1475-7516/2014/03/028`.

[Sch+14] Christian Schultz et al. "The high-z universe confronts warm dark matter: Galaxy counts, reionization and the nature of dark matter". In: *Monthly Notices of the Royal Astronomical Society* 442.2 (2014), pp. 1597–1609. ISSN: 0035-8711. DOI: `10.1093/mnras/stu976`. URL: `http://dx.doi.org/10.1093/mnras/stu976`.

[Esc+15] F. J. Escrihuela et al. "On the description of nonunitary neutrino mixing". In: *Phys. Rev. D* 92.5 (2015), p. 053009. DOI: `10.1103/PhysRevD.92.053009`. eprint: `1503.08879`.

[MT15] Alexander Merle and Maximilian Totzauer. "keV sterile neutrino dark matter from singlet scalar decays: basic concepts and subtle features". In: *Journal of Cosmology and Astroparticle Physics* 2015.06 (2015), pp. 011–011. ISSN: 1475-7516. DOI: `10.1088/1475-7516/2015/06/011`. URL: `http://dx.doi.org/10.1088/1475-7516/2015/06/011`.

[Ng+15] Kenny C. Y. Ng et al. "Improved limits on sterile neutrino dark matter using full-sky Fermi Gamma-Ray Burst Monitor data". In: *Physical Review D* 92.4 (2015), p. 043503. DOI: `10.1103/PhysRevD.92.043503`. arXiv: `1504.04027 [astro-ph.CO]`. URL: `https://arxiv.org/abs/1504.04027`.

[Tam+15] Takayuki Tamura et al. “An X-ray spectroscopic search for dark matter in the Perseus cluster with Suzaku”. In: *Publications of the Astronomical Society of Japan* 67.2 (2015), p. 23. DOI: 10.1093/pasj/psu156. arXiv: 1412.1869 [astro-ph.CO]. URL: https://arxiv.org/abs/1412.1869.

[Bau+16] Julien Baur et al. “Lyman-α Forests cool Warm Dark Matter”. In: *Journal of Cosmology and Astroparticle Physics* 2016.08 (2016), p. 012. DOI: 10.1088/1475-7516/2016/08/012. arXiv: 1512.01981 [astro-ph.CO]. URL: https://arxiv.org/abs/1512.01981.

[Cyb+16] R.H. Cyburt et al. “Big Bang Nucleosynthesis: 2015”. In: *Rev. Mod. Phys.* 88 (2016), p. 015004. DOI: 10.1103/RevModPhys.88.015004. arXiv: 1505.01076.

[NM16] A. Neronov and D. Malyshev. “Toward a full test of the<mml:math xmlns:mml=”http://www.w3.org/19
display=”inline”><mml:mrow><mml:mi>ν</mml:mi><mml:mi>MSM</mml:mi></mml:mrow></
neutrino dark matter model with Athena”. In: *Physical Review D* 93.6 (2016). ISSN: 2470-0029. DOI: 10.1103/physrevd.93.063518. URL: http://dx.doi.org/10.1103/PhysRevD.93.063518.

[PR16] Stephen Parke and Mark Ross-Lonergan. “Unitarity and the three flavor neutrino mixing matrix”. In: *Phys. Rev. D* 93 (11 June 2016), p. 113009. DOI: 10.1103/PhysRevD.93.113009. URL: https://link.aps.org/doi/10.1103/PhysRevD.93.113009.

[Rin+16] K. Rines et al. “Measuring the Masses of Galaxy Clusters”. In: *Astrophys. J.* 819 (2016), p. 63. DOI: 10.3847/0004-637X/819/1/63. arXiv: 1601.06092.

[Sch16] Aurel Schneider. “Astrophysical constraints on resonantly produced sterile neutrino dark matter”. In: *Journal of Cosmology and Astroparticle Physics* 2016.04 (2016), pp. 059–059. ISSN: 1475-7516. DOI: 10.1088/1475-7516/2016/04/059. URL: http://dx.doi.org/10.1088/1475-7516/2016/04/059.

[Aai+17] R. Aaij et al. “Search for the rare decay $K_S^0 \to \mu^+\mu^-$”. In: *Eur. Phys. J. C* 77 (2017), p. 678. DOI: 10.1140/epjc/s10052-017-5230-x. arXiv: 1706.00758 [hep-ex].

[Aba17] Kevork N. Abazajian. “Sterile neutrinos in cosmology”. In: *Physics Reports* 711–712 (2017), pp. 1–28. ISSN: 0370-1573. DOI: 10.1016/j.physrep.2017.10.003. URL: http://dx.doi.org/10.1016/j.physrep.2017.10.003.

[Bat+17] M. Battaglieri et al. “US Cosmic Visions: New Ideas in Dark Matter 2017: Community Report”. In: (2017). arXiv: 1707.04591 [hep-ph].

[Ble+17] Mattias Blennow et al. “Non-Unitarity, sterile neutrinos, and Non-Standard neutrino Interactions”. In: *JHEP* 04 (2017), p. 153. DOI: 10.1007/JHEP04(2017)153. eprint: 1609.08637.

[Cai+17] Yi Cai et al. “From the Trees to the Forest: A Review of Radiative Neutrino Mass Models”. In: *Front. Phys.* 5 (2017), p. 63. DOI: 10.3389/fphy.2017.00063. arXiv: 1706.08524 [hep-ph].

[HV17] Rasmus S. L. Hansen and Stefan Vogl. “Thermalizing Sterile Neutrino Dark Matter”. In: *Physical Review Letters* 119.25 (2017). ISSN: 1079-7114. DOI: 10.1103/physrevlett.119.251305. URL: http://dx.doi.org/10.1103/PhysRevLett.119.251305.

[Irš+17] Vid Iršič et al. “New constraints on the free-streaming of warm dark matter from intermediate and small scale Lyman- <mml:math xmlns:mml=”http://www.w3.org/1998/Math/MathML” display=”inline”><mml:mi>α</mml:mi></mml:math> forest data”. In: *Physical Review D* 96.2 (2017). ISSN: 2470-0029. DOI: 10.1103/physrevd.96.023522. URL: http://dx.doi.org/10.1103/PhysRevD.96.023522.

[Men+17] N. Menci et al. “Fundamental Physics with the Hubble Frontier Fields: Constraining Dark Matter Models with the Abundance of Extremely Faint and Distant Galaxies”. In: *The Astrophysical Journal* 836.1 (2017), p. 61. ISSN: 1538-4357. DOI: `10.3847/1538-4357/836/1/61`. URL: `http://dx.doi.org/10.3847/1538-4357/836/1/61`.

[Apr+18] E. Aprile et al. “Dark Matter Search Results from a One Ton-Year Exposure of XENON1T”. In: *Phys. Rev. Lett.* 121 (2018), p. 111302. DOI: `10.1103/PhysRevLett.121.111302`. arXiv: `1805.12562`.

[Ber+18] Jeffrey M. Berryman et al. “Lepton-number-charged scalars and neutrino beamstrahlung”. In: *Phys. Rev. D* 97 (7 Apr. 2018), p. 075030. DOI: `10.1103/PhysRevD.97.075030`. URL: `https://link.aps.org/doi/10.1103/PhysRevD.97.075030`.

[Du+18] N. Du et al. “Search for Invisible Axion Dark Matter with the Axion Dark Matter Experiment”. In: *Phys. Rev. Lett.* 120 (2018), p. 151301. DOI: `10.1103/PhysRevLett.120.151301`. arXiv: `1804.05750`.

[Ant+19] Stefan Antusch et al. “Low scale type II seesaw: present constraints and prospects for displaced vertex searches”. In: *Journal of High Energy Physics* 2019.2 (2019). ISSN: 1029-8479. DOI: `10.1007/jhep02(2019)157`. URL: `http://dx.doi.org/10.1007/JHEP02(2019)157`.

[BFS19] Pasquale Di Bari, Michele Re Fiorentin, and Rome Samanta. “Representing seesaw neutrino models and their motion in lepton flavour space”. In: *JHEP* 03 (2019), p. 040. DOI: `10.1007/JHEP03(2019)040`.

[Boy+19] A. Boyarsky et al. “Sterile neutrino Dark Matter”. In: *Prog. Part. Nucl. Phys.* 104 (2019), pp. 1–45. DOI: `10.1016/j.ppnp.2018.07.004`. arXiv: `1807.07938`.

[GKK19] Srubabati Goswami, Vishnudath K. N., and Najimuddin Khan. “Constraining the minimal type-III seesaw model with naturalness, lepton flavor violation, and electroweak vacuum stability”. In: *Physical Review D* 99.7 (2019). ISSN: 2470-0029. DOI: `10.1103/physrevd.99.075012`. URL: `http://dx.doi.org/10.1103/PhysRevD.99.075012`.

[Hoo19] A. Hook. “TASI Lectures on the Strong CP Problem and Axions”. In: *PoS TASI2018* (2019), p. 004. DOI: `10.22323/1.333.0004`. arXiv: `1812.02669`.

[JF19] Lucas Johns and George M. Fuller. “Self-interacting sterile neutrino dark matter: The heavy-mediator case”. In: *Physical Review D* 100.2 (2019). ISSN: 2470-0029. DOI: `10.1103/physrevd.100.023533`. URL: `http://dx.doi.org/10.1103/PhysRevD.100.023533`.

[KZ19] Kevin J. Kelly and Yue Zhang. “Mononeutrino at DUNE: New signals from neutrinophilic thermal dark matter”. In: *Phys. Rev. D* 99 (5 Mar. 2019), p. 055034. DOI: `10.1103/PhysRevD.99.055034`. URL: `https://link.aps.org/doi/10.1103/PhysRevD.99.055034`.

[Abe+20] C. Abel et al. “Measurement of the permanent electric dipole moment of the neutron”. In: *Phys. Rev. Lett.* 124 (2020), p. 081803. DOI: `10.1103/PhysRevLett.124.081803`. arXiv: `2001.11966`.

[Agh+20] N. Aghanim et al. “Planck 2018 results. VI. Cosmological parameters”. In: *Astron. Astrophys.* 641 (2020), A6. DOI: `10.1051/0004-6361/201833910`. arXiv: `1807.06209`.

[Aoy+20] T. Aoyama et al. “The anomalous magnetic moment of the muon in the Standard Model”. In: *Phys. Rept.* 887 (2020), pp. 1–166. DOI: `10.1016/j.physrep.2020.07.006`. arXiv: `2006.04822 [hep-ph]`.

[B M+20] B. M. Roach et al. “NuSTAR tests of sterile-neutrino dark matter: new galactic bulge observations and combined impact”. In: *Phys. Rev. D* 101 (2020), p. 103011. DOI: 10.1103/PhysRevD.101.103011. eprint: 1908.09037.

[BR20] Paolo Bellan and Marco Roccia. “A non-minimal tree-level seesaw at dimension nine”. In: *JHEP* 05 (2020), p. 123. arXiv: 2002.00000 [hep-ph].

[Est+20] I. Esteban et al. “The fate of hints: updated global analysis of three-flavor neutrino oscillations”. In: *JHEP* 09 (2020), p. 178. DOI: 10.1007/JHEP09(2020)178. arXiv: 2007.14792.

[Gou+20a] Andre de Gouvea et al. “Dodelson-Widrow Mechanism in the Presence of Self-Interacting Neutrinos”. In: *Physical Review Letters* 124.8 (2020). ISSN: 1079-7114. DOI: 10.1103/physrevlett.124.081802. URL: http://dx.doi.org/10.1103/PhysRevLett.124.081802.

[Gou+20b] André de Gouvêa et al. “Dodelson-Widrow Mechanism in the Presence of Self-Interacting Neutrinos”. In: *Physical Review Letters* 124.8 (2020). ISSN: 1079-7114. DOI: 10.1103/physrevlett.124.081802. URL: http://dx.doi.org/10.1103/PhysRevLett.124.081802.

[Kel+20] Kevin J. Kelly et al. “Origin of sterile neutrino dark matter via secret neutrino interactions with vector bosons”. In: *Physical Review D* 101.11 (2020). ISSN: 2470-0029. DOI: 10.1103/physrevd.101.115031. URL: http://dx.doi.org/10.1103/PhysRevD.101.115031.

[XZ20] Zhi-zhong Xing and Shun Zhou. “The minimal seesaw and leptogenesis models”. In: *Phys. Rev. D* 102 (2020), p. 095017. DOI: 10.1103/PhysRevD.102.095017.

[Bri+21] Torsten Bringmann et al. “Dark Matter from Exponential Growth”. In: *Physical Review Letters* 127.19 (2021). ISSN: 1079-7114. DOI: 10.1103/physrevlett.127.191802. URL: http://dx.doi.org/10.1103/PhysRevLett.127.191802.

[Ega+21] Daniel Egana-Ugrinovic et al. “The cosmological evolution of self-interacting dark matter”. In: *Journal of Cosmology and Astroparticle Physics* 2021.05 (2021), p. 013. ISSN: 1475-7516. DOI: 10.1088/1475-7516/2021/05/013. URL: http://dx.doi.org/10.1088/1475-7516/2021/05/013.

[Kop21] J. Kopp. “Sterile Neutrinos as Dark Matter Candidates”. In: (2021). October 27, 2021. URL: https://arxiv.org/abs/2109.00767.

[YZF21] Ben Yan, Shu-Min Zhao, and Tai-Fu Feng. *Electric dipole moments of neutron and heavy quarks c, t in CP violating $U(1)_X SSM$*. 2021. arXiv: 2011.08533 [hep-ph]. URL: https://arxiv.org/abs/2011.08533.

[Abb+22] T.M.C. Abbott et al. “Dark Energy Survey Year 3 Results: Cosmological Constraints from Galaxy Clustering and Weak Lensing”. In: *Phys. Rev. D* 105 (2022), p. 023520. DOI: 10.1103/PhysRevD.105.023520. arXiv: 2105.13549.

[Ake+22] M. Aker et al. “Direct neutrino-mass measurement with sub-electronvolt sensitivity”. In: *Nature Phys.* 18 (2022), pp. 160–166. DOI: 10.1038/s41567-021-01463-1. arXiv: 2105.08533 [hep-ex].

[Ben+22] Cristina Benso et al. “Sterile neutrino dark matter production in presence of nonstandard neutrino self-interactions: An EFT approach”. In: *Physical Review D* 105.5 (2022). ISSN: 2470-0029. DOI: 10.1103/physrevd.105.055016. URL: http://dx.doi.org/10.1103/PhysRevD.105.055016.

[Wor+22a] R.L. Workman et al. "Review of Particle Physics". In: *Prog. Theor. Exp. Phys.* 2022.8 (2022), p. 083C01. DOI: 10.1093/ptep/ptac097.

[Wor+22b] R.L. Workman et al. "Review of Particle Physics". In: *Prog. Theor. Exp. Phys.* 2022 (2022), p. 083C01. DOI: 10.1093/ptep/ptac097.

[An+23] Rui An et al. "Can Neutrino Self-interactions Save Sterile Neutrino Dark Matter?" In: *The Astrophysical Journal Letters* 954.1 (2023), p. L18. ISSN: 2041-8213. DOI: 10.3847/2041-8213/acf049. URL: http://dx.doi.org/10.3847/2041-8213/acf049.

[Bri+23a] Torsten Bringmann et al. "Minimal sterile neutrino dark matter". In: *Physical Review D* 107.7 (2023). ISSN: 2470-0029. DOI: 10.1103/physrevd.107.l071702. URL: http://dx.doi.org/10.1103/PhysRevD.107.L071702.

[Bri+23b] Torsten Bringmann et al. "Minimal sterile neutrino dark matter". In: *Phys. Rev. D* 107 (7 Apr. 2023), p. L071702. DOI: 10.1103/PhysRevD.107.L071702. URL: https://link.aps.org/doi/10.1103/PhysRevD.107.L071702.

[AV24] Maria Dias Astros and Stefan Vogl. *Boosting the production of sterile neutrino dark matter with self-interactions*. 2024. arXiv: 2307.15565 [hep-ph]. URL: https://arxiv.org/abs/2307.15565.

[Fuy+24] Kaori Fuyuto et al. "Sterile neutrino dark matter within the νSMEFT". In: *JHEP* 2024.9 (2024), p. 042. DOI: 10.1007/JHEP09(2024)042. arXiv: 2405.00119 [hep-ph].

[Li24] Jinjing Li. "Latest oscillation results from Daya Bay". In: (2024). arXiv: 2410.00738 [hep-ex]. URL: https://arxiv.org/abs/2410.00738.

[CHZ25] Zi-Qiang Chen, Xi-He Hu, and Ye-Ling Zhou. *An exact parametrization of minimal seesaw model*. 2025. arXiv: 2505.04279 [hep-ph]. URL: https://arxiv.org/abs/2505.04279.

Acknowledgments

I am deeply grateful to Francesco D'Eramo for our useful meetings, his overall great supervision, and for his liveliness in doing so. I realise the value of being guided well in my first attempt at actual research, and with this experience I very much look forward to our future years as collaborators. Additionally, I would like to thank Luca Vecchi for his accurate comments during our pleasant discussions in the final phase of the thesis, showing me the assumptions hidden in my own writing.

Then, of course, I would like to thank my mother Jacqueline, my father Ton, and my brother Conall for their continuous emotional and practical encouragement throughout my entire education. It simply would not have been possible without them. Also to Mikela, who has been extremely patient and caring throughout the entire process, I owe many thanks. I have never received anything but support and kindness.

Finally, to my dear classmates Ulaş Fırat Noyan and Vinka Dakić, I am grateful for reminding me on a weekly basis that Padova offers more than a university: thanks for all the fun.